NASA-CR-134490, Part I
WANL-M-FR-74-005
SEPTEMBER 1974

FINAL REPORT

INTERDIFFUSION BEHAVIOR OF TUNGSTEN OR RHENIUM AND GROUP V AND VI ELEMENTS AND ALLOYS OF THE PERIODIC TABLE PART I

by

F. G. Arcella

Prepared for

National Aeronautics and Space Administration

NASA Lewis Research Center

Cleveland, Ohio 44135

Contract NAS 3-13231

Astronuclear Laboratory

Westinghouse Electric Corporation

WESTINGHOUSE ELECTRIC CORPORATION P. O. BOX 10864 - PITTSBURGH, PENNSYLVANIA 15236

NOTICE

This report was prepared as an account of Government-sponsored work. Neither the United States, nor the National Aeronautics and Space Administration (NASA), nor any person acting on behalf of NASA:

A.) Makes any warranty or representation, expressed or implied, with respect to the accuracy, completeness, or usefulness of the information contained in this report, or that the use of any information, apparatus, method, or process disclosed in this report may not infringe privately-owned rights; or

B.) Assumes any liabilities with respect to the use of, or for damages resulting from the use of, any information, apparatus, method or process disclosed in this report.

As used above, "person acting on behalf of NASA" includes any employee or contractor of NASA, or employee of such contractor, to the extent that such employee or contractor of NASA or employee of such contractor prepares, disseminates, or provides access to any information pursuant to his employment or contract with NASA, or his employment with such contractor.

Requests for copies of this report should be referred to

National Aeronautics and Space Administration
Scientific and Technical Information Facility
P. O. Box 33
College Park, Maryland 20740

1 Report No	2 Government Accession No	3 Recipient's Catalog No
NASA CR-134490		

4 Title and Subtitle	5 Report Date
Interdiffusion Behavior of Tungsten or Rhenium and Group V and VI Elements and Alloys of the Periodic Table - Part I	September, 1974
	6 Performing Organization Code

7 Author(s)	8 Performing Organization Report No.
F. G. Arcella	WANL-M-FR-74-005
	10. Work Unit No

9 Performing Organization Name and Address	11. Contract or Grant No
Westinghouse Astronuclear Laboratory P. O. Box 10864 Pittsburgh, Pennsylvania 15236	NAS 3-13231
	13. Type of Report and Period Covered
12 Sponsoring Agency Name and Address	Final Report
National Aeronautics and Space Administration Cleveland, Ohio 44135	14 Sponsoring Agency Code

15 Supplementary Notes

Project Manager, R. A. Lindberg, NASA Lewis Research Center, Cleveland, Ohio

16 Abstract

Arc cast W, CVD W, CVD Re, and powder metallurgy Re materials were hot isostatically pressure welded to ten different refractory metals and alloys (Cb, Cb-1Zr, Ta, Ta-10W, T-111, ASTAR-811C, W-25Re, Mo-50Re, W-30Re-20Mo, etc.) and thermally aged at 10^{-8} torr at 1200, 1500, 1630, 1800, and 2000°C for 100 to 2000 hours. Electron beam microprobe analysis was used to characterize the interdiffusion zone width of each couple system as a function of age time and temperature. Each system was least squares fitted to the equation:

$$\ln\left(\frac{\Delta X^2}{t}\right) = \frac{B}{T} + A$$

where ΔX is net interdiffusion zone width, t is age time, and T is age temperature. Extrapolations of interdiffusion zone thicknesses to 10,000 hours were made. Classic interdiffusion analysis was performed for several of the systems by Boltzmann-Matano analysis. A method of inhibiting Kirkendall voids from forming during thermal ageing of dissimilar metal junctions was devised and experimentally demonstrated. An electron beam weld study of Cb-1Zr to Re and W-25Re demonstrated the limited acceptability of these welds.

The report is presented in two parts. Part I contains the results and discussion of the experimental investigation. Part II contains detailed descriptions of experimental and analytical procedures utilized in conducting experimental program presented in Part I.

17 Key Words (Suggested by Author(s))	18. Distribution Statement
Tungsten, Rhenium, Diffusion, Refractory Metal Interdiffusion, Chemical Interdiffusion, Autoclave Hot Isostatic Pressure Welding, Kirkendall Void Inhibition, Electron Beam Welding, Electron Beam Microprobe Analysis	Unclassified, and unlimited.

19 Security Classif (of this report)	20. Security Classif. (of this page)	21. No of Pages	22 Price*
Unclassified	Unclassified	248	

* For sale by the National Technical Information Service Springfield Virginia 22151

FOREWORD

This final report describes work performed for the National Aeronautics and Space Administration under Contract NAS 3-13231 by the Westinghouse Astronuclear Laboratory. Mr. R. A. Lindberg of the Lewis Research Center was the NASA Program Manager.

The program was administered for the Westinghouse Astronuclear Laboratory by Mr. R. W. Buckman, Jr. Dr. F. G. Arcella was the principal investigator.

Assistance in several key task areas is appreciably acknowledged:

Autoclave HIP Welding: G. G. Lessman, D. R. Stoner and R. P. Sprecace
Metallographic Preparation: S. Laciak and R. Sabolcik
Microprobe Analysis: A. W. Danko and R. W. Conlin
Electron Beam Weld Study: L. G. Stemann
Program Consulation: R. W. Buckman, Jr., and R. A. Lindberg

This study was performed from July, 1970 to July, 1973.

Astronuclear Laboratory

TABLE OF CONTENTS

TABLE OF CONTENTS (Cont'd.)

LIST OF ILLUSTRATIONS

List of Illustrations (Continued)

List of Illustrations (Continued)

List of Illustrations (Continued)

List of Illustrations (Continued)

List of Illustrations (Continued)

List of Illustrations (Continued)

List of Illustrations (Continued)

List of Tables

List of Tables (Continued)

I. SUMMARY

Dissimilar metal joints in thermionic power conversion systems can degrade through material interdiffusion. Such degradation effects occur (1) as cracks in brittle intermetallic phases which form in the juncture; (2) as Kirkendall voids which form in one side of the juncture; (3) or as an impurity which reduces the emittance efficiency of the diode. In order to resolve the time dependency of these effects, an experimental study was performed. Four diode emitter materials, (1) arc cast tungsten; (2) CVD tungsten; (3) powder metallurgy rhenium; and (4) CVD rhenium were autoclave hot isostatic pressure or hot press welded to each of the structural support alloys listed below:

Cb
Cb-1Zr
Ta
Ta-10W
T-111
ASTAR811C
Mo-50Re
W-30.9Re-20.1Mo
W-25Re
W or Re

The resulting bimetallic interdiffusion couples were vacuum aged for periods of 100, 1000, and 2000 hours at 1200, 1500, 1630, 1800, and 2000°C. Metallographic investigation as well as electron microprobe trace and spot count scans were employed to analyze the extent of interdiffusion as a function of age time and temperature. Computer programs were employed to correct the microprobe analysis data for fluorescense and adsorption and also to perform the Boltzmann-Mantano analysis of the interdiffusion concentration profiles. Engineering

relationships were established to predict the extent of interdiffusion for each system as a function of age temperature and age time. These relations are expressed for each couple system in the form:

$$\ln\left(\frac{\Delta X^2}{t}\right) = \frac{B}{T} + A \qquad (1)$$

where ΔX is the net interdiffusion zone width (cm)

t is the age time at temperature (sec)

T is the age temperature (^{o}K)

and A, B are constants.

Table 1 presents the parameters A and B for equation (1) for the interdiffusion systems studied.

High remperature solid state interdiffusion between two metallurgically joined metals of widely different melting points can also result in a coalescence of vacancies in the lower melting point material. The resulting pores form in a plane on one side of the juncture and can result in fracture in that plane, as well as through leakage of cesium plasma or containment gases. A method was devised to retard the formation of these Kirkendall voids, and a cursory investigation showed it to be quite successful.

Although all of the selected diffusion junctions survived the one age thermal cycle without fracture, several observations could be noted. Welded (hot isostatic pressure) interfaces with Re are not recommended for long term elevated temperature service due to brittle intermetallic phases and cracks which formed in the diffusion interface during short term thermal ageing. Nonplanar joints such as tubular (concentric cylinder) face joints with Re to Ta all cracked and fractured in the interdiffusion zone. Tungsten joined to columbium

Table 1. Parameters to Predict Net Interdiffusion Zone Width As a Function of Age Time (t-seconds) and Temperature (T - °K)

$$\ln\left(\frac{\Delta X^2}{t}\right) = B\left(\frac{1}{T}\right) + A$$

(with 95% confidence limits)

System	A	B
W/Cb, Cb-1Zr	-3.8689 ± 0.2266	-37,390 ± 2810
Re/Cb, Cb-1Zr	-0.4899 ± 0.2266	-43,880 ± 3060
W/Ta, Ta-10W	-7.3385 ± 0.1891	-35,290 ± 2210
W/T-111, ASTAR	-3.3585 ± 0.1530	-44,720 ± 3760
Re/Ta, Ta-10W	-7,1024 ± 0.0980	-35,020 ± 1100
Re/T-111, ASTAR	-6.4489 ± 0.1374	-36,560 ± 1730
W/Mo-50Re	+0.1554 ± 0.1921	-45,140 ± 4500
Re/Mo-50Re	-8,4797 ± 0.1466	-30,140 ± 2940
W/W-30.9Re-20.1Mo	-7.2084 ± 0.1719	-34,750 ± 3890
Re/W-30.9Re-20.1Mo	-9.3027 ± 0.1440	-28,580 ± 3290
W/Re	-4.4641 ± 0.3317	-41,300 ± 7470
W/W-25Re	-2.1992 ± 0.4407	-47,100 ± 9930
Re/W-25Re	+2.4148 ± 0.5513	-53,990 ± 11,900

and tantalum alloys were not subject to joint cracking but were susceptible to considerable Kirkendall void formation. The most acceptable joints for long term high temperature service should be those of W to alloys such as T-111 or ASTAR-811C after being pretreated for Kirkendall void inhibition.

Studies were also conducted into the weldability of Re/Cb-1Zr and Cb-1Zr/W-25Re systems. EB weld parameters such as beam energy, width, traverse speed, sample geometry, etc. were evaluated.

Successful electron beam welds were produced between Cb-1Zr alloy and W-25Re or Re. These joints had braze characteristics in that the lower melting point Cb-1Zr was melted against the more refractory material, and little intermixing occurred. Due to the brittle nature of these welds and the limited extent of this study, employment of junctions of these materials cannot be recommended for specific application without more definitive characterization.

II. INTRODUCTION

In-core and out-of-core thermionic power nuclear reactors operate on the principle of thermal emission of electrons. Metals with low electron thermal emission energies are heated to elevated temperatures, 1500 to 1800°C, where the electrons are emitted, traverse a short gap, typically 5 to 10 mils (0.25 mm) and are collected on an adjacent, lower temperature metal. Such diodes typically employ tungsten or rhenium as the emitter material, and columbium, for instance, as the collector material.

Problems occur in that the most ideal emitter materials, rhenium or tungsten, are not necessarily the best high temperature strength or load bearing materials, nor the most easily joined materials. Consequently, the pure emitter materials must be joined to more sophisticated refractory metal alloys to satisfy fabrication or structural requirements. Joining these materials is accomplished by (1) hot isostatic pressure (HIP) welding in an autoclave; (2) hot press joining; (3) electron beam (EB) welding; or (4) chemical vapor deposition.

Most of the diverse properties that occur in the material juncture region result from:

- Material intermixing
- Formation of brittle intermetallic phases
- Thermal expansion mismatching of phases
- Kirkendall void formation
- Penetration by diffusing structural materials to the emitter surfaces

and are dependent upon/or strongly influenced by the rate of interdiffusion (intermixing) of the parent binary metal combinations at elevated temperatures. For instance, thin interdiffusion zones composed of brittle intermetallic phases are most resistant to thermal cycling or stress fracture than thicker zones. Also, the thermionic emission efficiency can be reduced by the introduction (diffusion) of trace levels of other elements from structural support members to the emitter surfaces. The ability to predict the extent of interdiffusion between emitter/

structural material combinations would be valuable in the design selection of diode components.

This study quantitatively characterized the interdiffusion behavior of tungsten or rhenium emitter materials to several refractory metals and their alloys. Predictive models of the extent of interdiffusion as a function of material combination and temperature for long age (application) times were resolved. Also, the various material combinations selected for analysis were studied for juncture cracking, Kirkendall porosity, and interphase growth. Figure 1 presents a guide to the operational sequence of events followed in the performance of this study.

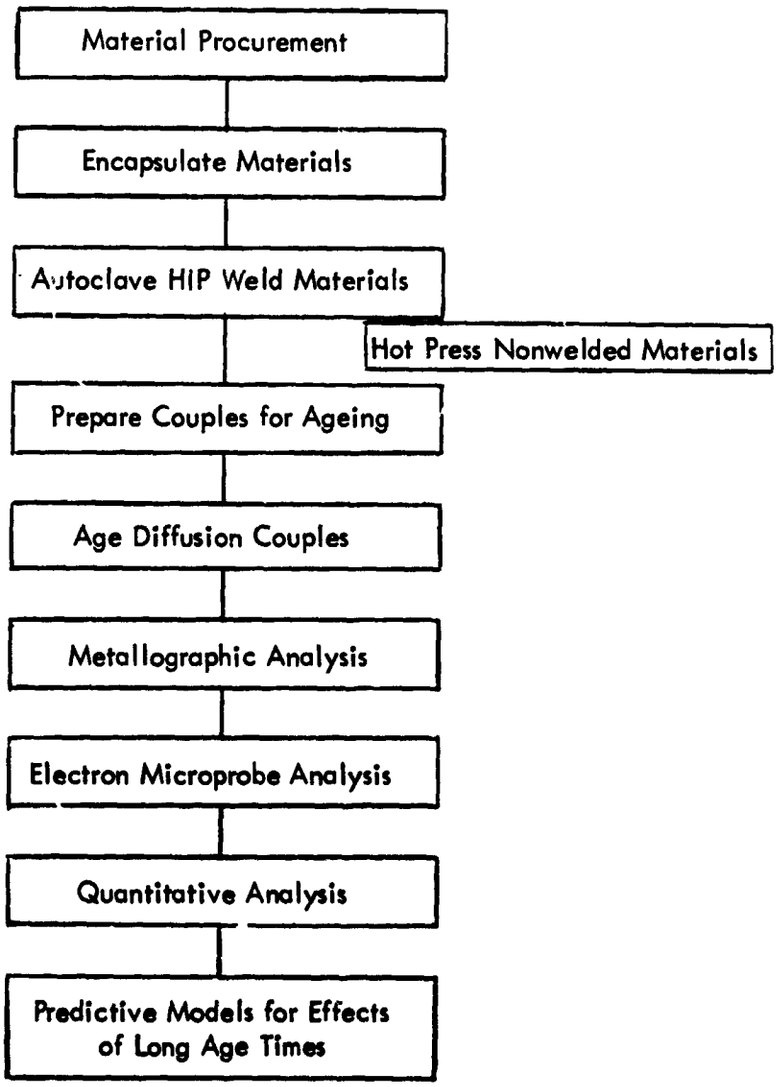

Figure 1. Program Sequence

III. MATERIAL SYSTEMS AND SOURCES

Although many emitter materials could have been selected for this study, tungsten and rhenium were chosen for their high temperature properties and general acceptance as leading thermionic emitter candidates. Chemical vapor deposition (CVD), arc cast, and powder metallurgy product materials were selected to resolve if any structural effects could be observed in the measured interdiffusion zone growth analysis. Selections of alloy structural support materials were made on the basis of (1) a good cross-section (representation) of alloy bases (i.e., columbium base, tantalum base, tungsten base, molybdenum-rhenium base), (2) general acceptability to high temperature structural support applications, and (3) possibilities for observing the effect of sequential alloy additions on interdiffusion rates (i.e., Ta, Ta-10W, T-111, ASTAR811C). Table 2 presents the diffusion couple combinations that were selected for detailed experimental study.

Selections of the experimental age temperatures to employ were bounded by the following constraints. Age temperatures for each alloy were restricted to that temperature regime where they would normally be employed. Also, the tungsten or rhenium to alloy couple was investigated for possible low melting eutectic conditions which could occur upon interdiffusion. Thus, Cb and Cb-1Zr systems were diffusion aged at 1200, 1500, 1630, and 1800°C while W-25Re systems were aged at 1500, 1630, 1800, and 2000°C.

Since all of the systems, due to their differing characteristics, interdiffuse at different rates, selection of experimental age times was critical. For instance, 100 hours at 1500°C for the W/Cb-1Zr couple combination would result in sufficient interdiffusion for accurate experimental measurement. However, ageing W/W-25Re for 100 hours at 1500°C would be analytically impractical. In order to select the optimum experimental age time/age temperature conditions to impose upon the selected material couple combinations, an engineering

Table 2. Diffusion Couple Material Combinations Selected for Study

Emitter Side		Alloy Side
W (arc cast)	to	Cb
W (CVD (100))*		Cb-1Zr
Re (powder metal product)		Ta
Re (CVD (0001))*		Ta-10W
		T-111
		ASTAR811C
		[illegible]-50Re
		W-30.9Re-20.1Mo
		W-25Re (arc cast)
		W or Re
4 emitter materials		10 structure materials

* Miller indices (100) indicating (100) planes parallel to junction plane.

level interdiffusion model was derived. This model, utilizing experimental results from similar material couple systems and relative entropy correlations, was used to predict the extent of interdiffusion for the couple systems selected for this program*. Thus, the optimum age times necessary to generate readily analyzable (microprobe) interdiffusion zones of adequate dimension were quantitatively predicted with this model. The model, presented in Part II, Appendix C, is also applicable to other diffusion couple material combinations not presented in Table 1.

With the aforementioned considerations as a guide, the age temperatures and times for the material combinations selected were resolved as illustrated in Tables 3 and 4. These tables also contain the predicted interdiffusion zone widths as derived from the model. Thus, in Table 3, for tungsten couples, columns one and two describe the age cyclic history planned for the material couples, and the remaining ten columns denote (by dots) the selected age cycle treatment for each alloy combination. Short age times at low temperatures (1200°C) were avoided as were long age times at elevated temperatures. As a selection criteria, only time/temperature conditions which resulted in a predicted interdiffusion zone width of 3.8×10^{-3} cm (1.5 mils) (or 5.1×10^{-3} cm (2 mils) at a 45 degree angle to the interdiffusion interface) or greater were accepted.

Since the effects of small impurity levels in the couple materials could influence the diffusion characteristics, high purity starting materials were desired. Table 5 lists the couple materials used for the study and their trace chemistries. Vendor chemistries were verified with random checks by our own analysis. Alloy constituencies are presented in Table 6 and were also verified by our own analysis.** Purchase order materials specifications were written to minimize constituent impurities, yet still permit economic alloy manufacture.

---

* Part II, Appendix C, Interdiffusion Predictive Model

**Electron beam microprobe analysis, relative intensity ratio

Table 3. Tungsten Couples - Age Schedule (Couple Analysis) with Predicted Interdiffusion Width

Code Tungsten A = Arc Cast W
B = CVD W ⊥ 100

Shown: Predicted interdiffusion zone width (cm x 10^3) (138 couples) *

Age T (°C)	Age t (hrs.)	Couples 13	13	13	17	13	17	13	13	13	13	Sums
2000	2000											
	1000				•22.70•		•>•	•32.10•	•<•	•>•	•56.60•	12
	100				• 7.18•		•>•	•10.15•	•<•	•>•	•17.96•	12
	10											
1800	2000											
	1000	•38.50•	•38.50•	•13.92•	• < •	•>•	•>•	•18.85•	•<•	•>•	•28.95•	20
	100	•12.18•	•12.18•	• 4.39•	• < •	•>•	•>•	• 5.94•	•<•	•>•	• 9.16•	20
	10											
1500	2000			•10.79•	• < •	•>•	•>•	•12.95•	•<•	•>•		14
	1000	•16.08•	•16.08•	• 7.61•	• < •	•>•	•>•	• 9.1o•	•<•	•>•	•11.90•	20
	100	• 5.08•	• 5.08•								• 3.79•	6
	10	•11.91•	•11.91•	• 8.02•								
1200	2000	• 4.69•	• 4.69•	• 3.16•	• < •	•>•	•>•					12
	1000	• 8.44•	• 8.44•	• 5.66•	• < •	•>•	•>•					12
	100											
	10											
As Bonded		•	•	•	•	•	•	•	•	•	•	10
		A B	A B	A B	A B	A B	A B	A B	A B	A B	A B	138
		Cb	Cb-1Zr	Ta	Ta-10W	T-111	ASTAR 811C	Re	W-25Re	W-30.9Re 20.1Mo	Mo-50Re	

* Note: > or < denotes zone width greater or less than primary alloy.

Table 4. Rhenium Couples - Age Schedule (Couple Analysis) with Predicted Interdiffusion Width

Code Rhenium C = Powder Metallurgy Product
D = CVD Re ⊥ 0001

Shown: Predicted interdiffusion zone width (cm x 10^3) (134 couples) *

Age T (°C)	Age t (hrs.)	Couples: 13	13	13	17	13	17	13	13	15	7	Sums
2000	2000				•43.50•		• > •	•32.15•	•< •	•78.20•	32.15•	11
	1000				•13.80•		• > •	•10.15•	•< •	•24.35•	10.15•	11
	100											
	10											
1800	2000											
	1000	•43.30•	•43.30•	•23.85•	• <	• •> •	• > •	•18.85•	•< •	•38.10•	18.85•	19
	100	• 5.38•	• 5.38•	• 2.97•	• <	• •> •	• > •	• 2.34•	• •	•12.03•	5.94•	19
	10	13.69	13.69	7.54								
1500	2000			•15.23•	• <	• •> •	• > •	•12.95•	•< •	•21.15•	12.95•	15
	1000	•16.48•	•16.48•	•10.78•	• <	• •> •	• > •	• 9.16•	•< •	•15.08•	9.16•	19
	100	• 5.21•	• 5.21•							• 4.75•		6
	10											
1200	2000											12
	1000	•10.78•	•10.78•	• 8.43•	• <	• •> •	• > •					12
	100	• 7.61•	• 7.61•	• 5.95•	• <	• •> •	• > •					
	10											
As Bonded		•	•	•	•	•	•	•	•	•	•	134
		C D	C D	C D	C D	C D	C D	C D	C D	C D	C D	D
		Cb	Cb-1Zr	Ta	Ta-10W	T-111	ASTAR 811C	W-25Re	W-30.9Re 20.1Mo	Mo-50Re	W	

* Note: > or < denotes zone width greater or less than primary alloy.

Table 5. Program Materials and Their Chemistries (in ppm (Wt))

Impurity	Cb	Cb -1Zr	Ta	Ta 10W	T-111	ASTAR 811C	W 25Re	Mo 50Re	W Re Mo	W arc	W CVD	Re Powder	Re CVD	Mo lids	Ta sheet
C	50	50	<30	7	60	300	40/39	37	3	20/19	20	41	18	250/10	20/33
O	100	60	50	22	80	<50	<50/5	20	4	30/5	<5	5	40	<10/61	47/250
H	2.3	3.2	1.5	1.7	5	< 1	1.4		<1		9		11	< 1	< 5
N	40	30	20	11	22	10	35/140	50	<1	9	11	70	9	< 1/65	18
Al	<20	<20	<20	<20			<20		<20	<10	2		100		<10
Ca	<10		<10						<10	<10					<10
Co	<10	<10	< 5	<10	< 5	< 5	60		<20	<10					<10
Cr	<10	<20	<10	<10	<10		<20		<20	10	< 1		7		<10
Cu	<40	<40	< 2	<10	<20		<40		<10	1	3		1		<10
Fe	<50	<50	42	<20	<20	35	100/150		34	3	3	700	8	<40	35
Pb	<20	<20	< 5	<10			<20		<50	<10					
Mg	<20	<20	<10	< 5			<20		<10	<10					<10
Mn	<20	<20	<10	<10			<20		<10	<10					<10
Ni	<20	<20	10	<20	<10	<10	<20		<20	20	< 1		4	<10	<10
Si	<50	<50	11	<25	<20		<100		<20	<10	20		20	<30	<10
Sn	<10	<10	<10	<10			<20		<20	<10					<10
F	-	-	-	-			-		-	10	9				
Re	-	-	-	-			-		-	<30					
Hf	<80	-	<200	<50			-		-	<100					
Cb	-	-	91	145	450	940	125/50		-	<50					100
Ta	290	<500	-	-			-		-	<50					
B	< 1	< 1	< 1	< 5			< 1		-	< 5					
Cd	-	< 5	-	<10			< 5		-	<10					
Na	<25	-	<10	-			-		30	<10					
Ti	<40	<40	<10	<25			<20		<20	<10	< 1		50		<10
V	<20	<20	<10	<20	<10	<10	<20		-	<10					<10
Li	-	-	-	-			-		-	<10					
Be	-	-	-	-			-		-	<20					
Mo	<20	<20	<10	<50	<10	<10	275/300		20.1	-	10	100	80		<10
Zr	-	1.0	-	-	<500		-		-						<10

Table 6. Alloy Chemistries and Properties

Alloy	Composition	Source
Cb	Cb	Wah Chang
Cb-1Zr	Cb-1.0Zr	Wah Chang
Ta	Ta	Wah Chang
Ta-10W	Ta-9.2W	Wah Chang
T-111	Ta-8.2W-1.9Hf	Wah Chang
ASTAR811C	Ta-8.1W-1.4Re-0.9Hf-0.03C	Wah Chang
Mo-50Re	Mo-49.5Re	Cleveland Refractory Metals
W-Re-Mo	W-30.9Re-20.1Mo	G. E. Cincinnati
Re (powder met)	Re	Cleveland Refractory Metals
W (arc cast)	W	Westinghouse Astronuclear
Re (CVD)	Re	San Fernando Laboratory
W (CVD)	W	San Fernando Laboratory
W-25Re (arc cast)	W-25.6Re	Wah Chang
Mo*	Mo	Climax Molybdenum

* Molybdenum used to encapsulate couple material for autoclave HIP-weld process.

The CVD tungsten and CVD rhenium were investigated for preferred orientation by x-ray diffraction tests. X-ray diffraction peaks are recorded at varying x-ray angles by planes (h k l) parallel to the sample surface. Only certain planes give reflections and peaks[1]. Structure factor calculations for tungsten (BCC) show that only planes with Miller indices h + k + l = even number will result in reflections. Thus, the (100) plane will not yield a peak, whereas the (200), (110), etc., will. A similar analysis applies to rhenium (HCP), and again only certain planes will yield reflections. Table 7 presents the relative diffraction peak intensities for randomly oriented tungsten and rhenium, and the CVD products used in this study. The CVD tungsten was found to be very strongly oriented with the (200) planes ({100} family) parallel to the surface; and thus diffusion occurred perpendicular ($\perp$) to the {100} family of planes. The CVD rhenium was also highly oriented with the (0002) planes ({0001} family) parallel to the surface; and thus diffusion occurred perpendicular ($\perp$) to the {0001} family of planes.

Table 7. Comparison of Relative X-Ray Diffraction Peak Intensities for Random and CVD Oriented Materials

Tungsten			Rhenium		
Plane (hkl)	I/I_1[1] (random)	I/I_1[2] CVD	Plane (hkl)	I/I_1[1] random	I/I_1[2] CVD
100	100	1	100	32	---
200	15	100	002	34	100
211	23	2	101	100	---
220	8	---	102	11	---
310	11	---	110	22	---
222	4	---	103	[illegible]	---
321	18	---	200	3	---
400	2	---	112	20	---
			201	15	---
			004	2	15
			202	3	---
			104	2	---
			203	7	---
			210	3	---
			211	15	---
			114	8	---
			212	5	---
			105	8	---
			204	2	---
			300	5	---

[1] Relative intensity; Diffraction peak intensity divided by intensity of maximum peak. These data traceable to NBS reports.

[2] Relative intensity; NAS 3-13231 CVD materials (tests at WANL).

IV. FORMATION OF DIFFUSION COUPLES

Autoclave hot isostatic pressure (HIP) welding was selected as the mode of forming the diffusion couples. This method was chosen because it could accommodate a large number of couple welds (all of the scheduled program couples) in one autoclave cycle. Also, the HIP welding process could affect metallurgical, surface to surface welds at low temperatures with minimal material interdiffusion. Figure 2 illustrates, conceptually, the HIP welding sequence employed. The diffusion couple fabrication sequence began with surface preparation operations.

The materials to be surface welded to form diffusion couples were received in the form of sheets (3.20 cm (1.250 inches) wide by 0.20 cm (0.080 inches)* thick by random length). Lengths of 6.35 cm (2.50 inches) were cut by shearing or by carbide cutoff wheel. All material surfaces were smooth (32 RMS or better) and flat. Light polishing with 600 emery paper and water was used to remove the faint surface oxides. The 3.20 cm (1.250 inches) by 6.35 cm (2.50 inches) sheet were then cleaned by subsequent

- Scrubbing with an abrasive cleaner
- Rinsing in hot tap water
- Rinsing in boiling distilled water
- Rinsing in ethyl alcohol
- and air drying.

The surfaces were then chemically etched as follows:

Cb Cb-1Zr	65 parts HNO_3 - 35 parts HF 1 minute at 120°F
Ta Ta-10W T-111 ASTAR811C	15 parts H_2SO_4 20 parts HF 20 parts HNO_3, 45 parts water 5 minutes at room temperature

* 0.080 inch thickness determined by diffusion analysis boundary conditions. See Part II, Appendix G, Diffusion Analysis.

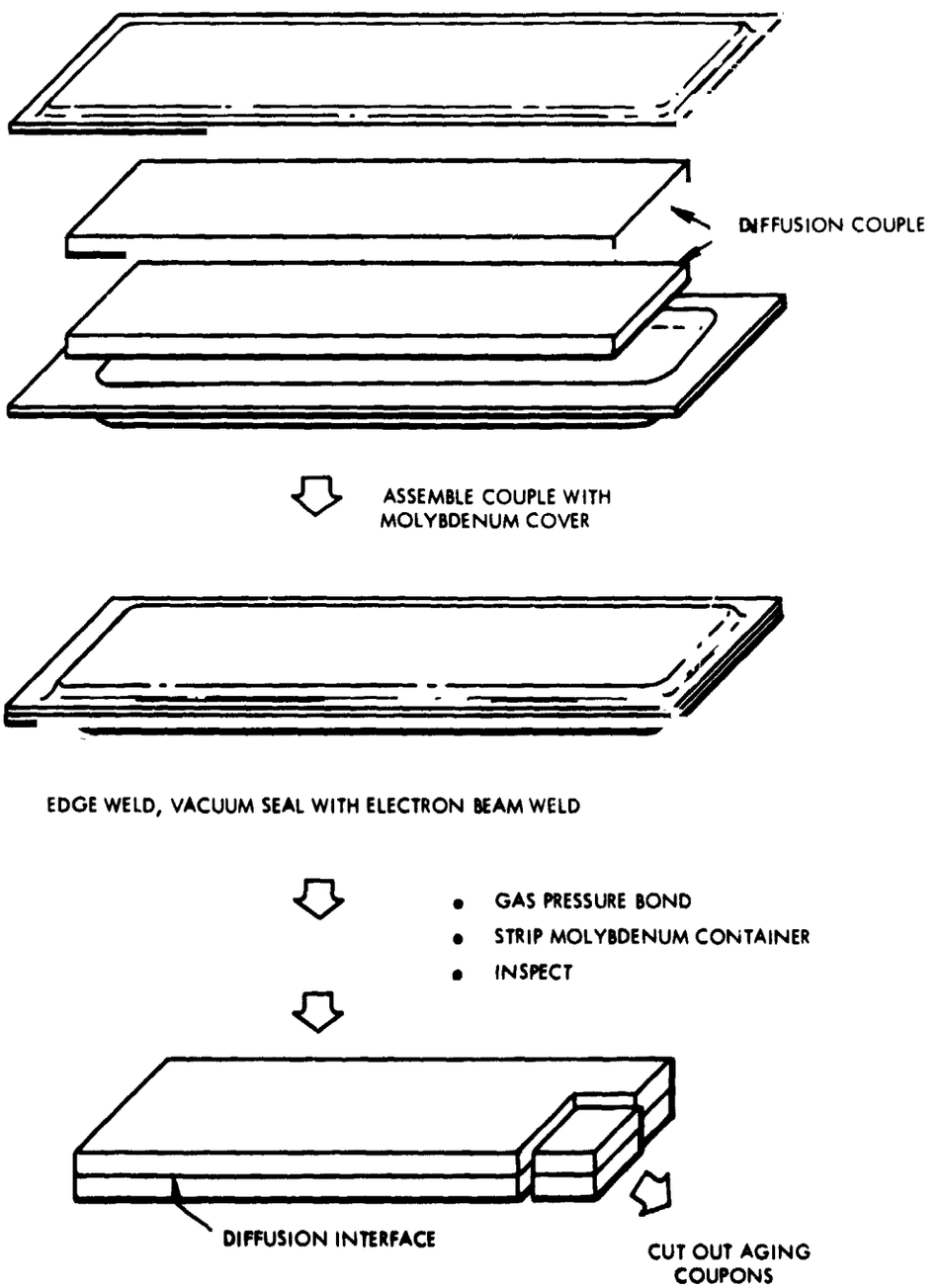

Figure 2. Fabrication of Diffusion Couples with Tungsten or Rhenium Grain Orientation Normal to the Diffusion Interface

W, Re, W-Re-Mo, Mo-50Re	No etch
W-25Re	30 parts HNO_3 - 20 parts HF - 50 parts water
Mo	Hot chromic acid

Molybdenum container cans were drawn to the geometry illustrated in Figure 2 from 0.051 cm (0.020 inches) thick arc cast molybdenum sheet product. Prior to the assembly of diffusion couple materials in each molybdenum container, all components were vacuum degassed at 900°C at 10^{-8} torr for 2 hours. During the degassing cycle, all components were individually wrapped in tantalum foil envelopes. Figure 3 presents a molybdenum HIP-weld can in the process of assembly. A tantalum foil sheet 0.0051 cm (0.002 inches) thick by 3.20 x 12.70 cm (1.25 by 5.00 inches) was placed in the bottom of the can. Next, the tungsten or rhenium half of the planned couple combination was wound with 0.0051 cm (0.002 inches) diameter W-1.0%ThO_2 wires at 0.08-0.16 cm (1/32 - 1/16 inch) intervals. The wires served as interface locators in the welded couples and were involved in the analytical treatment. The wires had been sonic degreased and were pulled through an alcohol lubricated cloth grip in order to remove oil and grease. The alloy half of each couple was then placed on the tungsten or rhenium half, another 0.0051 cm (0.002 inches) tantalum foil added, and the flat sheet molybdenum lid was placed over the couples. The assembly was held together with "C" clamps until joined by welding.

Precautions were taken to insure that contamination through handling would not occur. All assembly and handling operations were performed with teflon tipped tweezers or by cotton over plastic gloves. Care was taken not to rub or touch iron bearing materials on expected weld surfaces. The diffusion couple materials were also cross-loaded in the containment cans

Figure 3. Preautoclave HIP Weld Assembly Sequence of Couple Materials and Encapsulation Can. (Can 2D Containing W_{CVD}/Ta-10W and W_{CVD}/T-111 Diffusion Couple Combinations)

for redundancy. Thus, as in Figure 3, half of the can contained one alloy to tungsten couple material, and the other half of the can contained another alloy to tungsten couple combination. Thus, if one can failed in the HIP welding cycle, a backup capability was present. Also, the cross loading did not mix tungsten and rhenium in one can nor did it mix alloy materials of widely varying composition. In total, 48 cans were prepared for the autoclave HIP welding operation.

Once assembled, the cans were placed in a TIG weld box, and after a twelve hour evacuation at 10^{-4} N/m^2 (10^{-6} torr) were welded on three sides (edges) in an argon environment. Box atmospheres were normally in the 2 ppm oxygen and 3 ppm moisture range, continuously monitored during the weld cycle. Following this weld operation, the cans were immediately placed in an EB weld chamber, evacuated for 12 hours at 10^{-4} N/m^2 (10^{-6} torr), and EB weld sealed on the fourth (short) edge that had been left open.

The sealed molybdenum cans were then dye penetrant inspected for weld cracks or flaws and were also helium leak checked. This operation was performed in two steps. The sealed cans were placed in a retort which was evacuated and backfilled with helium to 15 psig and held for 15 minutes. Upon removal, the cans were plunged into a methanol bath where bubbles would indicate a gross leak. Following this operation, the cycle was repeated, and the cans were helium mass spectrograph leak checked and compared to a 10^{-9} cc (STP)/sec standard leak. Leaking cans were opened, and their contents cleaned, and transferred to a new container.

Initially, problems were encountered with the welds of several of the molybdenum cans. Post weld embrittlement and leaks (cracks) in areas adjacent to the welds were found only in cans with chemistries of 10-20 ppm or less carbon and 10 ppm oxygen. Molybdenum cans with 250 ppm carbon and 10 ppm oxygen were leak (crack) free. Apparently, the high carbon is necessary to counteract the oxygen and to prevent "hot tearing" as a result

of the weld process. Leaking cans were either replaced with cans of high carbon molybdenum or were resealed in a second can of tantalum.

Two autoclave trial HIP-weld parameter evaluation cycles with a cross section of planned material junctions showed that operation at 1450°C at 193 MN/m^2 (28,000 psi) for 45 minutes was adequate to achieve 100 percent surface welding of all couple material combinations. Thus, the couple cans were placed in four, four-inch diameter by 6-inch deep molybdenum containment buckets and placed in the autoclave furnace. Autoclave thermal control problems prevented achievement of the temperature goals in this third cycle and a fourth full load cycle was made. During this fourth full load cycle, three of the five heating zones in the autoclave furnace shorted and burned through, and all of the couple combinations did not reach the desired 1450°C temperature. Figure 4 shows the typical appearance of the post-HIP cycle molybdenum cans. A complete description of autoclave procedures followed, and their rationale is presented in Part II, Appendix D, HIP-Welding Operation and Practices.

Table 8 reviews the HIP weld autoclave cycles employed in this study, while Table 9 presents the results of the fourth HIP weld cycle. Post-HIP weld helium mass spectrograph leak checks of the cans (noted in Table 9) revealed that those couples, which did not weld acceptably, were primarily in cans that failed the leak check. The acceptability of the weld-interface for each material combination was determined by metallographic observation. For instance, Figure 5 shows typical interface conditions for accepted tungsten welds, while Figures 6 and 7 illustrate typical, accepted rhenium interfaces. Those welds not accepted generally appeared as illustrated in Figure 8. Those combinations not welding acceptably (as denoted in Table 9) were separated for hot press welding. The remaining, welded couple combinations continued their processing cycle as follows:

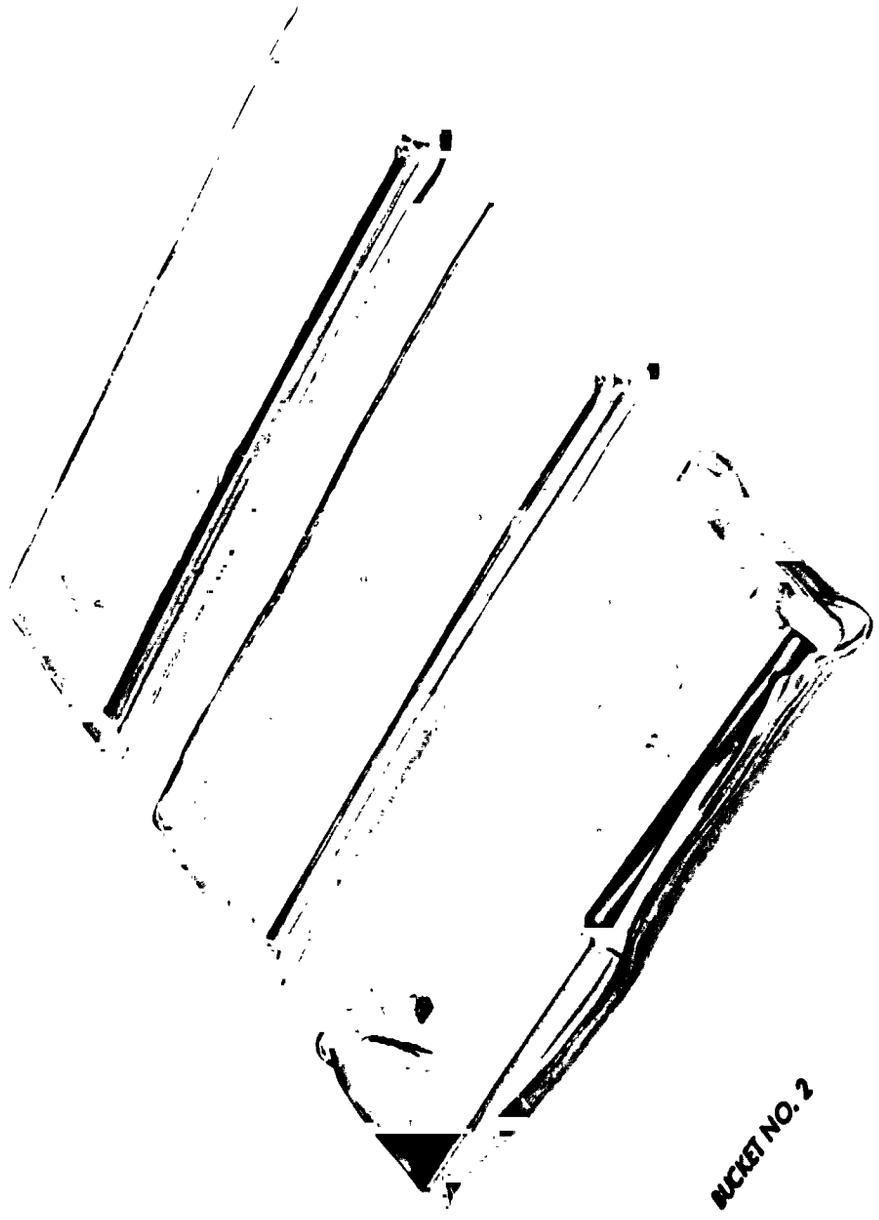

Figure 4. Post HIP-Weld Cycle Appearance of Molybdenum Container Cans

Table 8. Diffusion Couple Evaluation - HIP Weld Cycles

Cycle	Purpose	Results
1	Evaluate HIP-weld T-P conditions for alloys of program.	Molybdenum HIP-weld cans leaked due to oxygen hot tearing. Showed need to add getters (T-111 chips) and baffles to furnace and need to employ high carbon molybdenum cans.
2	Evaluate HIP-weld T-P conditions for alloys of program.	Welding conditions of 193 MN/m^2 (28,000 psi) at 1450°C for 40 minutes yielded 95-100% welding of all alloys in the program. T-111 chips and Ta foil baffles prevent oxygen hot tearing of high carbon molybdenum cans.
3	HIP-weld of all program diffusion couples at T-P conditions of cycle 2.	Problems in autoclave furnace control. 100% welding of Re/Cb, Re/Cb-1Zr, W/Cb, and W/Cb-1Zr. Other couples partially welded.
4	HIP-weld of remainder of program couples.	Achieved 65% of desired program couple welds. Furnace melt-through precludes further cycles.

Table 9. HIP-Weld Yield of Diffusion Couples from Autoclave Cycle 4

Can Number	Couple Combination (Primary Side)[1] X/Y	Post-Cycle He Leak Check of Containment Can[2]	% Welded (Subjective Evaluation)	Acceptable for Ageing and Analysis	Can Repackaged for Hot-Press Welding of Couple
1a	$\widehat{W}$arc/Cb	OK	100%	Yes	---
1b	$\widehat{W}$/Cb-1Zr	OK	100%	Yes	---
1c	$\widehat{W}$/Ta-10W	OK	50%	No	Yes
1d	$\widehat{W}$/Ta	OK	100%	Yes	--
1e	$\widehat{W}$/T-111	OK	60%	No	Yes
1f	$\widehat{W}$/Astar811C	OK	50%	No	Yes
1g	$\widehat{W}$/W-25Re	OK	0%	No	Yes
1h	$\widehat{W}$/W30.9Re2Q.1Mo	Leak	50%	No	Yes
1i	$\widehat{W}$/Mo-50Re	Leak	0%	No	Yes
1j	$\widehat{W}$/Re_p	Leak	30%	No	Yes
2a	W_{CVD}/Cb	OK	100%	Yes	--
2b	W_{CVD}/Cb-1Zr	OK	100%	Yes	--
2c	W_{CVD}/Ta	OK	100%	Yes	--
2d	W_{CVD}/Ta-10W	OK	95%	Yes	--
2e	W_{CVD}/T-111	Leak	0%	No	Yes
2f	W_{CVD}/Astar811C	Leak	0%	No	Yes
2g	W_{CVD}/W-25Re	OK	50%	No	Yes

[1] Secondary side of cans contain backup couples

[2] Couple cans post-autoclave helium leak checked

Table 9 (Continued)

Can No.	Couple Combination (Primary Side)[1] X/Y	Post-Cycle He Leak Check of Containment Can[2]	% Welded (Subjective Evaluation)	Acceptable for Ageing and Analysis	Can Repackaged for Hot Press Welding of Coupling
2h	W_{CVD}/W30.9Re20.1Mo	OK	50%	No	Yes
2i	W_{CVD}/Mo-50Re	Leak	5%	No	Yes
2j	W_{CVD}/Re_P	OK	95%	Yes	--
3a	Re_P/Cb	OK	100%	Yes	--
3b	Re_P/Cb-1Zr	OK	100%	Yes	--
3c	Re_P/Ta	OK	100%	Yes	--
3d	Re_P/Ta-10W	OK	100%	Yes	--
3e	Re_P/ASTAR811C	OK	40%	No	Yes
3g	Re_P/W-25Re	OK	90%	Yes	--
3h	Re_P/W30.9Re20.1Mo	OK	100%	Yes	--
3i	Re_P/Mo-50Re	OK	100%	Yes	--
4a	Re_{CVD}/Cb	OK	100%	Yes	--
4b	Re_{CVD}/Cb-1Zr	OK	100%	Yes	--
4c	Re_{CVD}/Ta	OK	100%	Yes	--
4d	Re_{CVD}/Ta-10W	OK	100%	Yes	--
4e	Re_{CVD}/T111	OK	100%	Yes	--
4f	Re_{CVD}/ASTAR811C	OK	50%	No	Yes
4g	Re_{CVD}/W-25Re	Leak	50%	No	Yes
4h	Re_{CVD}/W30.9Re20.1Mo	OK	100%	Yes	--
4i	Re_{CVD}/Mo-50Re	OK	100%	Yes	--
4j	Re_{CVD}/W	OK	60%	No	Yes

Summary: Acceptable Yield = 59%
Couple cans leaking (post-cycle) = 18%
Cans to be hot pressed = 16 units

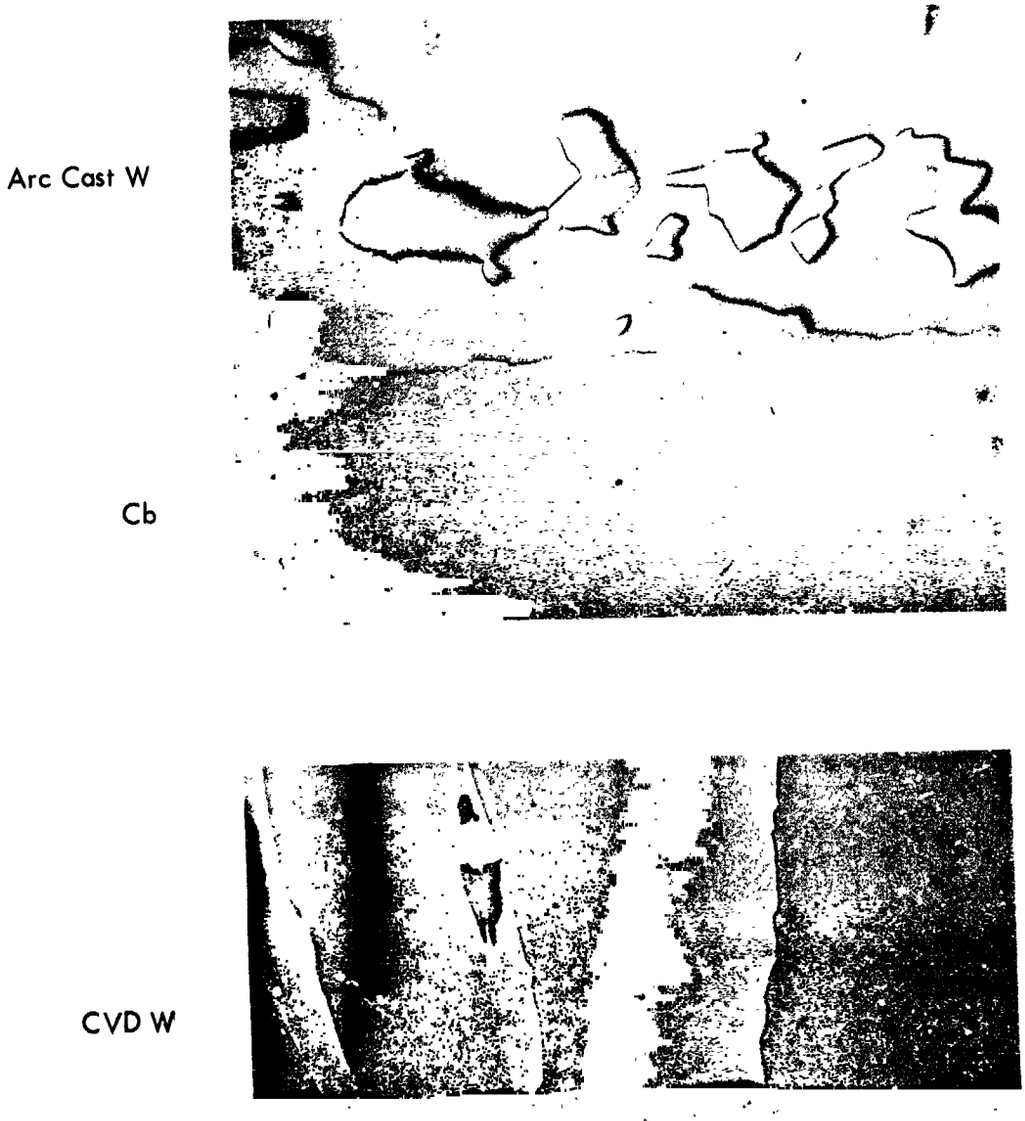

Figure 5. The Arc Cast-W/Cb and the CVD-W/Ta Interface at 400X (Oblique Light) Demonstrating Acceptable HIP-Weld Junctures

Figure 6. The Powder Metallurgy Re/Ta Interface at 1000X, Oblique Light (This Magnification was Necessary in Order to see into the Interface Zone) Illustrating Acceptable HIP-Weld Junction

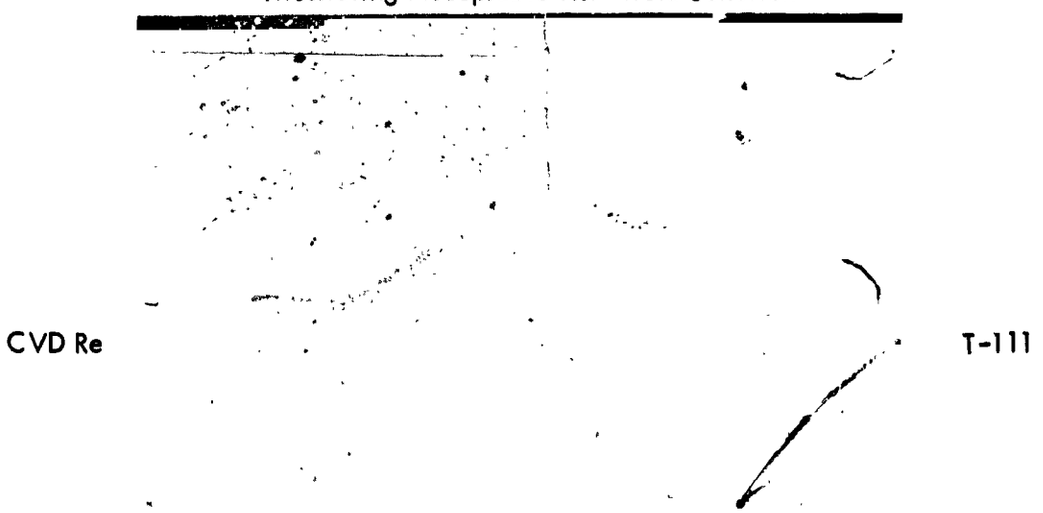

Figure 7. The CVD-Re/T-111 Interface at 1000X (Oblique Light) Illustrating Acceptable HIP-Weld Junction

Figure 8. Typical Partially HIP-Welded Interface Requiring Further Welding in the Hot Press Facility (Arc Cast W/ASTAR 811C at 400X, Oblique Light)

Post autoclave cycle vacuum outgassing treatments at 900°C for 1 hour at 10^{-6} torr were employed to remove hydrogen introduced by the autoclave operation*.

The degree of welding of each couple combination as presented in Table 9 was established by cutting off 0.320 cm (0.125 inches) from the end of each molybdenum can and metallographically inspecting the weld interface. Those material combinations that were welded (visual, subjective analysis) were cut to 1.59 x 1.27 cm (0.625 x 0.500 inch) diffusion couples with a diamond cutoff wheel. The perimeter of each couple was coated with a strippable latex, and the molybdenum can faces (lateral surfaces) were removed by etching in nitric acid. The previously mentioned 0.005 cm (0.002 inch) tantalum foil can liner prevented lateral attack of the couples. Alpha-numeric identification characters were scribed into the tungsten face of each couple with a carbide tip vibratool**. Annealing of a W/Ta couple at 2650°C for 10 hours*** showed that the scribe marks would not disappear through surface diffusion effects. The prepared couples were then scrubbed with an abrasive cleaner and rinsed in distilled water and alcohol. A 10^{-6} torr vacuum anneal at 900°C for 3 hours was used to prepare the couples for ageing+. The couples were again wrapped in tantalum foil during this outgas anneal.

Those diffusion couple combinations not joined by HIP weld practice were prepared for hot press joining. Surface preparation was identical to that described for the HIP weld materials. A parameter evaluation hot press cycle was made with a stack of the following material sequence:

Ta/ASTAR811C/W/T-111/W-30.9Re-20.1Mo/W/W-25Re/T-111/Ta.

At 2000°C, 12.4 MN/m^2 (1800 psi) for 15 minutes, the ASTAR811C and T-111 welds to W were 70-90 percent successful, while the W-25Re and W-30.9Re-20.1Mo welds were only

* Part II, Appendix D, HIP-Welding Operation and Practices.
** Diffusion Couple Age/Identification Chart presented in Part II, Appendix F.
*** Accelerated diffusion test.
\+ See Part II, Appendix K, Section 1. Minimizing Interdiffusion During Vacuum Outgassing Anneals.

30% successful. A second cycle at 2100°C, 20.7 MN/M^2 for 20 minutes yielded 100 per cent welding of all junctions. Microprobe traces across these sample weld interfaces indicated weld zones of less than 6 microns. Part II, Appendix E, Hot Press Operation, describes the practice and facilities to join the couple combinations designated in Table 9.

In order to achieve the necessary stress to effect hot press welding, the 6.45 x 3.18 cm (2.500 x 1.250 inch) HIP weld sheets were cut to 1.27 x 3.18 (0.500 inches wide x 1.250 inches long) and stacked as follows:

Mo/Alloy/W/Mo/Alloy/W/Mo/ - - - -
↑ Interface ↑ Interface

Thus, after hot press welding, the welded stack of materials was immersed in nitric acid, and the preferential etch removal of the molybdenum released the alloy/tungsten diffusion couples.

These individual diffusion couple pieces were also surface polished, chemically cleaned, and vacuum outgassed* under the same conditions as previously described for the HIP welded couples.

*See Part II, Appendix K, Section 1, Minimizing Interdiffusion During Vacuum Outgassing Anneals

V. DIFFUSION AGING CYCLES

The age temperature/time conditions selected for each of the diffusion couple combinations are presented in Tables 3 and 4. Three age times (100, 1000, and 2000 hours) and four age temperatures (2000, 1800, 1500, 1200°C) were selected as described previously. Part II, Appendix F, Diffusion Couple Age/Identification Chart, illustrates the number of diffusion couples in the program (323), and the number of couples per age cycle. Table 10 summarizes the age time/temperature matrix by illustrating the number of couples to be aged for each condition. As can be seen, nine age cycles were required. Since three furnaces were available for the program, Table 11 was necessary to affect the optimum schedule for furnace utilization and calendar time.

Three ultra-high vacuum, sputter ion pumped, cold wall vacuum furnaces were used for the diffusion ages. One furnace was tantalum resistance heated (1200°C cycles) and two were tungsten mesh resistance heated (1500, 1800, and 2000°C cycles). The furnaces were manufactured by Varian Associates of Palo Alto, California. Hot zones are 10.2 cm (4-inches) diameter by 15.2 cm (6-inches) long and were shielded by tungsten foil reflectors. The furnaces were pumped by 500 l/sec diode sputter ion pumps and operated, typically, at 1×10^{-6} N/m^2 (1×10^{-8} torr) or lower for all of the age cycles employed. A water-cooled copper cold wall surrounds the radiation shields and split cylinder resistance heater to maintain the sputter ion pump and vacuum chamber at as low a temperature as possible. All seals were made with crushable copper gaskets. Titanium sublimation pumps are located in the chamber bottom and were only used during temperature ramps to operating conditions. Tantalum foil shields were employed to protect the furnace from line of sight exposure to sublimed titanium. These furnaces are completely described in prior reports.[2]

The furnaces could be temperature controlled either through standard proportional controllers, or a saturable core reactor thermowatt converter system. Bare wire thermocouples were used

Table 10. Interdiffusion Furnace Age Treatments

T°C	Age Time		
	2000 hrs	1000 hrs	100 hrs
2000	-	C (30)*	G (23)
1800	-	D (52)	H (47)
1500	A (39)	E (47)	I (12)
1200	B (24)	F (24)	-

* (parenthesis denote number of diffusion couples per age treatment)

Table 11. Furnace Age - Time Chart for Interdiffusion Study

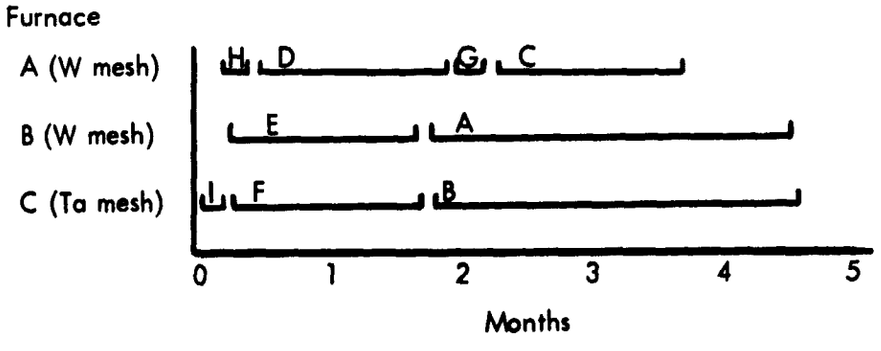

in the hot zone with ceramic insulation (ThO_2) for shield feedthroughs. W/W-26Re thermocouples were used at 2000 and 1800°C while Pt/PtRh thermocouples were used at 1500 and 1200°C. Continuous trace millivolt recorders were used to monitor temperature conditions throughout the age periods. Temperature variations did not exceed $\pm$ 20°C for all of the ages.

Prior to actual ageing cycles, the furnaces were charged with simulated couple loads and power requirements for each age temperature were determined. With this calibration the ramp times from 800°C to 1200, 1500, 1800, and 2000°C were determined. These ramp tests were made to ascertain the time corrections for time at temperature*. For instance, ramp times from 800°C to 1500°C were less than 2 minutes, while quench times back to 800°C were less than 5 minutes. These short times were due to the low thermal mass in the furnace hot zone. Since the ratio of interdiffusion coefficients for tungsten/rhenium interdiffusion[3] is

$$\frac{\tilde{D}\ (800^{\circ}C)}{\tilde{D}\ (1200^{\circ}C)} = 0.0045 \qquad (2)$$

and the two ramp times are short (2 minutes up ramp Δt_u, 5 minutes quench Δt_q), the average age time correction would be

$$t_{age}\ (\text{corrected}) = t_{age}\ (\text{experimental}) + \frac{\Delta t_u + \Delta t_q}{2} \qquad (3)$$

For the minimum age of 100 hours, the correction would be

$$\frac{\Delta t_u + \Delta t_q}{2} = 0.058 \text{ hours} \qquad (4)$$

or 0.058%. The ramp time corrections to the 1800 and 2000°C age temperatures are also lower. Thus, ramp time corrections to the age temperature were not necessary in this study.

The diffusion couples to be aged for each time-temperature cycle were placed on a special EDM fabricated tungsten support stand. Figure 9 illustrates the couples for age 1** placed

* See Part II, Appendix K, Section 2, Corrections to Age Time due to Furnace Time-Temperature Ramps.

** See Table 10 and Part II, Appendix F, Diffusion Couple Age/Identification Chart.

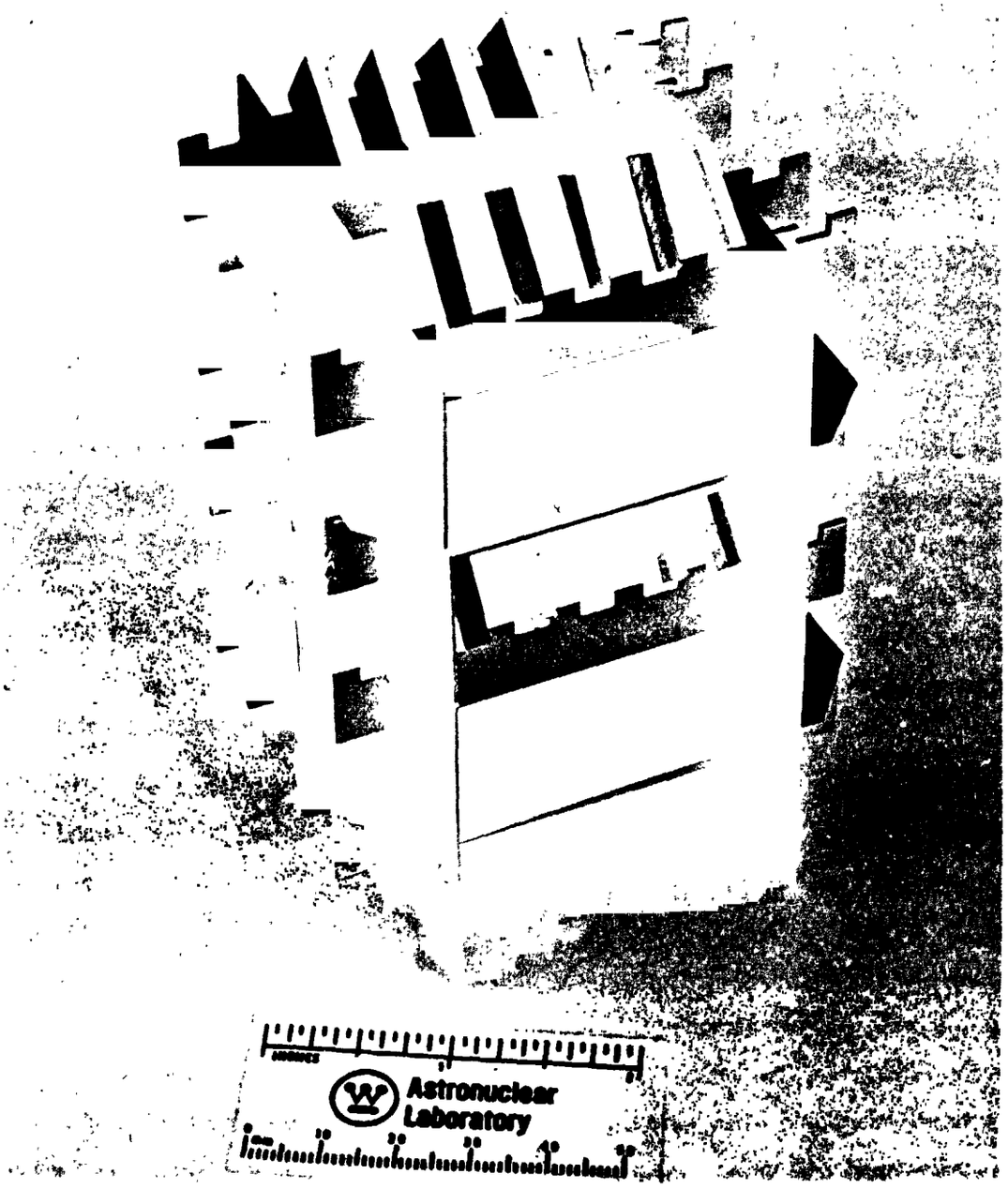

Figure 9. Demonstrating the Placement of Support Stands and Couples for Diffusion Age I (1500°C, 100 Hours)

upon the support structure. Each couple contacts the stand at only two support points, thus permitting thermal expansion without stresses. A complete identification map of each couple's furnace location in each age cycle was retained. Tungsten foil interlayers between the stands prevented couples from falling out of the hot zone if they slipped from the stand. These foils also acted with top and bottom foils to prevent axial temperature drops in the hot zone. Figure 10 illustrates diffusion couple placement inside the heater sheath in the age furnace.

Once the furnace was loaded, thermocouples placed, and vacuum chamber sealed (27.3 cm (10-3/4 inch) "Wheeler" flange seated on a crushable round copper gasket), the chamber was baked out for 12 hours at 200°C after being evacuated with a turbomolecular pump. Initial power heating to 900°C and a five to ten hour hold were affected to outgas the system. Subsequent power ramps to temperature were rapid (previously described), and pressures did not exceed 1.2×10^{-3} N/m^2 (1×10^{-5} torr) during this startup cycle. The pressure always dropped below 1.2×10^{-6} N/m^2 (1×10^{-8}) within a few hours (with titanium sublimation pumping), and no pressure problems were encountered for any of the age cycles.

Power versus elapsed time and temperature versus elapsed time continuous plots were made during the age cycles to observe trends in control. Temperature deviations did not exceed $\pm$ 20°C for any of the age cycles*. One cycle, age E, 1500°C for 1000 hours, did encounter a temperature problem. Although the thermocouple reading indicated 1500°C, the optical pyrometer reading was 1630°C. This discrepancy was not resolved until after the cycle had been terminated. The 20.3 cm (8-inch) long 8 pin (1/8 inch diameter each) thermocouple feedthrough into the furnace was removed. It was found that some teflon bore insulators were not present, thus the thermocouple wires were shorting at each end of the metallic feedthrough, and since the internal end was hot, a stray emf was affecting the temperature reading. This problem was corrected for subsequent cycles in this furnace.** Optical pyrometer readings on the

* See Part II, Appendix K, Section 5, Error Contribution to Interdiffusion Analysis due to Variance in Age Temperature.

** Employment of the 1630°C optical pyrometer temperature reading was later validated by the interdiffusion analysis.

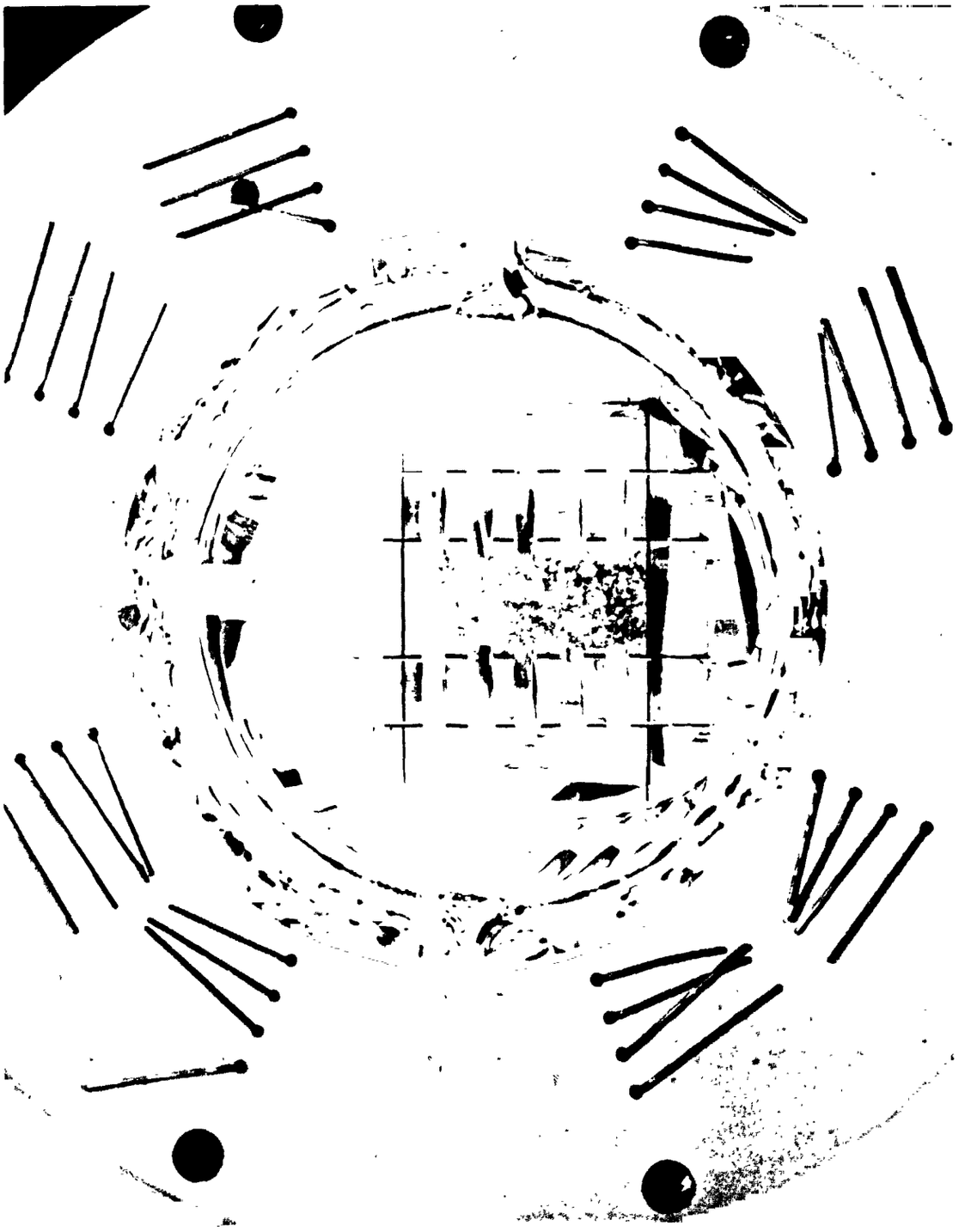

Figure 10. View Downward into the Tantalum Heater Sheath Hot Zone Illustrating Diffusion Couple Placement in the Age Furnace

other age cycles correlated well with thermocouple readings and were recorded as a backup to thermocouple failure. The sight glass employed was shielded from incident metal vapor from within the furnace except for the few seconds required to take temperature readings.

Age cycle shutdown procedures involved shutting the power off at the end of the cycle time period and permitting the furnace to cool under vacuum. The diffusion couples were removed from the furnace, inspected visually for irregularities, and sealed in individual envelopes until delivered for metallographic preparation.

VI. INTERDIFFUSION ANALYSIS

In order to completely describe the interdiffusion characteristics of the selected tungsten or rhenium diffusion couple combinations, several modes of analysis were required. Engineering analysis and interdiffusion zone width predictive models required electron microprobe trace data across the interdiffusion interface, photomicrographs to illustrate the effects of interdiffusion, and some microhardness information through the interdiffusion zone. Diffusion analysis by Boltzmann-Mantano techniques required electron microprobe spot count profiles across the interdiffusion interface, and correction programs for absorption, fluorescense, etc. Prior to performing these tasks, however, was the task of metallographic preparation.

All diffusion couples studied in this investigation were prepared for both metallographic examination and electron microprobe analysis. Each sample, as submitted, was first ground on a bimetal edge perpendicular to the wrapped tungsten wire being used for both orientation and calibration purposes. After this initial grinding, the sample was carefully mounted in a 2.5 cm (one inch) diameter mold using Hysol R8-2038 Resin (H4-3410 Hardener) saturated with a filler medium consisting of 150 mesh powdered porcelain. The prepared mount was inserted into a low vacuum oven for 10 minutes and then cured and hardened by raising the oven temperature to 60°C (140°F) for a minimum 2-hour period. The cooled mounted sample was then transversely cut in half, and all further metallographic operations were performed on this cut surface. This technique of preparing the samples for metallographic analysis prevented the brittle diffusion zones from cracking during sectioning; and at the same time, the added porcelain filler aids in keeping the exposed sample surfaces flat during the subsequent grinding-polishing operations*.

Samples for metallographic examination were ground successively on 120, 240, 400, and 600 grit silicon carbide papers with water as the coolant. Using automatic grinding apparatus, the

* See Part II, Appendix K, Section 3, Potential Error in Interdiffusion Zone Width Measurement due to Improper Metallographic Mounting

grinding cycle was one minute at 14 Kg (30 pounds) pressure on each grinding paper used. In some cases more than one grinding paper of a particular size was necessary. Normally, six mounted samples could be run at the same time using the Buehler Automet polishing attachment.

The next step consisted of a rough polish on Buehler AB silk cloth using a slurry of 0.3 micron Al_2O_3 (Linde "A") as the abrasive and an automatic cycle of two minutes and 14 Kg (30 pounds) pressure.

The final polish was made on Buehler AB Microcloth using one of the two following acid-polish mediums. For Group 1 couples consisting of W/W25Re, W/W-Re-Mo, W/Mo50Re, Re/W25Re, Re/W-Re-Mo, Re/Mo50Re, and W/Re refractory alloy combinations, the acid-polish used was 10 grams Cr_2O_3 and 10 grams Jeweler's Rouge in 100 ml of water. For Group 2 couples consisting of W/Cb, W/Cb1Zr, W/Ta10W, W/T111, W/ASTAR811C, Re/Cb, Re/Cb1Zr, Re/Ta10W, Re/T-111, and Re/ASTAR811C refractory alloy combinations, the acid-polish used was 100 ml of an acid solution consisting of 250 ml water, 50 grams Cr_2O_3, 35 ml orthophosphoric acid and 3 ml H_2SO_3 mixed with 200 ml water containing approximately 75 grams .05 micron Al_2O_3 (Linde "B").

To reveal the microstructure of the diffusion zone, Group 1 couples (W) were swab-etched with a solution consisting of 40 ml conc. HCl, 20 ml conc. HNO_3, and 30 ml 48% hydrofluoric acid while Group 2 couples (Re) were swab-etched with a solution consisting of 10 grams potassium ferricyanide, 10 grams of potassium hydroxide in 100 ml water.

For electron microprobe analysis, the metallographic samples were prepared only through the final polish stage. No etching was performed on microprobe samples in order to prevent preferential constituent dissolution and perturbed results.

Post-age interdiffusion concentration profiles were resolved by electron microprobe analysis. Two types of analysis were performed. The interdiffusion zone of every diffusion couple in the

program was traced with a continuous scan at 90 or 45 degrees (depending upon zone width) to the interface plane. For binary couples, one element was traced. For ternary or higher couples, two or more elements were traced. Selected diffusion couples were also spot count traversed at 2, 4, or 8 micron intervals at 90 or 45 degrees to the interface plane. The equipment, techniques. and correction factors (Colby Computer Program) employed are described below.

To determine the composition profiles for the refractory metal alloy diffusion interfaces, the Applied Research Laboratories Model AMX electron probe microanalyzer was used. Quantitative analysis was performed by calculating the weight fraction of an element in the sample under study by determining the ratios of characteristic x-ray intensities generated by the electron beam in the sample to that generated from a pure standard of the same element.

In this investigation the operating parameters of the microprobe were set at 25.0 KV accelerating potential and 0.1 μA beam current. The electron beam was adjusted to a 1 micron spot size using an aluminum oxide standard for focusing and aligning the beam. The generated x-rays were diffracted by a dispersive scanner having a LiF analyzing crystal and proportional counter detector. The intensity data was recorded either on a X-Y recorder or a scaler-typewriter output translator. Quantitative composition results were computed from the digital data by a modified MAGIC computer program as described in Part II, Appendix J.

Normally the samples were scanned at 45 degrees to the diffusion zone; the angle of traverse being positioned with the aid of a protractor eyepiece used with the light optical microscope system. For a few cases where the diffusion zone was very wide, a 90 degree traverse was used for the analysis.

For the X-Y recorder continuous scans of the diffusion zone, the traverse speed was set to 16 microns per minute. In those cases of wide diffusion zone bands, the traverse speed was

increased to 196 microns per minute. The acquisition of the ratemeter analog data was normally begun 100 microns before the diffusion edge and continued until no intensity change could be observed after passing through the diffusion zone.

The point count digital data was obtained by means of a stepping motor. As with the X-Y scanning method, the point count data was started 20 to 30 microns before the edge of the diffusion zone, and digital data was continuously obtained at 2 micron intervals until no further change in intensity could be observed. Background counts were taken before and after the element intensity peak in both matrix materials of the couple, averaged for each of the matrices and if necessary, prorated for each of the point counts through the diffusion zone.

The counting time was set to either 10 seconds or 1 second, the latter time used for the intermediate and wide diffusion zone couples. As stated previously, the scaler output was recorded on a special IBM typewriter through a data translator. It was this data that was prepared for input to the Raytheon 520 computer for calculating the compositions of the selected element in the refractory metal alloy couples.

Direct calibration of the electron probe microanalyzer as well as testing the correction calculations utilized in the modified Colby Computer Program were made by analyzing the NBS Standard Reference Material No. 482, Gold-Copper Wires for Microprobe Analysis. The nominal composition of these wires is shown in Table 12.

Although all samples of the series were run, the standardization of the microprobe was normally based only on Wire C, $Au_{60}Cu_{40}$ with the principle analysis being performed on the copper composition. The periodic calibration results are shown in Table 13.

Table 12. Gold-Copper Wires for Microprobe Analysis SRM 482

Wire	Name	Chemical Composition (weight percent)	
		Gold	Copper
A	Au100	100.00	--
B	Au80 Cu20	80.15	19.83
C	Au60 Cu40	60.36	39.64
D	Au40 Cu60	40.10	59.92
E	Au20 Cu80	20.12	79.85
F	Cu100	--	100.00

Table 13. Copper Results, Wire C, Au60 Cu40 SRM 482

Date Analyzed	Copper w/o
1 November, 1971	41.00
24 November, 1971	41.02
17 December, 1971	41.79
21 December, 1971	39.14

As shown in Table 13, the laboratory coupld duplicate the standards composition well within 5 percent of the NBS reported value.

A more meaningful analysis of the precision and accuracy obtained for typical couples analyzed in this study is shown in Tables 14, 15, and 16 on the analysis of 50Re50Mo matrices (containing 33.57 atomic percent rhenium) of three Re/50Re 50Mo couples identified as 41A1, 31A5, and 31A6. These three couples were aged at 1500, 1800, and 2000°C, respectively.

Primary emphasis in analytical treatment was devoted to engineering level analysis with the development of correlation equations. These equations permitted the net interdiffusion zone width of each diffusion couple material combination to be characterized as a function of age time, age temperature, and extrapolated time (to 10,000 hours) if so desired. Part II, Appendix G, Diffusion Analysis Methods, presents analytical techniques and methods necessary to the accurate resolution and characterization of interdiffusion information. The development and interrelationships between interdiffusion equations are also described in Appendix G.

On an engineering level, the interdiffusion characteristics of the tungsten or rhenium to alloy couple systems were described at each age temperature by relating the interdiffusion zone width, ΔX, to age time, t, as

$$\Delta X \alpha \sqrt{t} \qquad (5)$$

Table 14. Rhenium Analysis by WANL Electron Microprobe
Sample 41A1
1500°C/100 hours
50Re-Mo Matrix
(33.57 a/o Re)

Point Count	Rhenium (a/o)
1	33.54
2	33.54
3	33.54
4	33.51
5	33.95
6	33.51
7	33.80
8	33.89
9	33.93
$\bar{X}$ =	33.69
σ =	±0.20
3σ =	±0.60

Table 15. Rhenium Analysis by WANL Electron Microprobe
Sample 31A5
1800°C/1000 hours
50Re-Mo Matrix
(33.57 a/o Re)

Point Count	Rhenium (a/o)
1	32.63
2	32.87
3	32.41
4	32.14
5	32.61
6	31.58
7	32.87
8	32.83
9	32.06
$\bar{X}$ =	32.44
σ =	± .44
3σ =	±1.32

Table 16. Rhenium Analysis by WANL Electron Microprobe

Sample 31A6
2000°C/100 hours
50Re-Mo Matrix
(33.57 a/o Re)

Point Count	Rhenium (a/o)
1	33.33
2	34.30
3	33.18
4	34.40
5	34.79
6	33.78

$X = 33.96$

$\sigma = \pm .64$

$3\sigma = \pm 1.92$

where the interdiffusion zone width was determined from a microprobe trace concentration scan across the diffusion interface. A typical microprobe trace scan for this program determined the net interdiffusion zone width as that distance extending from 100/98 atomic percent tungsten. Resolution below $\pm$ 2 atomic percent was beyond the accuracy of the trace scan*. The net interdiffusion zone width dimensions were determined as the points at the extremeties of the concentration profile where the slope went to zero. These positions of zero slope were determined graphically. The dimension between the concentration profile extremeties of aged couples (i. e., net interdiffusion zone width) was corrected for as-welded conditions by subtracting the as-welded zone width. The error contribution of large as-welded zone widths is discussed in Part II, Appendix K (Section 7) and was found not to exceed 14 percent.

The accuracy of the measured and corrected interdiffusion zone widths was evaluated with the assistance of equation (6):

$$\ln \left(\frac{\Delta X^2}{t}\right) = \frac{B}{T} + A$$

where ΔX is net interdiffusion zone width (cm), t is age time (sec), T is age temperature (^{o}K), and A and B are constants. Equation (6) was developed from basic diffusion theory as presented in Part II, Appendix G. Thus, from equation (6) a plot of $\ln \left(\frac{\Delta X^2}{t}\right)$ versus 1/T will yield a straight line. Interdiffusion zone widths at one age temperature and several age times will all define one point. The resulting graph of equation (6) serves as an excellent check on the accuracy of the measured interdiffusion zone widths at any age temperature for all age times. Equation (6) also becomes an excellent predictive model for verifying the accuracy of equation (5) and permitting extrapolation to extended age times (beyond those employed experimentally). However, each interdiffusion couple system (W/Cb, Re/Ta, etc.) will require a separate set of constants (A, B) in order to use Equation (6) as a predictive model.

* Part II, Appendix K, Error Analysis, Section 1.

A predictive model, which describes the net interdiffusion zone widths for varying age times and temperatures, for tungsten or rhenium interdiffusion with elements of Group V and VI of the periodic table was derived. This model, described in Part II, Appendix C, relates the net interdiffusion zone width upon aging to the relative entropy level of the diffusion couple system. The predictive model developed in Appendix C presented the interdiffusion zone width, ΔX (cm), as

$$\ln \left(\frac{\Delta X^2}{t}\right) = 21.0 \left(\frac{T}{T_m}\right) - 37.5 \qquad (7)$$

where t is age time (sec.), T is age temperature (^{o}K), and T_m is the lowest melting point in the combined diffusion couple system (i.e., eutectic for binary system). This is the model that was employed to predict the level of interdiffusion expected for the couple materials selected for this study. Experimental age times and temperatures were selected with the assistance of this model in order to project adequate interdiffusion for microprobe analysis. The accuracy of the predictive model with respect to the experimental results will be discussed in a later section.

The microprobe spot count analyses were employed for diffusion analysis of the individual couple systems. Diffusion analysis, as described in Part II, Appendix G, showed that for components of dissimilar melting points, Gaussian (error function) concentration/penetration profiles would not occur, and non-Gaussian analysis would be required. Such concentration profiles required employment of the Boltzmann-Matano analysis to describe the interdiffusion coefficient as a function of tungsten or rhenium concentration and as a function of age temperature. The Boltzmann-Matano equation

$$\tilde{D}(c) = -\frac{1}{2t} \frac{1}{\left(\frac{2c}{2x}\right)_c} \int_c^{C_{max}} x\,dc \qquad (8)$$

was solved with the aid of the Hartley computer program* for interdiffusion zones with intermediate phases, and by the Lifshin** computer program for solid solution, non-Gaussian concentration profiles.

The results of these diffusion analyses were presented as ln $\tilde{D}$ versus concentration plots for each age temperature for each material system studied. The results of analysis at several age temperatures were summarized as

$$\ln \tilde{D} \text{ vs } 1/T \tag{9}$$

relations. Only the following systems were analyzed:

Cb/W
Cb/Re
Ta/W
Ta/Re
Re/Mo-50Re
Re/W

This is because other systems formed partial couples (i.e., W/Ta-10W, W/W-25Re) and would have yielded the same information as total couples, or formed ternary systems such that the ternary constituent could no longer be ignored (i.e., Re/T-111, Re/Ta-10W, W/Mo-50Re, Re/W-30.9Re-20.1Mo, etc.) Ternary analysis was not attempted in such systems as W/Mo-50Re and W/W-30.9Re-20.1Mo since more experimental information would have been required.

* Part II, Appendix H, Hartley Computer Program for Boltzmann-Matano Diffusion Analysis.
** Part II, Appendix I, Lifshin-Hammemann Computer Program for Boltzmann-Matano Diffusion Analysis.

VII. RESULTS AND OBSERVATIONS

The results of the interdiffusion analyses are presented as a function of alloy family. The sequence followed is presented as tungsten or rhenium interdiffusion with (1) columbium systems; (2) tantalum systems; (3) molybdenum-rhenium systems; (4) molybdenum-rhenium-tungsten systems; and (5) tungsten-rhenium systems.

Tables 17 through 20 summarize the corrected, experimental interdiffusion zone widths (98 to 2 atomic percent tungsten or rhenium) found from analyzing the microprobe trace scans. This experimental information was treated and is presented in this section to quantitatively characterize the interdiffusion behavior of the material couple combinations of this study.

A. COLUMBIUM SYSTEMS

1. Columbium-Tungsten Systems

The columbium-tungsten system diffusion couples form solid solution, interdiffusion zones. All junctions were formed by autoclave HIP welds resulting in minimal zero condition interdiffusion zones. Figure 11 illustrates that an extrapolation of measured interdiffusion zone widths (ΔX meas) to time zero results in an intercept at approximately 0.80×10^{-3} cm. This agreed well with the microprobe trace measured as welded zone widths of 0.48 and 0.72×10^{-3} cm. Analysis of columbium and columbium-1 zirconium to arc cast tungsten and CVD tungsten interdiffusion zone widths is summarized in Table 21.

Figure 12 shows that although some scatter exists at 1200°C, there is essentially no detectable difference between the systems. A grain boundary diffusion effect for preferentially oriented CVD tungsten grains was not discerned, and the scatter at 1200°C can be assigned to experimental errors and the small ΔX values found. Least squares computer analysis established the columbium-tungsten interdiffusion model as

Table 17. Experimental Interdiffusion Zone Widths (cm x 10^3) for Arc Cast Tungsten*

Age Temp. (°C)	Age Time (hrs.)	Couple Alloy									
		Cb	Cb-1Zr	Ta	Ta-10W	T-111	ASTAR 811C	W-ReMo	Mo-50Re	W-25Re	Re
2000	2000	--	--	--	--	--	--	--	--	--	--
	1000	--	--	--	25.67	--	24.47	24.47	96.60	19.21	34.37
	100	--	--	--	7.21	--	5.43	8.69	23.75	6.10	24.48
1800	2000	--	--	--	--	--	--	--	--	--	--
	1000	29.42	30.62	8.61	7.97	4.75	5.77	7.38	40.20	7.92	10.83
	100	9.84	11.04	3.08	1.67	1.79	1.64	3.59	14.69	2.37	2.10
1500	2000	--	--	3.56	2.28	1.77	1.45	4.51	--	3.06	3.09
1630	1000	16.72	16.62	3.94	5.86	3.36	2.37	6.17	15.79	2.43	5.07
1500	100	1.72	1.78	--	--	--	--	--	2.09	--	--
1200	2000	0.66	1.75	0.29	0.57	**	**	--	--	--	--
	1000	0.69	0.73	**	0.40	**	**	--	--	--	--
	100	--	--	--	--	--	--	--	--	--	--
As-Welded		0.48	--	0.48	--	1.58	--	1.43	2.20	--	1.77
Couple Formation ***		HIP	HIP	HIP	HP	HP	HP	HP	HP	HP	HP

* Zone widths given corrected for as-welded condition
** Inadequate interdiffusion for analysis
***HIP = Hot Isostatic Pressure Welding
HP= Hot Pressure Welding

Table 18. Experimental Interdiffusion Zone Width (cm x 10^3) for CVD Tungsten*

Age Temp. (°C)	Age Time (hrs.)	Couple Alloy									
		Cb	Cb-1Zr	Ta	Ta-10W	T-111	ASTAR 811C	W-ReMo	Mo-50Re	W-25Re	Re
2000	2000	--	--	--	--	--	--	--	--	--	--
	1000	--	--	--	24.32	--	22.83	22.52	108.5	19.68	37.70
	100	--	--	--	7.29	--	6.94	10.98	32.0	6.88	19.85
1800	2000	--	--	--	--	--	--	--	--	--	--
	1000	30.68	34.18	7.56	9.07	5.95	6.24	12.17	39.70	11.15	13.90
	100	9.63	9.91	2.98	2.81	2.14	2.50	3.64	10.94	1.60	2.00
1500	2000	--	--	2.97	4.85	1.67	1.42	3.75	--	0.85	2.61
1630	1000	15.37	17.27	6.27	5.41	3.97	3.46	6.47	16.81	2.38	5.15
1500	100	1.54	2.04	--	--	--	--	--	1.41	--	--
1200	2000	0.90	0.61	0.50	0.29	**	**	--	--	--	--
	1000	0.33	0.81	0.28	0.35	**	**	--	--	--	--
	100	--	--	--	--	--	--	--	--	--	--
As-Welded		--	0.72	--	--	--	--	--	--	0.94	--
Couple Formation ***		HIP	HIP	HIP	HIP	HP	HP	HP	HP	HP	HP

* Zone widths given corrected for as-welded condition

** Inadequate interdiffusion for analysis

***HIP = Hot Isostatic Pressure Welding

HP = Hot Pressure Welding

Table 19. Experimental Interdiffusion Zone Widths (cm x 10^3) for Powder Metallurgy Rhenium*

Age Temp. (°C)	Age Time (hrs.)	Couple Alloy								
		Cb	Cb-1Zr	Ta	Ta-10W	T-111	ASTAR 811C	W-ReMo	Mo-50Re	W-25Re
2000	2000	--	--	--	--	--	--	--	--	--
	1000	--	--	--	26.64	--	26.88	35.83	43.24	61.60
	100	--	--	--	7.94	--	8.57	9.34	11.12	17.65
1800	2000	--	--	--	--	--	--	--	--	--
	1000	34.09	32.24	11.57	10.55	10.36	Cracked	15.48	16.59	13.90
	100	12.14	14.44	4.22	3.38	4.09	3.35	8.13	5.88	2.78
1500	2000	--	--	3.16	5.02	3.24	2.71	7.27	8.54	2.86
1630	1000	18.14	16.31	6.00	5.76	5.14	6.40	8.49	10.93	6.07
1500	100	1.52	3.16	--	--	--	--	--	2.09	--
1200	2000	0.36	--	0.46	0.64	**	0.61	--	--	--
	1000	0.34	--	0.38	0.56	**	0.35	--	--	--
	100	--	--	--	--	--	--	--	--	--
As-Welded		0.91	--	0.66	--	0.72	1.34	0.72	0.66	1.96
Couple Formation***		HIP	HIP	HIP	HIP	HIP	HP	HIP	HIP	HP

* Zone widths given corrected for as-welded condition
** Inadequate interdiffusion for analysis
***HIP = Hot Isostatic Pressure Welding
HP = Hot Pressure Welding

Table 20. Experimental Interdiffusion Zone Widths (cm x 10^3) for CVD Rhenium*

Age Temp. (°C)	Age Time (hrs.)	Couple Alloy									
		Cb	Cb-1Zr	Ta	Ta-10W	T-111	ASTAR 811C	W-ReMo	Mo-50Re	W-25Re	W
2000	2000	--	--	--	--	--	--	--	--	--	--
	1000	--	--	--	26.19	--	27.56	27.43	35.53	46.30	28.09
	100	--	--	--	8.24	--	7.56	9.68	11.23	11.60	4.70
1800	2000	--	--	--	--	--	--	--	--	--	--
	1000	31.13	32.13	11.79	8.73	9.71	Cracked	18.97	15.42	N/A	8.83
	100	10.80	12.06	4.16	3.12	4.16	2.85	6.68	6.90	2.54	1.60
1500	2000	--	--	2.99	3.47	3.32	1.92	7.94	8.14	1.34	2 08
1630	1000	16.38	15.33	5.12	5.80	5.27	6.20	10.07	10.89	7.72	3.76
1500	100	1.38	2.67	--	--	--	--	--	1.62	--	--
1200	2000	0.83	1.27	0.65	0.43	**	0.45	--	--	--	--
	1000	0.86	0.43	0.34	0.34	**	0.23	--	--	--	--
	100	--	--	--	--	--	--	--	--	--	--
As-Welded		--	0.57	--	--	0.72	1.34	--	--	--	2.10
Couple Formation ***		HIP	HIP	HIP	HIP	HIP	HP	HIP	HIP	HP	HP

* Zone widths given corrected for as-welded condition
** Inadequate interdiffusion for analysis
***HIP = Hot Isostatic Pressure Welding
HP = Hot Pressure Welding

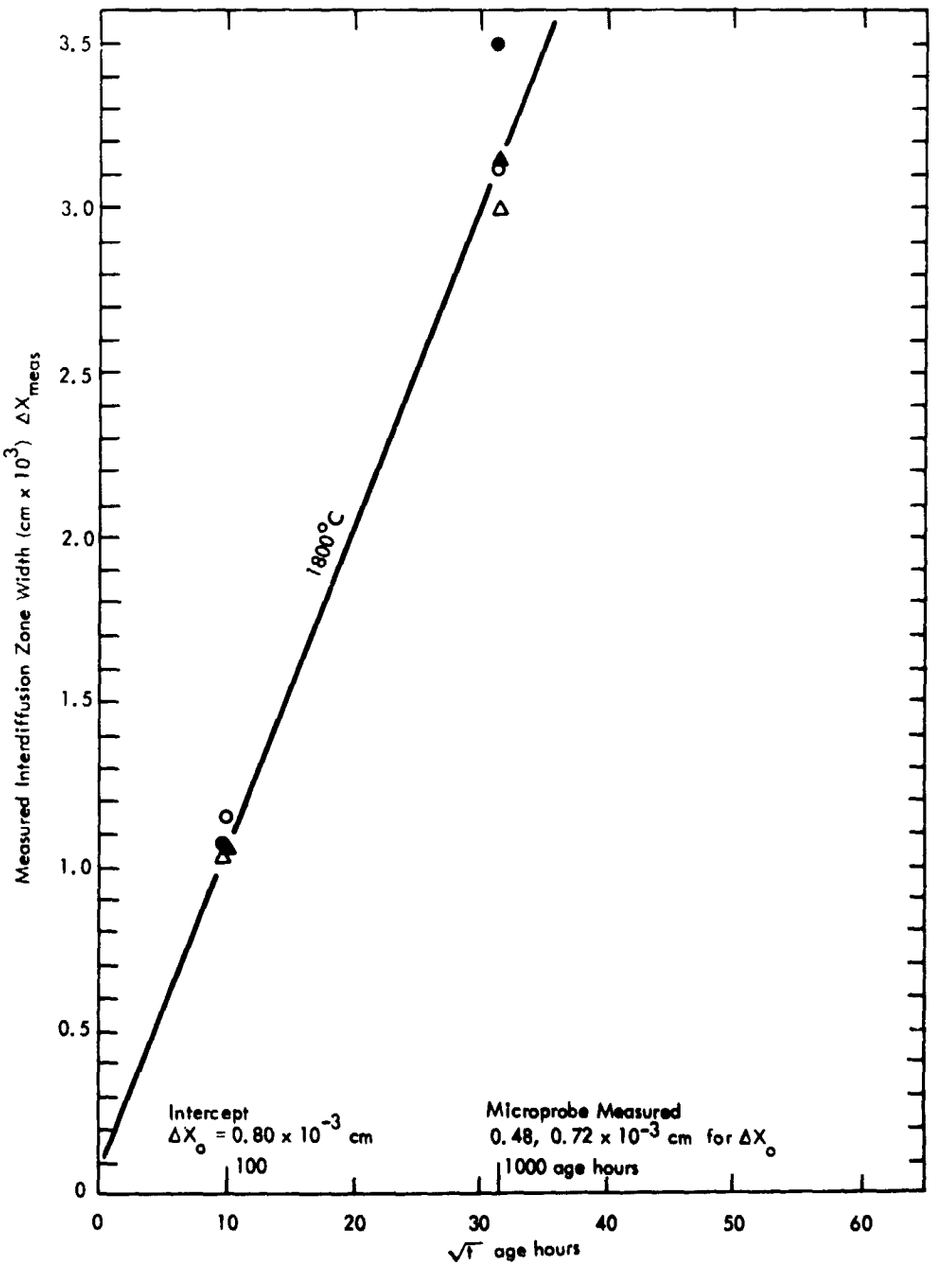

Figure 11. Extrapolation of Measured Interdiffusion Zone Widths to Zero Time to Establish Zero Condition for the W/Cb System

Table 21. Columbium-Tungsten Couple Systems Corrected Interdiffusion Zone Widths

Columbium Couple	Age Temp. (°C)	Age Time t (hrs.)	Age Time t ($sec \times 10^{-6}$)		ΔX Interdiffusion Zone Width ($cm \times 10^{3}$) *	$\Delta X^2/t$ (cm^2/sec)
Cb/W_{arc} **	1800	1000	3.60	Δ	29.42	2.41×10^{-10}
		100	0.36		9.84, 9.54	2.69×10^{-10}, 2.53×10^{-10}
	1630	1000	3.60		16.72, 17.50	7.76×10^{-11}, 8.52×10^{-11}
	1500	100	0.36		1.72	8.22×10^{-12},
	1200	2000	7.20		0.66	6.02×10^{-14}
		1000	3.60		0.69	1.32×10^{-13}
Cb-1Zr/W_{arc}	1800	1000	3.60	O	30.62	2.61×10^{-10}
		100	0.36		11.04	3.38×10^{-10}
	1630	1000	3.60		17.05, 16.62	8.09×10^{-11}, 7.68×10^{-11}
	1500	100	0.36		1.78	8.84×10^{-12},
	1200	2000	7.20		1.75	4.25×10^{-13}
		1000	3.60		0.73	1.49×10^{-13}
Cb/W_{CVD} ***	1800	1000	3.60	▲	30.68	2.61×10^{-10}
		100	0.36		9.63	2.58×10^{-10}
	1630	1000	3.60		15.37	6.56×10^{-11}
	1500	100	0.36		1.54	6.59×10^{-12}
	1200	2000	7.20		0.90	1.12×10^{-13}
		1000	3.60		0.33	3.03×10^{-14}
Cb-1Zr/W_{CVD}	1800	1000	3.60	●	34.18	3.25×10^{-10}
		100	0.36		9.91	2.73×10^{-10}
	1630	1000	3.60		17.27	8.29×10^{-11}
	1500	100	0.36		2.04	1.15×10^{-11}
	1200	2000	7.20		0.61	5.09×10^{-14}
		1000	3.60		0.81	1.80×10^{-13}

* Zone width = cm x 10^3, i.e., 1.72 = 1.72 x 10^{-3} cm
Zone width also corrected by as-welded condition

** W_{arc} = arc cast tungsten

*** W_{CVD} = chemical vapor deposited tungsten, from WF_6, (100) planes

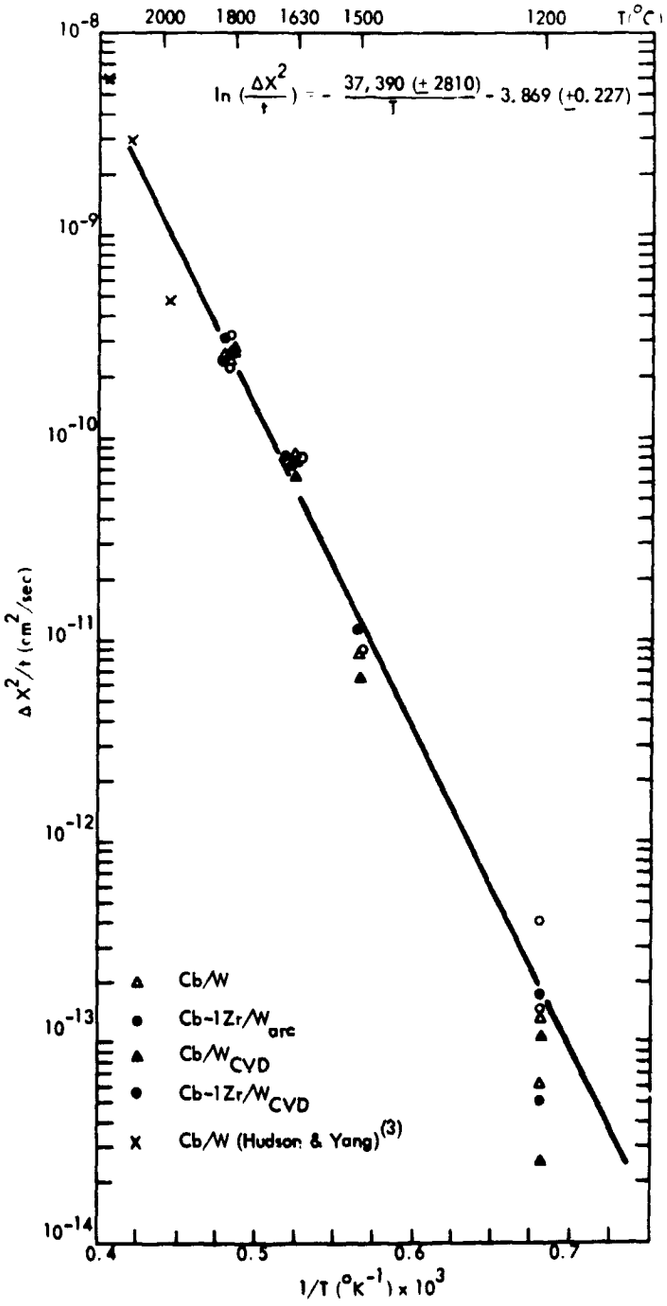

Figure 12. Arrhenius Model for Interdiffusion Zone Width in the Columbium-Tungsten Couple Systems

$$\ln\left(\frac{\Delta X^2}{t}\right) = -\frac{37,390\ (\pm 2810)}{T} - 3.869\ (\pm 0.227) \qquad (10)$$

where ΔX is interdiffusion zone width from 98 to 2 atomic percent tungsten in centimeters, t is age time in seconds, and T is age temperature in ^{o}K. Ninety-five percent confidence limits are presented. Note that columbium-tungsten interdiffusion zone width data from Hudson and Yang[3] correlate well with the data presented here.

Figure 13 presents the interdiffusion zone width information as a function of age time, and extrapolations to long age times are provided with equation (10) from Figure 12. A least squares fit correlation coefficient of 0.934 was found for equation (10). This correlation was surprising in light of the gross Kirkendall porosity which occurred on the columbium side of the interface in this system. Figure 14 presents the as-welded columbium/CVD tungsten interface in contrast to Figures 15 and 16 which present the same interface after 1000 hours of ageing at 1630 and 1800°C, respectively. The void structure, although presenting a reduced cross sectional area to interdiffusion, did not appear to effect the extrapolation capabilities of equation (10). Perhaps the reduced area for constituent flux was counteracted by rapid surface diffusion effects within the voids. Also, by the time the pores became gross, the interdiffusion kinetics were quite reduced.

For Boltzmann-Mantano analysis of the columbium-tungsten systems, the columbium-1 zirconium alloy can be treated as columbium*. Electron microprobe spot count traverses were made on samples**

1AA-5	1800°C	1000 hours
1AA-4	1500°C	100 hours
1AA-2	1200°C	1000 hours

* Refer to Part II, Appendix G, Diffusion Analysis Methods (consideration of ternary components).

** Part II, Appendix F, Diffusion Couple Age/Identification Chart.

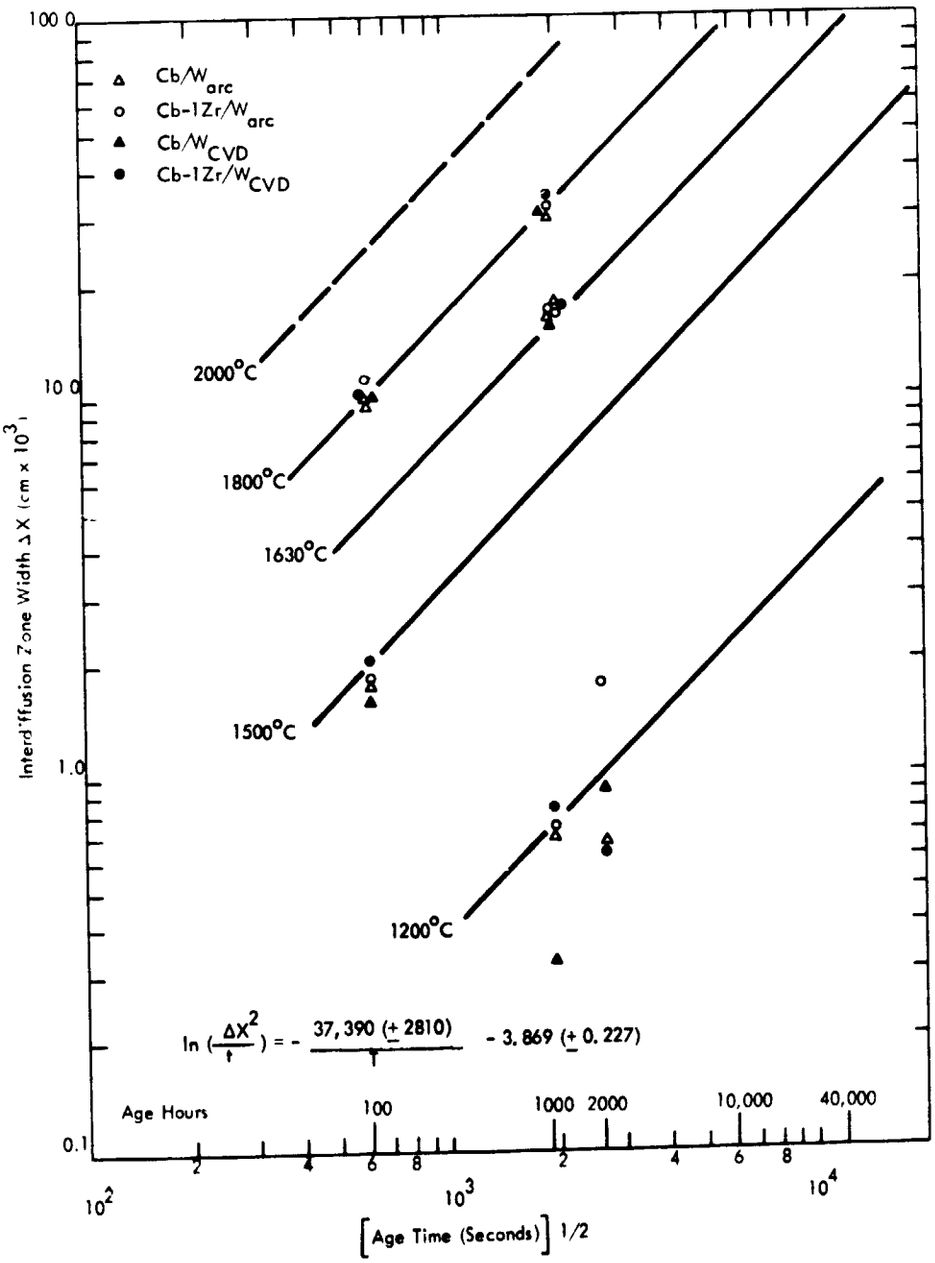

Figure 13. Illustrating Extrapolation of Zone Widths to Long Age Times for Columbium-Tungsten Interdiffusion

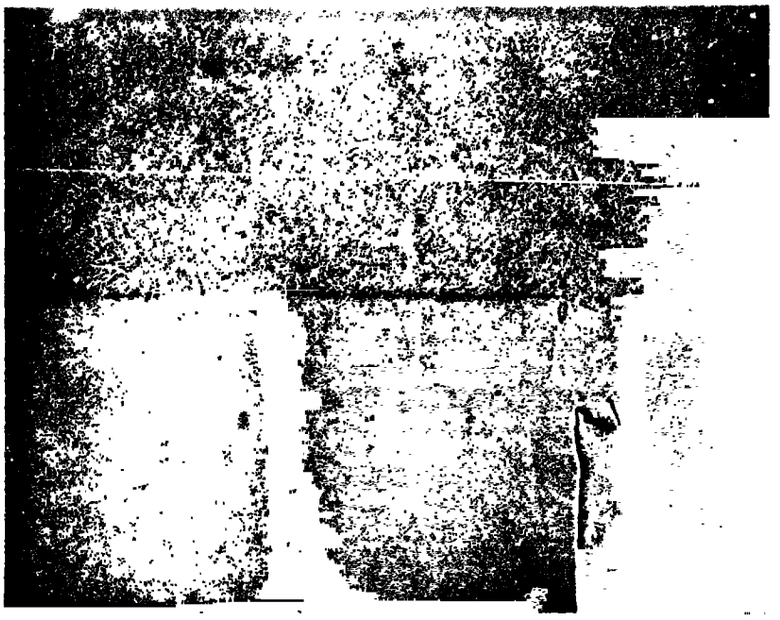

Figure 14. As-Welded Interface of Columbium/CVD Tungsten Couple (2AA-7) at 400X.

Figure 15. Interface of Columbium/Arc Cast Tungsten Interface After 1000 hours at 1630°C (1AA-3) at 200X

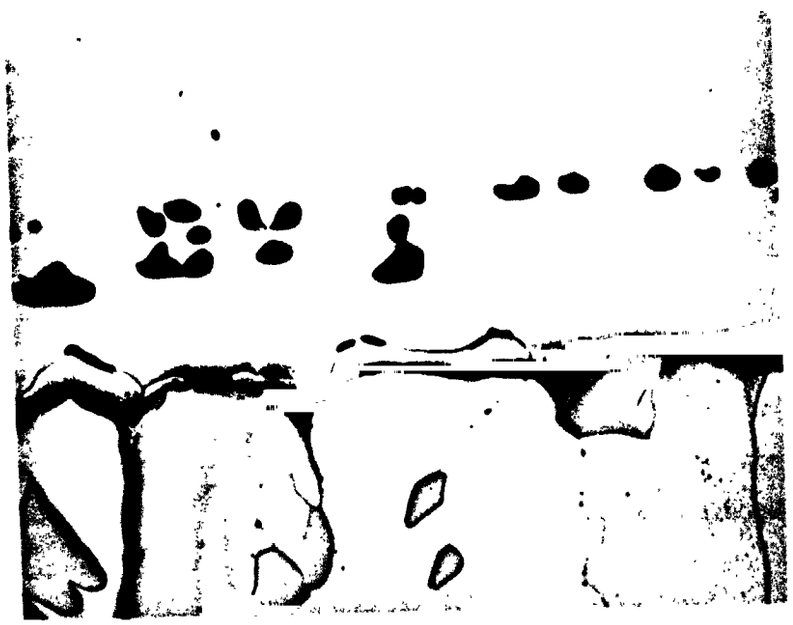

Figure 16. Interface of Columbium/CVD Tungsten Interface After 1000 hours at 1800°C (2AA-6) at 200X

and the Colby MAGIC* corrected concentration profiles were loaded into the Lifshin-Hannemann** Boltzmann-Mantano analysis computer program. Figure 17 illustrates the microprobe corrected interdiffusion concentration profile of sample 1AA-5 as presented by Calcomp plot subroutine. Figures 18, 19 and 20 present the resulting interdiffusion coefficients as a function of concentration of tungsten at 1200, 1500, and 1800°C. Figure 20, interdiffusion at 1800°C, closely approaches the form found by Hehemann and Leber[4], and reported by Vergasova[5].

Figure 21 presents the Arrhenius interdiffusion relation for columbium-tungsten interdiffusion as resolved in this study. Agreement of interdiffusion coefficient and slope (activation energy) with that presented by Hehemann and Leber[4] is excellent and falls properly within the respective self-diffusion coefficients. Although Hehemann and Leber did not quantize the interdiffusion coefficient, it could be expressed (generally) as

$$\tilde{D}\left(\frac{cm^2}{sec}\right) = 9.21 \times 10^{-7} \exp\left[-\frac{52,400}{RT}\right] \qquad (11)$$

for 50 to 95 atomic percent tungsten, where T is in °K and R is the gas constant (1.987 cal/mole-°K).

2. Columbium-Rhenium Systems

The columbium-rhenium systems' diffusion couples form an intermediate phase (X) interdiffusion zone. All junctions were formed by autoclave HIP-welds, resulting in minimal zero condition interdiffusion zones. Microprobe trace measured as-welded zone widths were 0.91 and 0.57×10^{-3} centimeters. Analysis of columbium and columbium-1 zirconium to rhenium (powder metallurgy and CVD product) interdiffusion zone widths is summarized in Table 22.

* Part II, Appendix J, Colby Computer Program for Correcting Microprobe Intensity Analysis.
** Appendix I, Lifshin-Hannemann Computer Program for Boltzmann-Mantano Diffusion Analysis.

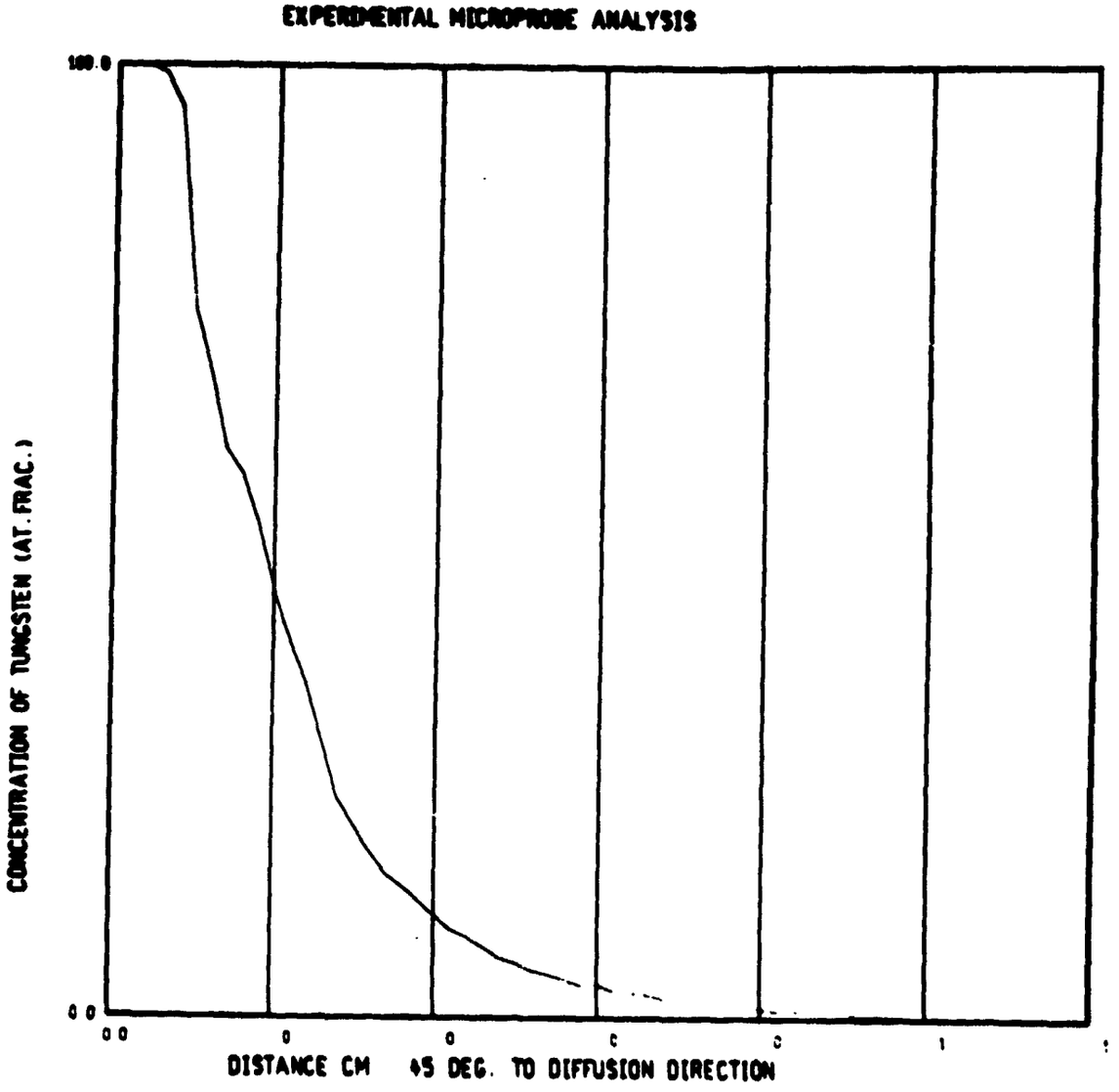

Figure 17. Computer Calcomp Plot of Corrected Microprobe Interdiffusion Concentration Profile for Cb/W Couple 1AA-5, 1500°C for 100 Hours

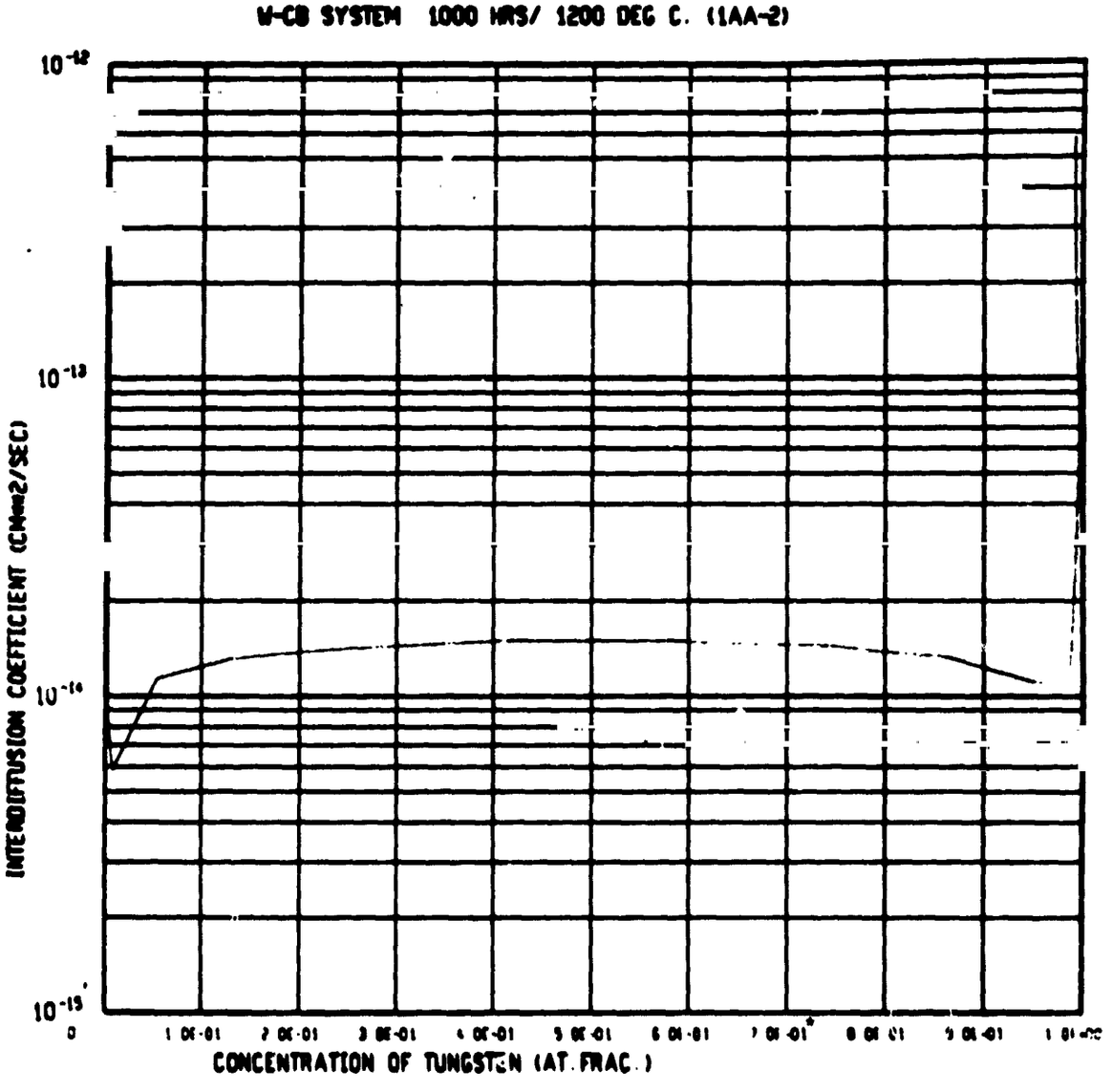

* 7.0 E-01 = 7.0×10^{-1} = 0.7

Figure 18. Columbium-Tungsten Interdiffusion Coefficient at 1200°C

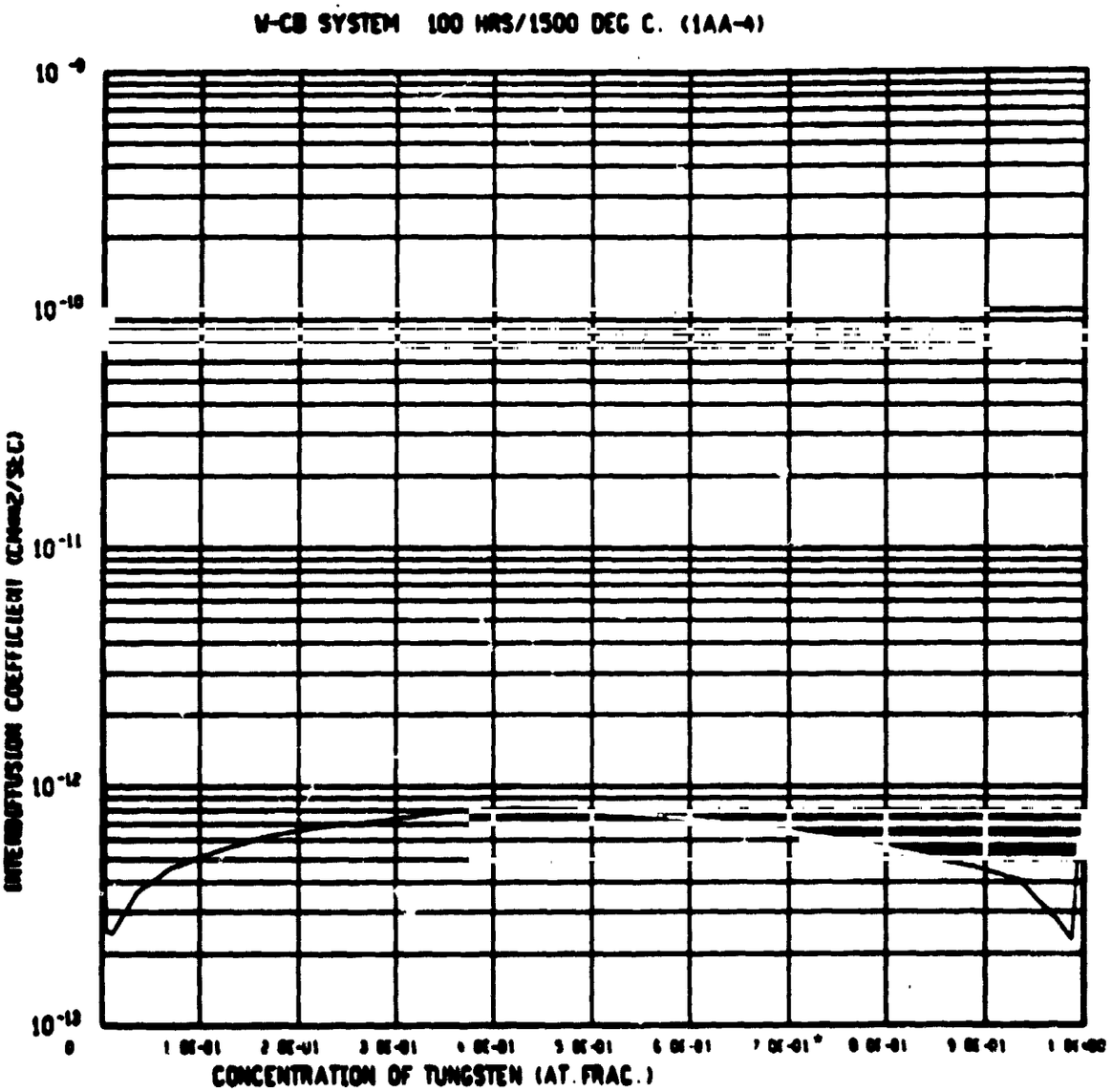

* 7.0 E-01 = 7.0×10^{-1} = 0.7

Figure 19. Columbium-Tungsten Interdiffusion Coefficient at 1500°C

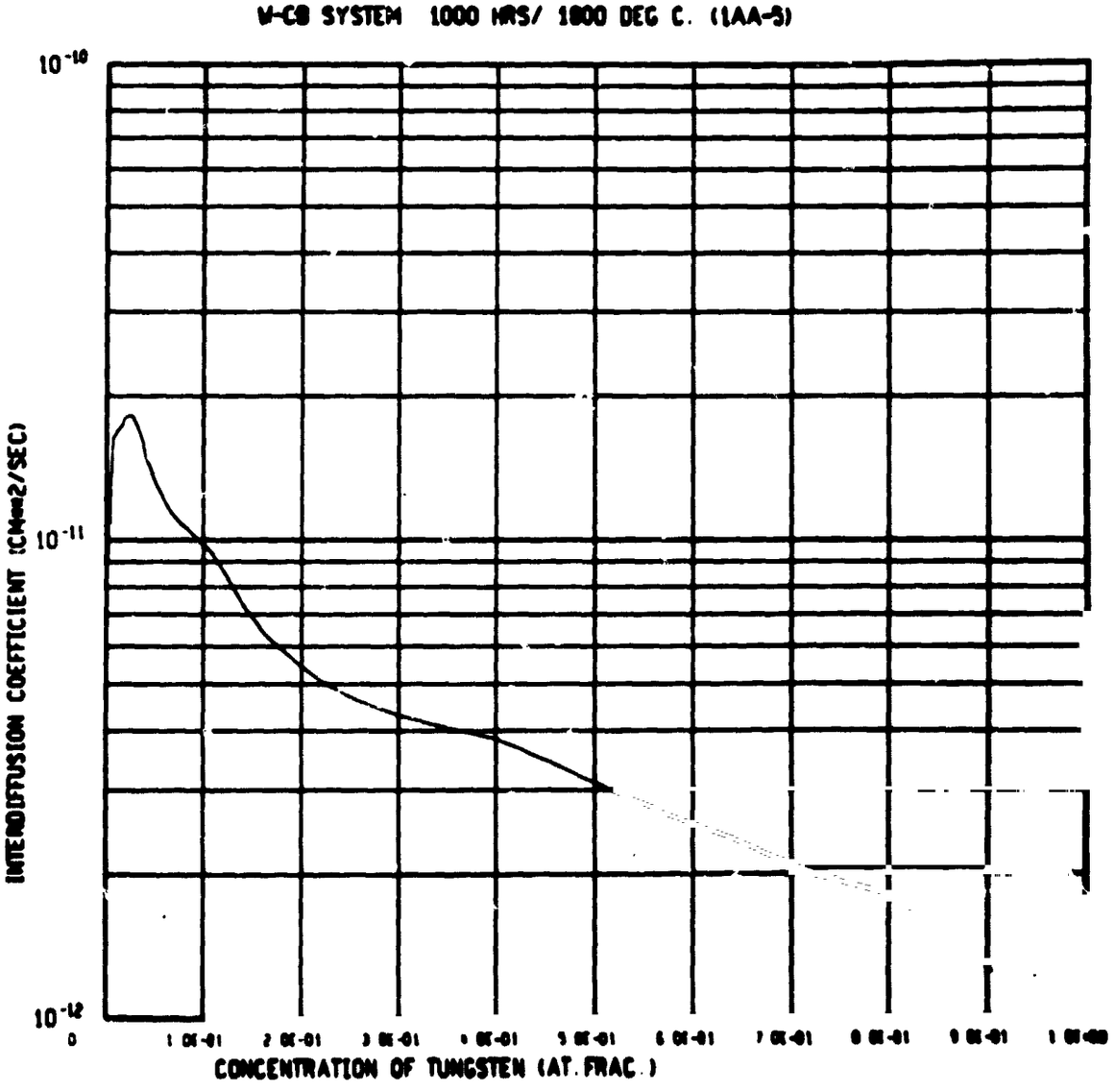

Figure 20. Columbium-Tungsten Interdiffusion Coefficient at 1800°C

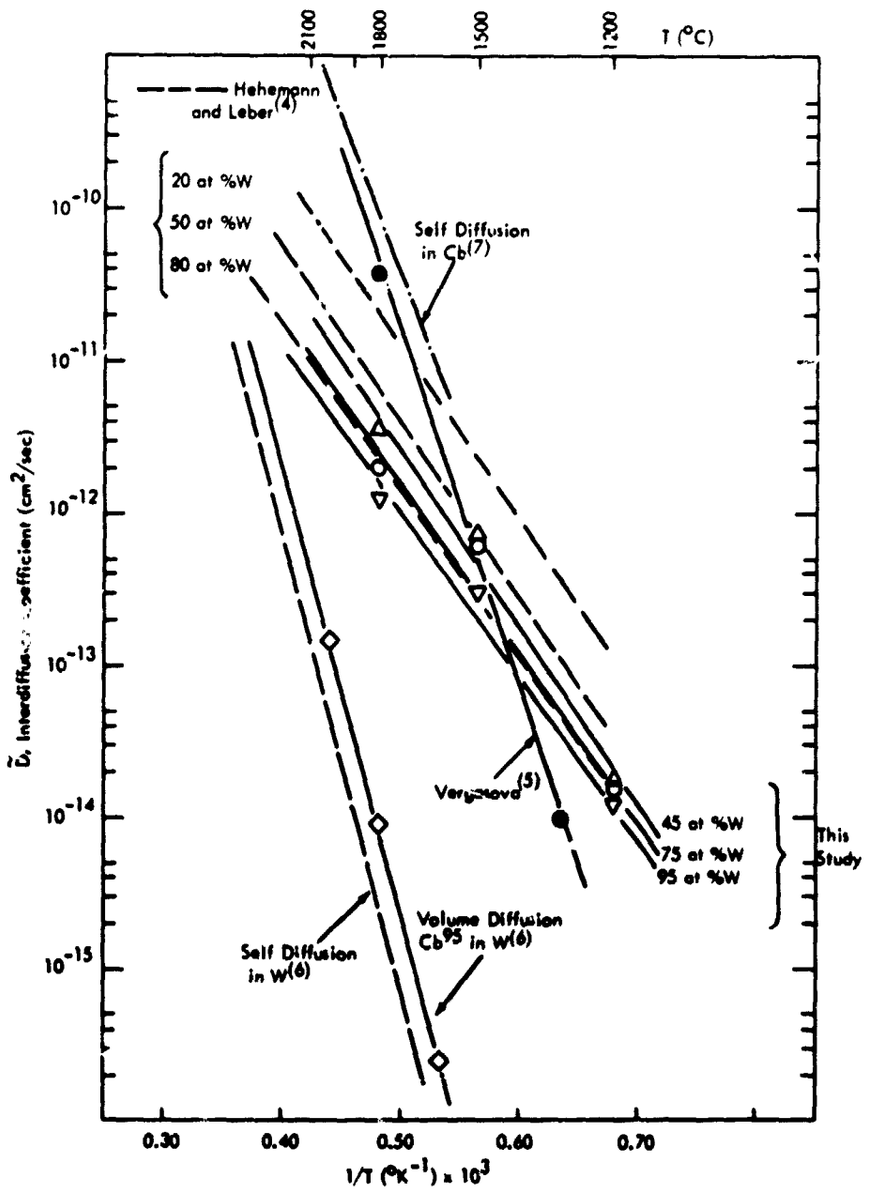

Figure 21. Arrhenius Interdiffusion Coefficient-Temperature Relation for the Columbium-Tungsten System

Table 22. Columbium-Rhenium Couple Systems Corrected Interdiffusion Zone Widths

Columbium Couple	Age Temp. (°C)	Age Time t (hrs.)	Age Time t (sec x 10^{-6})		ΔX Interdiffusion Zone Width (cm x 10^3)*	$\Delta X^2/t$ (cm^2/sec)
Cb/Re_P**	1800	1000	3.60	□	34.09	3.23×10^{-10}
		100	.36		11.37, 12.14	3.59×10^{-10}, 4.10×10^{-10}
	1630	1000	3.60		18.14	9.14×10^{-11}
	1500	100	.36		1.52	6.42×10^{-12}
	1200	2000	7.20		0.36	1.77×10^{-14}
		1000	3.60		0.43, 0.34	5.14×10^{-14}, 3.21×10^{-14}
Cb-1Zr/Re_P	1800	1000	3.60	◇	32.24	2.89×10^{-10}
		100	.36		14.44, 14.38	5.79×10^{-10}, 5.75×10^{-10}
	630	1000	3.60		16.31	7.40×10^{-11}
	500	100	.36		3.16	2.78×10^{-11}
	1200	2000	7.20		--+	--
		1000	3.60		--+	--
Cb/Re_{CVD}***	1800	1000	3.60	■	31.13	2.69×10^{-10}
		100	.36		10.80	3.24×10^{-10}
	1630	1000	3.60		16.38	7.46×10^{-11}
	1500	100	.36		1.38	5.29×10^{-12}
	1200	2000	7.20		0.83	9.51×10^{-14}
		1000	3.60		0.86	2.04×10^{-13}
Cb-1Zr/Re_{CVD}	1800	1000	3.60	◆	32.13	2.87×10^{-10}
		100	.36		12.06	4.04×10^{-10}
	1630	1000	3.60		15.33	6.53×10^{-11}
	1500	100	.36		2.67	1.98×10^{-11}
	1200	2000	7.20		1.27	2.24×10^{-13}
		1000	3.60		0.43	5.14×10^{-14}

* Zone width = cm x 10^3, also corrected by as-welded condition

** Re_P = powder metallurgy rhenium product

*** Re_{CVD} = chemical vapor deposited rhenium

\+ Insufficient interdiffusion for accurate analysis

Figure 22 shows that although some scatter exists at 1200 and 1500°C, there is no detectable difference between the systems. A grain boundary diffusion effect for preferentially oriented CVD rhenium grains was not discerned, nor did the presence of zirconium influence the interdiffusion zone widths. Least squares computer analysis established the columbium-rhenium interdiffusion model as

$$\ln\left(\frac{\Delta X^2}{t}\right) = -\frac{43,880\ (\pm 3060)}{T} - 0.490\ (\pm 0.249 \qquad (12)$$

where ΔX is interdiffusion zone width from 98 to 2 atomic percent rhenium in centimeters, t is age time in seconds, and T is age temperature in °K. Ninety-five percent confidence limits are shown. Literature reviews were unable to reveal other sources of information for this system for comparative purposes.

Figure 23 presents the interdiffusion zone width information as a function of age time, and extrapolations to long age times are provided with equation (12) from Figure 22. A least squares fit correlation coefficient of 0.866 was found for equation (12).

Although Kirkendall voids were not produced in this system for the temperatures and age times employed, photomicrographs revealed a brittle X phase in the interdiffusion zone. The X phase was only found to be cracked after long age periods (1000 hours), and is exhibited in Figures 24 and 25.

For Boltzmann-Matano analysis of the columbium-rhenium systems, the columbium-1 zirconium alloy was treated as columbium*. Electron microprobe spot count traverses were made on samples**:

* Refer to Part II, Appendix G, Diffusion Analysis Methods (consideration of ternary components).
** Part II, Appendix F, Diffusion Couple Age/Identification Chart.

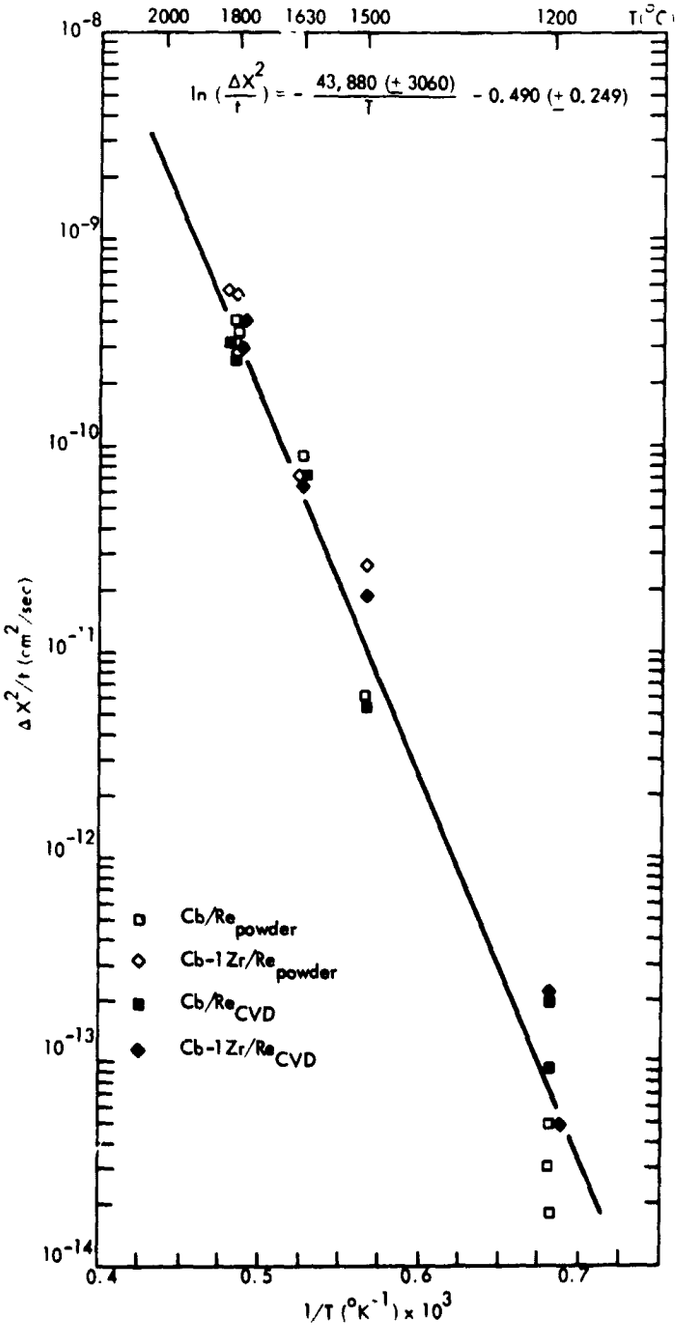

Figure 22. Arrhenius Model for Interdiffusion Zone Widths in the Columbium-Rhenium Couple Systems

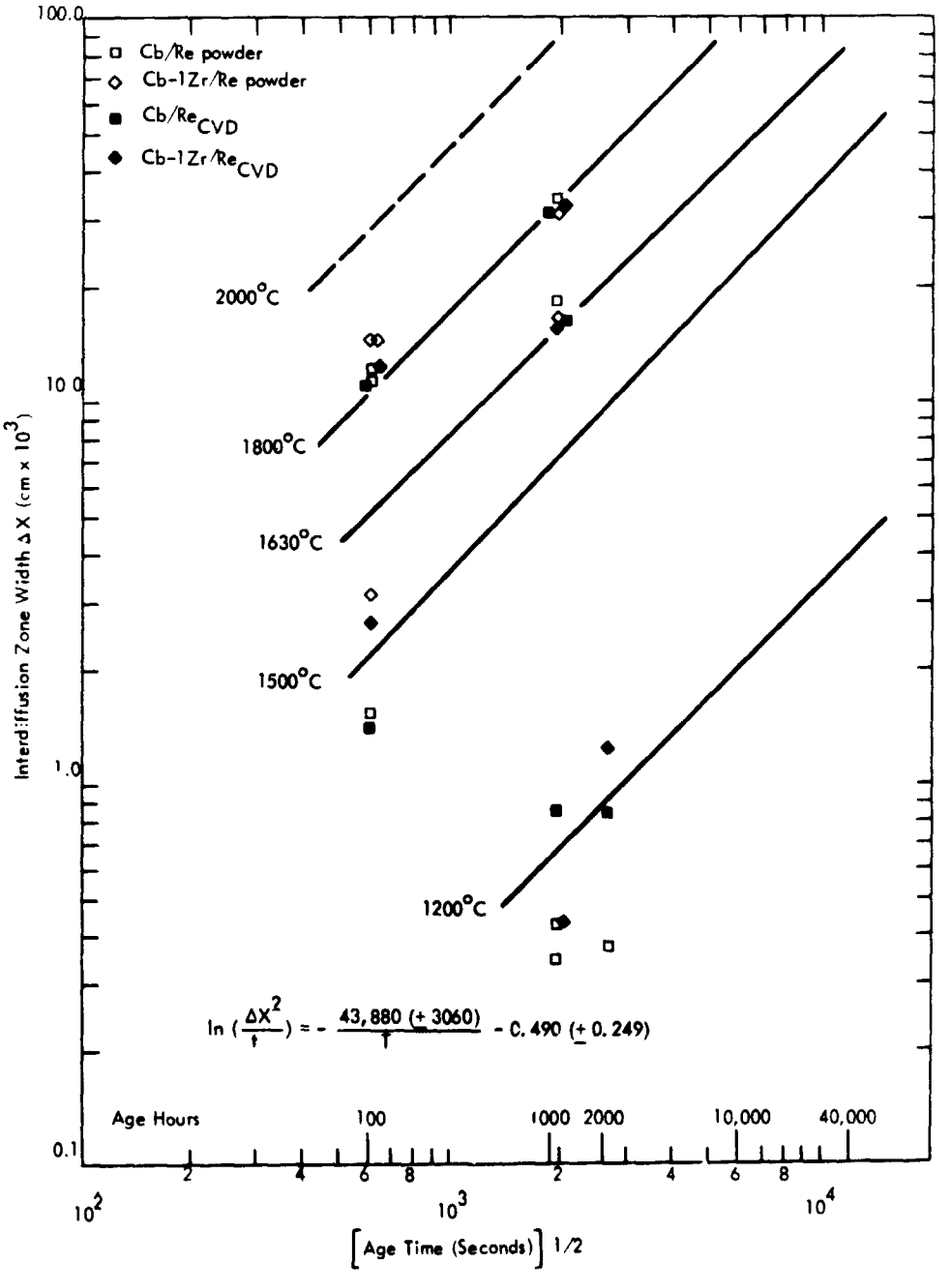

Figure 23. Illustrating Extrapolation of Zone Widths to Long Age Times for Columbium-Rhenium Interdiffusion

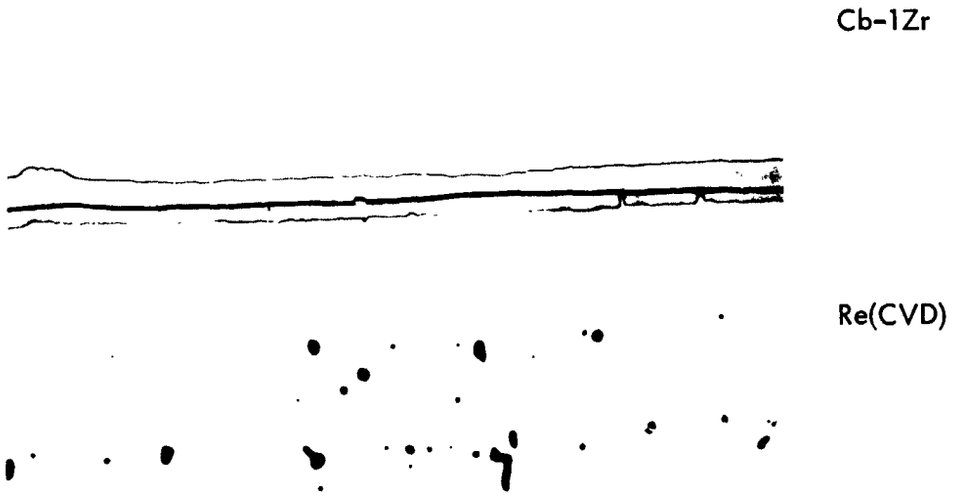

Figure 24. Cracked, Intermediate X Phase in Columbium-1 Zirconium/ CVD Rhenium Interdiffusion Zone After 1000 Hours at 1630°C (4BA-4) at 200X

(Porosity is result of CVD deposition process in CVD Re)

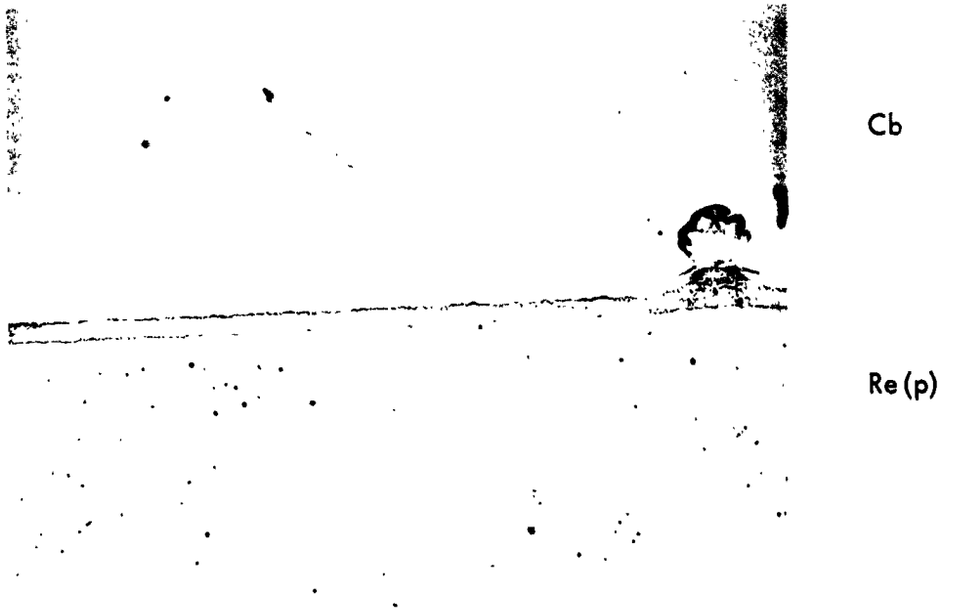

Figure 25. Intact X Phase in Columbium-Rhenium Interdiffusion Zone After 100 Hours at 1800°C (3AA-5) at 200X

(Note marker wire in Cb)

3AA-5	1800°C	1000 hours
3BA-3	1500°C	100 hours
4AA-1	1200°C	1000 hours

and the Colby MAGIC* corrected concentration profiles were loaded into the Hartley** Boltzmann-Matano analysis computer program after being fitted, in probability coordinates, for curve smoothing. Figure 26 illustrates the microprobe corrected interdiffusion concentration profile of sample 3AA-5 as presented by Calcomp plot subroutine.

Figure 27 presents the smoothed concentration profile generated by the least squares fit routine (in probability coordinates) of the Hartley program. The two X phase concentration discontinuities agree rather well with published phase diagrams for rhenium-columbium. Figures 28, 29, and 30 present the resulting interdiffusion coefficients as a function of rhenium concentration at 1200, 1500 and 1800°C. The absence of two phase regions in Figure 28 is due to the small interdiffusion zone and the steep (few data points concentration gradient found at 1200°C.

Figure 31 presents the Arrhenium interdiffusion relation for columbium-rhenium interdiffusion as resolved in this study. The interdiffusion coefficients fall closely below that for columbium self-diffusion and are plotted as mean $\tilde{D}$ values for each phase region. Self-diffusion data for rhenium was not found in the literature (probably due to a lack of long lived rhenium isotopes with adequate emission properties). The low activation energy (slope) of the α phase line may be more measurement error than real, since very few data points were available in this region, and the Hartley Program distorts near boundaries. The interdiffusion coefficient can be expressed for each phase as:

$$\tilde{D}_{\beta}\left(\frac{cm^2}{sec}\right) = 8.24 \times 10^{-4} \exp\left[-\frac{73,400}{RT}\right] \qquad (13)$$

* Part II, Appendix J, Colby Computer Program for Correcting Microprobe Intensity Analysis.

** Part II. Appendix H, Hartley Computer Program for Boltzmann-Mantano Diffusion Analysis.

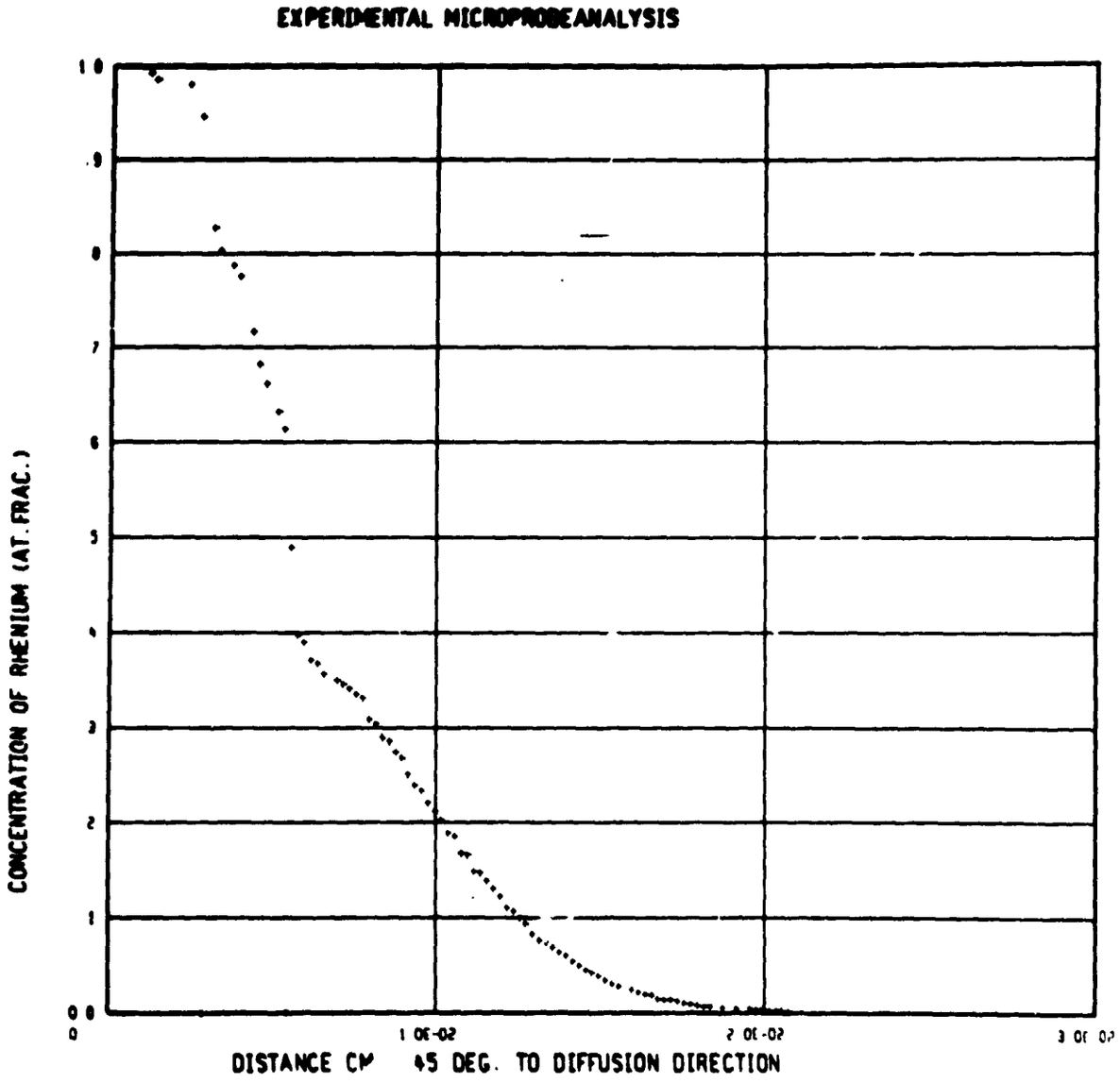

Figure 26. Colby MAGIC Corrected Input Profile to Hartley Boltzmann-Matano Program for Columbium-Rhenium Interdiffusion at 1800°C for 1000 Hours (34A-5) as Plotted by Calcomp

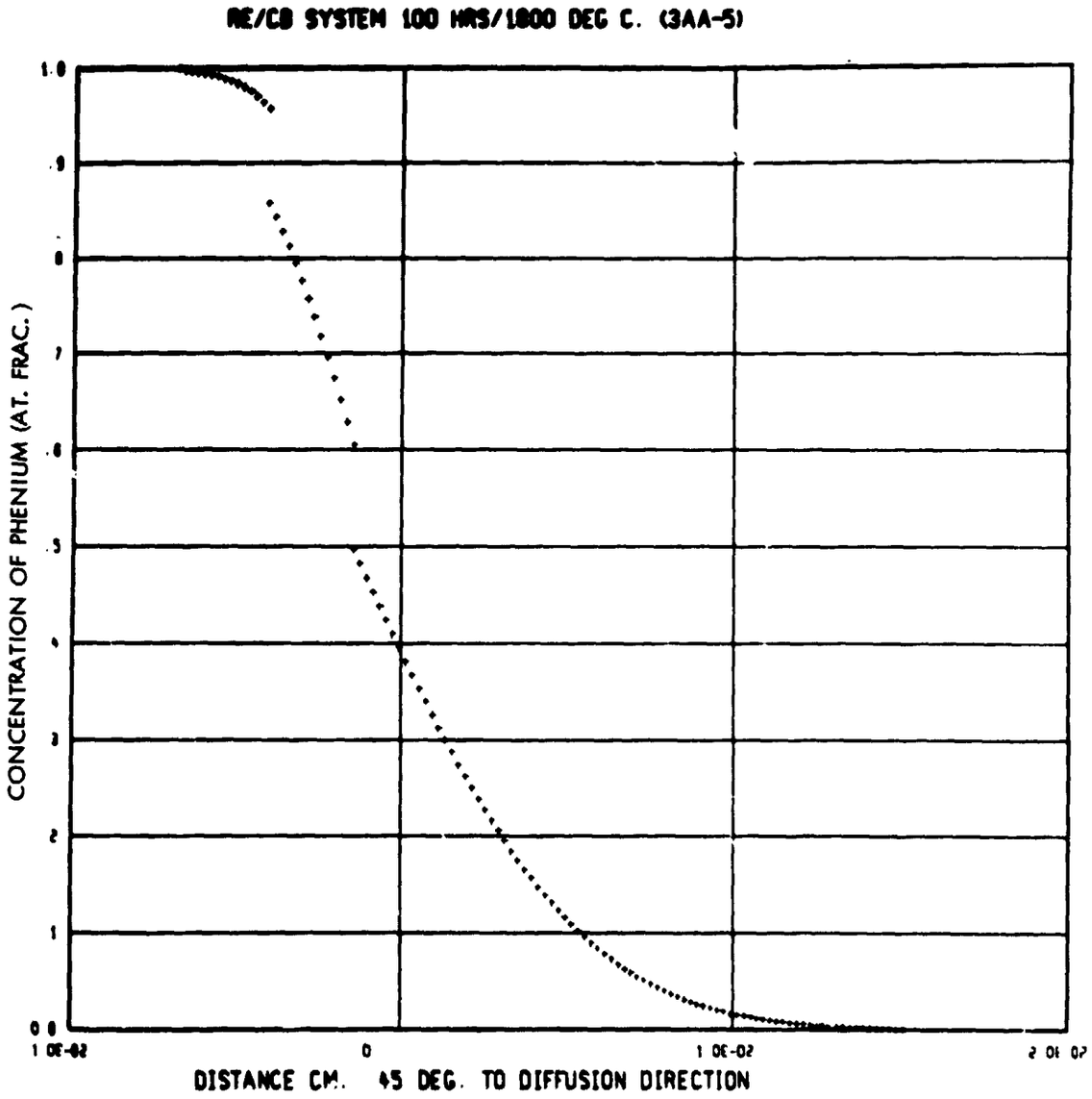

Figure 27. Regenerated (least squares fit) Concentration Profile from Data in Figure VII-16.

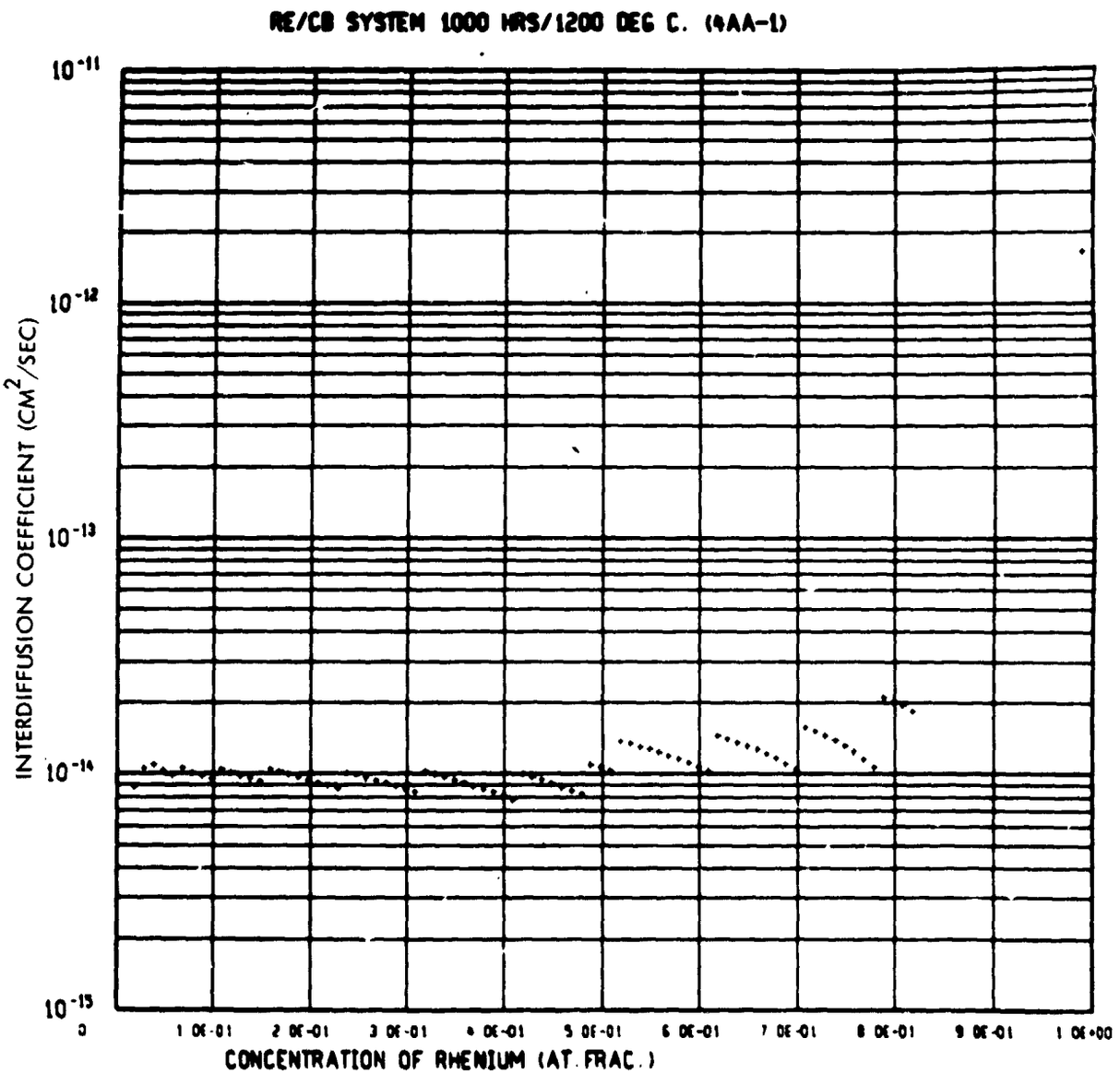

Figure 28. Columbium-Rhenium Interdiffusion Coefficient at 1200°C (4AA-1).

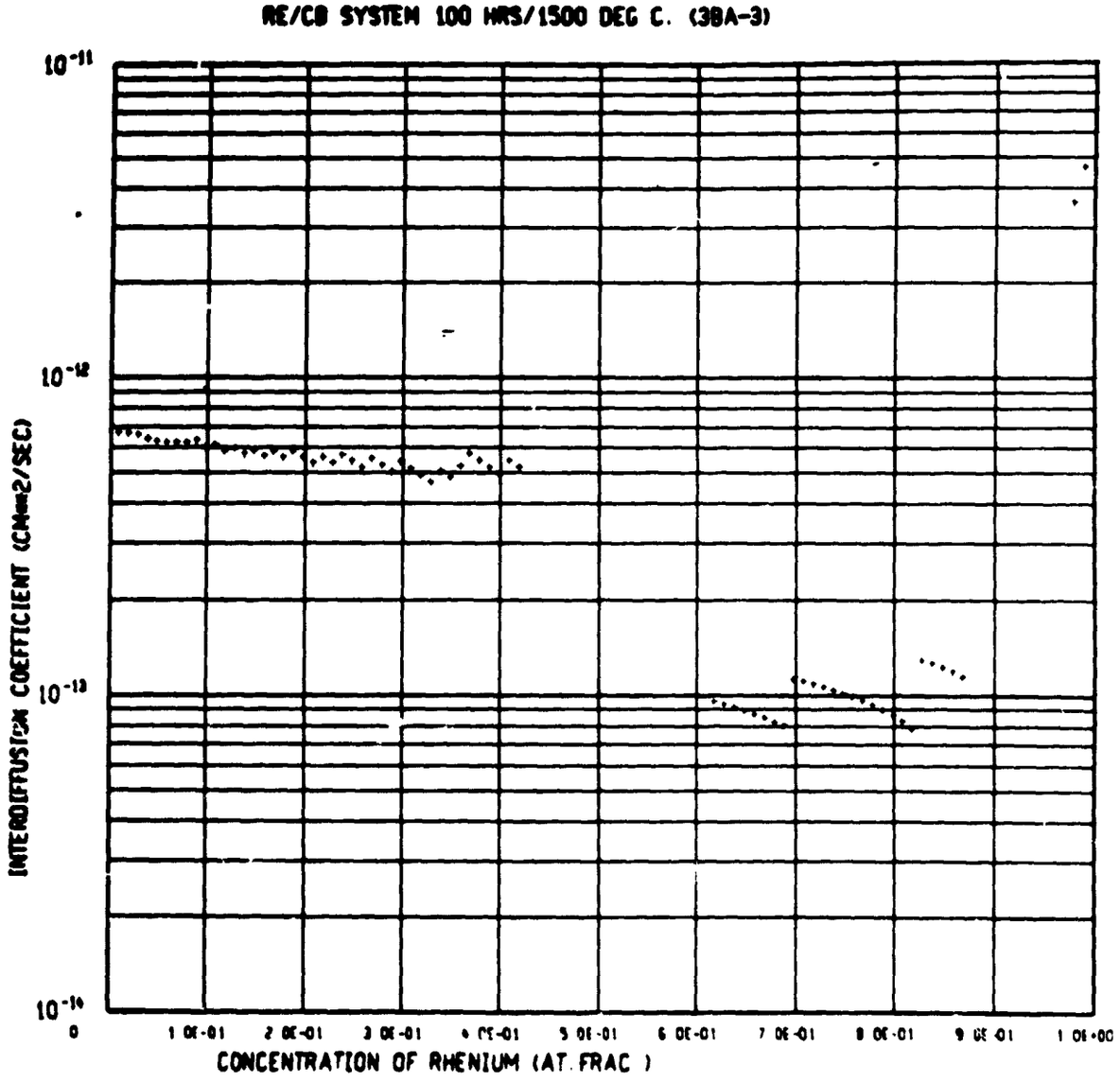

Figure 29. Columbium-Rhenium Interdiffusion Coefficient at 1500°C (3BA-3)

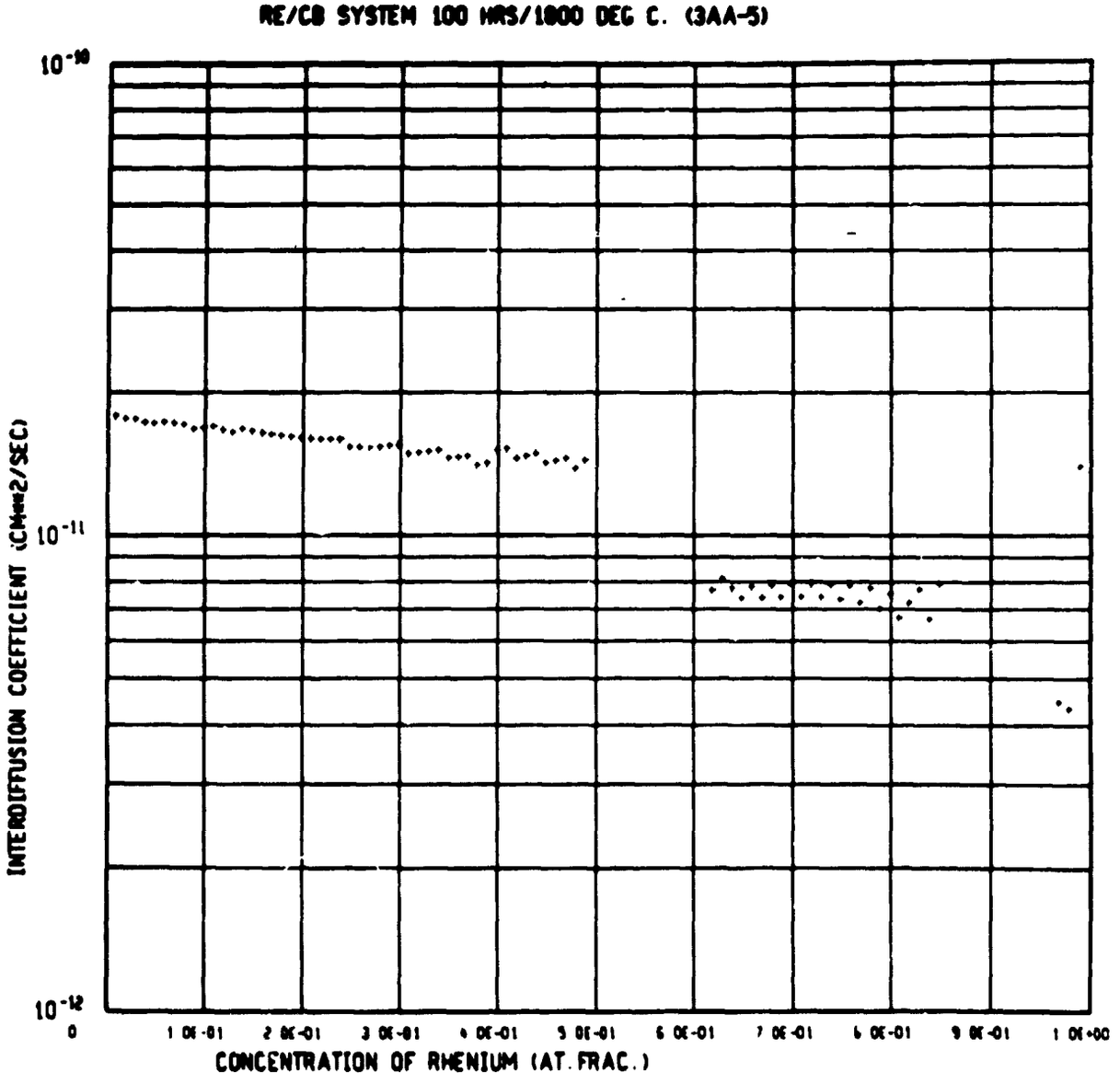

Figure 30. Columbium-Rhenium Interdiffusion Coefficient at 1800°C (3AA-5)

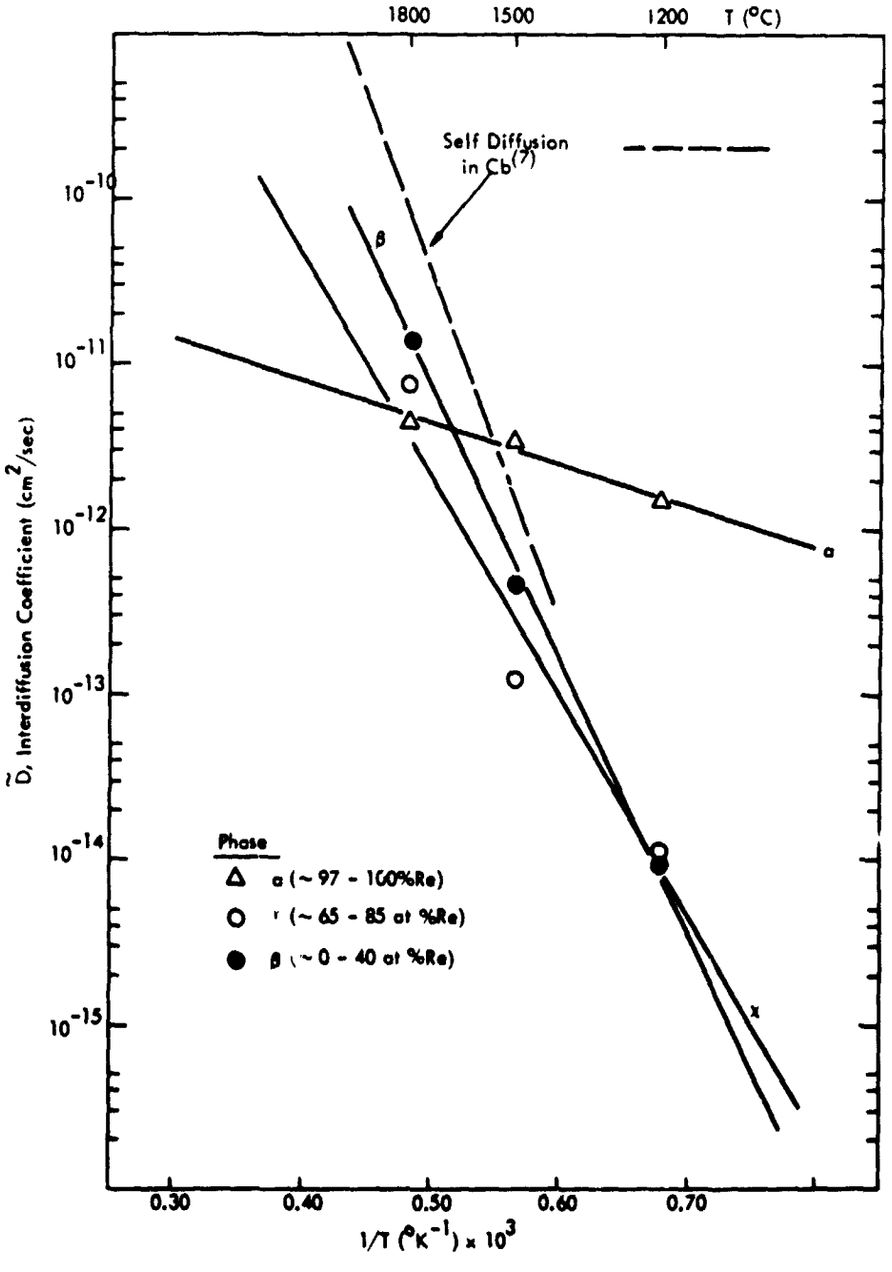

Figure 31. Arrhenius Interdiffusion Coefficient-Temperature Relation for the Columbium-Rhenium System

$$\tilde{D}_X \left(\frac{cm^2}{sec}\right) = 8.75 \times 10^{-6} \exp\left[-\frac{60,000}{RT}\right] \qquad (14)$$

for the concentration regions of the phase diagram where they apply, and where T is in ^{o}K, and R is the gas constant (1.987 cal/mole-^{o}K).

B. TANTALUM SYSTEMS

1. Tantalum-Tungsten Systems

The tantalum-tungsten system diffusion couples form solid-solution, interdiffusion zones. Of the four arc cast and CVD tungsten to tantalum and tantalum-10 tungsten couple systems, only arc cast tungsten to tantalum-10 tungsten couples were formed by hot pressing. The other three systems were formed by autoclave HIP welding. Microprobe trace measured as-welded zone widths were 0.48×10^{-3} centimeters. Analysis of tantalum-tungsten interdiffusion zone widths are summarized in Table 23.

Figure 32 shows that although some scatter exists, there is essentially no detectable difference between the systems. A grain boundary diffusion effect for preferentially oriented CVD tungsten grains was not discerned. Least squares computer analysis established the tantalum-tungsten interdiffusion model as

$$\ln\left(\frac{\Delta X^2}{t}\right) = -\frac{35,290\ (\pm 2210)}{T} - 7.339\ (\pm 0.189) \qquad (15)$$

where ΔX is net interdiffusion zone width (affected zone) in centimeters, t is age time in seconds, and T is age temperature in ^{o}K. Ninety-five percent confidence limits are shown. Note that tantalum-tungsten interdiffusion zone width data from Hudson and Yang[3] correlate well with the data presented here.

Table 23. Tantalum-Tungsten Couple Systems Corrected Interdiffusion Zone Widths

Columbium Couple	Age Temp. (°C)	Age Time (t) (hrs.)	Age Time (t) ($sec \times 10^{-6}$)		ΔX Interdiffusion Zone Width ($cm \times 10^3$)*	$\Delta X^2/t$ (cm^2/sec)
Ta/W_{arc}**	1800	1000	3.60	Δ	8.61	2.08×10^{-11}
		100	.36		3.08	2.64×10^{-11}
	1630	1000	3.60		3.94	4.30×10^{-12}
	1500	2000	7.20		3.56	1.76×10^{-12}
	1200	2000	7.20		0.29	1.17×10^{-14}
		1000	3.60		--+	--
Ta/W_{CVD}***	1800	1000	3.60	▲	7.56	1.59×10^{-11}
		100	.36		2.98	2.47×10^{-11}
	1630	1000	3.60		6.27	1.09×10^{-11}
	1500	2000	7.20		2.97	1.23×10^{-12}
	1200	2000	7.20		0.50	3.41×10^{-14}
		1000	3.60		0.28	2.18×10^{-14}
Ta-10W/W_{arc}	2000	1000	3.60	○	25.67	1.83×10^{-10}
		100	.36		7.21	1.44×10^{-10}
	1800	1000	3.60		7.97	1.77×10^{-11}
		100	.36		1.67	7.75×10^{-12}
	1630	1000	3.60		5.85	9.52×10^{-12}
	1500	2000	7.20		2.28	7.23×10^{-13}
	1200	2000	7.20		0.57	4.52×10^{-14}
		1000	3.60		0.40	4.34×10^{-14}
Ta-10W/W_{CVD}	2000	1000	3.60	●	24.32	1.64×10^{-10}
		100	.36		7.29	1.48×10^{-10}
	1800	1000	3.60		9.07	2.28×10^{-11}
		100	.36		2.81, 3.53, 3.33	2.20×10^{-12}, 3.46×10^{-11}, 3.08×10^{-11}
	1630	1000	3.60		5.41	8.13×10^{-12}
	1500	2000	7.20		4.85	3.27×10^{-12}
	1200	2000	7.20		0.29	1.16×10^{-14}
		1000	3.60		0.35	3.41×10^{-14}

* Zone width = cm x 10^3, i.e., 1.72 = 1.72×10^{-3}cm
Zone width also corrected for as-welded condition

** W_{arc} = arc cast tungsten

*** W_{CVD} = chemical vapor deposited tungsten, from WF_6, (100) planes

\+ Insufficient interdiffusion for accurate analysis

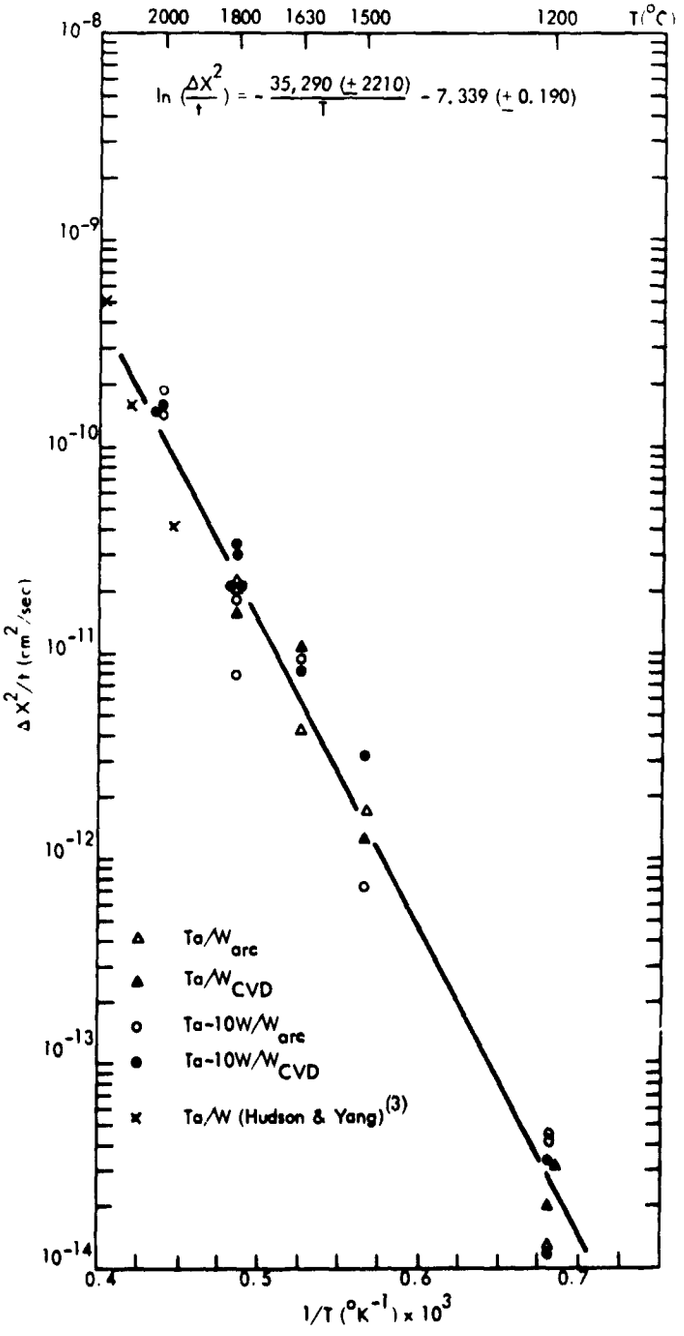

Figure 32. Arrhenius Model for Interdiffusion Zone Widths in the Tantalum-Tungsten Couple Systems

C-2

Figure 33 presents the interdiffusion zone width information as a function of age time, and extrapolations to long age times are provided with equation (15) from Figure 32. A least squares fit correlation coefficient of 0.897 was found for equation (15).

A Kirkendall void structure formed on the tantalum side of the interface at 2000, 1800, 1630, and 1500°C but was not as advanced as that observed in the columbium-tungsten system. Voids were not observed at 1200°C. Voids appeared after ageing at 1500°C and were generally spherical or oblate. Ageing at 1800°C resulted in two types of void structure, spherical again (Figure 34), and also elongated (Figure 35). Figure 34 illustrates the joining of several spherical voids to form an elongated void. The presence of the different void structures did not appear to depend on method of couple formation (HIP-weld or hot press), on the alloy constituency (i.e., tantalum or tantalum-10 tungsten), or on the age time (since voids formed at 1800°C and 100 hours were elongated -- see Figure 34). Interestingly, the void density after 2000°C ages was much reduced over that at 1630 or 1800°C. It appears that Kirkendall voids will not form at low or elevated temperatures but only at some intermediate temperature. This consideration is evaluated in more detail in Section 9, Kirkendall Void Problems.

For Boltzmann-Matano analysis of the tantalum-tungsten systems, only the tantalum-tungsten couples were evaluated since tantalum-10 tungsten alloy couples formed partial couples*. Electron microprobe spot count traverses were made on samples**

1DA-5	1800°C	1000 hours
1DA-3	1500°C	100 hours
2CA-1	1200°C	1000 hours

and the Colby MAGIC*** corrected concentration profiles were loaded into the Lifshin-

* Refer to Part II, Appendix G, Diffusion Analysis Methods
** Part II, Appendix F, Diffusion Couple Age/Identification Chart
*** Part II, Appendix J, Colby Computer Program for Correcting Microprobe Intensity Analysis

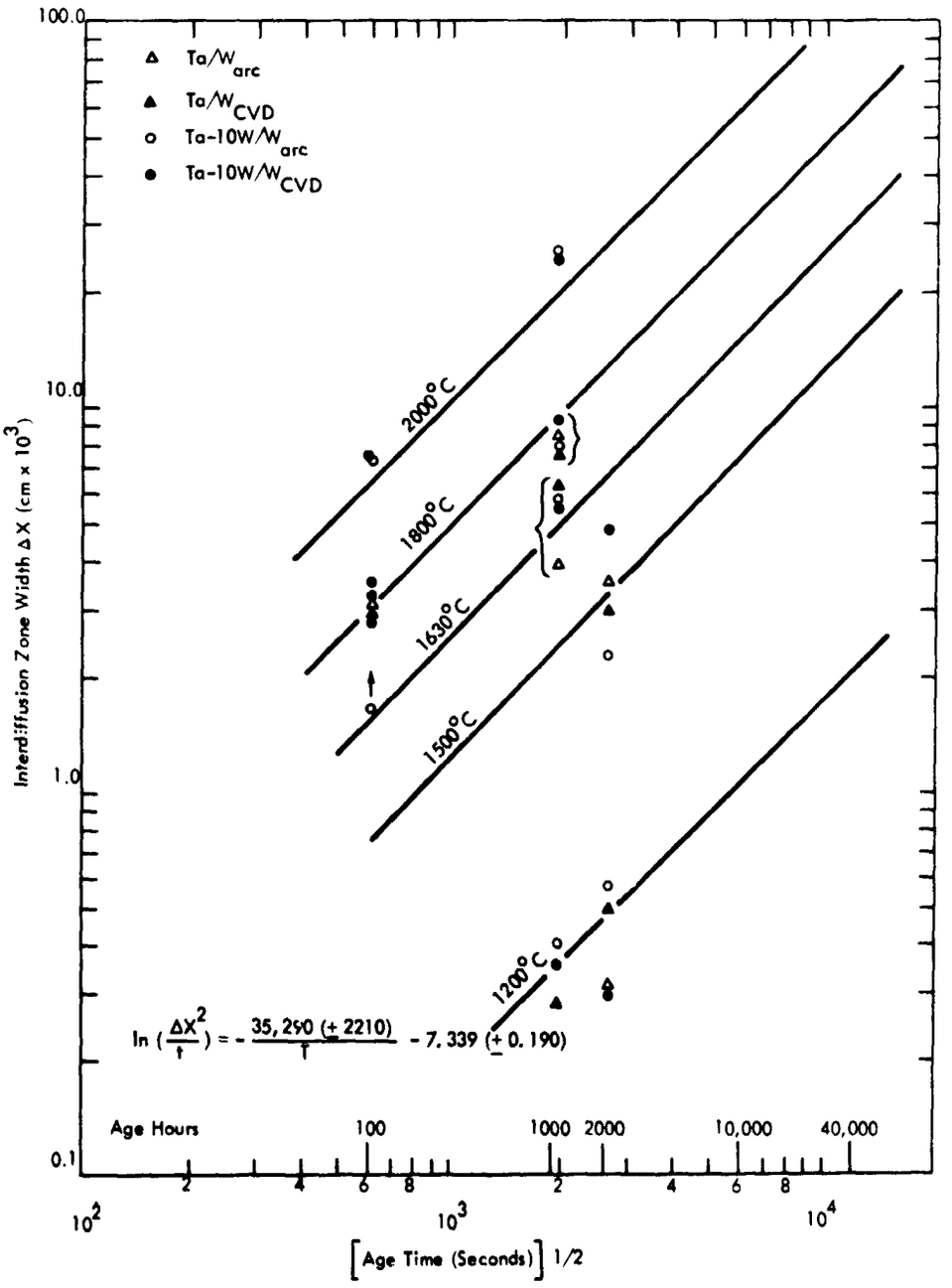

Figure 33. Illustrating Extrapolation of Zone Widths to Long Age Times for Tantalum-Tungsten Interdiffusion

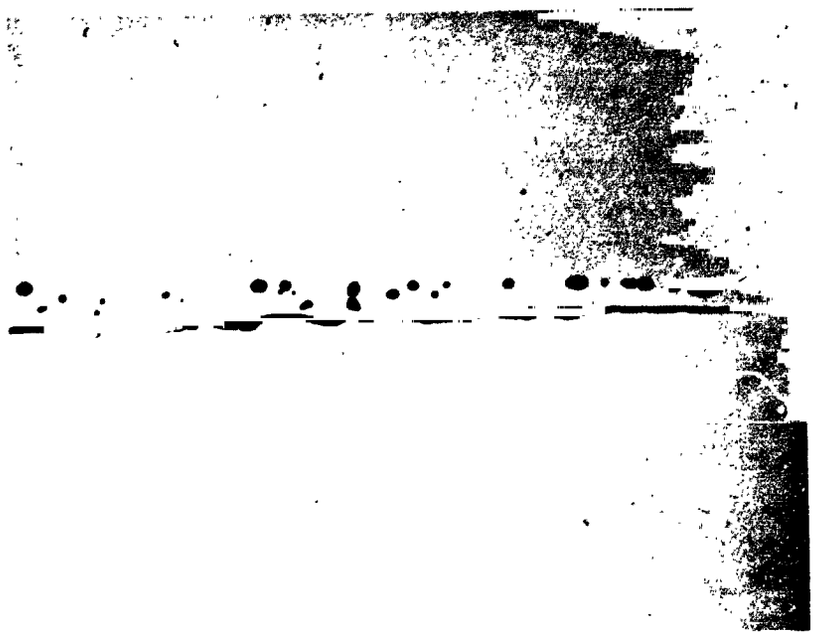

Figure 34. Illustrating Spherical Voids in Tantalum-10 Tungsten/Tungsten (arc cast) System After Ageing at 1800°C for 1000 hours (1CA-5) at 200X

Figure 35. Illustrating Elongated Voids in Tantalum-Tungsten (CVD) System After Ageing at 1800°C for 1000 hours (2CA-6) at 200X

Hannemann* Boltzmann-Matano analysis computer program. Figure 36 illustrates the microprobe corrected interdiffusion concentration profile of sample 1DA-5 as presented by Calcomp plot subroutine. Figures 37, 38, and 39 present the resulting interdiffusion coefficients as a function of concentration of tungsten at 1200, 1500, and 1800°C.

Figure 40 presents the Arrhenius interdiffusion relation for tantalum-tungsten interdiffusion. as resolved in this study. Aggrement of interdiffusion coefficient and slope (activation energy) with that presented by Ivanov[8] is excellent and falls properly within the respective self-diffusion coefficients. Analysis of interdiffusion by Tregubov[9] at 2000°C also agrees quite well with this study. Although Tregubov could not express his results in the Arrhenius form, that of Ivanov (Q = 120.5 to 110 Kcal/mole, D_o = 1.54 to 42 cm^2/sec) does not agree with the coefficients developed here:

$$\tilde{D}\left(\frac{cm^2}{sec}\right) = 1.07 \times 10^{-3} \exp\left[-\frac{70,300}{RT}\right] \qquad (16)$$

for 10 atomic percent tungsten, and

$$\tilde{D}\left(\frac{cm^2}{sec}\right) = 4.45 \times 10^{-4} \exp\left[-\frac{72,500}{RT}\right] \qquad (17)$$

for 60 to 90 atomic percent tungsten, where T is in °K and R is the gas constant (1.987 cal/mole-°K). This disagreement is probably due to Ivanov's data being in a very restricted temperature range and thus leading to greater error in slope for extended extrapolations.

2. Tantalum Alloy-Tungsten Systems

The tantalum alloy (T-111, ASTAR811C)**-tungsten (arc cast, CVD) system diffusion couples form solid solution, interdiffusion zones. All four couple systems were formed by hot press welding, thus resulting in slightly larger zero condition interdiffusion zones than for HIP-

* Part II, Appendix I, Lifshim-Hannemann Computer Program for Boltzmann-Matano Diffusion Analysis.

** T-111 Alloy is Ta-8.2W-1.9Hf
ASTAR811C is Ta-8.1W-1.4Re-0.9Hf

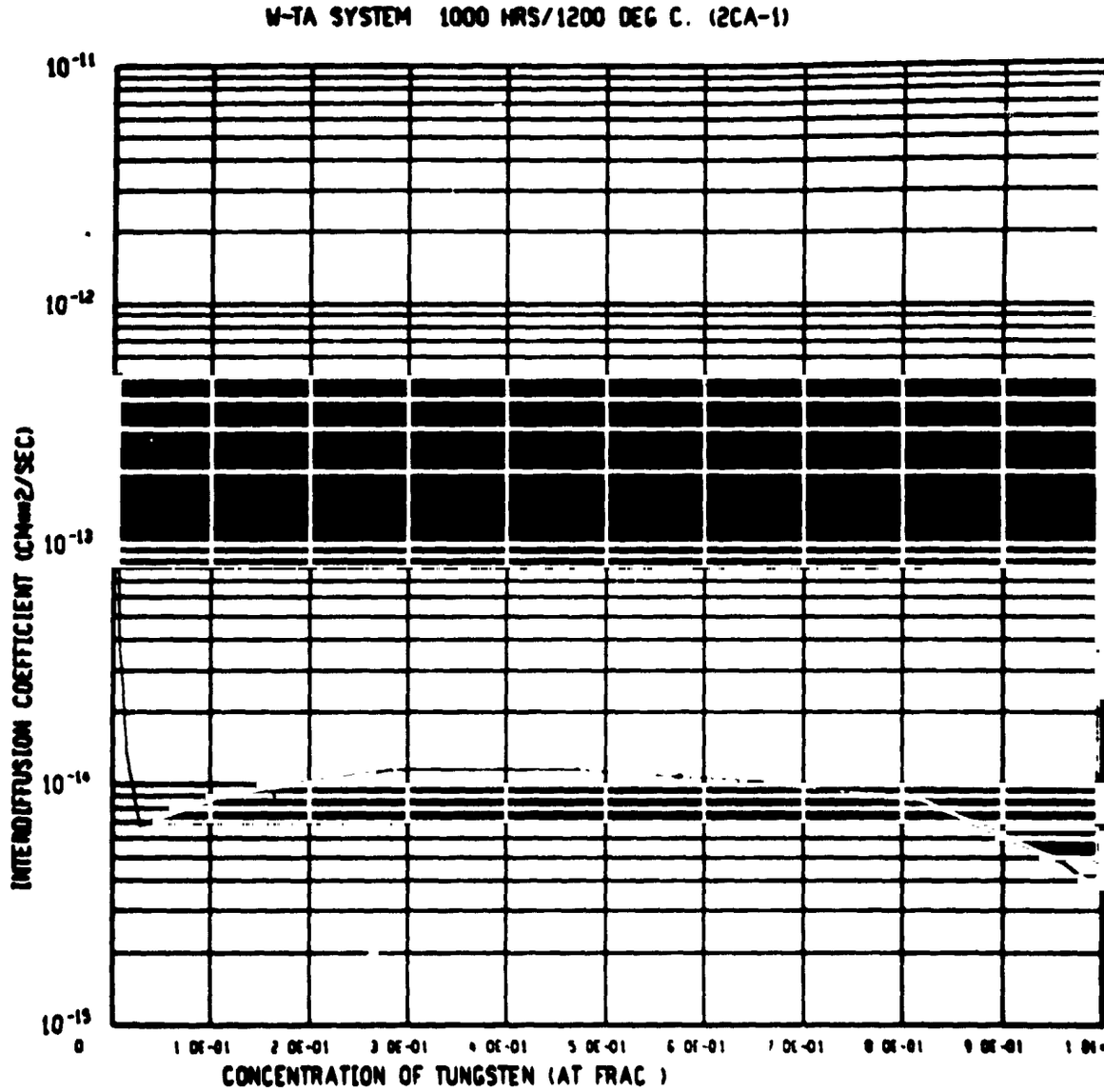

Figure 36. Microprobe Corrected Interdiffusion Concentration Profile of Sample 1DA-5 After Ageing for 1000 hours at 1800°C

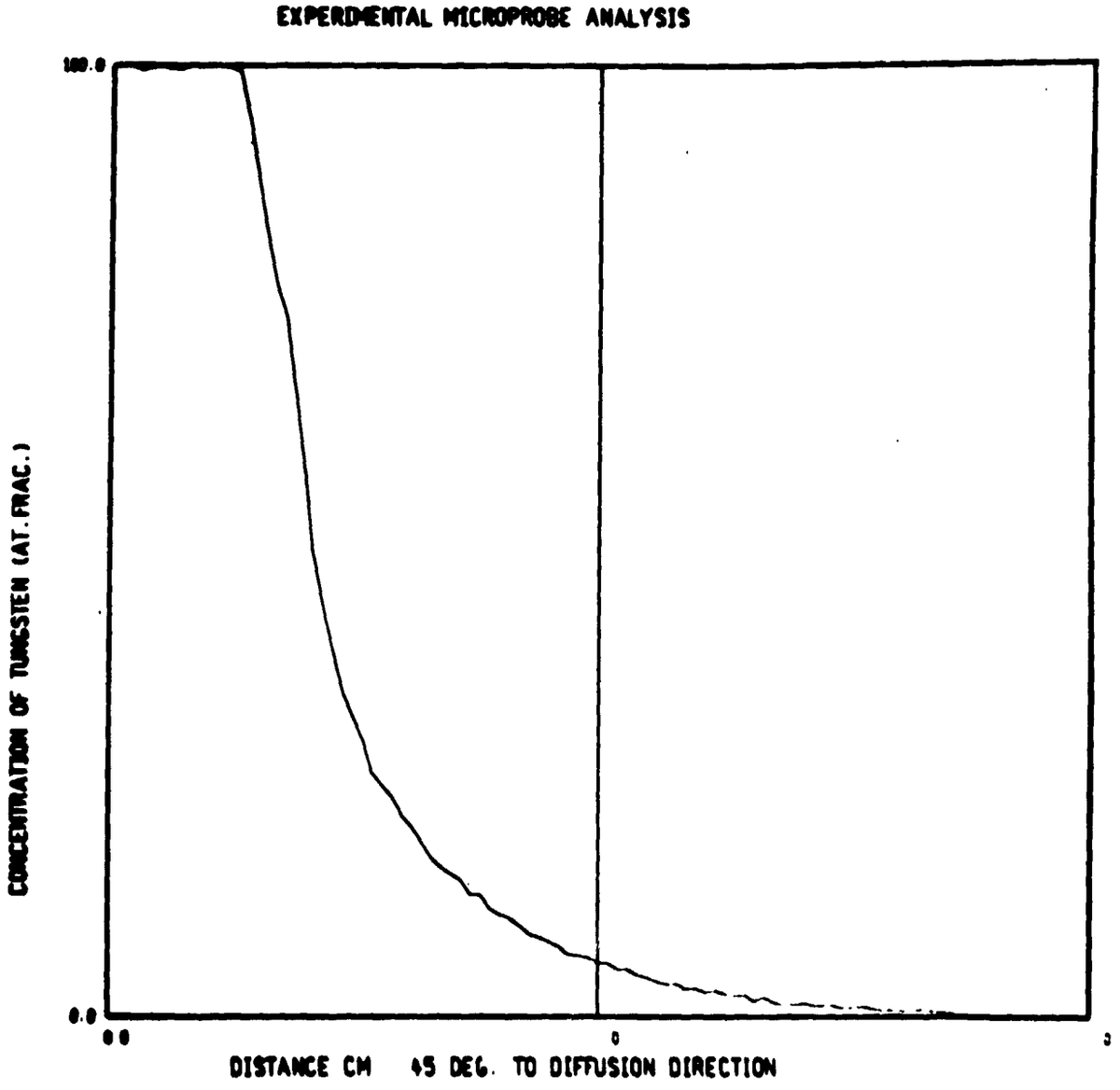

Figure 37. Tantalum-Tungsten Interdiffusion Coefficient at 1200°C

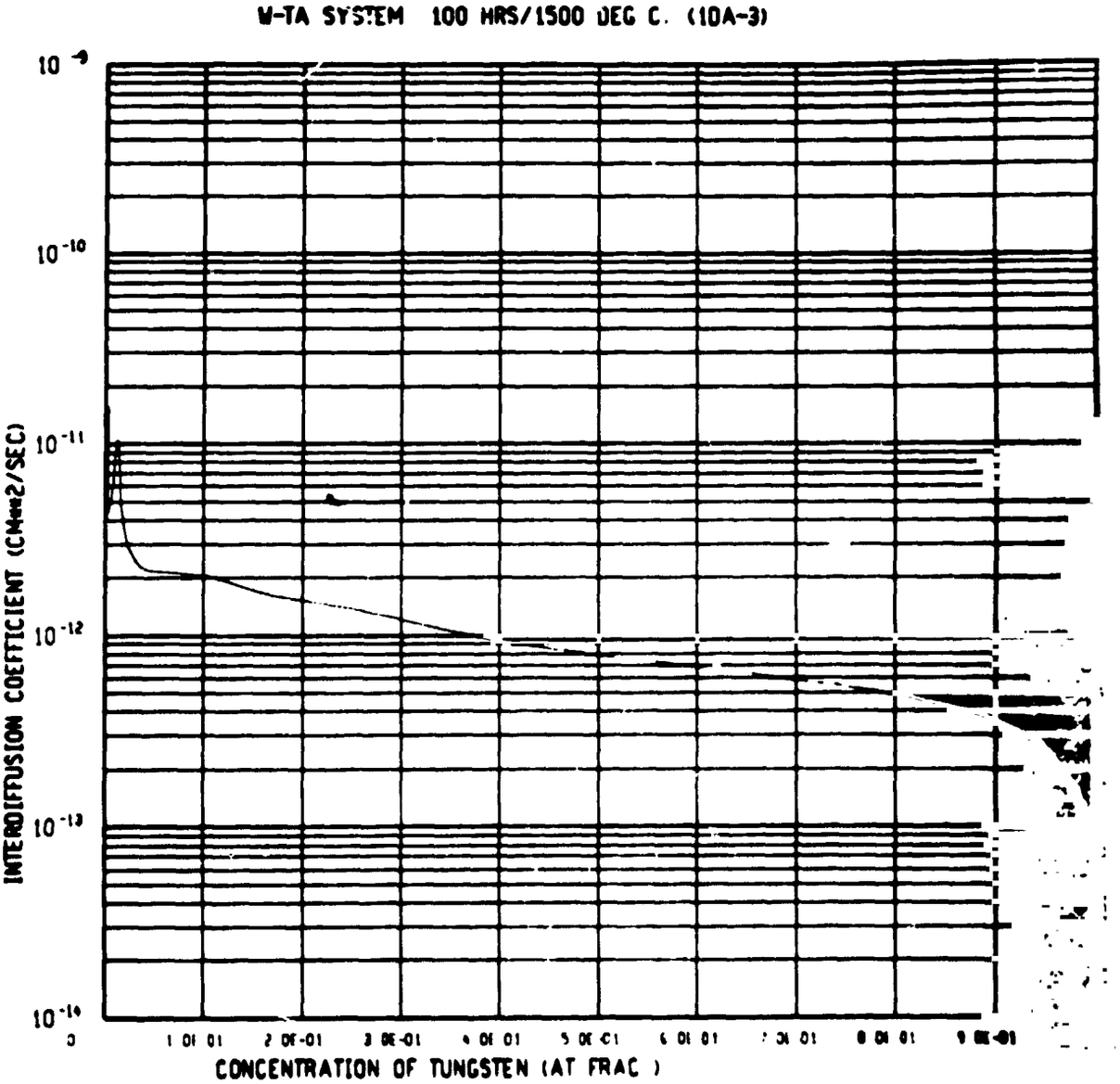

Figure 38. Tantalum-Tungsten Interdiffusion Coefficient at 1500°C

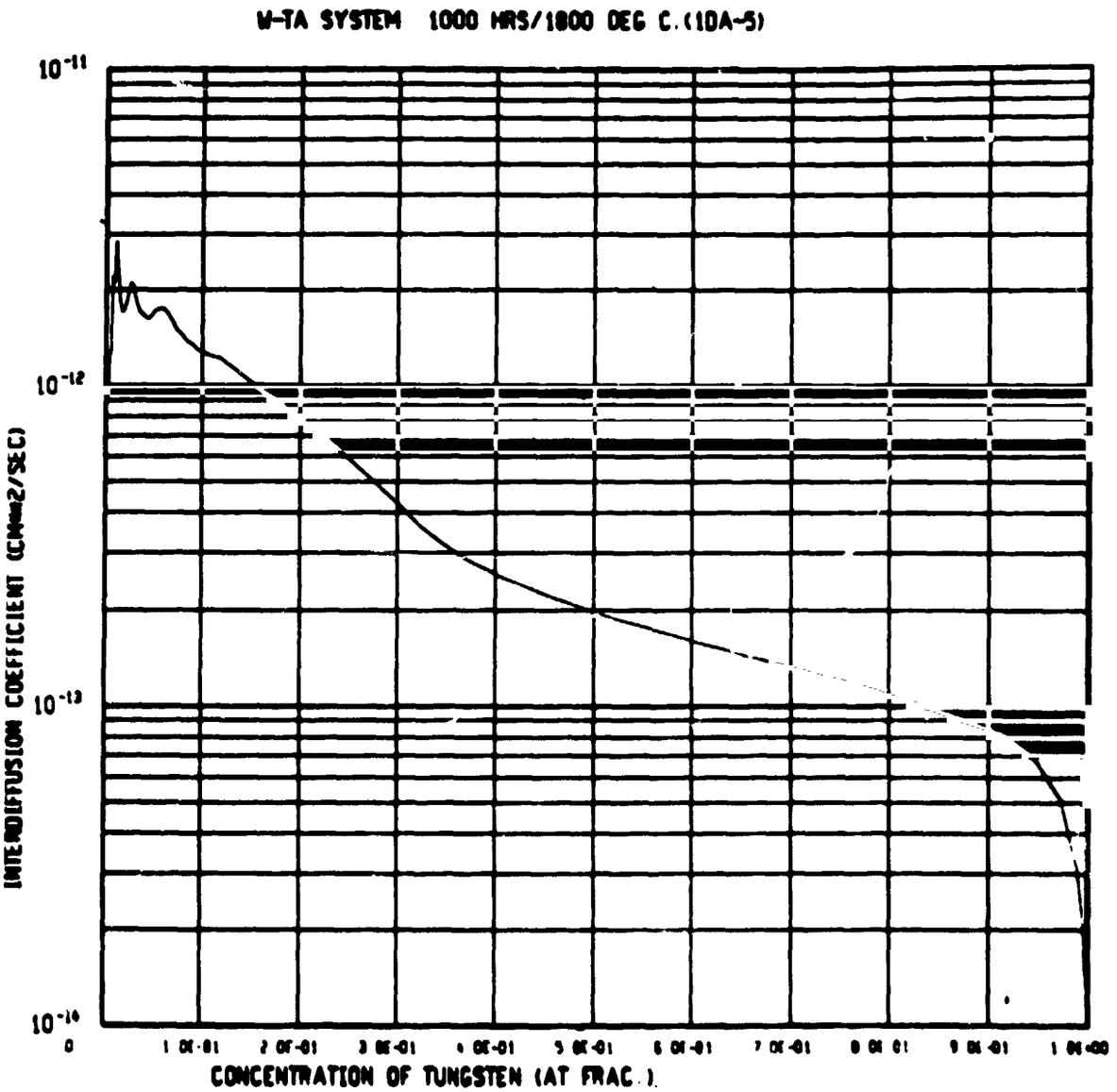

Figure 39. Tantalum-Tungsten Interdiffusion Coefficient at 1800°C

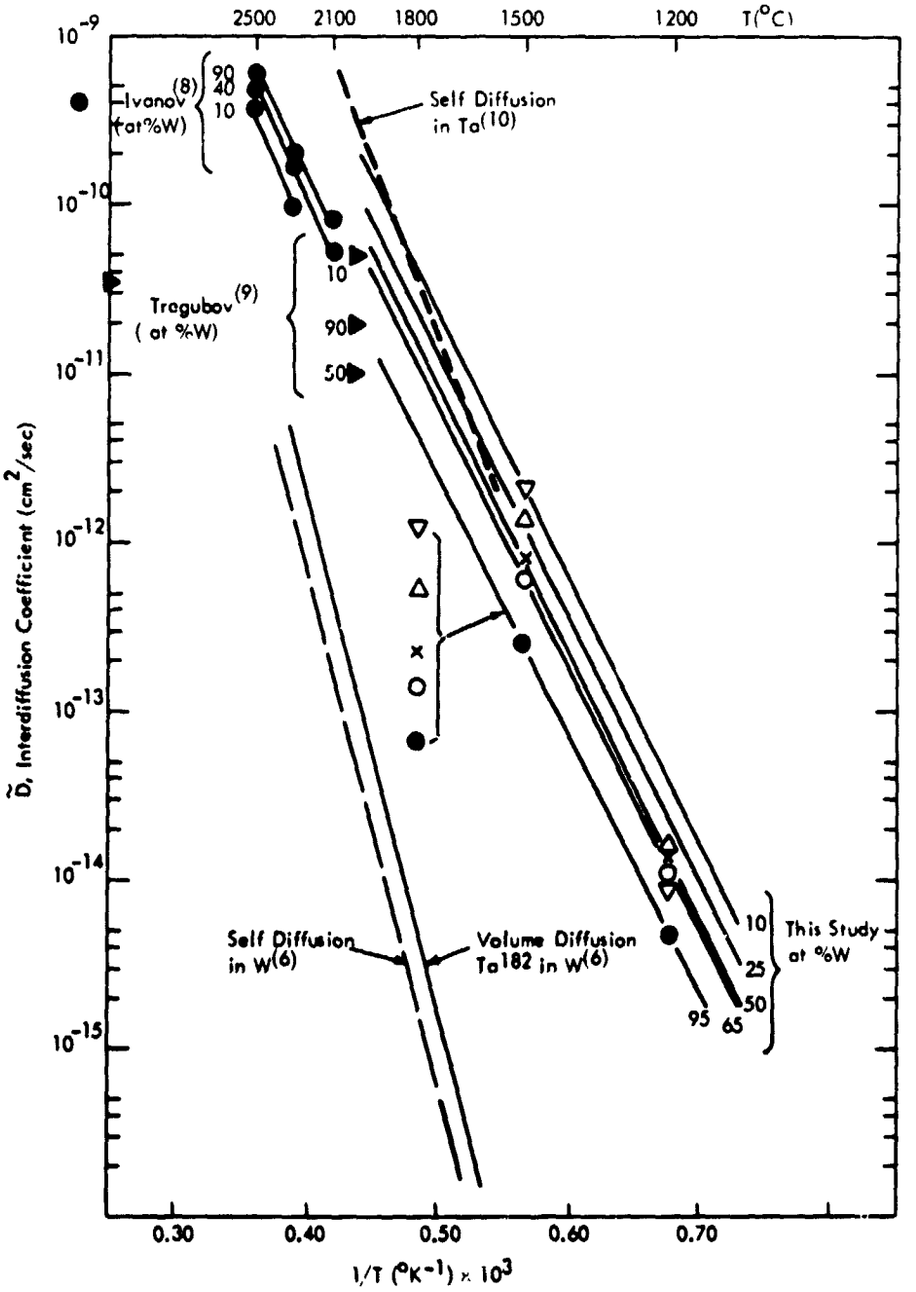

Figure 40. Arrhenius Interdiffusion Coefficient-Temperature Relation for the Tantalum-Tungsten System

welded couples. Figure 41 illustrates that an extrapolation of measured interdiffusion zone widths (ΔX meas) for 1800°C ages to time zero results in an intercept at 2.0×10^{-3} cm. This value agreed well with the microprobe trace measured as welded zone widths of 1.5 and 1.6×10^{-3} cm. Analysis of T-111 and ASTAR811C to arc cast and CVD tungsten interdiffusion zone widths is summarized in Table 24.

Figure 42 shows that very little scatter existed for this system and that there is no detectable difference between the systems. A slight trend for tungsten interdiffusion zone widths to exceed those of tantalum can be noted in Table 24, but is not conclusive. A grain boundary diffusion effect for preferentially oriented CVD tungsten grains was not discerned, nor did the difference in alloy base (Hf, Re) constituents influence the interdiffusion zone widths. Interdiffusion zone widths at 1200°C were not discernable above the zero condition as welded correction and thus were not included in the analysis. Least squares computer analysis established the tantalum alloy-tungsten interdiffusion model as

$$\ln\left(\frac{\Delta X^2}{t}\right) = -\frac{44,720\ (\pm 3760)}{T} - 3.359\ (\pm 0.153) \qquad (18)$$

where ΔX is the net interdiffusion zone width (affected zone) in centimeters, t is age time in seconds, and T is age temperature in °K. Ninety-five percent confidence limits are shown. Literature reviews were unable to reveal other sources of information for this system for comparison purposes.

Figure 43 presents the interdiffusion zone width information as a function of age time, and extrapolations to long age times are provided with equation (18) from Figure 42. A least squares fit correlation coefficient of 0.815 was found for equation

Kirkendall void structure was not as pronounced as in the binary tantalum-tungsten system couples and consisted of occasional spherical voids on the alloy side of the interface. No elongated

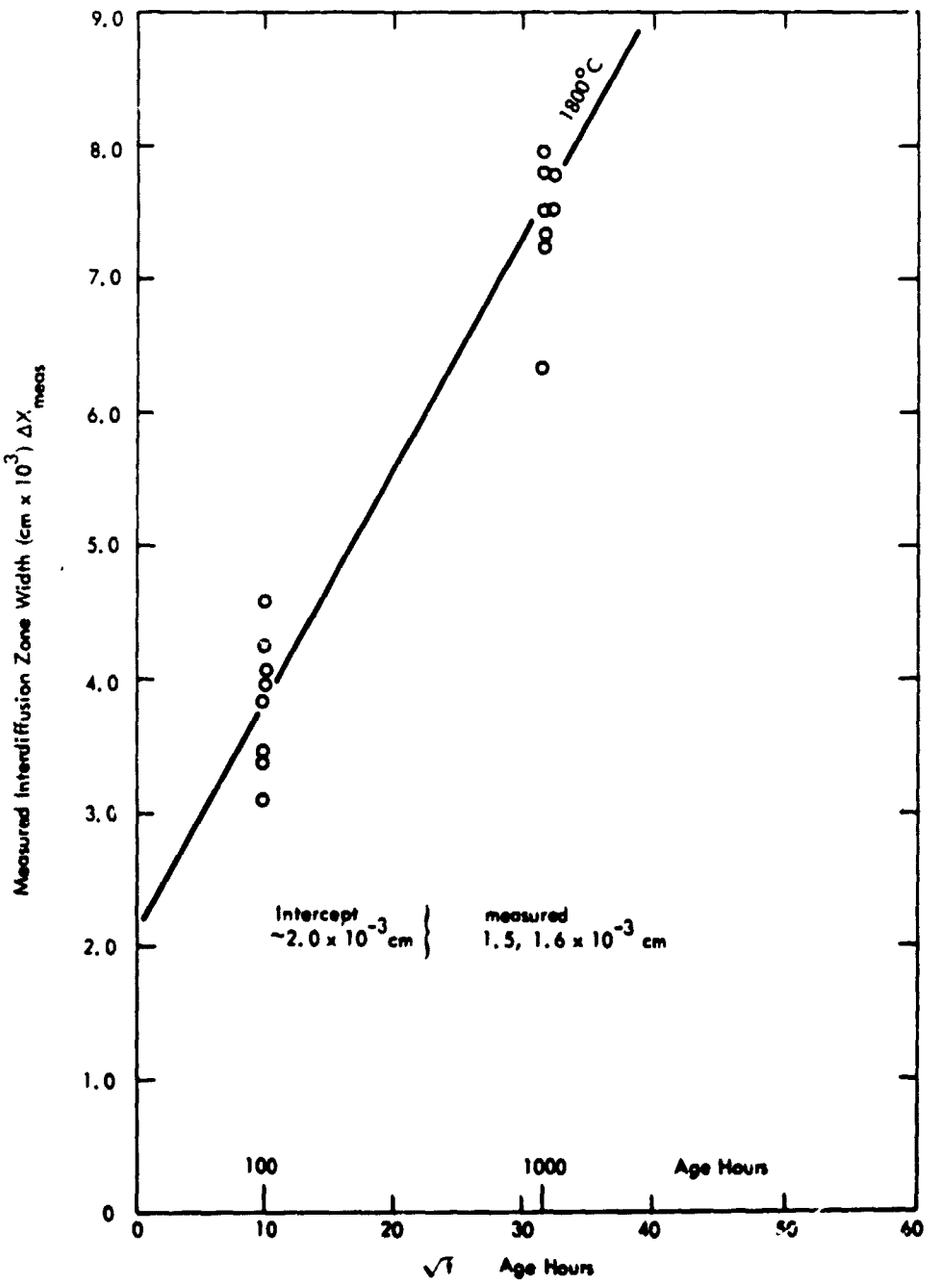

Figure 41. Extrapolation of Measured Interdiffusion Zone Widths to Zero Time to Establish Zero Condition for the Tantalum Alloy-Tungsten System

Table 24. T-111/ASTAR811C - Tungsten Couple Systems
Corrected Interdiffusion Zone Widths

Tantalum Alloy Couple	Age Temp. (°C)	Age Time, Hrs.	Age Time, (sec x 10^{-6})	ΔX Interdiffusion Zone Width (cm x 10^3)* Ta Curve	ΔX Interdiffusion Zone Width (cm x 10^3)* W Curve	$\Delta X^2/t$ (cm x 10^3)* (Ta Curve)	$\Delta X^2/t$ (cm x 10^3)* (W Curve)
T-111/W_{arc}**	1800	1000	3.60	□ 4.75	⊡ 5.62	□ 6.27 x 10^{-12}	⊡ 8.79 x 10^{-12}
		100	0.36	1.79	2.21	8.89 x 10^{-12}	1.36 x 10^{-11}
	1630	1000	3.60	3.36	3.08	3.14 x 10^{-12}	2.63 x 10^{-12}
	1500	2000	7.20	1.77	1.97	4.36 x 10^{-13}	5.40 x 10^{-13}
	1200	2000	7.20	--+	--+	--+	--+
		1000	3.60	--+	--+	--+	--+
T-111/W_{CVD}***	1800	1000	3.60	■ 5.95	◆ 6.28	■ 9.83 x 10^{-12}	◆ 1.09 x 10^{-11}
		100	0.36	2.14	2.08	1.27 x 10^{-11}	1.20 x 10^{-11}
	1630	1000	3.60	3.97	4.07	4.37 x 10^{-12}	4.60 x 10^{-12}
	1500	2000	7.20	1.67	1.56	3.88 x 10^{-13}	3.38 x 10^{-13}
	1200	2000	7.20	--+	--+	--+	--+
		1000	3.60	--+	--+	--+	--+
ASTAR/W_{arc}	2000	1000	3.60	○ 24.47	⊕ 20.61	○ 1.68 x 10^{-11}	⊕ 1.18 x 10^{-10}
		100	0.36	5.43	6.30	8.19 x 10^{-11}	1.10 x 10^{-10}
	1800	1000	3.60	5.77	5.71	9.23 x 10^{-12}	9.06 x 10^{-12}
		100	0.36	1.50, 1.64	2.34, 1.88	6.25, 7.47 x 10^{-12}	1.52 x 10^{-11}
							9.83 x 10^{-12}
	1630	1000	3.60	2.37	2.82	1.56 x 10^{-12}	2.21 x 10^{-12}
	1500	2000	7.20	1.45	1.74	2.92 x 10^{-13}	4.18 x 10^{-13}
	1200	2000	7.20	+	--+	--+	--+
			3.60	--+	--+	--+	--+
ASTAR/W_{CVD}	2000	1000	3.60	● 22.83	◆ 25.21	● 1.45 x 10^{-10}	◆ 1.77 x 10^{-10}
		100	0.36	6.94	6.58	1.34 x 10^{-10}	1.20 x 10^{-10}
	1800	1000	3.60	6.24	6.16	1.08 x 10^{-11}	1.06 x 10^{-11}
		100	0.36	2.50, 1.91	2.61, 2.96	1.73, 1.01, 1.89	2.43 x 10^{-11}
	1630	1000	3.60	3.46	3.40	3.33 x 10^{-12}	3.22 x 10^{-12}
	1500	2000	7.20	1.42	1.70	2.80 x 10^{-13}	4.02 x 10^{-13}
	1200	2000	7.20	--+	--+	--+	--+
		1000	3.60	--+	--+	--+	--+

* Zone width = cm x 10^3, i.e., 1.72 = 1.72 x 10^{-3}cm
Zone widths also corrected for as-welded condition

** W_{arc} = arc cast tungsten

*** W_{CVD} = chemical vapor deposited tungsten, from WF_6, (10 [illegible] ines.

\+ Insufficient interdiffusion for accurate analysis.

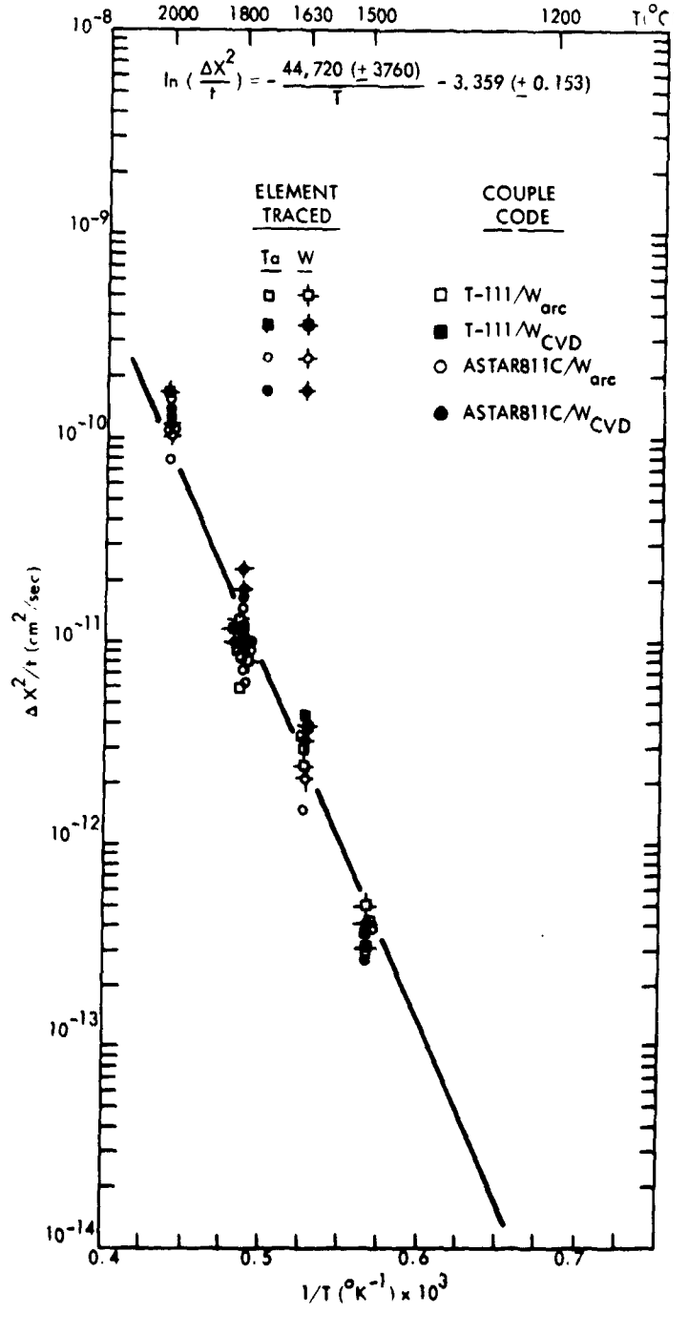

Figure 42. Arrhenius Model for Interdiffusion Zone Width in the Tantalum Alloy-Tungsten Couple System

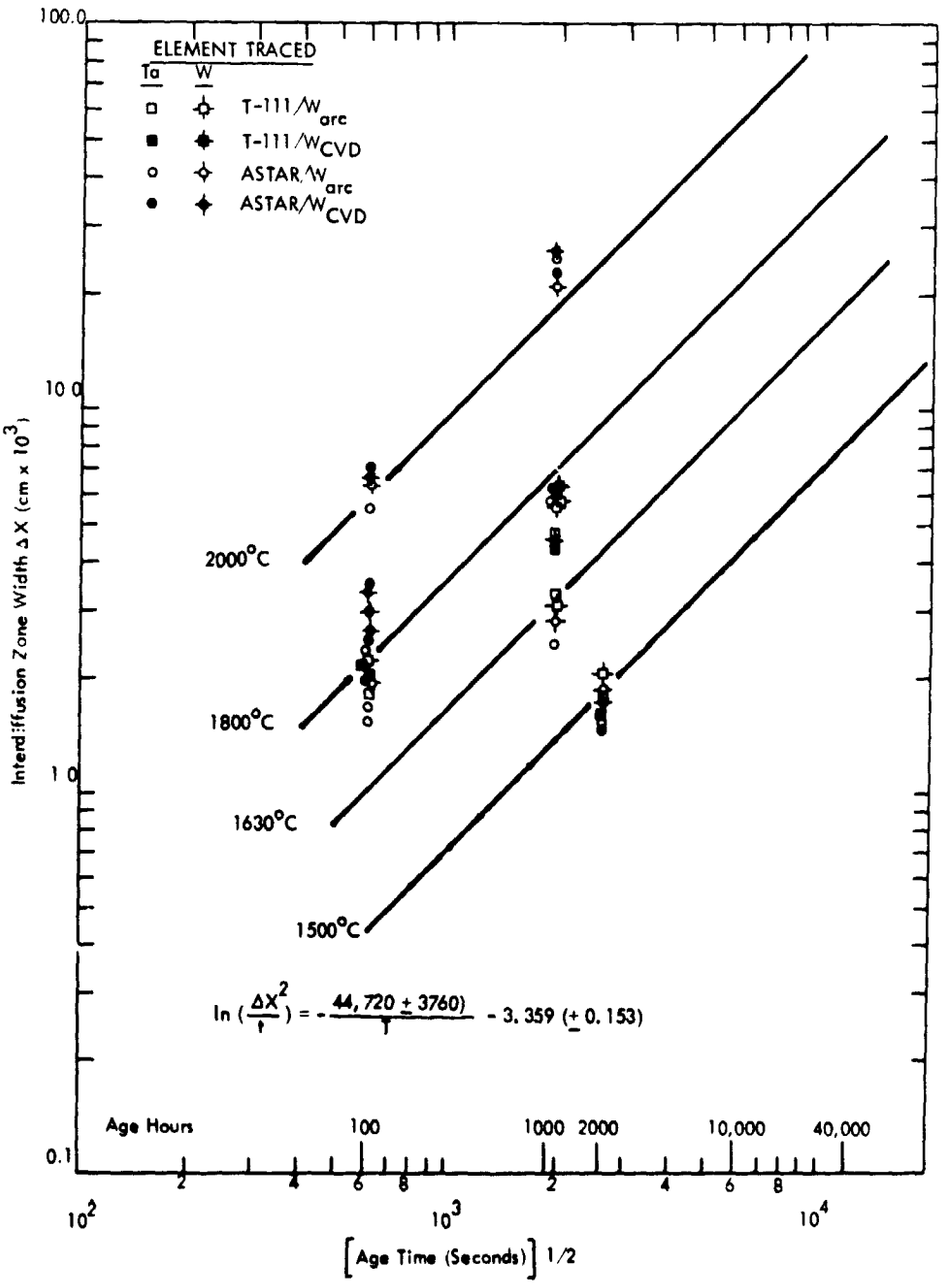

Figure 43. Illustrating Extrapolation of Zone Widths to Long Age Times for Tantalum Alloy (T-111, ASTAR811C)-Tungsten Interdiffusion

or interconnecting voids were observed. Since Kirkendall voids did form to a slightly greater extent in tantalum-10 tungsten, only the additions of hafnium or rhenium to T-111 or ASTAR-811C could have been responsible for the reduced void structure in these alloys.

Boltzmann-Matano diffusion analysis was not performed on the T-111, ASTAR811C to tungsten interdiffusion couples since the effects of ternary additions (hafnium, rhenium) appeared to perturb the systems from true binary behavior.

3. Tantalum-Rhenium Systems

The tantalum-rhenium systems diffusion couples form an intermediate phase (χ) interdiffusion zone. All junctions were formed by autoclave HIP-welds, resulting in minimal zero condition interdiffusion zones. Tantalum and tantalum-10 tungsten were joined to CVD and powder metallurgy product rhenium. Microprobe trace measured as-welded zero condition zone widths were 0.66×10^{-3} cm. Extrapolations of measured interdiffusion zone widths (from samples aged at 1800 and 2000°C) to time zero resulted in intercepts at 0.60 to 1.00×10^{-3} cm (Figure 44). Analysis of tantalum and tantalum-10 tungsten to powder metallurgy and CVD rhenium interdiffusion zone widths is summarized in Table 25. The tantalum-10 tungsten alloy forms a ternary couple with rhenium but was included in this couple system since the tungsten was not expected to contribute the deviations that hafnium would (T-111, ASTAR811C).

Figure 45 shows that very little scatter existed for this system, and that there is no obvious difference between the systems. A slight tendency for powder metallurgy rhenium couples to exhibit larger interdiffusion zone widths could be due to statistical scatter. A grain boundary diffusion effect for preferentially oriented CVD rhenium grains was not discerned nor did the presence of tungsten (alloy constituent) influence the interdiffusion zone widths. Interdiffusion zones at low temperatures (1500, 1200°C) possessed more statistical scatter, but this was due to measured zone widths being of the same order of magnitude as zero condition zone widths.

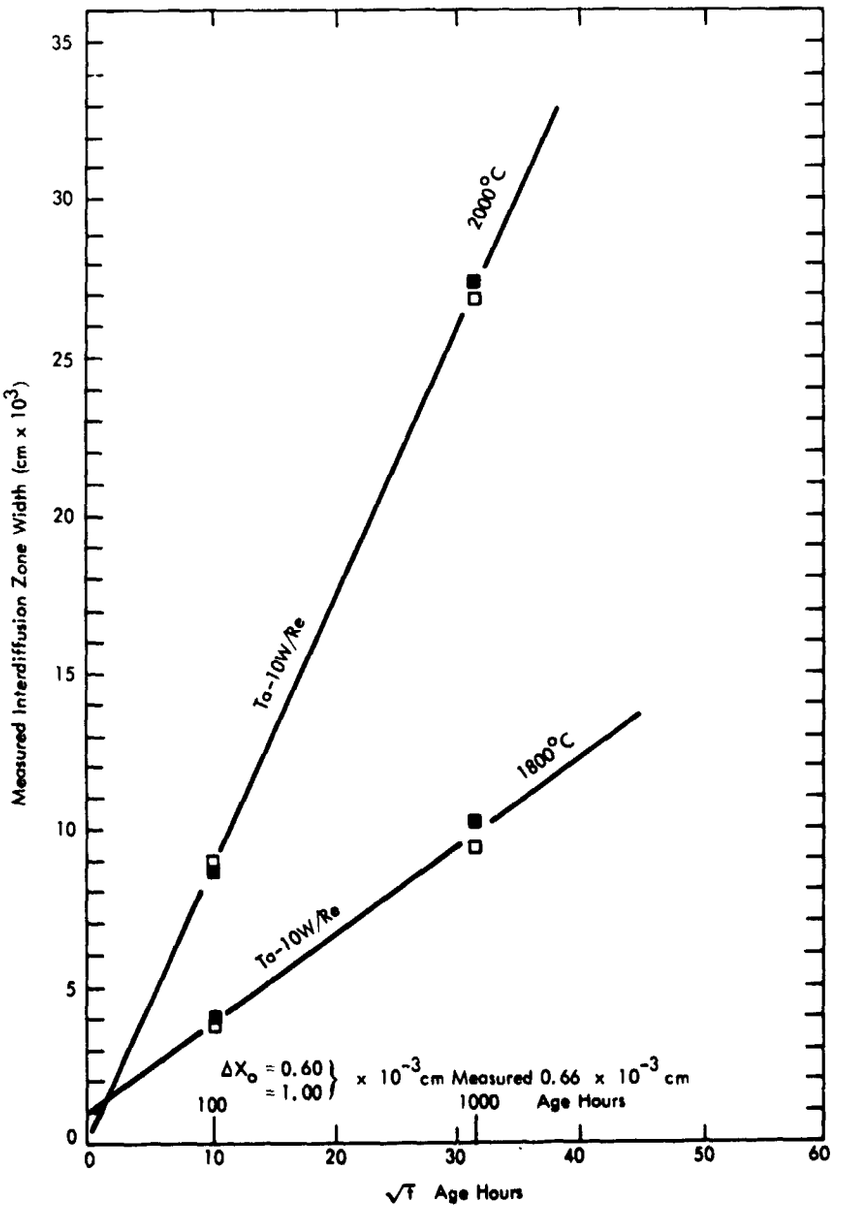

Figure 44. Extrapolation of Measured Interdiffusion Zone Widths to Zero Time to Establish Zero Condition for the Tantalum-Rhenium System

Table 25. Tantalum-Rhenium Couple Systems
Corrected Interdiffusion Zone Widths

Tantalum Couple	Age Temp. (°C)	Age Time (t) (hrs.)	Age Time (t) (sec. x 10^{-6})	ΔX Interdiffusion Zone Width (cm x 10^3)* Re	ΔX Interdiffusion Zone Width (cm x 10^3)* Ta	$\Delta X^2/t$ (cm^2/sec)	
Ta/Re_{powder}**	1800	1000	3.60	● 11.57	--	3.72×10^{-11}	
		100	.36	4.22	--	4.95×10^{-11}	
	1630	1000	3.60	6.00	--	1.0×10^{-11}	
	1500	2000	7.20	3.16	--	1.38×10^{-12}	
	1200	2000	7.20	0.46	--	2.98×10^{-14}	
		1000	3.60	0.38	--	4.01×10^{-14}	
Ta/Re_{CVD}***	1800	1000	3.60	○ 11.79	--	3.86×10^{-11}	
		100	.36	4.16	--	4.81×10^{-11}	
	1630	1000	3.60	5.12	--	7.29×10^{-12}	
	1500	2000	7.20	2.99	--	1.24×10^{-12}	
	1200	2000	7.20	0.65	--	5.93×10^{-14}	
		1000	3.60	0.34	--	3.21×10^{-14}	
Ta-10W/Re_P	2000	1000	3.60	■ 26.64	✚ 25.84	1.97×10^{-10}	1.86×10^{-10}
		100	.36	7.94	8.42	1.75×10^{-10}	1.97×10^{-10}
	1800	1000	3.60	10.55	11.17	3.09×10^{-11}	3.47×10^{-11}
		100	.36	3.38	4.04	3.18×10^{-11}	4.53×10^{-11}
	1630	1000	3.60	5.76	6.48	9.23×10^{-12}	1.17×10^{-11}
	1500	2000	7.20	5.02	5.05	3.50×10^{-12}	3.54×10^{-12}
	1200	2000	7.20	0.64	0.51	5.70×10^{-14}	3.64×10^{-14}
		1000	3.60	0.56	0.43	8.73×10^{-14}	5.14×10^{-14}
Ta-10W/Re_{CVD}	2000	1000	3.60	□ 26.19	✚ 25.84	1.91×10^{-10}	1.85×10^{-10}
		100	.36	8.24	8.45	1.89×10^{-10}	1.98×10^{-10}
	1800	1000	3.60	8.73	9.24	2.12×10^{-11}	2.38×10^{-11}
		100	.36	3.12	3.34	2.70×10^{-11}	3.10×10^{-11}
	1630	1000	3.60	5.80	6.09	9.35×10^{-12}	1.03×10^{-11}
	1500	2000	7.20	3.47	3.73	1.67×10^{-12}	1.93×10^{-12}
	1200	2000	7.20	0.39	0.43	2.12×10^{-14}	2.57×10^{-14}
		1000	3.60	0.34	--+	3.21×10^{-14}	--+

* Zone width = cm x 10^3, i.e., 1.72 = 1.72×10^{-3} cm
Zone width also corrected for as-welded condition

** Re_{powder} = powder metallurgy product rhenium

*** Re_{CVD} = chemical vapor deposited rhenium

\+ Not analyzed.

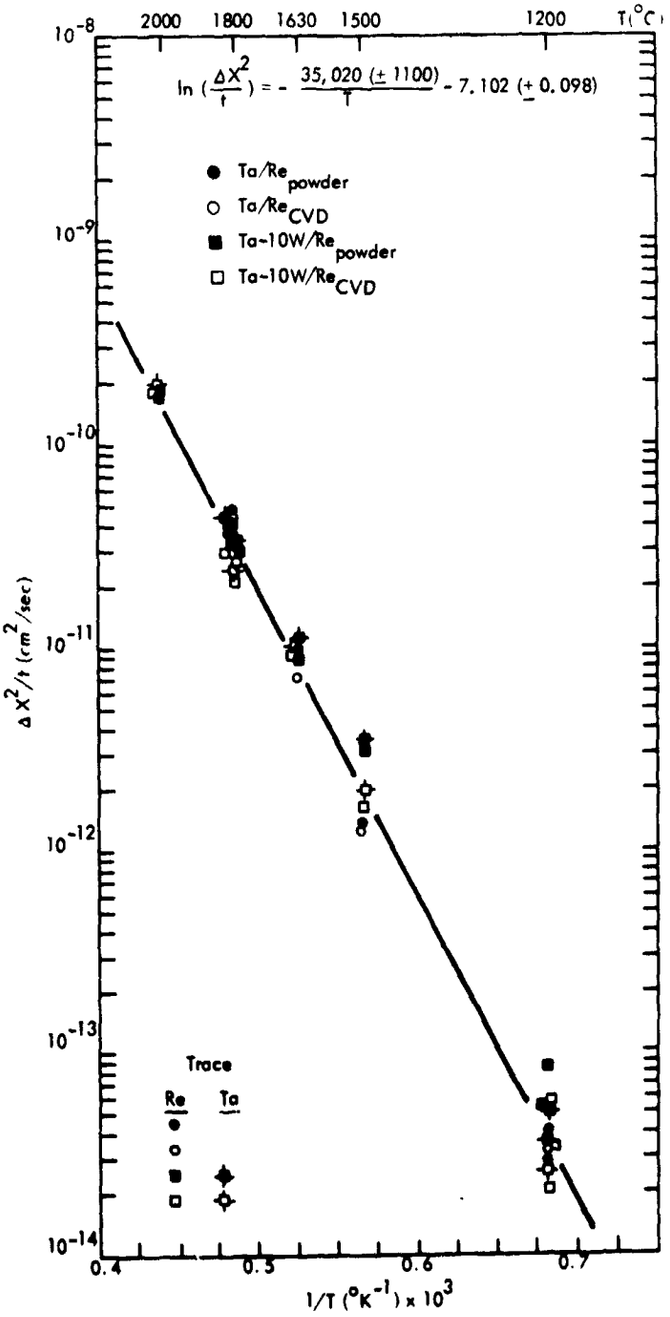

Figure 45. Arrhenius Model for Interdiffusion Zone Width in the Tantalum-Rhenium Couple System

Least squares computer analysis established the tantalum-rhenium interdiffusion model as:

$$\ln\left(\frac{\Delta X^2}{t}\right) = -\frac{35{,}020\ (\pm 1100)}{T} - 7.102\ (\pm 0.098) \qquad (19)$$

where ΔX is the net interdiffusion zone width (affected zone) in centimeters, t is age time in seconds, and T is age temperature in °K. Ninety-five percent confidence limits are shown. Literature reviews did not reveal other sources of zone width information for this system.

Figure 46 presents the interdiffusion zone width information as a function of age time, and extrapolations to long age times are provided with equation (19) from Figure 45. A least squares fit correlation coefficient of 0.971 was found for equation (19).

Although Kirkendall voids were not observed in this system for the age times and temperatures employed, photomicrographs revealed a brittle χ phase in the interdiffusion zone. Cracks in the χ phase were generally parallel to the weld zone and were not consistent in their appearance in the aged couples, i.e., some couples possessed cracks after 1000 hours at 1630°C, while some aged for 1000 hours at 1800°C and did not. Whether the cracks existed prior to/or were caused by metallographic treatment was not resolved. Figure 47 shows the uncracked χ phase interface after ageing a tantalum-CVD rhenium couple for 1000 hours at 1800°C. The holes in the CVD rhenium are the result of a deposition step and are not Kirkendall effects. Figure 48 illustrates the type of cracks appearing in the tantalum-10 tungsten/CVD rhenium system after ageing for 1000 hours at 2000°C.

For Boltzmann-Matano analysis of the tantalum-rhenium system, only pure tantalum to rhenium was considered. Electron microprobe spot count traverses were made on samples:*

3CA-6	1800°C	1000 hours
3CA-3	1630°C	1000 hours
3CA-1	1200°C	1000 hours

* Part II, Appendix F, Diffusion Couple Age/Identification Chart.

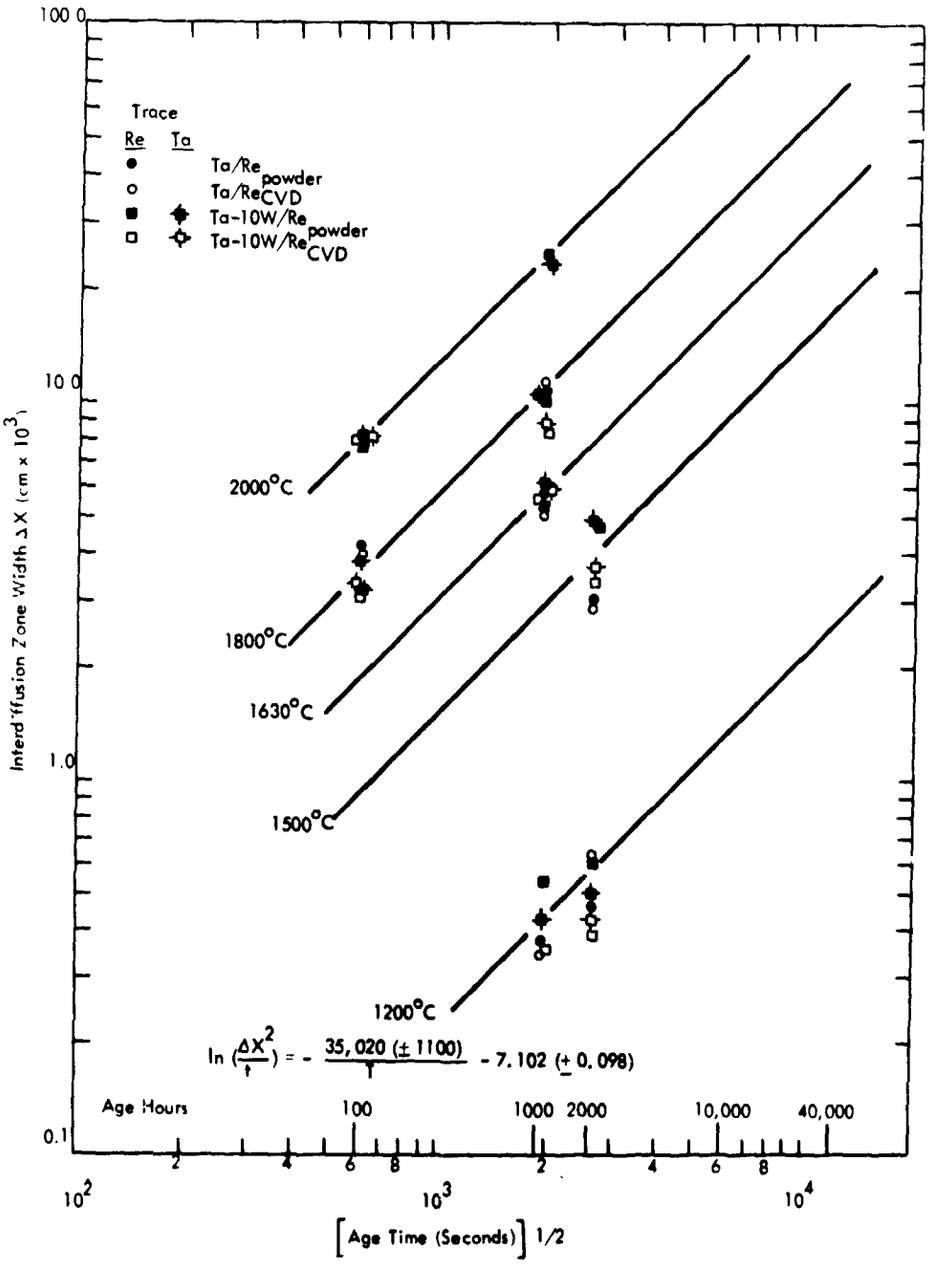

Figure 46. Illustrating Extrapolation of Zone Widths to Long Age Times for Tantalum-Rhenium Interdiffusion

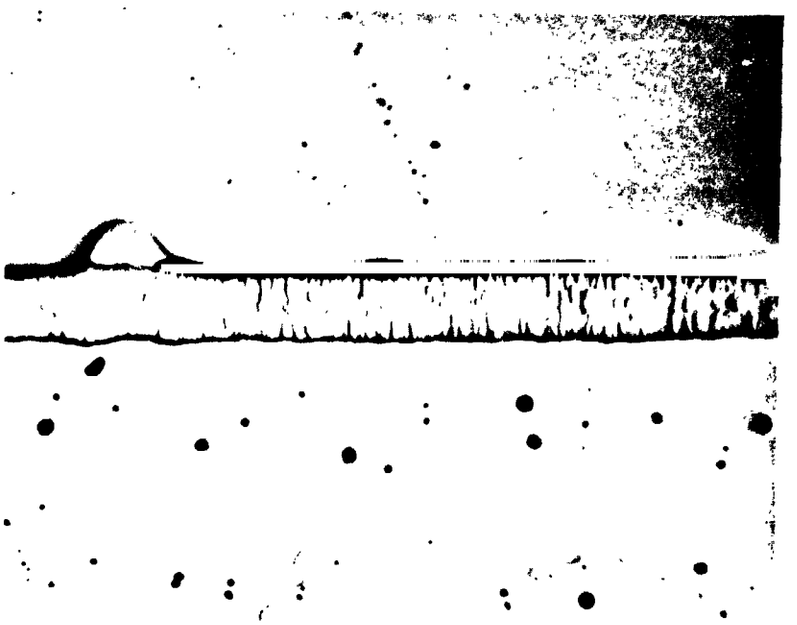

Figure 47. The Tantalum-CVD Rhenium X-Phase Interdiffusion Zone After Ageing at 1800°C for 2000 hours (4CA-6) at 200X

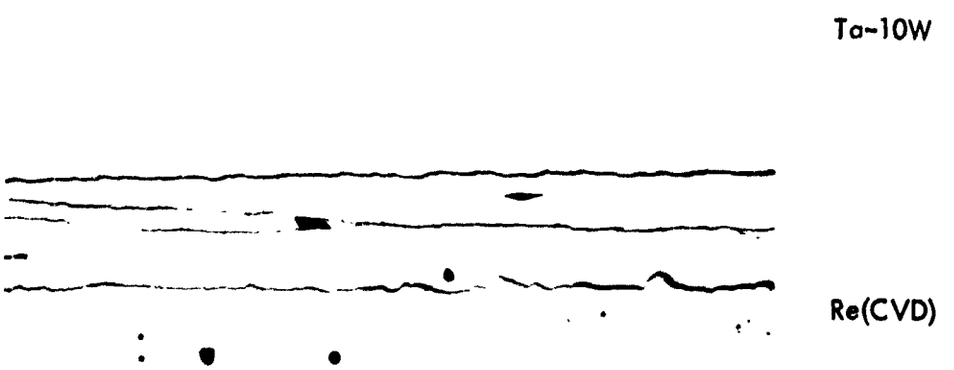

Figure 48. The Tantalum-10 Tungsten/CVD Rhenium Cracked X-Phase Interdiffusion Zone After Ageing at 2000°C for 1000 hours (4DA-8) at 200X

and the Colby MAGIC* corrected concentration profiles were loaded into the Hartley** Boltzmann-Matano analysis computer program after being fitted, in probability coordinates, for curve smoothing. Figure 49 illustrates the microprobe corrected interdiffusion concentration profile of sample 3CA-6 as presented by Calcomp plot subroutine. Figure 50 presents the smoothed concentration profile generated by the least squares fit routine (in probability coordinates) of the Hartley program. The two χ phase concentration discontinuities agree rather well with published phase diagrams for rhenium-tantalum. Figures 51, 52 and 53 present the interdiffusion coefficient as a function of rhenium concentration at 1200, 1630, and 1800°C. The absence of the interdiffusion phase regions in Figure 51 is due to the small interdiffusion zone and the steep (few data points) concentration gradient found at 1200°C (i.e., χ phase discontinuities were not discernable).

Figure 54 presents the Arrhenius interdiffusion relation for tantlum-rhenium interdiffusion as resolved in this study. The interdiffusion coefficients fall closely below that for tantalum self-diffusion and are plotted as mean $\tilde{D}$ values for each phase region. Self-diffusion data for rhenium was not found in the literature. Difficulty was encountered in resolving $\tilde{D}$ for the α phase (~ 99-100 atomic percent Re) due to the limited size of the phase field and the lack of data points in it and also due to the distortions which occur in the analytical code near phase boundaries. The interdiffusion coefficient can be expressed for each phase as:

$$\tilde{D}_{\beta} \left(\frac{cm^2}{sec}\right) = 3.71 \times 10^{-6} \exp\left[-\frac{62,500}{RT}\right] \qquad (20)$$

$$\tilde{D}_{\chi} \left(\frac{cm^2}{sec}\right) = 2.21 \times 10^{-5} \exp\left[-\frac{63,400}{RT}\right] \qquad (21)$$

for the concentration (phase) regions of the phase diagram where they apply, and where T is in °K and R is the gas constant (1.987 cal/mole-°K).

---

* Part II, Appendix J, Colby Computer Program for Correcting Microprobe Intensity Analysis.
** Part II, Appendix H, Hartley Computer Program for Boltzmann-Matano Diffusion Analysis.

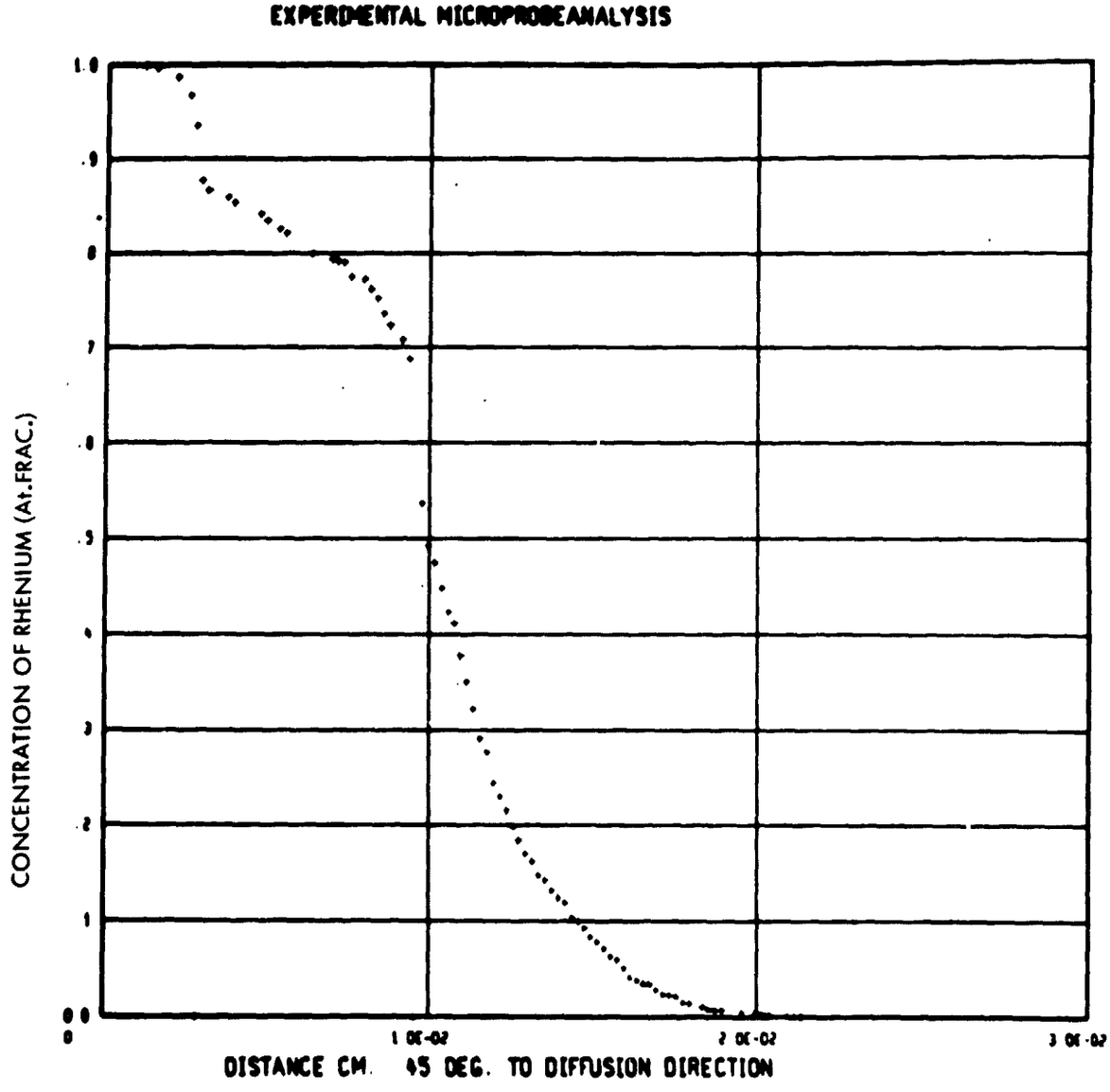

Figure 49. Colby MAGIC Corrected Input Profile to Hartley Boltzmann-Matano Program for Tantalum-Rhenium Interdiffusion at 1800°C for 1000 hours (3CA-6) as Plotted by Calcomp

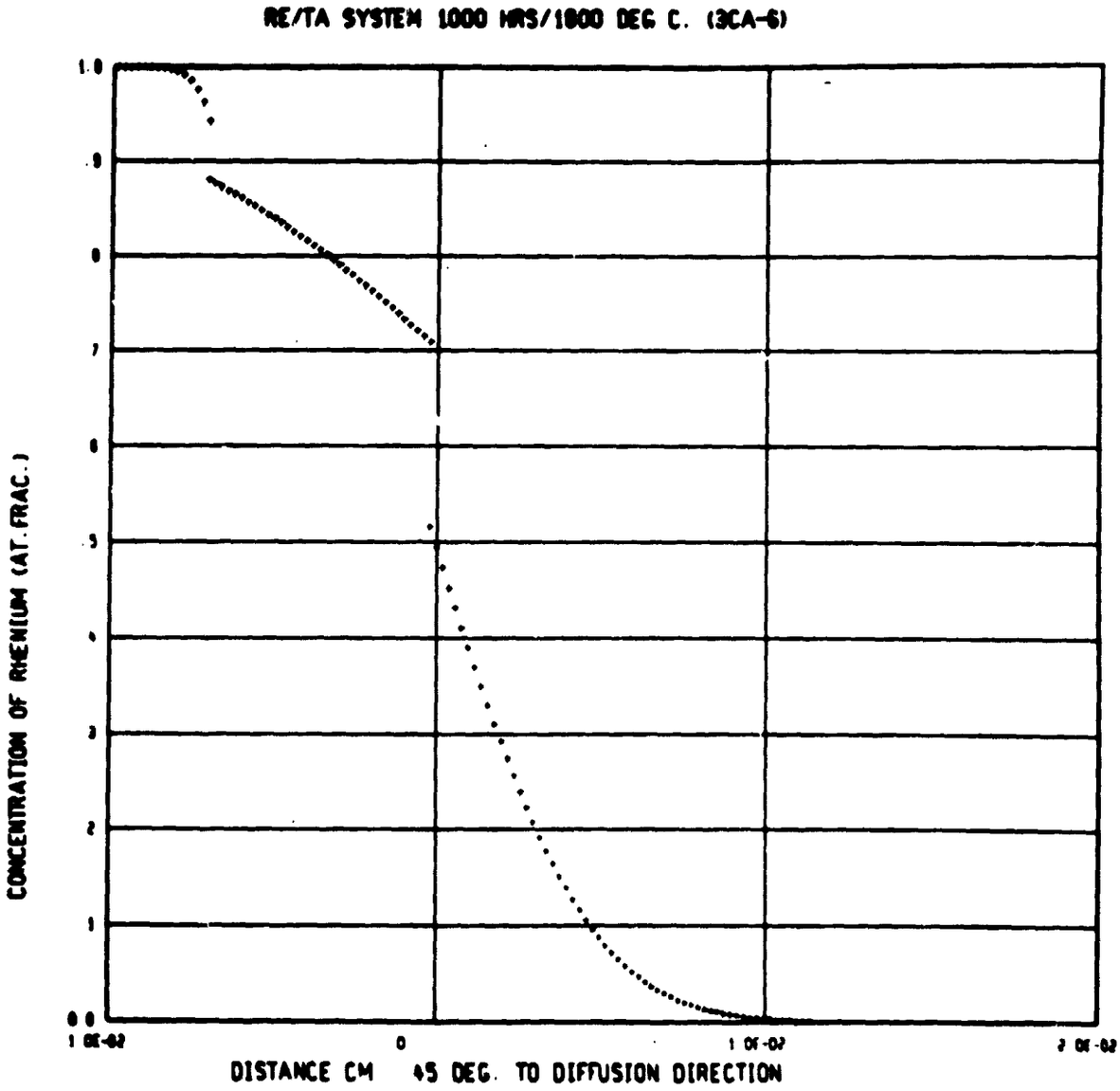

Figure 50. Regenerated (least squares fit) Concentration Profile From Data in Figure 49.

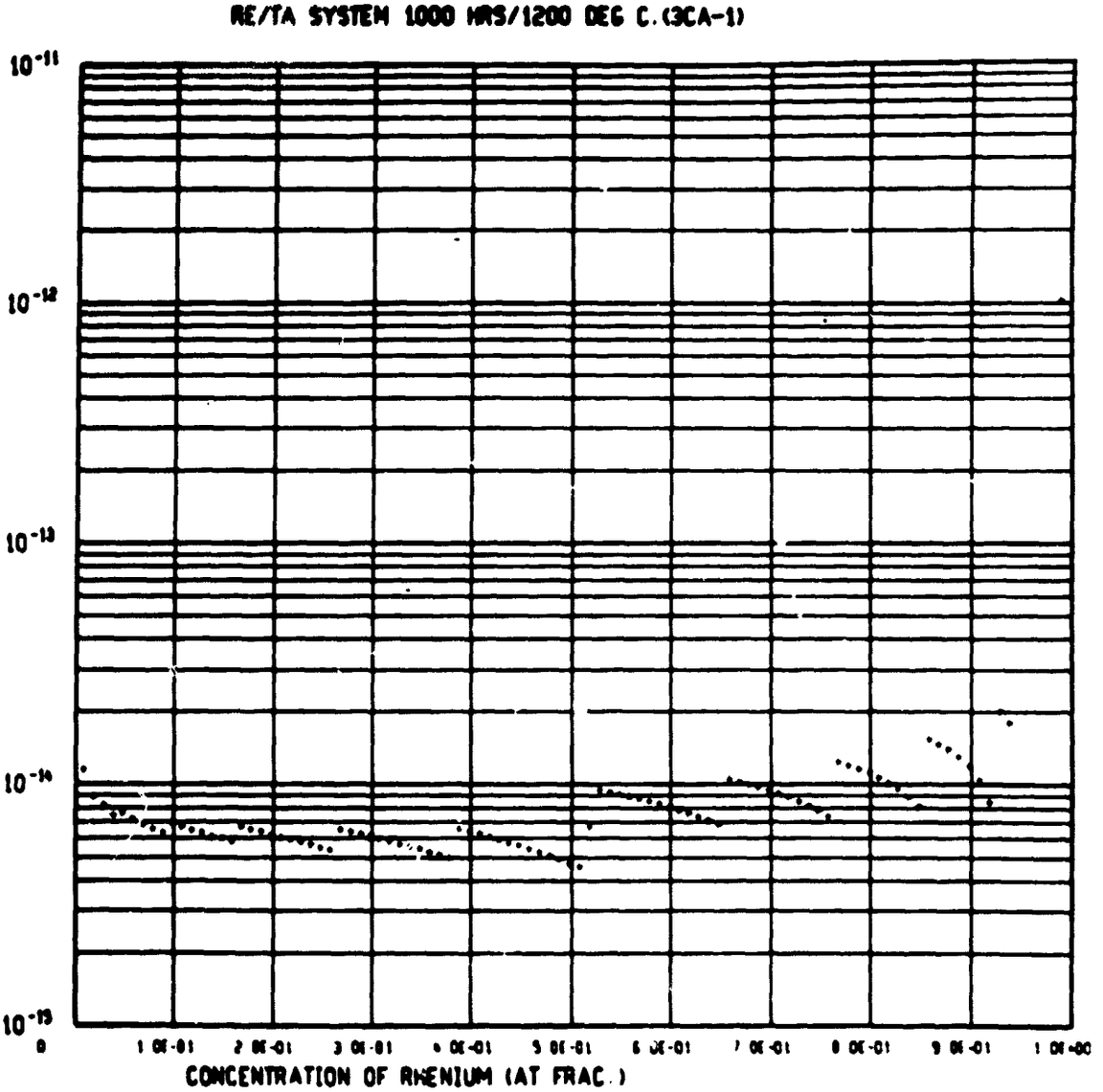

Figure 51. Tantalum-Rhenium Interdiffusion Coefficient at 1200°C (3CA-1)

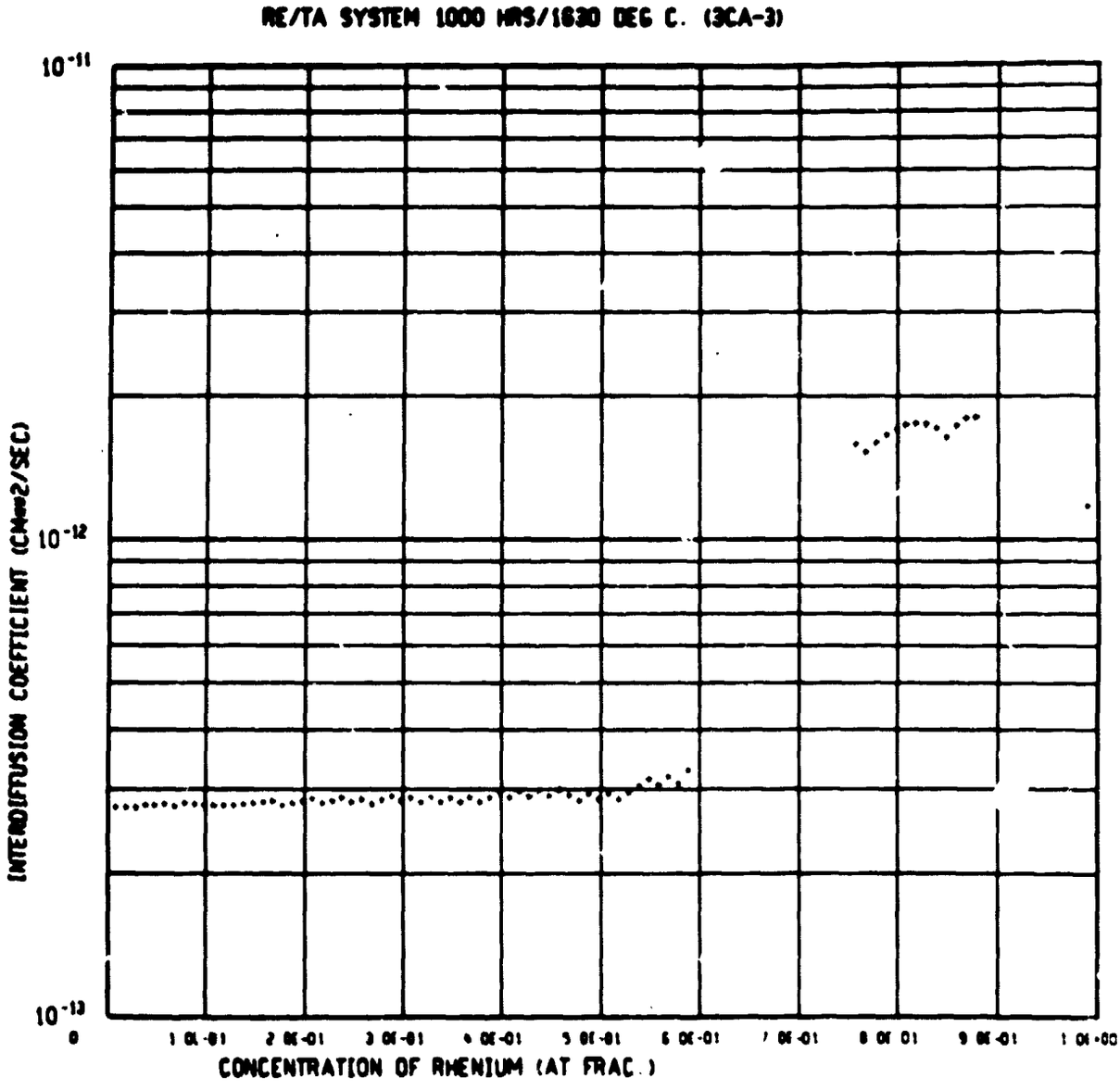

Figure 52. Tantalum-Rhenium Interdiffusion Coefficient at 1630°C (3CA-3)

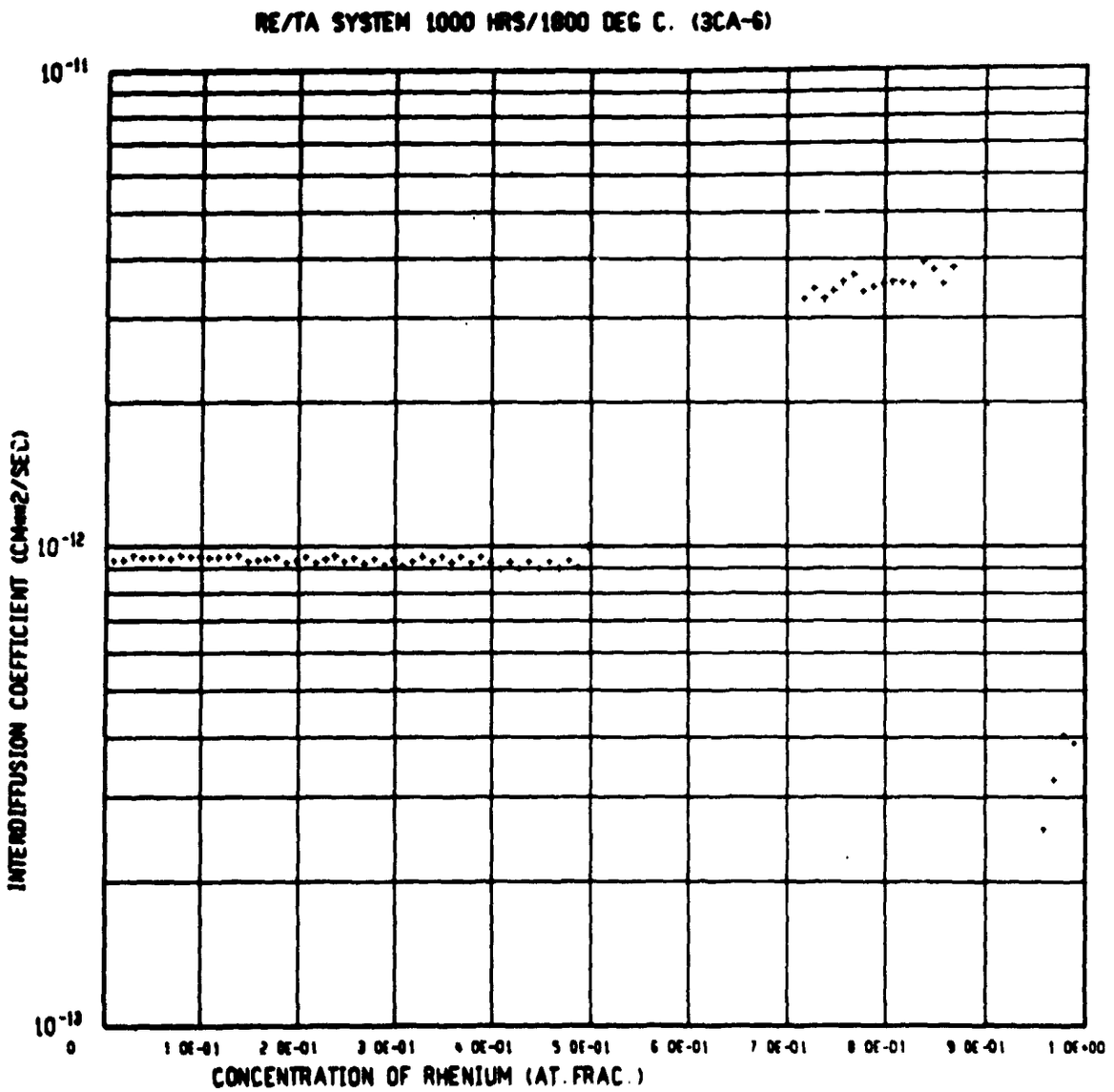

Figure 53. Tantalum-Rhenium Interdiffusion Coefficient at 1800°C (3CA-6)

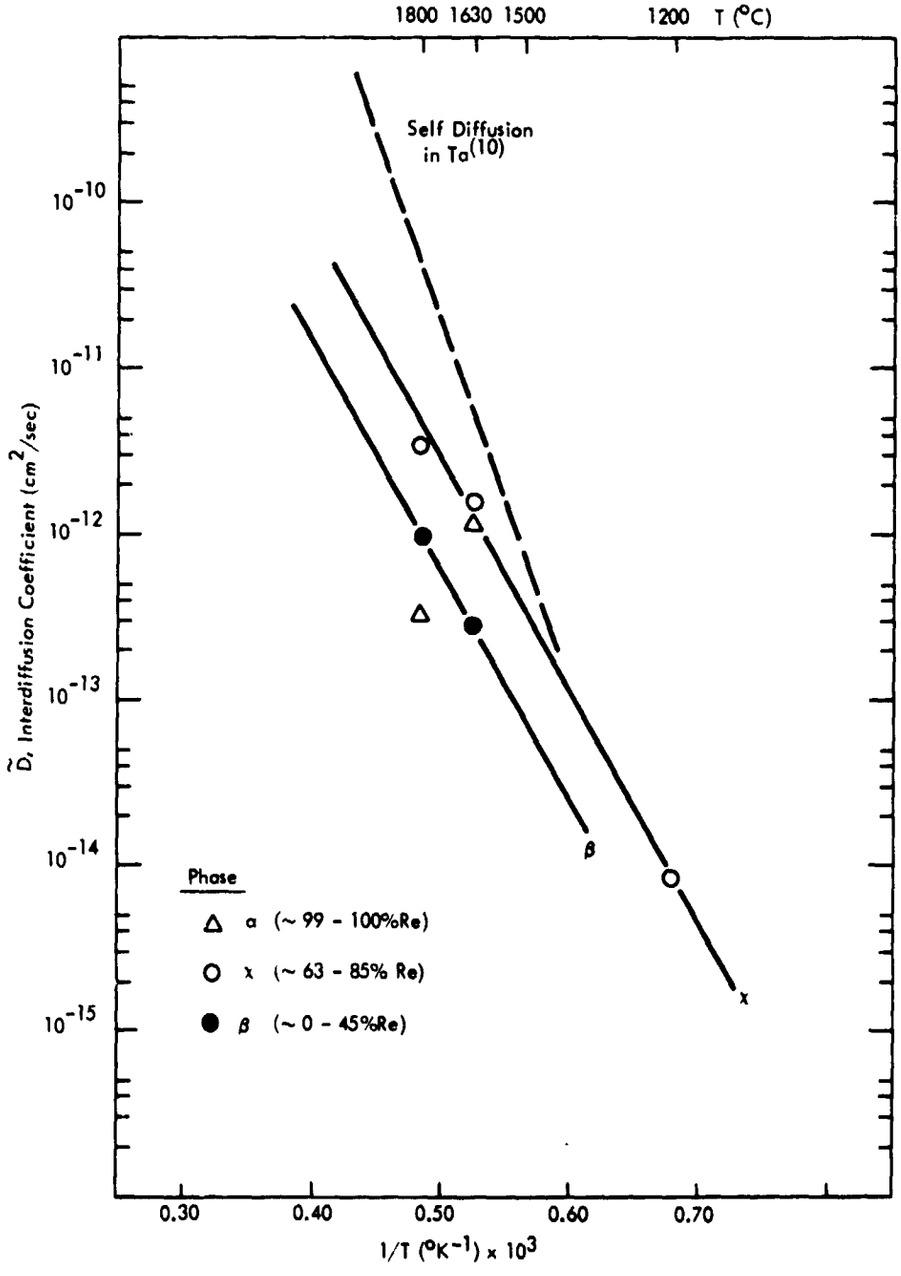

Figure 54. Arrhenius Interdiffusion Coefficient-Temperature Relation for the Tantalum-Rhenium System

4. Tantalum Alloy-Rhenium Systems

The tantalum alloy-rhenium systems diffusion couples form an intermediate phase (X) interdiffusion zone. The T-111 alloy-rhenium (CVD and powder metallurgy product) junctions were formed by autoclave HIP-welding, whereas the ASTAR811C-rhenium junctions were formed by hot press joining. Microprobe trace as-welded diffusion zones for the T-111 junctions were 0.72×10^{-3} cm, while those for the hot press joined ASTAR811C junctions were 1.34×10^{-3} cm. Extrapolations of measured interdiffusion zone widths (from samples aged at 1800 and 2000°C) to time zero resulted in intercepts at 0.90 to 1.80×10^{-3} cm (Figure 55). Analysis of T-111 and ASTAR811C to powder metallurgy and CVD rhenium interdiffusion zone widths is summarized in Table 26.

Figure 56 shows that very little scatter existed for this system and that there is no detectable difference between the systems. A grain boundary diffusion effect for preferentially oriented CVD rhenium grains was not discerned, nor did the difference in alloy base (Hf, Re) constituents influence the interdiffusion zone widths. Least squares computer analysis established the tantalum alloy-rhenium interdiffusion model as

$$\ln \left(\frac{\Delta X^2}{t} \right) = - \frac{36,560 \ (\pm 1730)}{T} - 6.449 \ (\pm 0.137) \qquad (22)$$

where ΔX is the net interdiffusion zone width (affected zone) in centimeters, t is the age time in seconds, and T is the age temperature in °K. Ninety-five percent confidence limits are shown. Literature reviews were unable to reveal other sources of information for this system for comparative purposes.

Figure 57 presents the interdiffusion zone width information as a function of age time, and extrapolations to long age times are provided with equation (22) from Figure 56. A least squares fit correlation coefficient of 0.939 was found for equation (22).

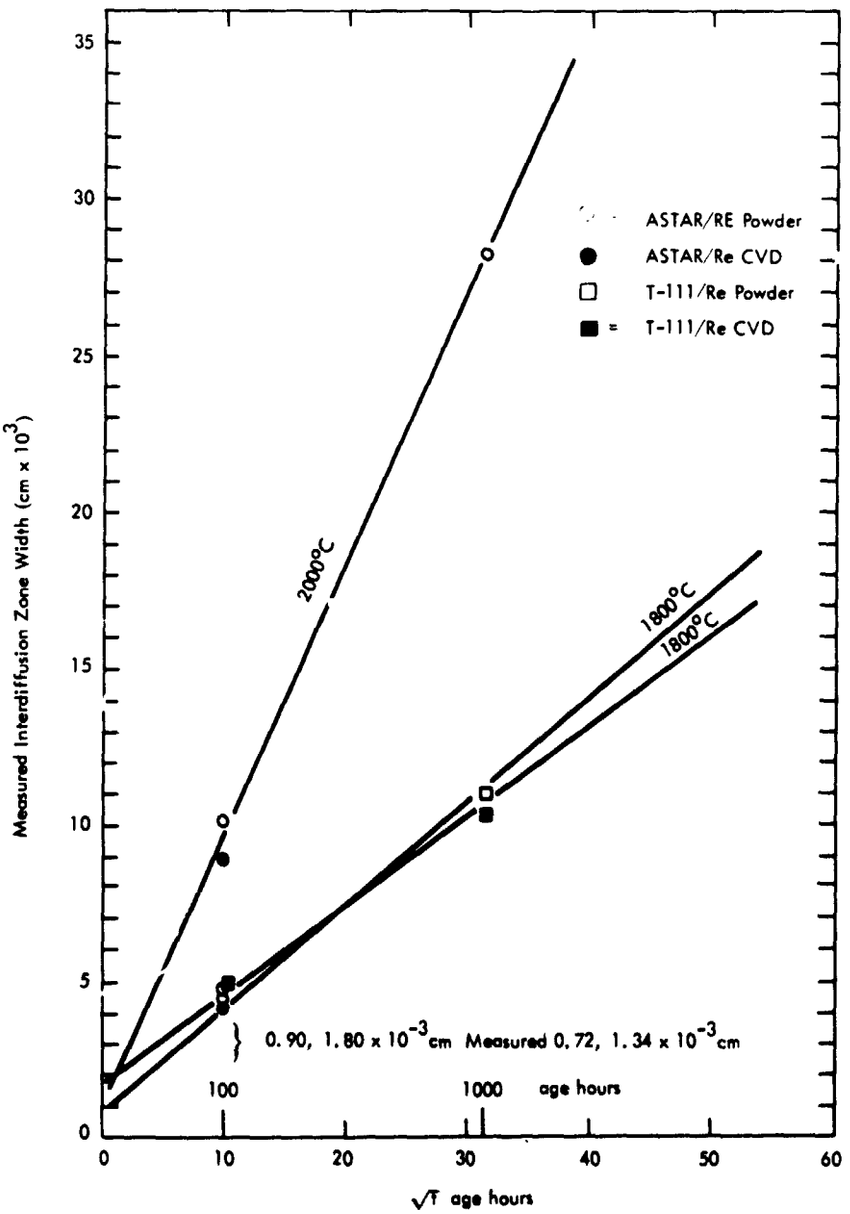

Figure 55. Extrapolation of Measured Interdiffusion Zone Widths to Zero Time to Establish Zero Conditions for the Tantalum Alloy-Rhenium System

Table 26. Tantalum Alloy-Rhenium Couple Systems
Corrected Interdiffusion Zone Widths

Tantalum Alloy Couple	Age Temp. (°C)	Age Time (t) (hrs.)	Age Time (t) (sec. x 10^{-6})	ΔX Interdiffusion Zone Width (cm x 10^3)* Re	ΔX Interdiffusion Zone Width (cm x 10^3)* Ta	$\Delta X^2/t$ (cm^2/sec) Re	$\Delta X^2/t$ (cm^2/sec) Ta
T-111/Re_{powder}**	1800	1000	3.60	□ 10.36	⊡ 10.51	2.98×10^{-11}	3.07×10^{-11}
		100	.36	4.09	3.99	4.65×10^{-11}	4.43×10^{-11}
	1630	1000	3.60	5.14	5.41	7.35×10^{-12}	8.14×10^{-12}
	1500	2000	7.20	3.24	3.29	1.46×10^{-12}	1.51×10^{-12}
	1200	2000	7.20	--+	--+	--+	--+
		1000	3.60	--+	--+	--+	--+
T-111/Re_{CVD}***	1800	1000	3.60	■ 9.71	◆ 9.65	2.62×10^{-11}	2.59×10^{-11}
		100	.36	4.16	3.52	4.81×10^{-11}	3.44×10^{-11}
	1630	1000	3.60	5.27	5.75	7.72×10^{-12}	9.19×10^{-12}
	1500	2000	7.20	3.32	3.16	1.53×10^{-12}	1.39×10^{-12}
	1200	2000	7.20	--+	--+	--+	--+
		1000	3.60	--+	--+	--+	--+
ASTAR/Re_{powder}	2000	1000	3.60	○ 26.88	◇ 27.47	2.01×10^{-10}	2.09×10^{-10}
		100	.36	8.57	8.76	2.04×10^{-10}	2.13×10^{-10}
	1800	1000	3.60	Cracked in Age Furnace			
		100	.36	3.35	3.62	3.12×10^{-11}	3.64×10^{-11}
	1630	1000	3.60	6.40	6.06	1.14×10^{-11}	1.02×10^{-11}
	1500	2000	7.20	2.71	2.57	1.02×10^{-12}	9.17×10^{-13}
	1200	2000	7.20	0.61	0.80	5.09×10^{-14}	8.90×10^{-14}
		1000	3.60	0.35	0.35	3.40×10^{-14}	3.40×10^{-14}
ASTAR/Re_{CVD}	2000	1000	3.60	● 27.56	◆ 28.58	2.11×10^{-10}	2.27×10^{-10}
		100	.36	7.56	8.81	1.59×10^{-10}	2.16×10^{-10}
	1800	1000	3.60	Cracked during age			
		100	.36	2.85	2.85	2.26×10^{-11}	2.26×10^{-11}
	1630	1000	3.60	6.20	6.11	1.07×10^{-11}	1.04×10^{-11}
	1500	2000	7.20	1.92	1.82	5.12×10^{-13}	4.61×10^{-13}
	1200	2000	7.20	0.45	0.41	2.82×10^{-14}	2.34×10^{-14}
		1000	3.60	0.23	0.31	1.47×10^{-14}	2.67×10^{-14}

* Zone width = cm x 10^3, i.e., 1.72 = 1.72 x 10^{-3}cm
Zone width also corrected for as-welded condition

** Re_{powder} = powder rhenium metallurgy product

*** Re_{CVD} = chemical vapor deposited rhenium

\+ Insufficient interdiffusion for accurate analysis

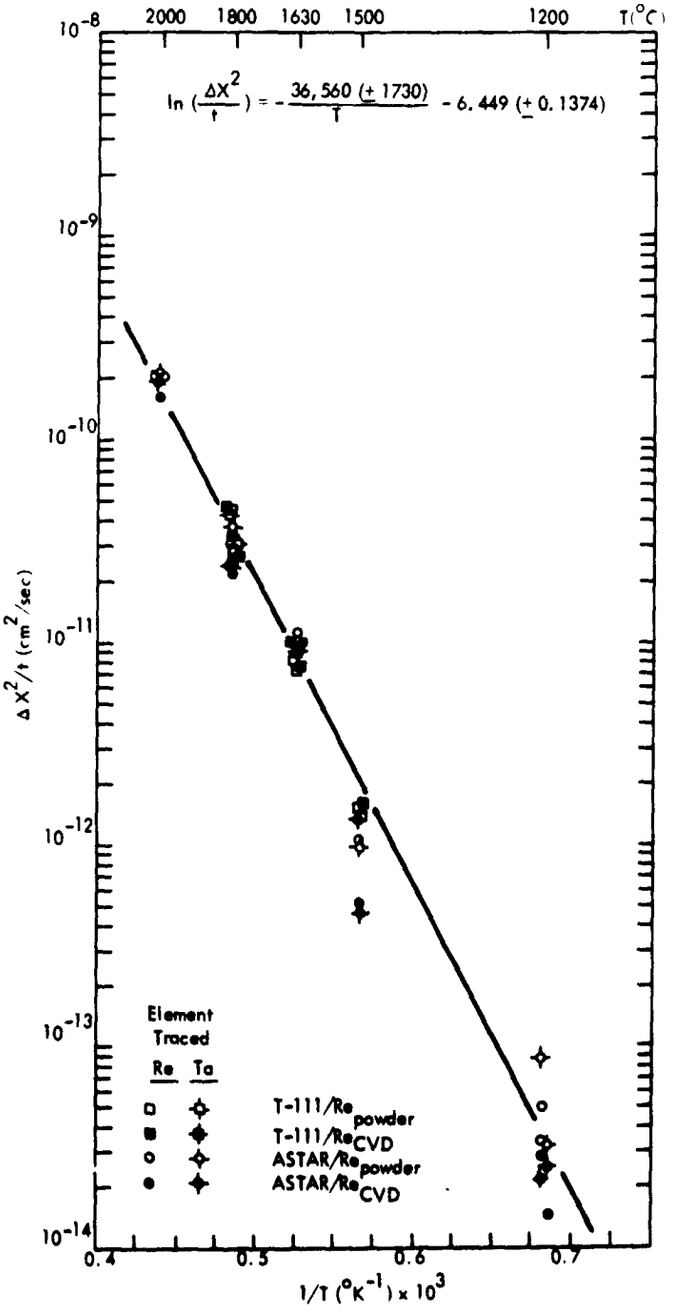

Figure 56. Arrhenius Model for Interdiffusion Zone Width in the Tantalum Alloy-Rhenium Couple System

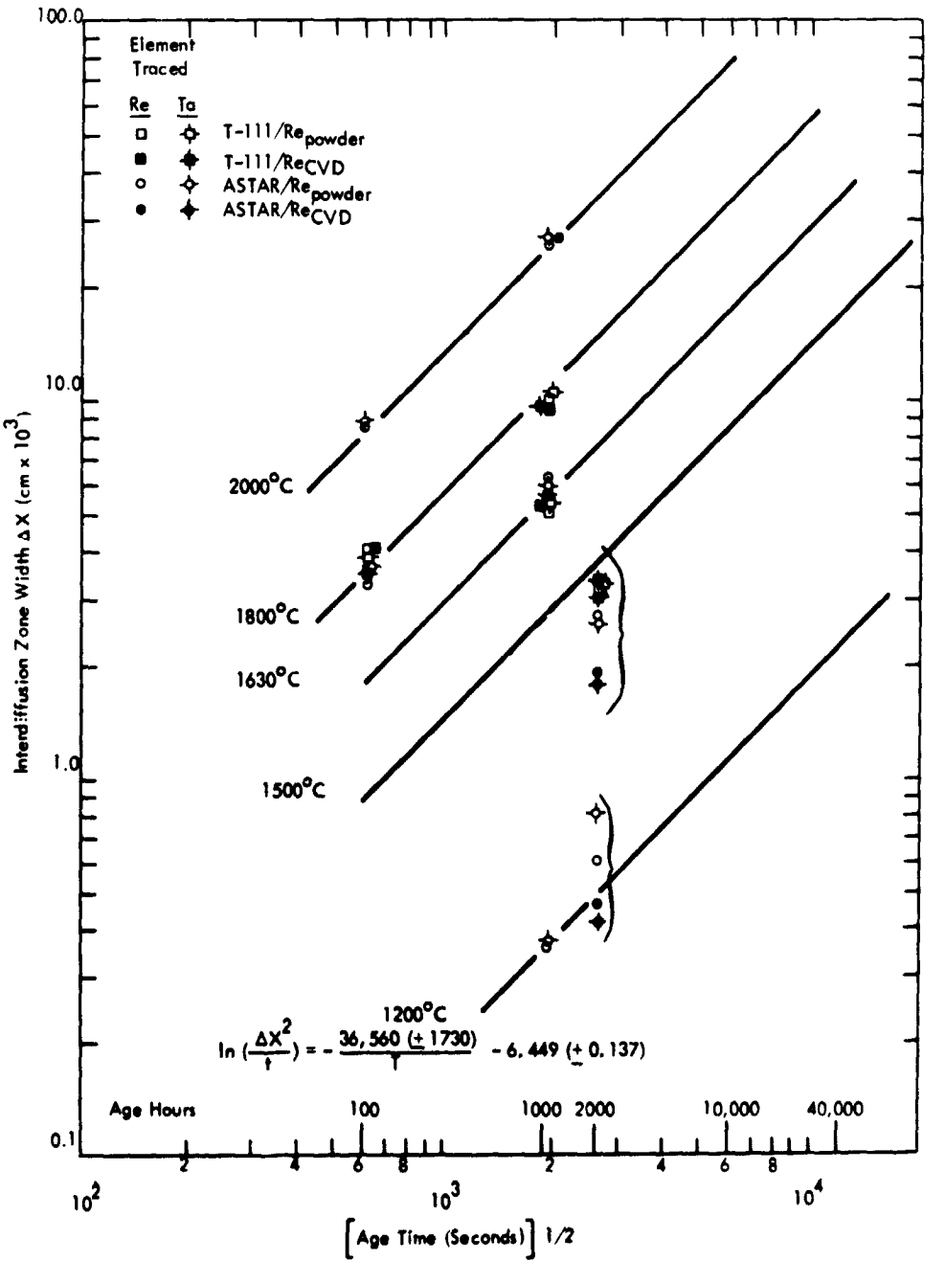

Figure 57. Illustrating Extrapolation of Zone Widths to Long Age Times for Tantalum Alloy (T-111, ASTAR811C)-Rhenium Interdiffusion

A Kirkendall void structure was not observed in the tantalum alloy-rhenium couple interdiffusion zones. ASTAR811C couples to CVD, and powder metallurgy rhenium possessed long cracks through the interdiffusion zone after ageing at 2000 and 1800°C for 1000 hours (Figure 58) but possessed no cracks after short 100 hour age at these temperatures. The T-111 couples aged at 1800°C for 1000 hours did not crack in the interdiffusion zone (Figure 59). It is probable that some interdiffusion zone width must be exceeded before cracking (thermal stress induced) will occur, and the additional presence of rhenium in ASTAR811C (over T-111) causes it to have a lower crack threshhold.

Boltzmann-Matano diffusion analysis was not performed on the T-111, ASTAR811C to rhenium interdiffusion zones since the effects of ternary and higher elemental additions could not be adequately described by the limited number of couple (alloy) combinations employed here.

C. MOLYBDENUM-RHENIUM SYSTEMS

1. Molybdenum-50Rhenium to Tungsten Systems

The molybdenum-50rhenium to tungsten (arc cast and CVD) diffusion couples form intermediate phase (discontinuous concentration profile) interdiffusion zones. Both tungsten system couples were formed by hot press joining. Microprobe trace measured as-welded zone widths were 2.2×10^{-3} cm. Figure 60 shows that an extrapolation of measured interdiffusion zone widths for 1800°C ages to time zero results in an intercept at 2.2×10^{-3} cm. Analysis of molybdenum-50rhenium interdiffusion with tungsten (arc cast and CVD) is summarized in Table 27.

Figure 61 shows that very little scatter existed for this system and that no discernible differences were found between the tungsten systems. A grain boundary diffusion effect for preferentially oriented CVD tungsten grains was not found. The interdiffusion zone widths

Figure 58. Illustrating Crack in Interdiffusion Zone (X Phase) of ASTAR811C-CVD Rhenium Diffusion Couple After Ageing at 2000°C for 1000 hours (4FA-8) at 200X

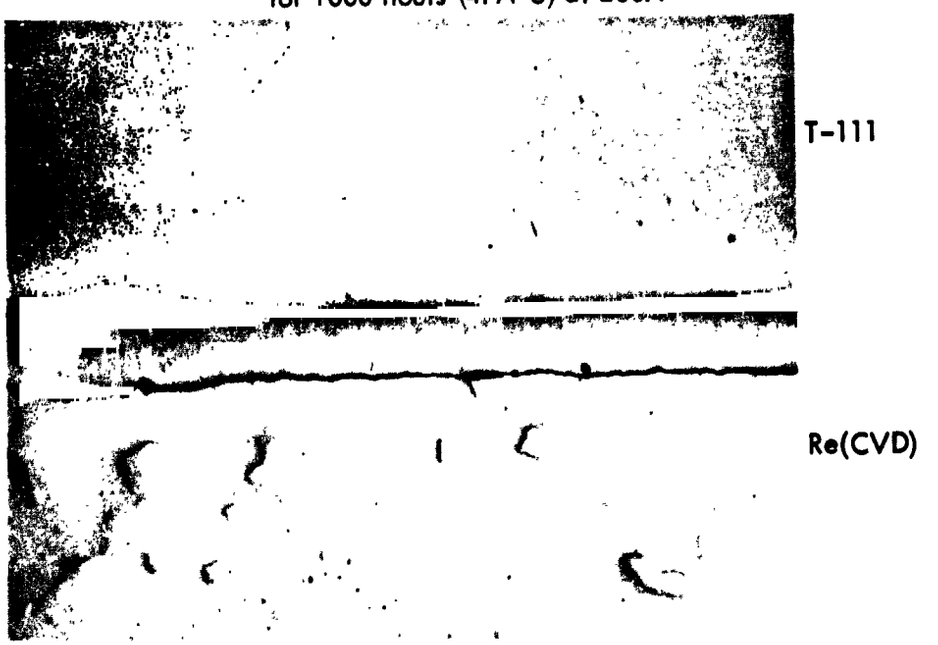

Figure 59. Interdiffusion Zone (X Phase) in T-111-Rhenium (powder metallurgy product) Diffusion Couple After Ageing at 1800°C for 1000 hours (3EA-6)at 200X

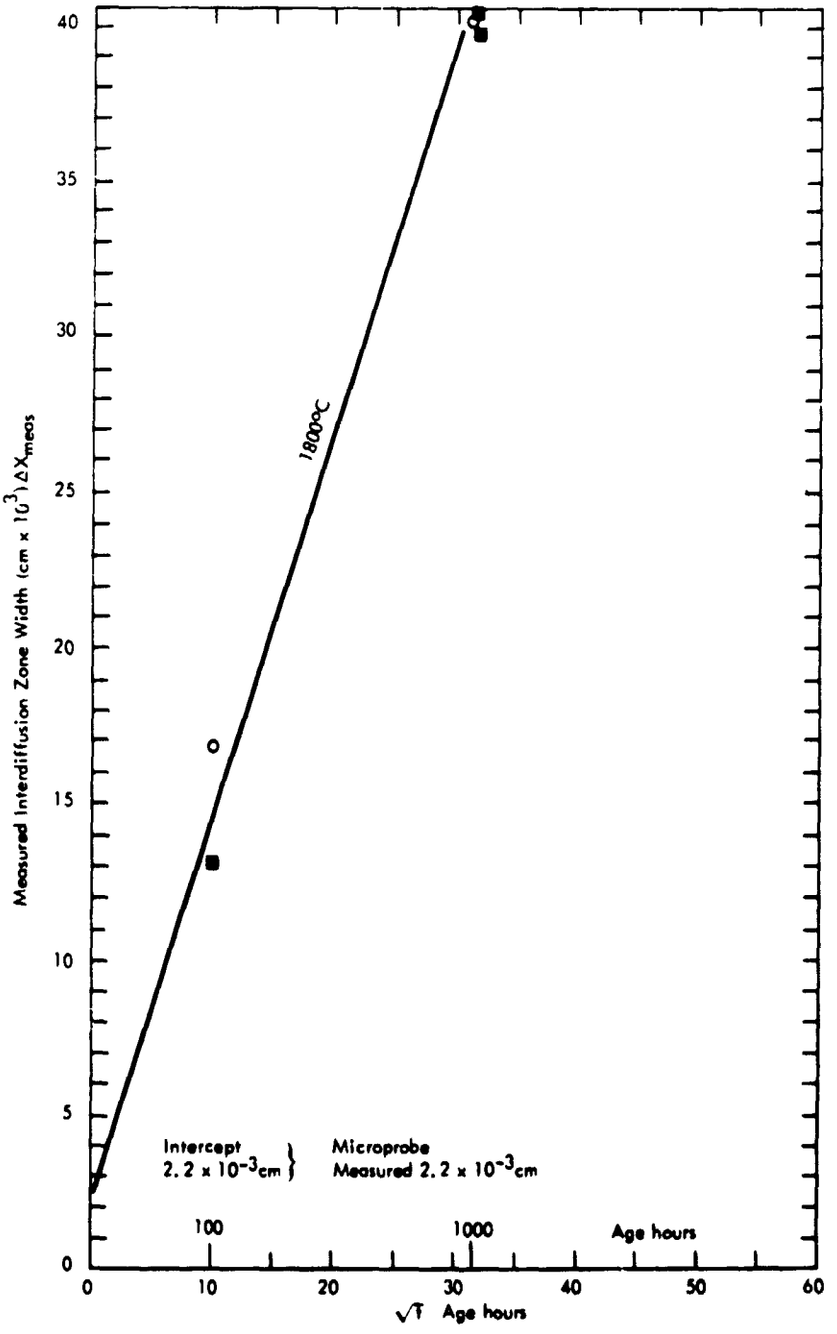

Figure 60. Extrapolation of Measured Interdiffusion Zone Widths to Zero Time to Establish Zero Condition for the Molybdenum-50Rhenium/Tungsten System

Table 27. Mo-50Re/Tungsten-Rhenium Couple Systems
Corrected Interdiffusion Zone Widths

Mo-50Re Alloy Couple	Age Temp. (°C)	Age Time (t) (hrs.)	Age Time (t) (sec. x 10^{-6})	ΔX Interdiffusion Zone Width (cm x 10^3)		$\Delta X^2/t$ (cm^2/sec)	
				W	Re		
Mo-50Re/W_{arc} **	2000	1000	3.60	○ 96.60	104.60	2.56×10^{-9}	3.04×10^{-9}
		100	.36	23.75	--+**	1.57×10^{-9}	--+**
	1800	1000	3.60	40.20	38.6	4.49×10^{-10}	4.14×10^{-10}
		100	.36	14.69	11.23	6.00×10^{-10}	3.50×10^{-11}
	1630	1000	3.60	15.79	15.79	6.93×10^{-11}	6.93×10^{-12}
	1500	100	.36	2.09	1.35	1.21×10^{-11}	5.06×10^{-12}
Mo-50Re/W_{CVD} ***	2000	1000	3.60	■ 108.5	98.2	3.27×10^{-9}	2.71×10^{-9}
		100	.36	32.0	29.30	2.85×10^{-9}	2.39×10^{-9}
	1800	1000	3.60	39.70, 42.30	16.15	4.38×10^{-10}, 4.97×10^{-10}	7.25×10^{-11}
		100	.36	10.94	10.11	3.32×10^{-10}	2.84×10^{-10}
	1630	1000	3.60	16.81	17.42	7.85×10^{-11}	8.43×10^{-11}
	1500	100	.36	1.41	0.49	5.52×10^{-12}	6.67×10^{-13}
Mo-50Re/$Re_{pdr.}$ +	2000	1000	3.60	□ --+**	43.24		5.20×10^{-10}
		100	.36	--+**	11.12		3.44×10^{-10}
	1800	1000	3.60	--+**	16.59		7.65×10^{-11}
		100	.36	--+**	5.88		9.61×10^{-11}
	1630	1000	3.60	--+**	10.93		3.32×10^{-11}
	1500	2000	7.20	--+**	8.54		1.01×10^{-11}
	1500	100	.36	--+**	2.09		1.21×10^{-11}
Mo-50Re/Re_{CVD} +*	2000	1000	3.60	● --+**	35.53		3.51×10^{-10}
		100	.36	--+**	11.23		3.50×10^{-10}
	1800	1000	3.60	--+**	15.42		6.61×10^{-11}
		100	.36	--+**	6.90		1.32×10^{-10}
	1630	1000	3.60	--+**	10.89		3.29×10^{-11}
	1500	2000	7.20	--+**	8.14		9.20×10^{-12}
	1500	100	.36	--+**	1.62, 1.42		7.29×10^{-12}, 5.56×10^{-12}

* Zone width = cm x 10^3, i.e., 1.72 = 1.72 x 10^{-3}cm
Zone width also corrected for as-welded condition

** W_{arc} = arc cast tungsten

*** W_{CVD} = chemical vapor deposited tungsten

\+ Re_{powder} = powder metallurgy rhenium

+* Re_{CVD} = chemical vapor deposited rhenium

+** Not analyzed

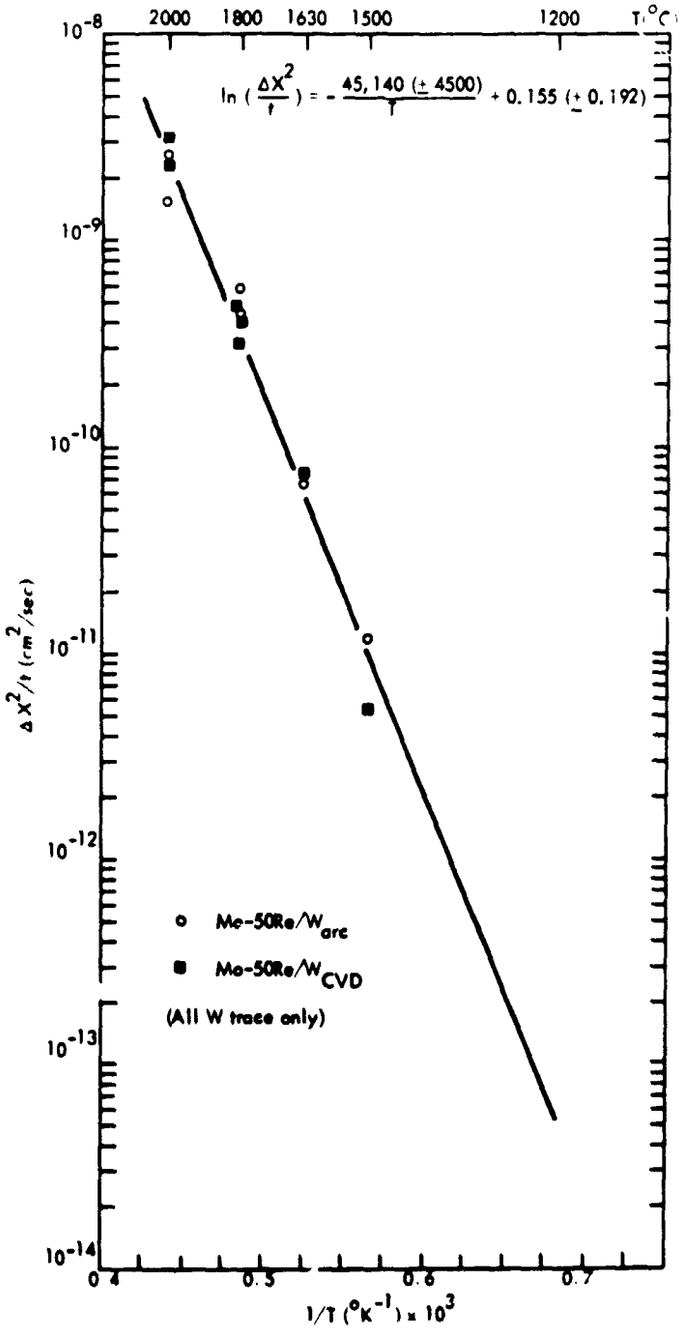

Figure 61. Arrhenius Model for Interdiffusion Zone Width in the Molybdenum-50Rhenium/Tungsten Couple System

measured were large compared to those of other systems, and since they exceeded zero time as-welded conditions by one order of magnitude, the result was very little data scatter. Least squares computer analysis established the molybdenum-50 rhenium/tungsten interdiffusion model as

$$\ln\left(\frac{\Delta X^2}{t}\right) = -\frac{45,140\ (\pm 4500)}{T} + 0.155\ (\pm 0.192) \qquad (23)$$

where ΔX is the net interdiffusion zone width (affected zone) in centimeters, t is age time in seconds, and T is age temperature in $^{\circ}K$. Ninety-five percent confidence limits are shown. Literature reviews did not reveal other sources of information for this system for comparison purposes.

Figure 62 presents the interdiffusion zone width information as a function of age time, and extrapolations to long age times are provided with equation (23) from Figure 61. A least squares fit correlation coefficient of 0.894 was found for equation (23).

Only tungsten concentration profiles were analyzed for Figures 61 and 62 since they formed the largest interdiffusion zone widths, and the rhenium zone widths were generally less than or equal to those of the tungsten trace. The tungsten zone widths exceeded those of rhenium at high temperatures and equaled them at low temperatures. This variation resulted because the molybdenum-50rhenium/tungsten diffusion couple is a strong ternary system. Whereas the diffusion path in a binary system is constant, that in a ternary system is variable. Figure 63 represents a typical interdiffusion concentration path in a ternary system. This sinusoidal effect is due to the different mobilities of the ternary constituents. If several phase fields were present in Figure 64, then the diffusion path would follow tie lines through two phase regions and could trace a surprisingly extended path. If C (in Figure 63) were tungsten, and A and B were molybdenum and rhenium, the interdiffusion path, which occurred in couples of tungsten to molybdenum-50rhenium would follow the trends exhibited. However, as Figure 64 demonstrates, a two phase field is intercepted by the interdiffusion path, and an intermediate phase (σ) is created in the interdiffusion zone.

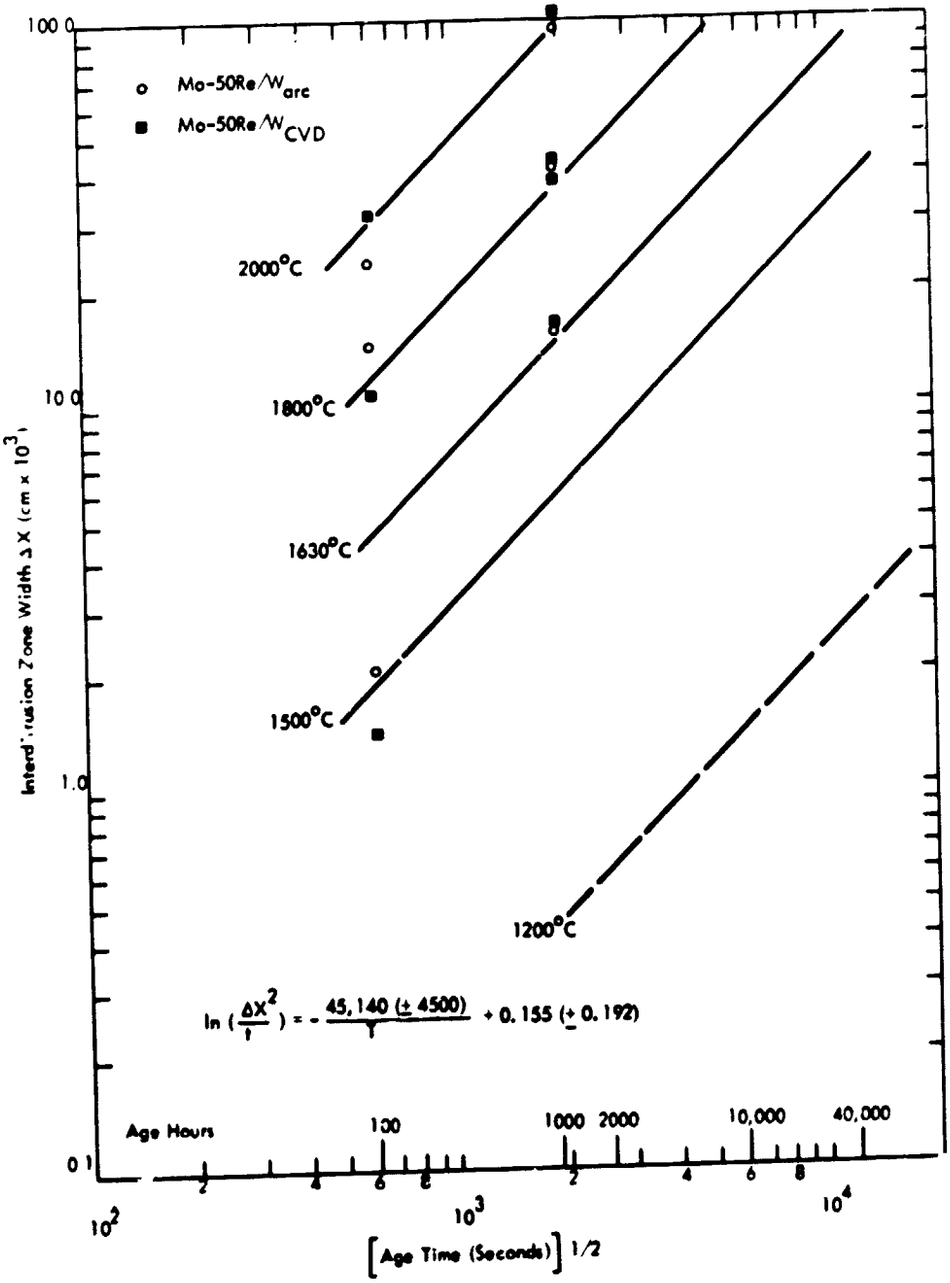

Figure 62. Illustrating Extrapolation of Zone Widths to Long Age Times for Molybdenum-50Rhenium/Tungsten Interdiffusion

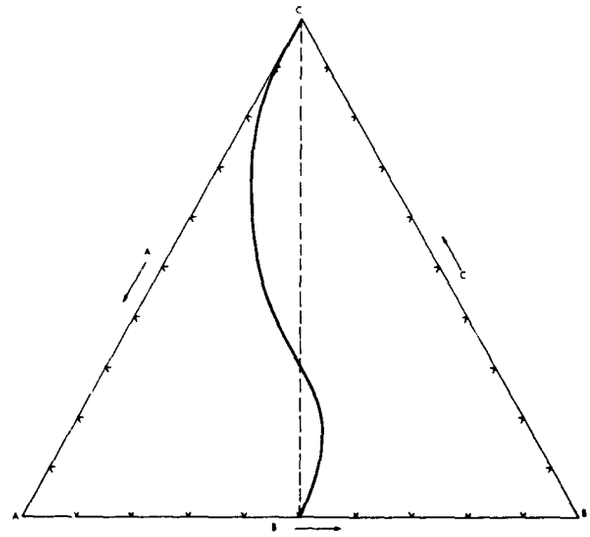

Figure 63. Illustrating Typical Diffusion Path for Ternary Couple C/50A-50B

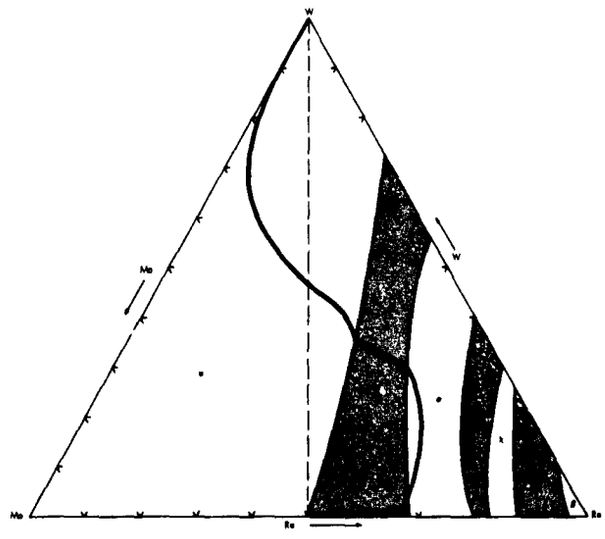

Figure 64. Interdiffusion Path of Tungsten to Molybdenum-50Rhenium Couples[11]

As exhibited in Figure 64, the diffusion path initially parallels the tungsten-molybdenum base of the ternary phase diagram, resulting in changes in tungsten and molybdenum concentration but following iso-rhenium concentration lines. Since molybdenum has the lowest melting point on its side of the interface, its preferred interdiffusion (higher mobility) with tungsten would be expected. The sinusoidal diffusion path is shallower at lower temperatures, resulting in more equal interdiffusion zone widths for tungsten and rhenium traces.

Binary Boltzmann-Matano interdiffusion analysis was not performed in this system due to its ternary character. Ternary Matano analysis could not be performed without significantly more couple combinations of varying composition for each age temperature.

Metallographic study of the interdiffusion zones for the couples of this system did show an intermediate phase in the interdiffusion zone. Figure 65 shows such a zone (σ phase) for a molybdenum-50 rhenium/tungsten couple aged at 1800°C for 100 hours. Kirkendall voids were not observed in the interdiffusion zone of this system. Interdiffusion zone cracking did not occur for any of the age temperatures or age times.

2. Molybdenum-50Rhenium to Rhenium Systems

The molybdenum-50rhenium to rhenium system diffusion couples form an intermediate phase (σ,χ) interdiffusion zone. All junctions were formed by autoclave HIP-welds, resulting in minimal interdiffusion zones. Molybdenum-50rhenium was joined to CVD and powder metallurgy product rhenium. Microprobe trace measured as-welded zero condition zone widths were 0.66×10^{-3} cm. Analysis of the interdiffusion zone widths for this system are presented in Table 27. (See Section C.1, Molybdenum-50Rhenium to Tungsten Systems.) Only rhenium concentration profiles were traced for this binary system.

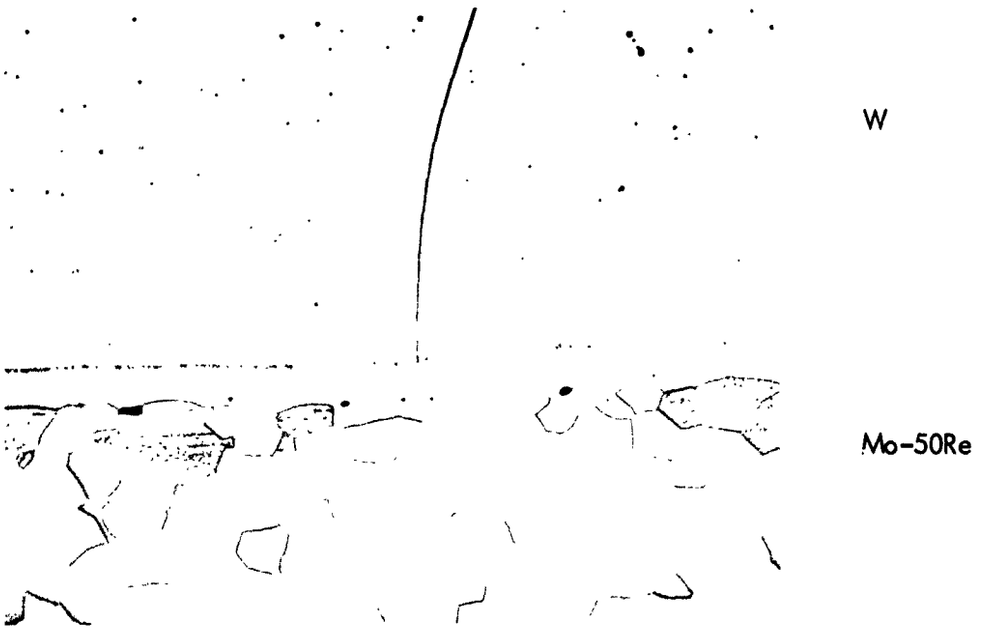

Figure 65. An Intermediate Phase (σ) Exists in the Interdiffusion Zone of the Molybdenum-50Rhenium/Tungsten Couple Aged at 1800°C for 100 hours (11A-3). View at 200X

Figure 66 shows that very little scatter existed for this system and that there is no difference between the systems. A grain boundary diffusion effect for preferentially oriented CVD rhenium grains was not observed. Least squares computer analysis established the molybdenum-50rhenium to rhenium interdiffusion model as:

$$\ln\left(\frac{\Delta X^2}{t}\right) = -\frac{30,140\ (\pm 2940)}{T} - 8.480\ (\pm 0.147) \qquad (24)$$

where ΔX is the net interdiffusion zone width (affected zone) in centimeters, t is age time in seconds, and T is age temperature in ^{o}K. Ninety-five percent confidence limits are shown. The interdiffusion zone width, ΔX, extends from 50 to 100 weight percent (33 to 100 atomic percent) rhenium. Literature reviews did not reveal other sources of zone width information for this system.

Figure 67 presents the interdiffusion zone width information as a function of age time, and extrapolations to long age times are provided with equation (24) from Figure 66. A least squares fit correlation coefficient of 0.929 was found for equation (24).

Although Kirkendall voids were not observed in this system for the age times and temperatures employed, photomicrographs did reveal a wide interdiffusion zone with σ and χ phases present (Figure 68). Interdiffusion zone cracking only occurred for the ages at 2000°C (Figure 69).

For Boltzmann-Matano analysis of the molybdenum-50rhenium to rhenium system, only rhenium concentration traces were analyzed. Electron microprobe spot count traverses were made on samples*:

31A-6	2000°C	100 hours
31A-5	1800°C	1000 hours
41A-1	1500°C	100 hours

* Part II, Appendix F, Diffusion Couple Age/Identification Chart

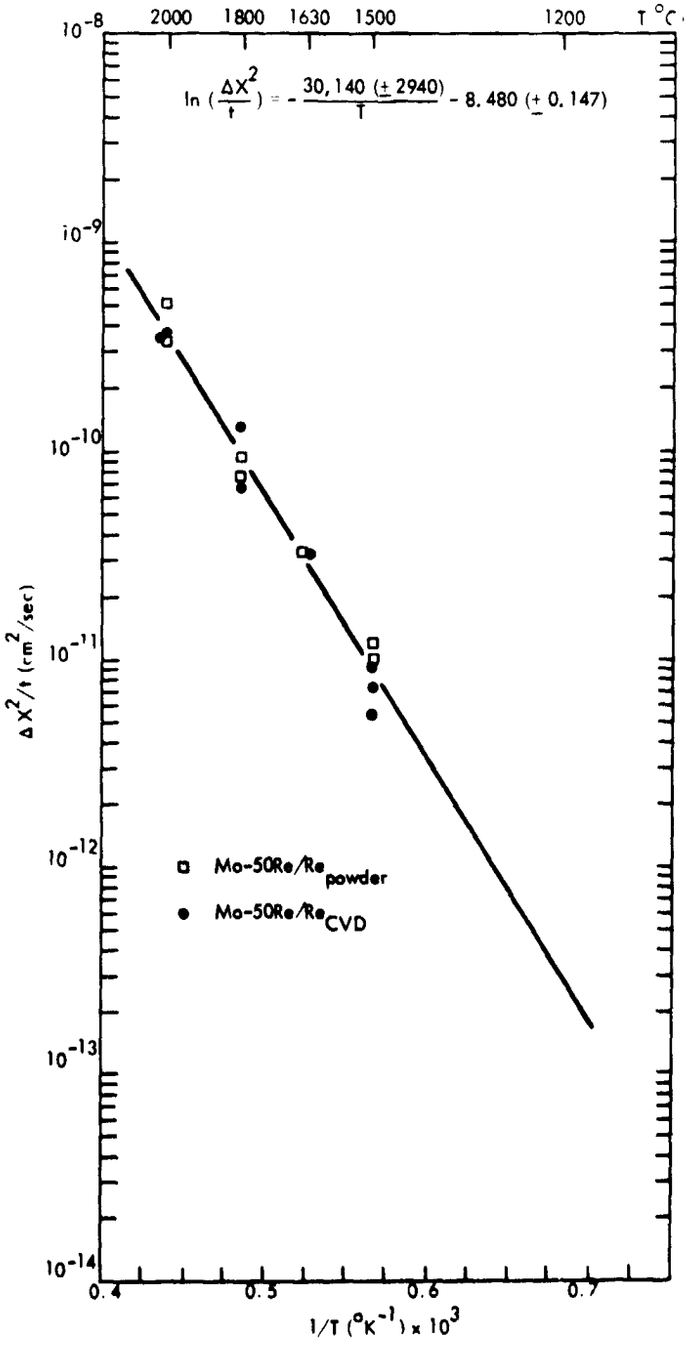

Figure 66. Arrhenius Model for Interdiffusion Zone Width in the Molybdenum-50Rhenium to Rhenium Couple System

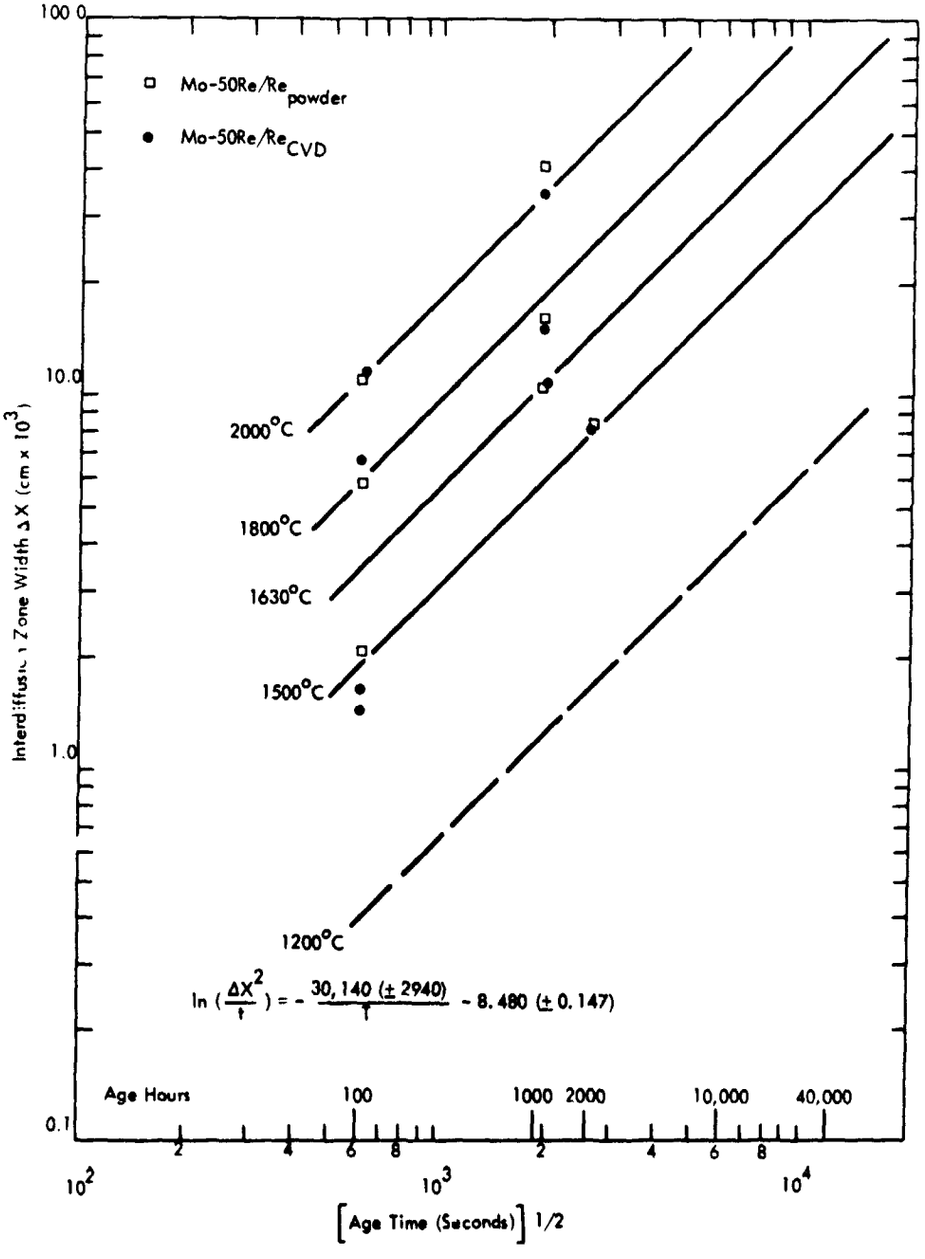

Figure 67. Illustrating Extrapolation of Zone Widths to Long Age Times for Molybdenum-50Rhenium to Rhenium Interdiffusion

Figure 68. The Molybdenum-50Rhenium to CVD Rhenium Interdiffusion Zone After Ageing at 1800°C for 1000 hours (41A-5) at 200X

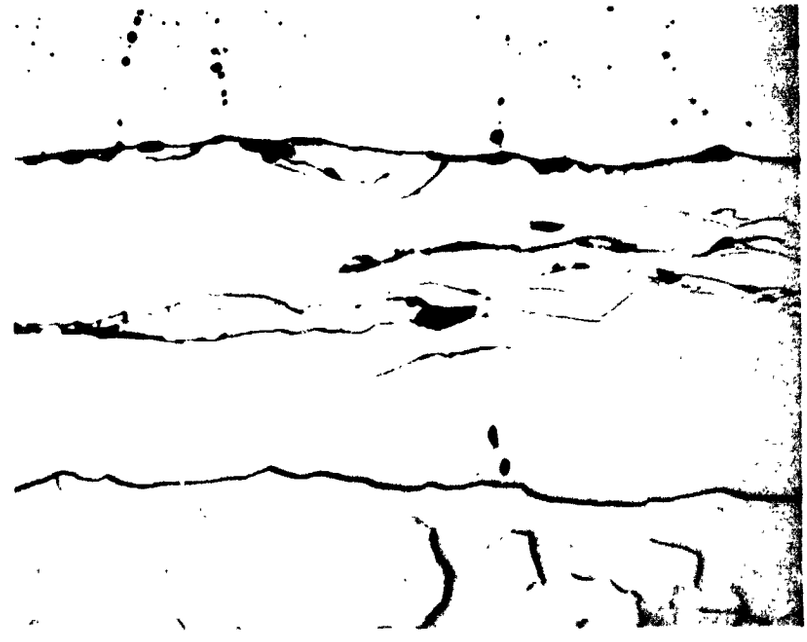

Figure 69. The Type of Cracking Which Occurred in the Molybdenum-50Rhenium to Rhenium Interdiffusion Zone After Ages at 2000°C (Couple 31A-7, 2000°C, for 1000 hours at 200X)

and the Colby MAGIC* corrected concentration profiles were loaded into the Hartley** Boltzmann-Matano analysis computer program after being fitted, in probability coordinates, for curve smoothing. Interdiffusion phase concentrations (limits) did not correspond to that for published phase diagrams.[11] For instance, at 1500°C the σ and χ phase regions should extend from .52 to .68 and .72 to .78 atom fraction rhenium, respectively. Concentration ranges in sample 41A-1 were .55 - .58 and .64 - .76 atomic fraction rhenium, respectively. This could be because the system was dynamic, and equilibrium conditions had not been established. Figures 70, 71, and 72 present the interdiffusion coefficients for this system as plotted by computer subroutine.

Interdiffusion coefficients at 1500°C (Figure 70) were only accurate in the χ phase due to the small σ phase limit and due to the previously described limited phase extent of the σ phase (0.72 - 0.78 atom fraction rhenium). Interdiffusion coefficients at 1800 and 2000°C were more accurately derived from larger phase field regions.

Figure 73 presents the Arrhenius interdiffusion relation for the molybdenum-rhenium system. The interdiffusion coefficients cross that for molybdenum self-diffusion, and are plotted as mean $\tilde{D}$ values for each phase region. Self-diffusion data for rhenium was not found in the literature. Due to the scatter in the calculated $\tilde{D}$ values, Arrhenius form predictive equations were not derived from Figure 73. The scatter is due to the difficulty in establishing $\tilde{D}$ values at 1500°C and to the small χ phase field at higher temperatures. The molybdenum-50rhenium to rhenium interdiffusion coefficient at 1500 to 2000°C is in the 10^{-11} to 10^{-12} cm^2/sec range.

3. Tungsten-Rhenium-Molybdenum to Tungsten

The tungsten-30.9rhenium-20.1molybdenum alloy to tungsten (CVD, arc cast) system diffusion couples form solid solution interdiffusion zones. Couples for this system were formed

*Part II, Appendix J, Colby Computer Program for Correcting Microprobe Intensity Analysis.
**Part II, Appendix H, Hartley Computer Program for Boltzmann-Matano Diffusion Analysis.

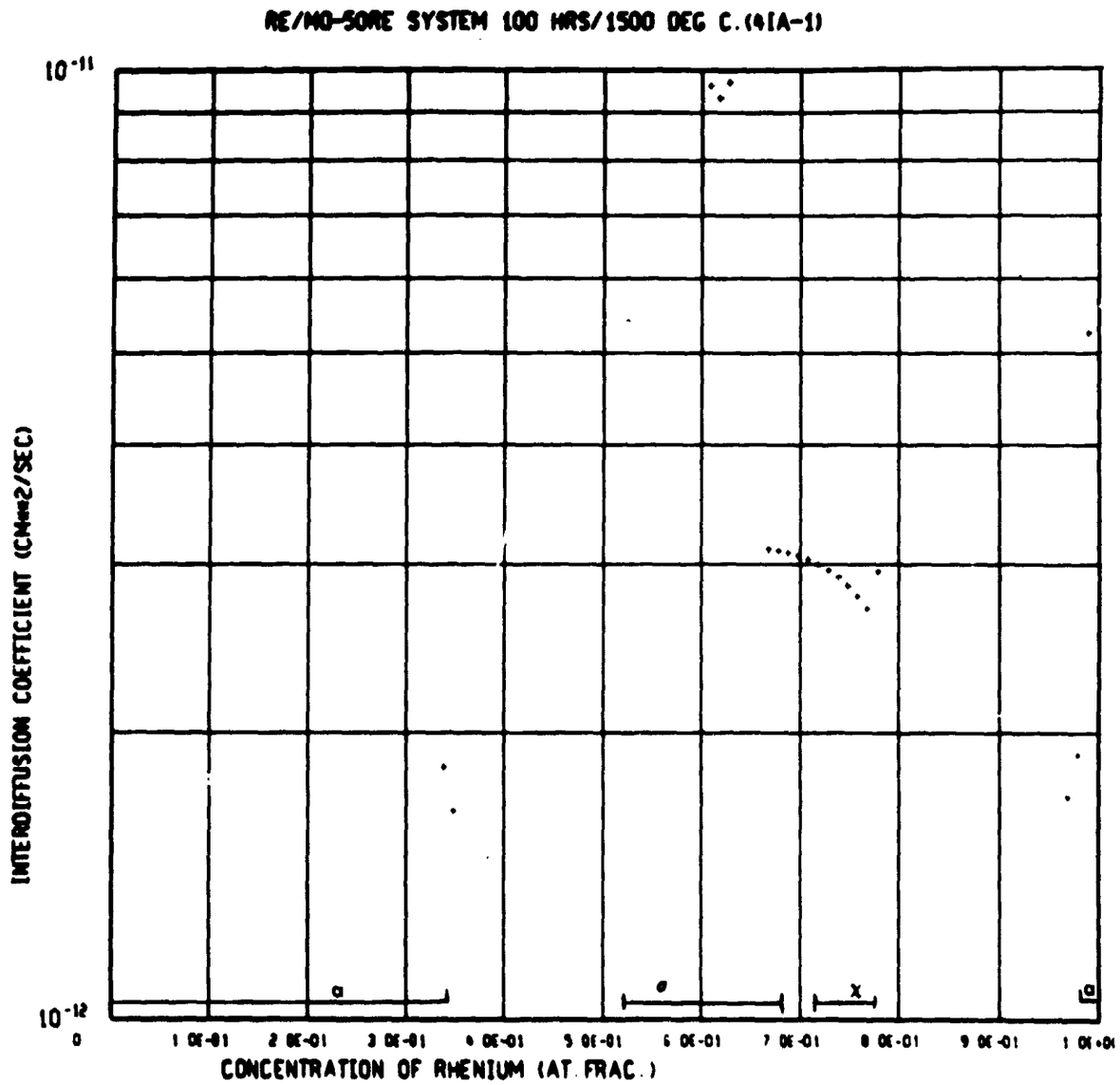

Figure 70. Molybdenum-50Rhenium to Rhenium χ Phase Interdiffusion Coefficient at 1500°C (41A-1)

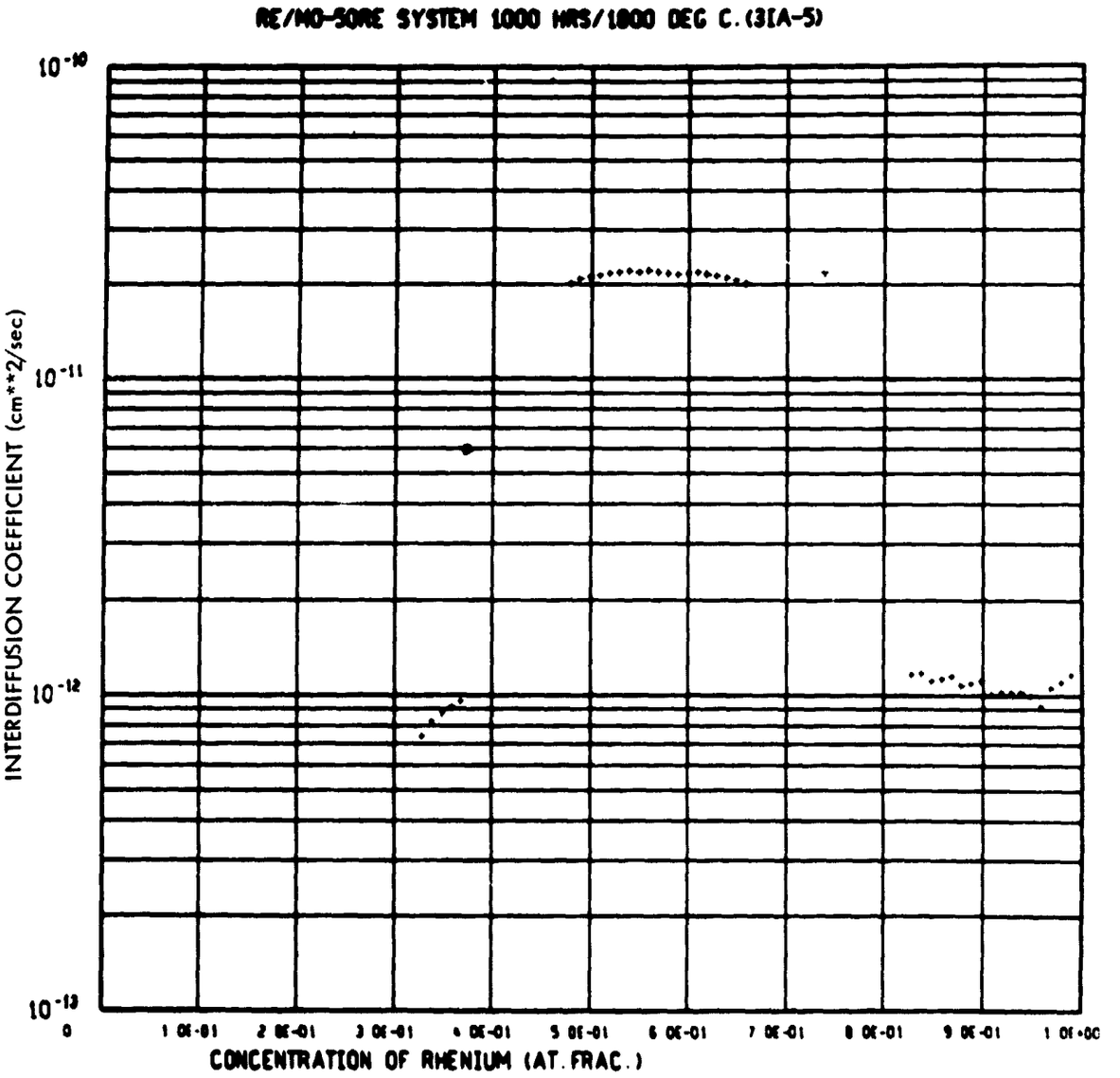

Figure 71. Molybdenum-50Rhenium to Rhenium Interdiffusion Coefficient at 1800°C (3IA-5)

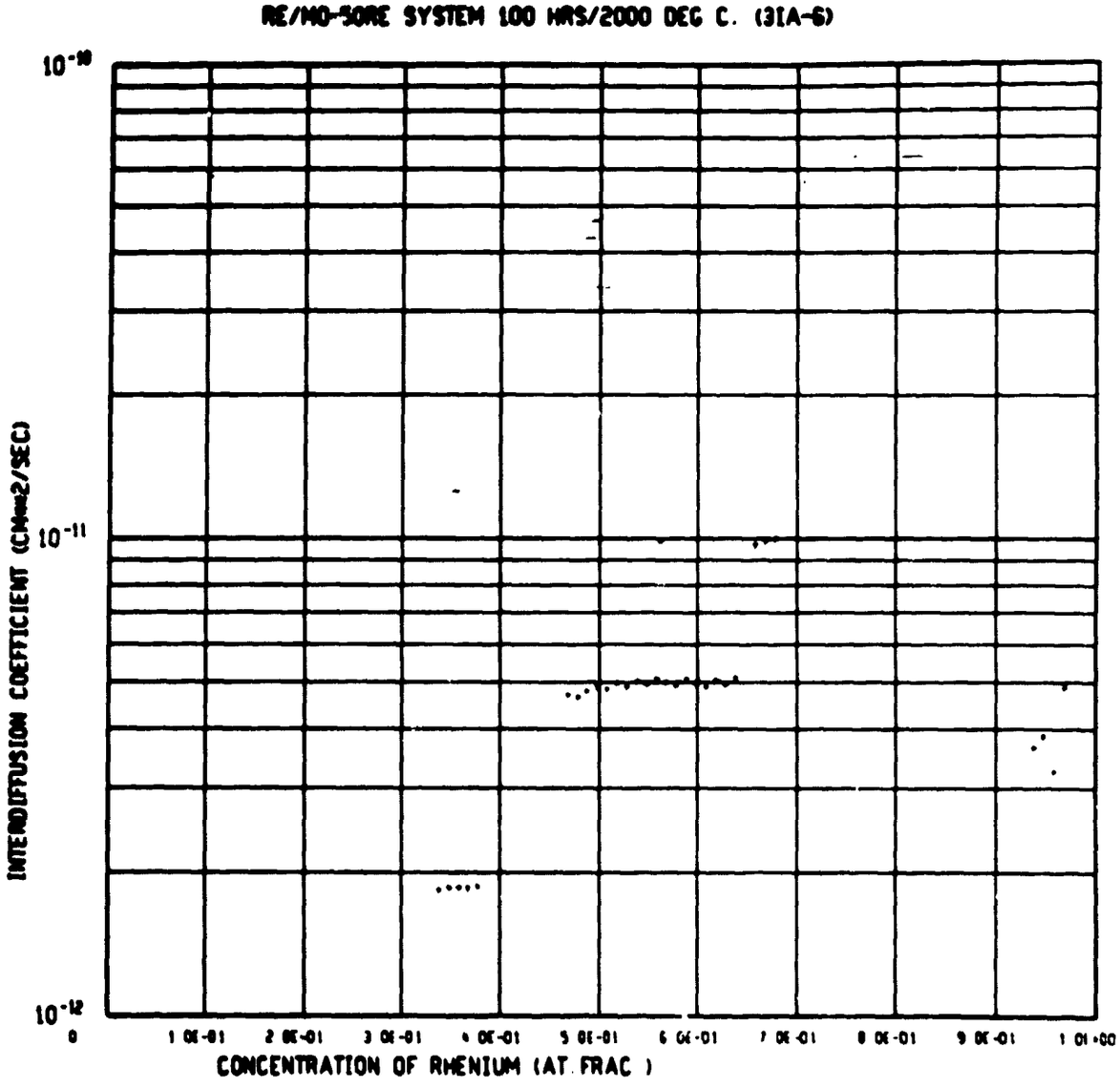

Figure 72. Molybdenum-50Rhenium to Rhenium Interdiffusion Coefficient at 2000°C (31A-6)

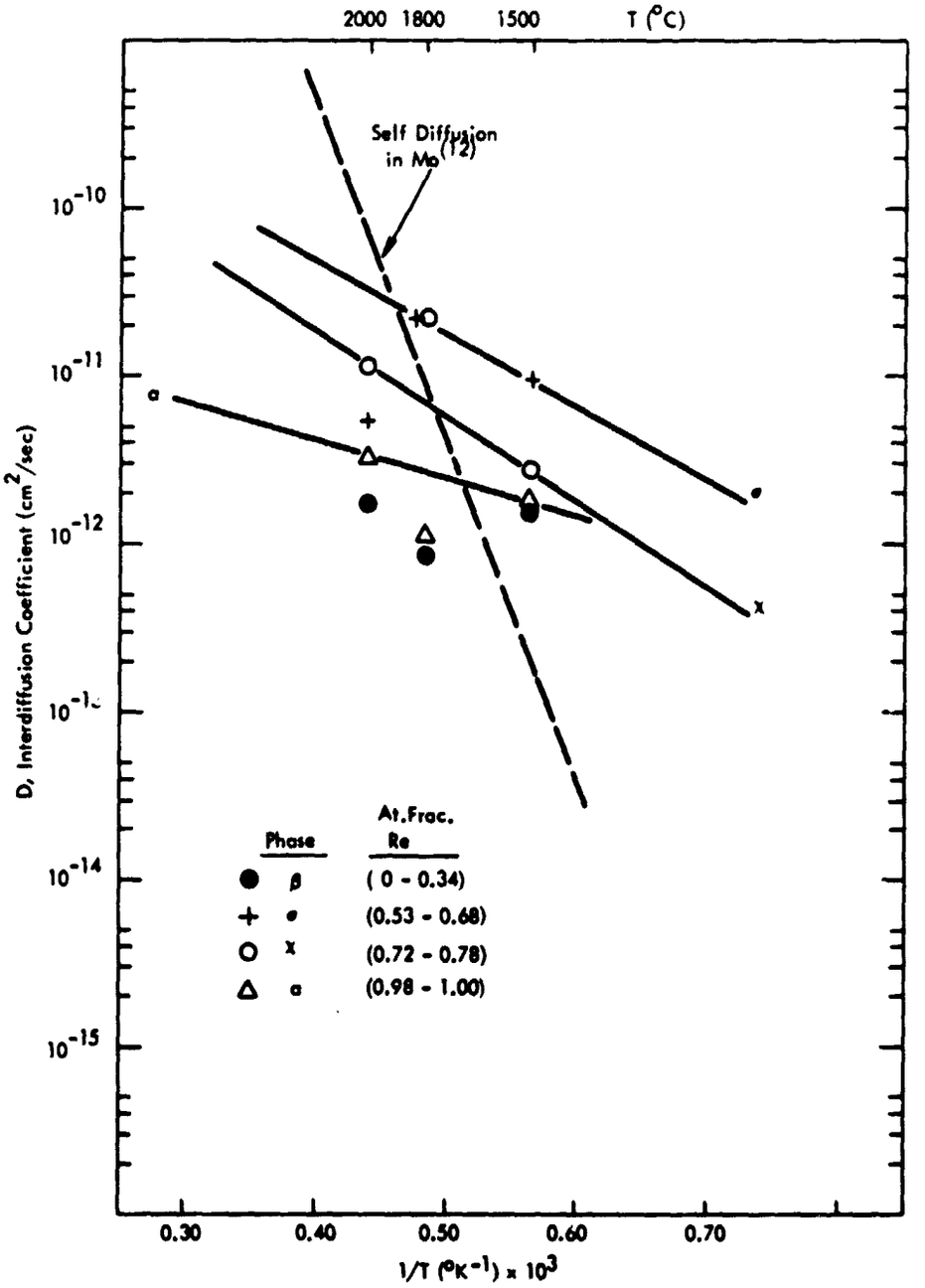

Figure 73. Arrhenius Interdiffusion Coefficient-Temperature Relation for the Molybdenum-Rhenium System

by hot press joining. Figure 74 illustrates that an extrapolation of measured interdiffusion zone widths (ΔX meas) for 1800°C ages to time zero results in an intercept at 1.45×10^{-3} cm. This value agreed well with the microprobe trace measured as-welded zone width of 1.40×10^{-3} cm. Analysis of tungsten-rhenium-molybdenum to tungsten interdiffusion zone widths is summarized in Table 28.

Figure 75 shows that very little scatter existed for this system and that there is no detectable difference between the systems. A grain boundary diffusion effect for preferentially oriented CVD tungsten grains was not observed. Least squares computer analysis established the tungsten-rhenium-molybdenum to tungsten interdiffusion model as:

$$\ln \left(\frac{\Delta X^2}{t} \right) = - \frac{34,750 \ (\pm 3890)}{T} - 7.208 \ (\pm 0.172) \qquad (25)$$

where ΔX is the net interdiffusion zone width (affected zone) in centimeters, t is age time in seconds, and T is age temperature in °K. Ninety-five percent confidence limits are shown. The interdiffusion zone width extends from 98 to 42 atomic percent tungsten, or 26 to 2 atomic percent rhenium. Both tungsten and rhenium interdiffusion zone widths are presented in Figure 75 with no one element being predominant in having a larger zone width (i.e., sinusoidal ternary path). Literature reviews did not reveal other sources of zone width information for this system.

Figure 76 presents the interdiffusion zone width information as a function of age time, and extrapolations to long age times are provided with equation (25) from Figure 75. A least squares correlation coefficient of 0.771 was found for equation (25).

Metallographic study of the interdiffusion zone revealed that neither Kirkendall voids nor intermediate phases were present. Cracking did not occur in the interdiffusion zone.

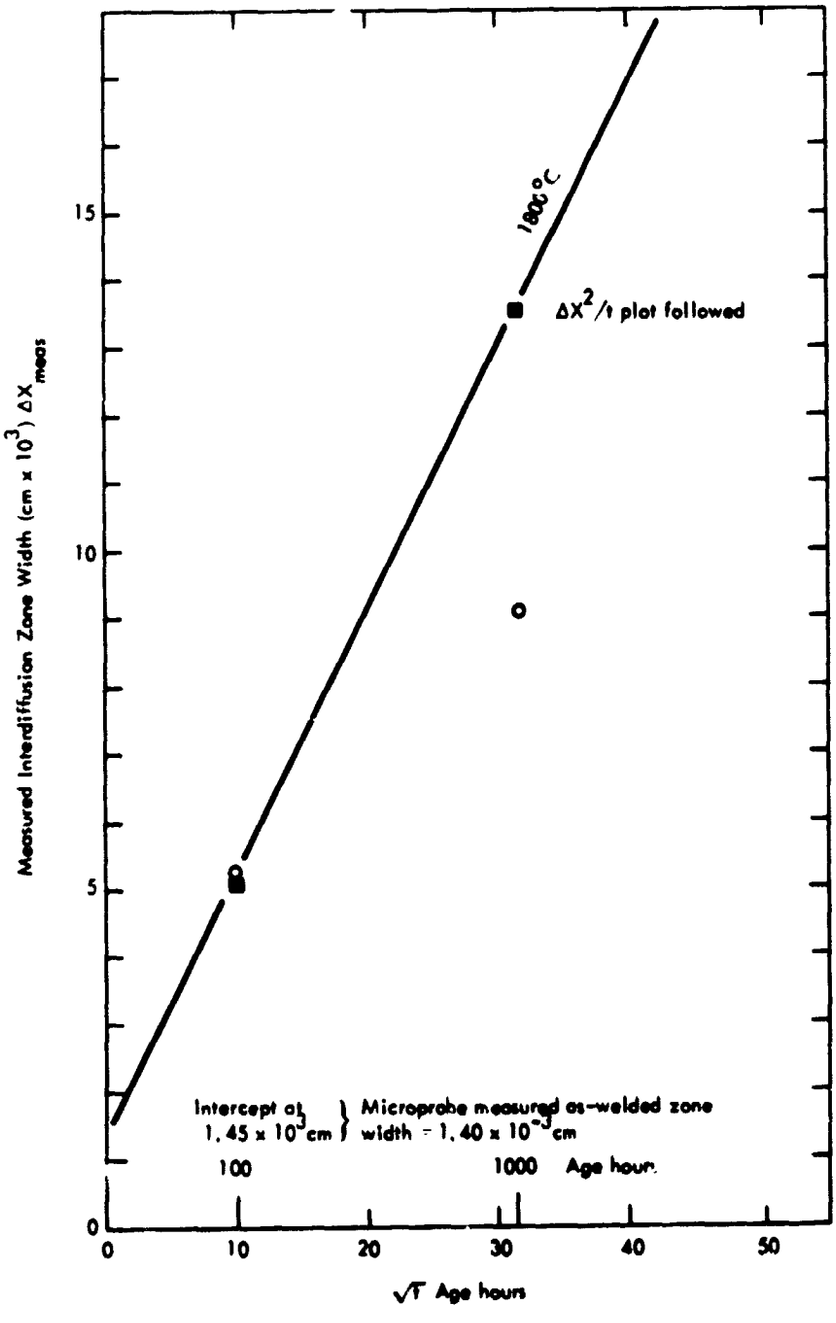

Figure 74. Extrapolation of Measured Interdiffusion Zone Widths to Zero Time to Establish As-welded Zone Width for the Tungsten-Rhenium-Molybdenum to Tungsten Diffusion Couples

Table 28. W-30.9Re-20.1Mo/Tungsten-Rhenium Couple Systems Corrected Interdiffusion Zone Widths

W-29Re-18Mo Couple	Age Temp. (°C)	Age Time (t) (hrs.)	Age Time (t) sec. ($\times 10^{-6}$)	ΔX Interdiffusion Zone Width (cm x 10^{-3})* W	ΔX Interdiffusion Zone Width (cm x 10^{-3})* Re	$\Delta X^2/t$ (cm^2/sec)	
W-Re-Mo/W_{arc}**	2000	1000	3.60	○ 22.47	◇ 22.97	1.40×10^{-10}	1.46×10^{-10}
		100	0.36	8.69	8.39	2.10×10^{-10}	1.96×10^{-10}
	1800	1000	3.60	7.38	7.31	1.51×10^{-11}	1.49×10^{-11}
		100	0.36	3.59	3.41	3.58×10^{-11}	3.23×10^{-11}
	1630	1000	3.60	6.17	5.62	1.06×10^{-11}	8.77×10^{-12}
	1500	2000	7.20	4.51	4.19	2.82×10^{-12}	2.44×10^{-12}
W-Re-Mo/W_{CVD}***	2000	1000	3.60	■ 22.52	◆ --	$1.4p \times 10^{-10}$	--
		100	0.36	10.98	10.56	3.36×10^{-10}	3.10×10^{-10}
	1800	1000	3.60	12.17	11.15	4.11×10^{-11}	3.44×10^{-11}
		100	0.36	3.64	4.59	3.68×10^{-11}	5.86×10^{-11}
	1630	1000	3.60	6.47	5.92	1.16×10^{-12}	9.74×10^{-12}
	1500	2000	7.20	3.75	4.37	1.96×10^{-12}	2.66×10^{-12}
W-Re-Mo/$Re^{+}_{pwdr.}$	2000	1000	3.60	□ --	◈ 35.83	--	3.57×10^{-10}
		100	0.36	9.85	9.34	2.70×10^{-10}	2.42×10^{-10}
	1800	1000	3.60	16.03	15.48	7.14×10^{-11}	6.68×10^{-11}
		100	0.36	8.17	8.13	1.86×10^{-10}	1.84×10^{-10}
	1630	1000	3.60	10.35	8.49	2.97×10^{-11}	2.11×10^{-11}
	1500	2000	7.20	7.09	7.27	6.99×10^{-12}	7.35×10^{-12}
W-Re-Mo/Re_{CVD}***	2000	1000	3.60	● --	✦ 27.43	--	2.09×10^{-10}
		100	0.36	9.65	9.68	2.54×10^{-10}	2.61×10^{-10}
	1800	1000	3.60	21.78	18.97	1.32×10^{-10}	1.00×10^{-10}
		100	0.36	7.37	6.68	1.51×10^{-10}	1.24×10^{-10}
	1630	1000	3.60	9.77	10.07	2.65×10^{-11}	2.82×10^{-11}
	1500	2000	7.20	8.52	7.94	1.01×10^{-11}	8.75×10^{-12}

* Zone width = cm x 10^{3}, i.e., $1.72 = 1.72 \times 10^{-3}$ cm
Zone width also corrected for as-welded condition

** W_{arc} = arc cast tungsten

*** W_{CVD} = chemical vapor deposited tungsten (W), rhenium (Re)

\+ Re_{powder} = powder metallurgy product rhenium

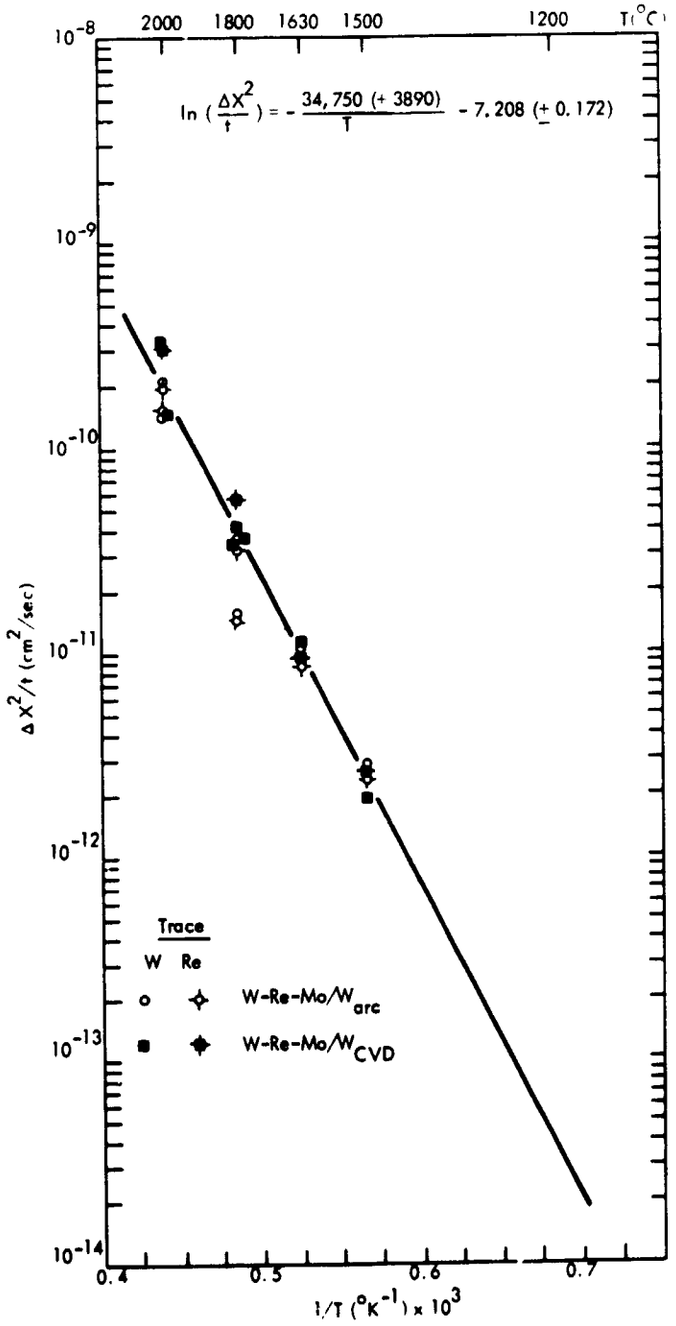

Figure 75. Arrhenius Model for Interdiffusion Zone Width in the Tungsten-Rhenium-Molybdenum to Tungsten Couple System

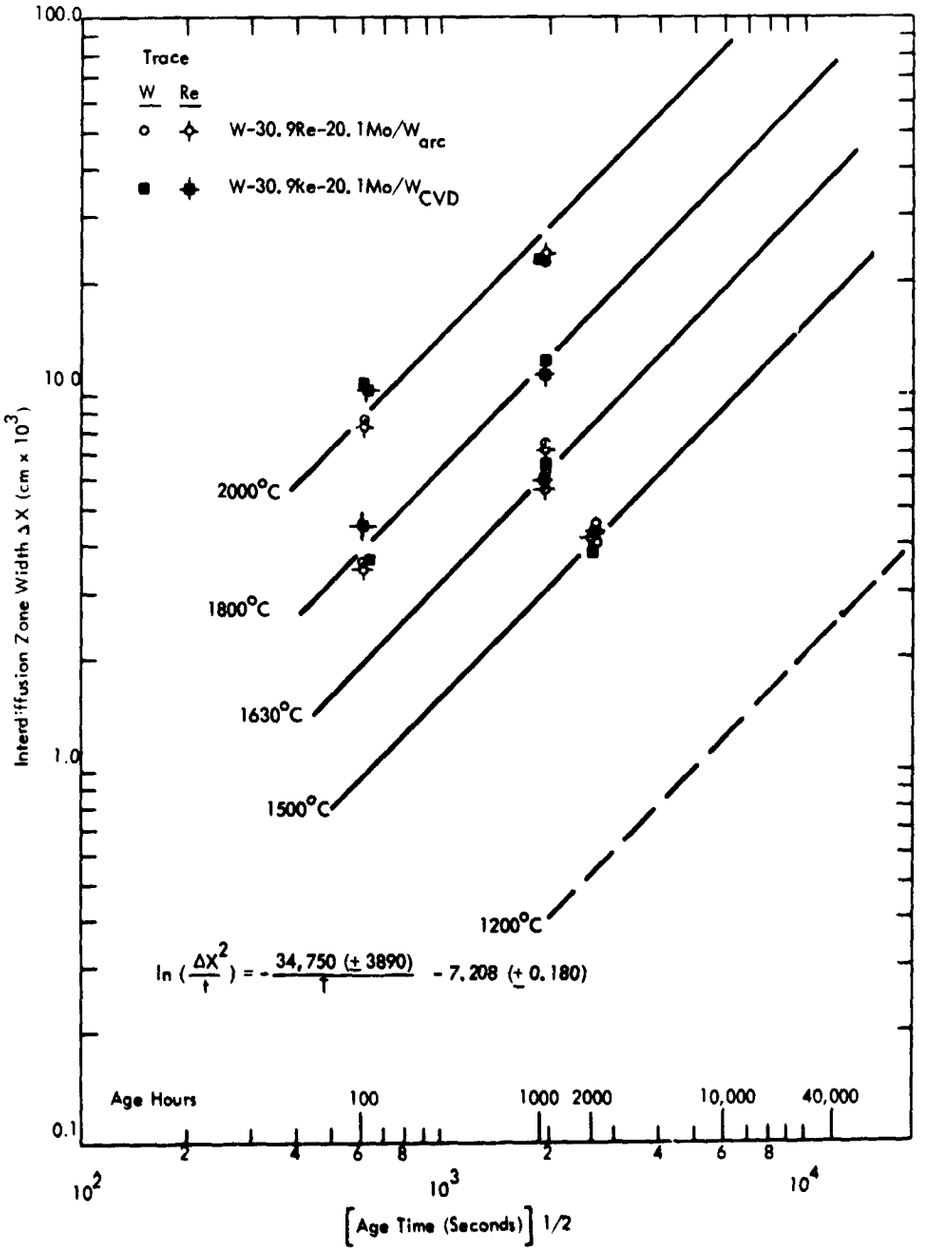

Figure 76. Illustrating Extrapolation of Zone Widths to Long Age Times for Tungsten-Rhenium-Molybdenum to Rhenium Interdiffusion

Boltzmann-Matano analysis was not performed for this system since it is a strong ternary system, and diffusion couples of several compositions would have been required.

4. Tungsten-Rhenium-Molybdenum to Rhenium

The tungsten-30.9rhenium-20.1molybdenum alloy to rhenium (CVD, powder metallurgy product) system diffusion couples form intermediate phase (discontinuous concentration profile) interdiffusion zones. Couples for this system were formed by autoclave pressure welding. Microprobe trace measured as-welded widths were 0.72×10^{-3} cm. Analysis of tungsten-rhenium-molybdenum to rhenium interdiffusion zone widths are summarized in Table 28.

Figure 77 shows that this system had little scatter and that there is no detectable difference between the systems. A grain boundary diffusion effect for preferentially oriented CVD rhenium grains was not observed. Least squares computer analysis established the tungsten-rhenium-molybdenum to rhenium interdiffusion model as:

$$\ln \left(\frac{\Delta X^2}{t}\right) = - \frac{28,580\ (\pm 3290)}{T} - 9.303\ (\pm 0.144) \qquad (26)$$

where ΔX is the net interdiffusion zone width (affected zone) in centimeters, t is age time in seconds, and T is age temperature in ^{o}K. Ninety-five percent confidence limits are shown. The interdiffusion zone width extends from 98 to 26 atomic percent rhenium, or from 42 to 2 atomic percent tungsten. Both tungsten and rhenium interdiffusion zone widths are presented in Figure 77 with no one element being predominate in having a larger zone width (i.e., sinusoidal ternary path). Literature reviews did not reveal other sources of zone width information for this system.

Figure 78 presents the interdiffusion zone width information as a function of age time, and extrapolations to long age times are provided with equation (26) from Figure 77. A least squares correlation coefficient of 0.791 was found for equation (26).

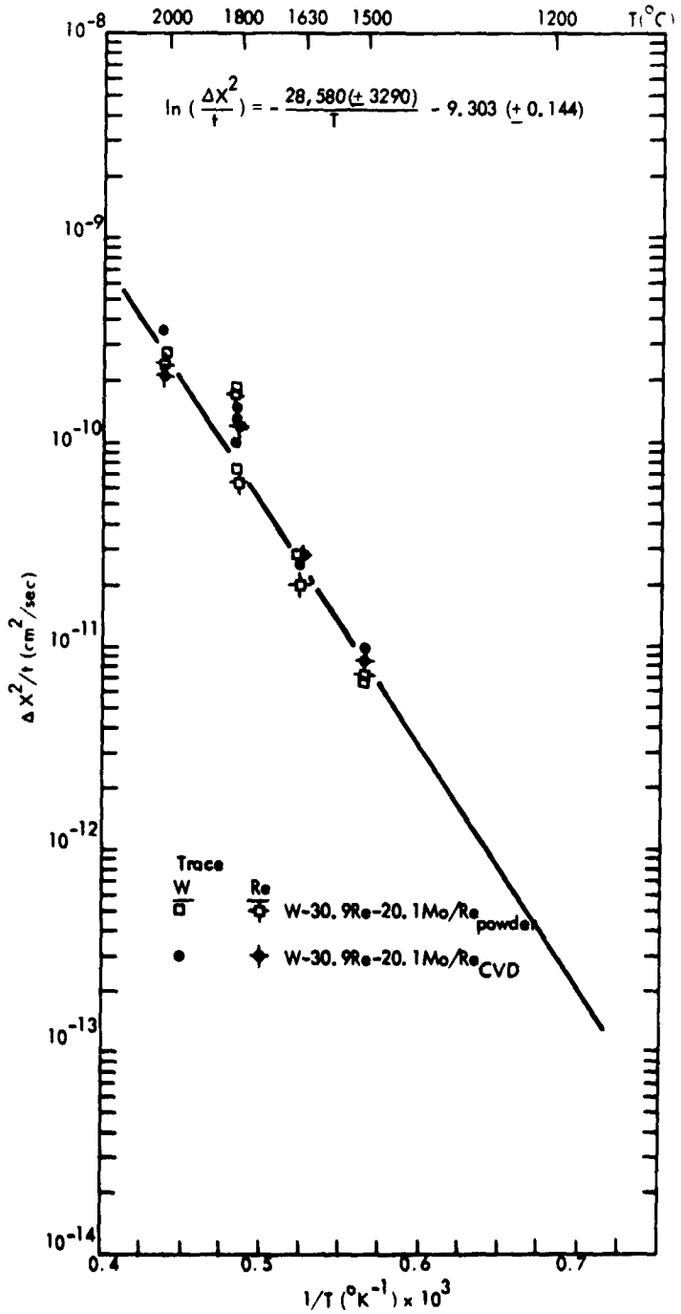

Figure 77. Arrhenius Model for Interdiffusion Zone Width in the Tungsten-Rhenium-Molybdenum to Rhenium Couple System

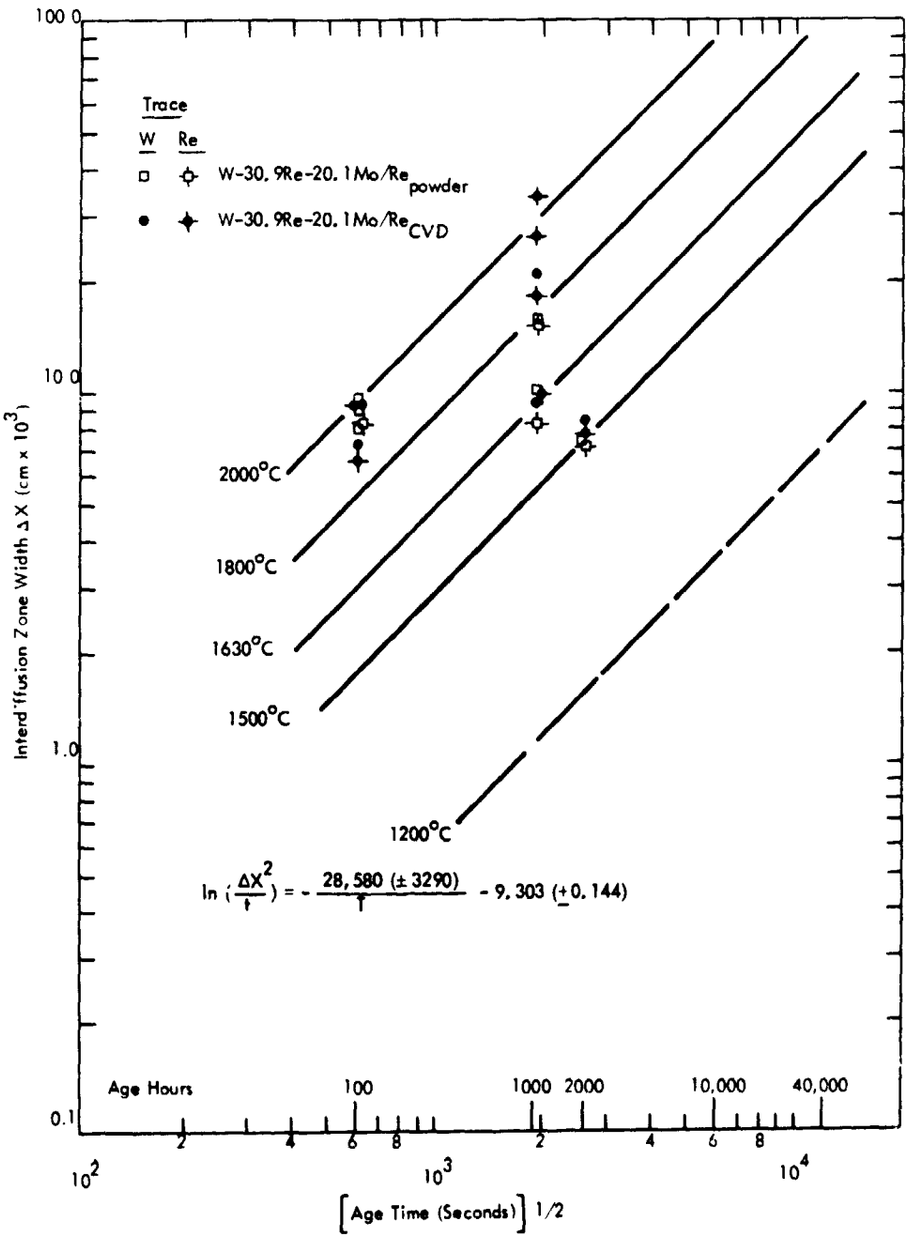

Figure 78. Illustrating Extrapolation of Zone Widths to Long Age Times for Tungsten-Rhenium-Molybdenum to Rhenium Interdiffusion

Kirkendall voids did not form in the interdiffusion zones of this system. Figures 79 and 80 illustrate the σ and χ phases which formed in the interdiffusion zone after ages at 1800°C. The small porosity on the rhenium side of the interdiffusion zone are the result of CVD processes and are not a Kirkendall effect.

Cracks were only observed in the interdiffusion zones of this sample system after ageing at 2000°C for 1000 hours. Figure 81 illustrates the small, randomly oriented cracks which occurred in the σ phase region of this system. The holes in the interdiffusion zone are associated with the tungsten-1 percent thoria marker wire and are typical of marker wire effects in this study. None of the couples of this system fractured.

Boltzmann-Matano analysis was not performed for this system since it is a strong ternary system, and diffusion couples of several compositions would have been required.

D. TUNGSTEN TO RHENIUM SYSTEMS

1. Tungsten to Rhenium

The tungsten to rhenium system diffusion couples form an interdiffusion zone with intermediate phases. The couples were all formed by hot press joining and were joined in the following structures:

W(arc cast)/Re (powder metallurgy product)
W(CVD product)/Re(powder metallurgy product)
W(powder metallurgy product)/Re(CVD product)

Microprobe trace measured as-welded zero condition zone widths were 1.77 to 2.10 x 10^{-3} cm. Analysis of tungsten to rhenium interdiffusion zone widths are summarized in Table 29.

Figure 79. Tungsten-30.9Rhenium-20.1Molybdenum to CVD Rhenium Interdiffusion Zone After 100 hours at 1800°C (4HA-3) at 200X.
Note the thin χ and wide σ phase zones in the couple.

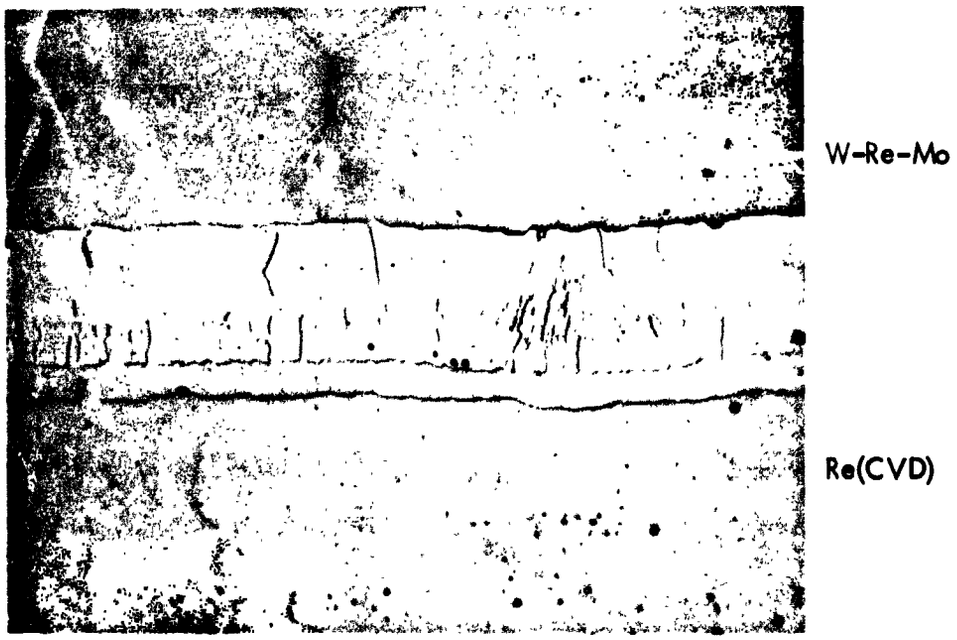

Figure 80. Tungsten-30.9Rhenium-20.1Molybdenum to CVD Rhenium Interdiffusion Zone after 1000 hours at 1800°C (4HA-4) at 200X.
The χ and σ phase zones have grown proportionally from the 100 hour age.

W-Re-Mo

Re(p)

Figure 81. Typical Randomly Oriented Interdiffusion Zone σ Phase Cracks Appearing in Tungsten-30.9Rhenium-20.1Molybdenum to Rhenium Couples After Ageing at 2000°C for 1000 hours (3HA-6) at 200X.

Table 29. Tungsten-Rhenium Couple Systems
Corrected Interdiffusion Zone Widths

Tungsten/ Rhenium Couple	Age Temp. (°C)	Age Time (t) (hrs.)	Age Time (t) (sec. $\times 10^{-6}$)		ΔX Interdiffusion Zone Width (cm $\times 10^{3}$)*	$\Delta X^2/t$ (cm^2/sec)
$W^{**}_{arc}/Re^{***}_{powder}$	2000	1000	3.60	■	34.37	3.28×10^{-10}
		100	0.36		24.48	1.66×10^{-10}
	1800	1000	3.60		10.83	3.26×10^{-11}
		100	0.36		2.10	1.23×10^{-11}
	1630	1000	0.36		5.07	7.15×10^{-12}
	1500	2000	7.20		3.09	1.33×10^{-12}
$W^{+}_{CVD}/Re^{***}_{powder}$	2000	1000	3.60	□	37.70	3.95×10^{-10}
		100	0.36		19.85	1.09×10^{-10}
	1800	1000	3.60		13.90	5.37×10^{-11}
		100	0.36		2.00	1.11×10^{-11}
	1630	1000	3.60		5.15	7.38×10^{-12}
	1500	2000	7.20		2.61	9.46×10^{-13}
$W^{***}_{powder}/Re^{+}_{CVD}$	2000	1000	3.60	X	28.09	2.19×10^{-10}
		100	0.36		4.70	6.14×10^{-11}
	1800	1000	3.60		8.83	2.16×10^{-11}
		100	0.36		1.60	7.11×10^{-12}
	1630	1000	3.60		3.76	3.93×10^{-12}
	1500	2000	7.20		2.08	6.02×10^{-13}

* Zone width = cm $\times 10^{3}$, i.e., $1.72 = 1.72 \times 10^{-3}$ cm
Zone width also corrected for as-welded condition.

** W_{arc} = arc cast tungsten product

*** Re_{powder} = powder metallurgy rhenium product

\+ W_{CVD} = chemical vapor deposited tungsten product

Figure 82 shows that some scatter existed for this system but could not be assigned to any material structure differences. The scatter was more pronounced as a result of elevated temperature ageing than low temperature ageing, contrary to the results for all of the other systems in this study. Work of Hudson and Yang[13] agrees rather well at elevated temperatures but differs by a factor of 3 (in zone width) at lower temperatures. The difference could be the result of joining techniques (hot press for this study versus CVD to a substrate) or neglect of corrections for as-welded conditions at zero age time. Least squares computer analysis established the tungsten-rhenium interdiffusion model as:

$$\ln\left(\frac{\Delta X^2}{t}\right) = -\frac{41,300\ (\pm 7470)}{T} - 4.464\ (\pm 0.332) \qquad (27)$$

where ΔX is the net interdiffusion zone width (affected zone) in centimeters, t is age time in seconds, and T is age temperature in $^{\circ}K$. Ninety-five percent confidence limits are shown.

Figure 83 presents the interdiffusion zone width information as a function of age time, and extrapolations to long age times are provided with equation (27) from Figure 82. A least squares fit correlation coefficient of 0.584 was found for equation (27).

Metallographic investigation of the interdiffusion zone revealed that Kirkendall voids did not occur in this system. Both σ and χ phases were observed in the interdiffusion zone (Figure 84). Interdiffusion zone cracks were not observed in any of the couples for this system. The CVD tungsten developed a definite grain boundary related porosity after 2000 hours at 2000°C (Figure 85). This porosity was probably the result of the CVD process (fluorine content), but did not adversely perturb the interdiffusion characteristics of the couple system. The voids present in the interdiffusion interface (Figure 85) only occurred in the areas where CVD grain boundary porosity occurred. Similar porosities were not observed in the CVD rhenium couple material but were present to a lesser extent in the powder metallurgy tungsten material.

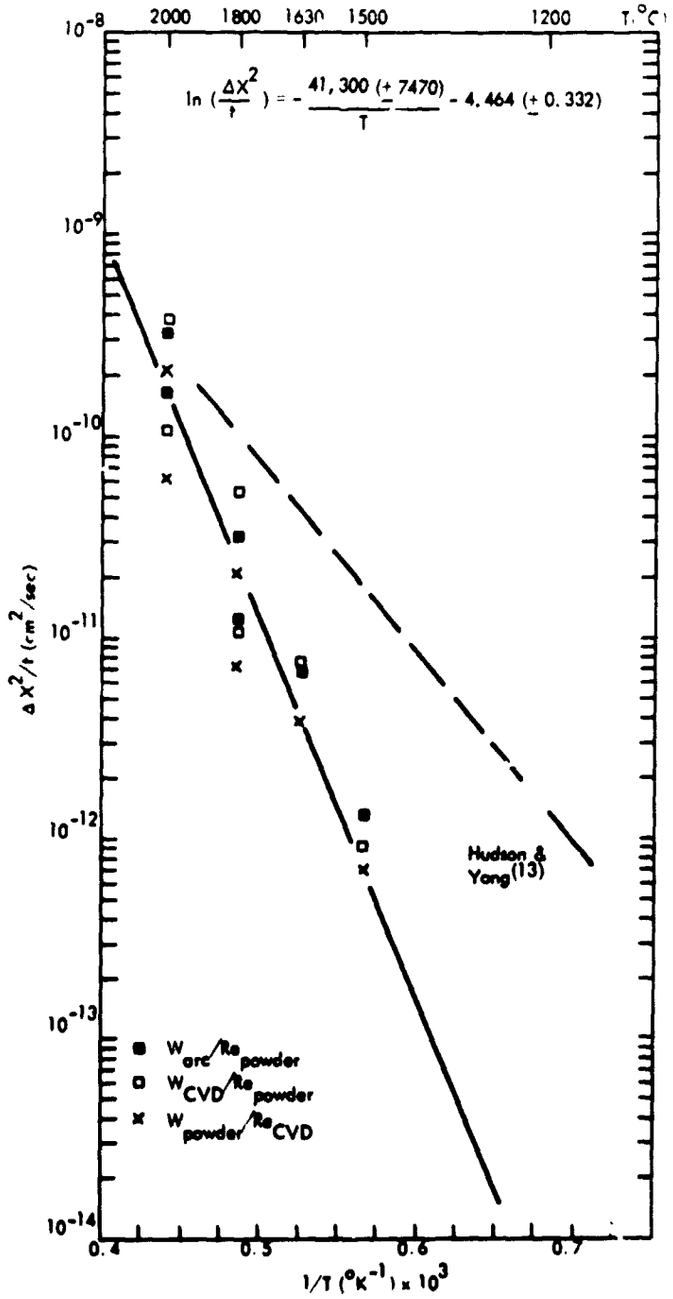

Figure 82. Arrhenius Model for Interdiffusion Zone Width in the Tungsten-Rhenium Couple System

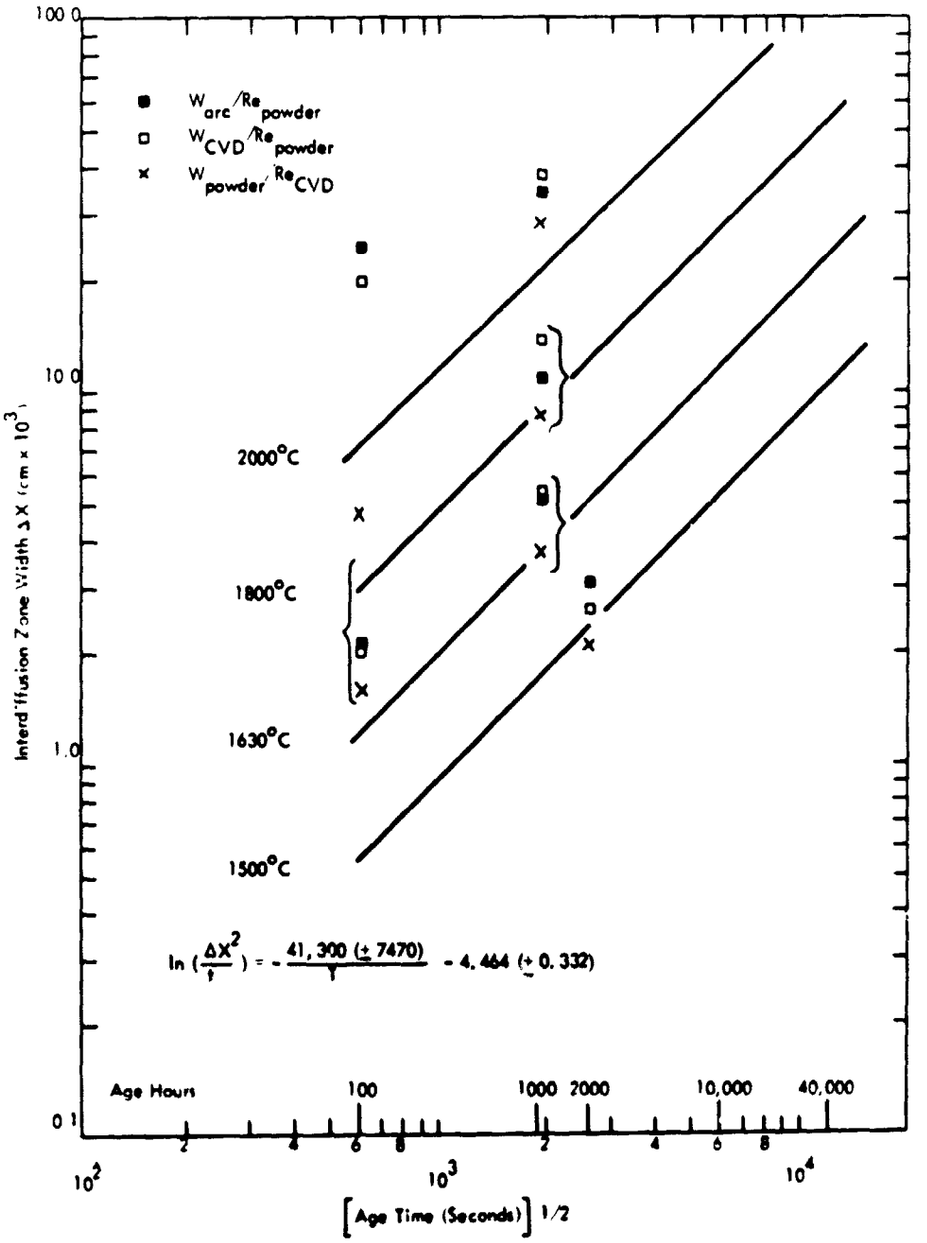

Figure 83. Illustrating Extrapolation of Zone Widths to Long Age Times for Tungsten-Rhenium Interdiffusion

Figure 84. The σ and χ Phases were Present in All Tungsten to Rhenium Interdiffusion Zones. This couple (2JA-4) aged at 1800°C for 1000 hours (at 200X).

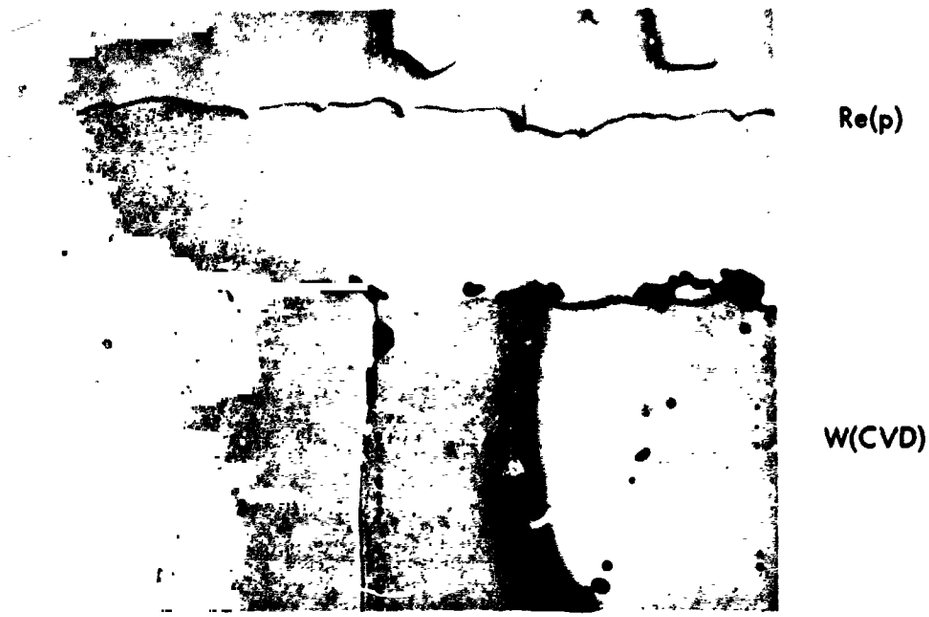

Figure 85. Grain Boundary Porosity Occurred in the CVD Tungsten Couple Tungsten Couple Materials after 1000 hours at 2000°C (Couple 2JA-6 at 200X)

Perusal of Figures 84 and 85 will reveal that the χ phase does not appear to be present after 2000°C ageing. This observation was repeated for all tungsten to rhenium couples for 2000°C age only. Since published phase diagrams establish a χ phase to 2200°C, its absence at 2000°C could only be assigned to its small concentration span at this temperature (i. e., 73 to 74 atomic percent), and thus low visibility on a concentration gradient trace. However, when the relative concentration-distance profiles were plotted on probability paper (Hartley Boltzmann-Matano computer analysis), a discontinuity in this concentration area verified the existance of the χ phase.

For Boltzmann-Matano analysis of the tungsten-rhenium system, only pure tungsten to rhenium was considered. Other couples, such as tungsten to tungsten-25rhenium and rhenium to tungsten-25rhenium form partial couples and will yield the same results. Electron microprobe spot c unt traverses were made on samples:*

4JA-6	2000°C	1000 hours
4JA-4	1800°C	1000 hours
2JA-1	1630°C	1000 hours

and the Colby MAGIC** corrected concentration profiles were loaded into the Hartley*** Boltzmann-Matano analysis computer program after being fitted, in probability coordinates, for curve smoothing. Figure 86 illustrates the microprobe corrected interdiffusion concentration profile of sample 2JA-1 as presented by Calcomp plot subroutine. Phases present from pure tungsten to rhenium are β, σ, χ, α. Figure 87 presents the smoothed concentration profile generated by the least squares fit routine (in probability coordinates) of the Hartley program. The σ and χ phase concentration limits agreed with published phase diagrams. Figures 88, 89, and 90 present the interdiffusion coefficient as a function of tungsten concentration at 1630, 1800, and 2000°C. Only the σ and χ phase interdiffusion coefficients

* Part II, Appendix F, Diffusion Couple Age/Identification Chart.
** Part II, Appendix J, Colby Computer Program for Correcting Microprobe Intensity Analysis.
*** Part II, Appendix H, Hartley Computer Program for Boltzmann-Matano Diffusion Analysis.

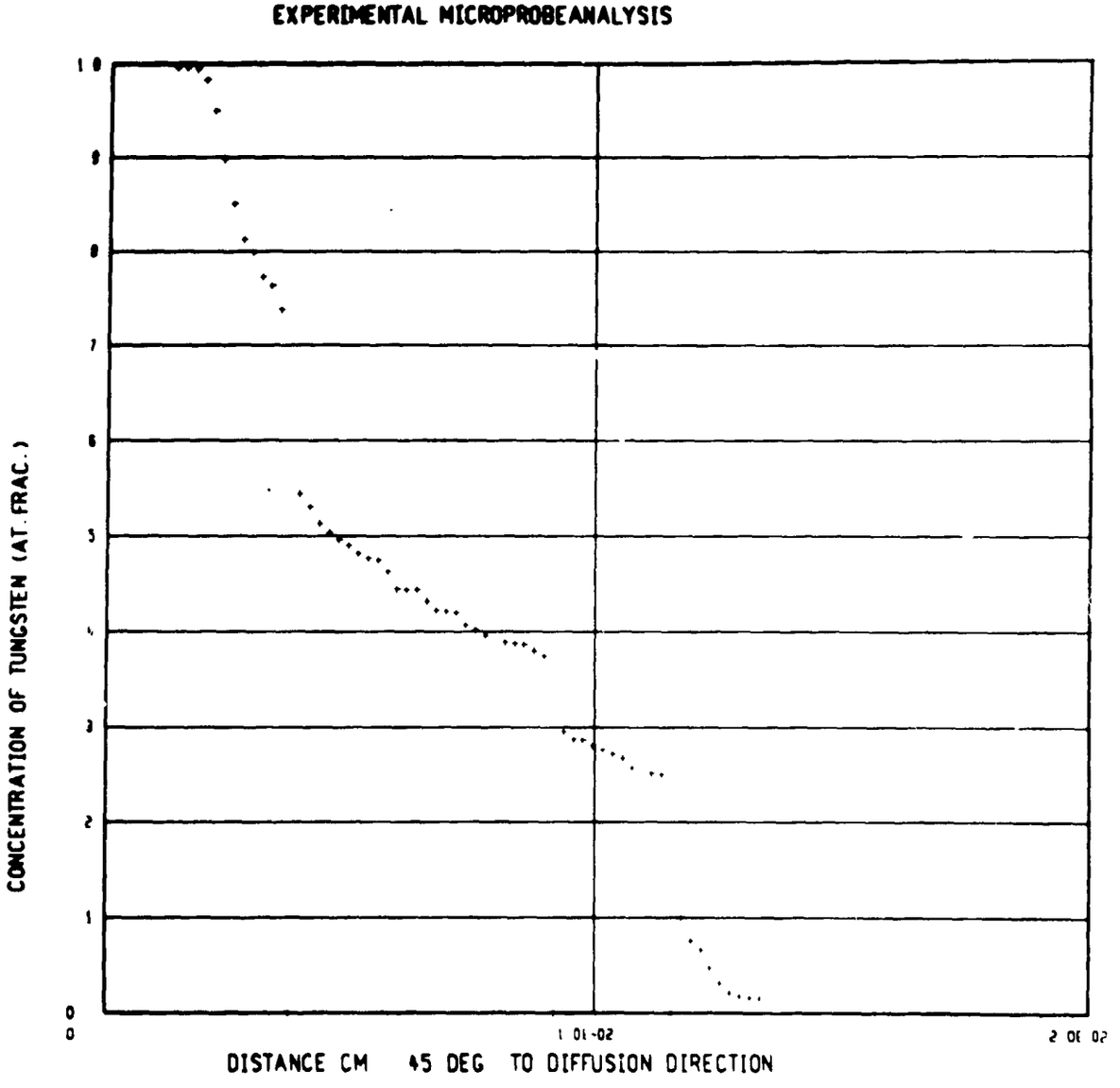

Figure 86. Colby MAGIC Corrected Input Profile to Hartley Boltzmann - Matano Program for Tungsten-Rhenium Interdiffusion at 1630°C for 1000 hours (2JA-1) as Plotted by Calcomp

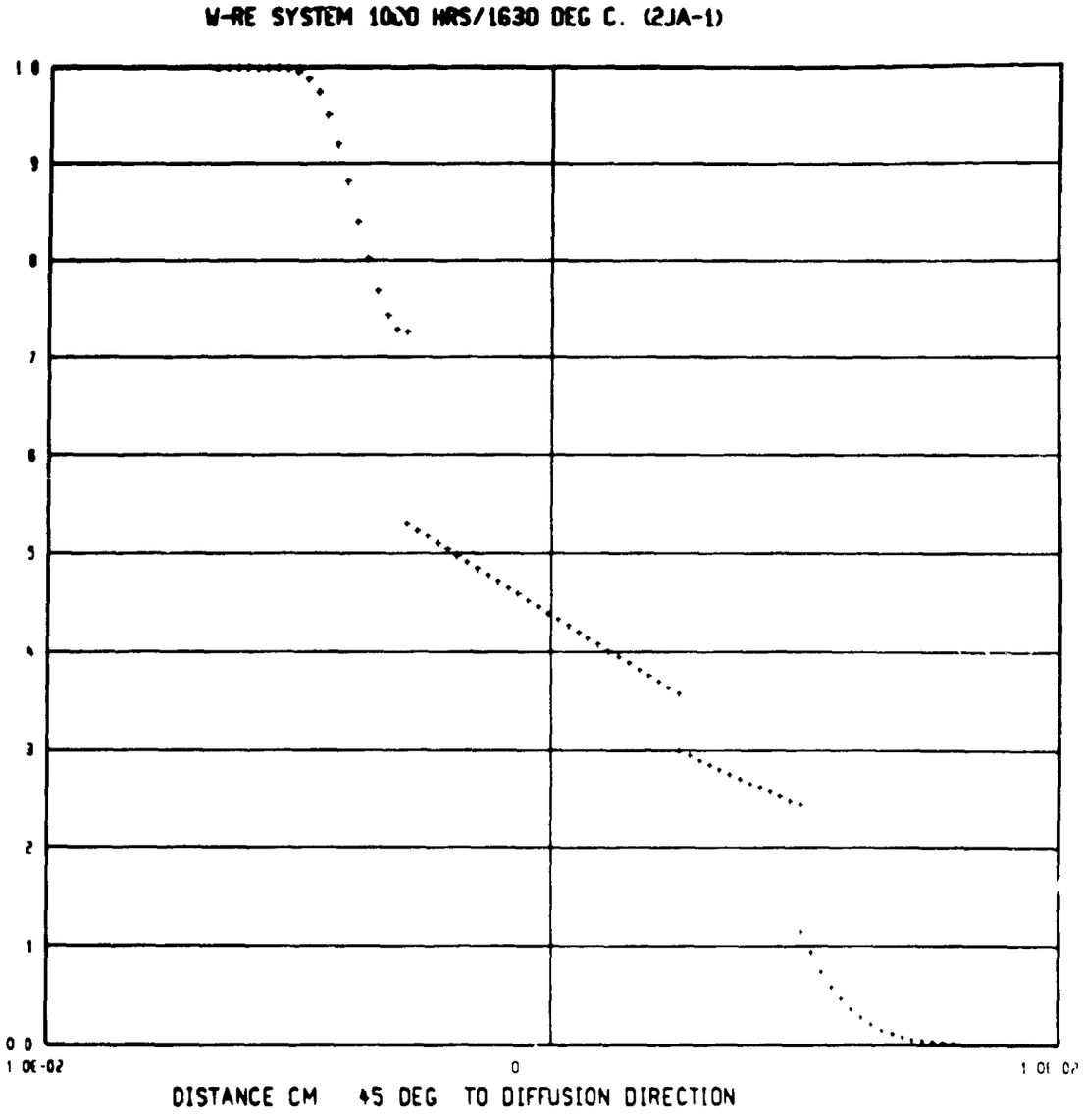

Figure 87. Regenerated (least squares fit) Concentration Profile from Data in Figure VII-77.

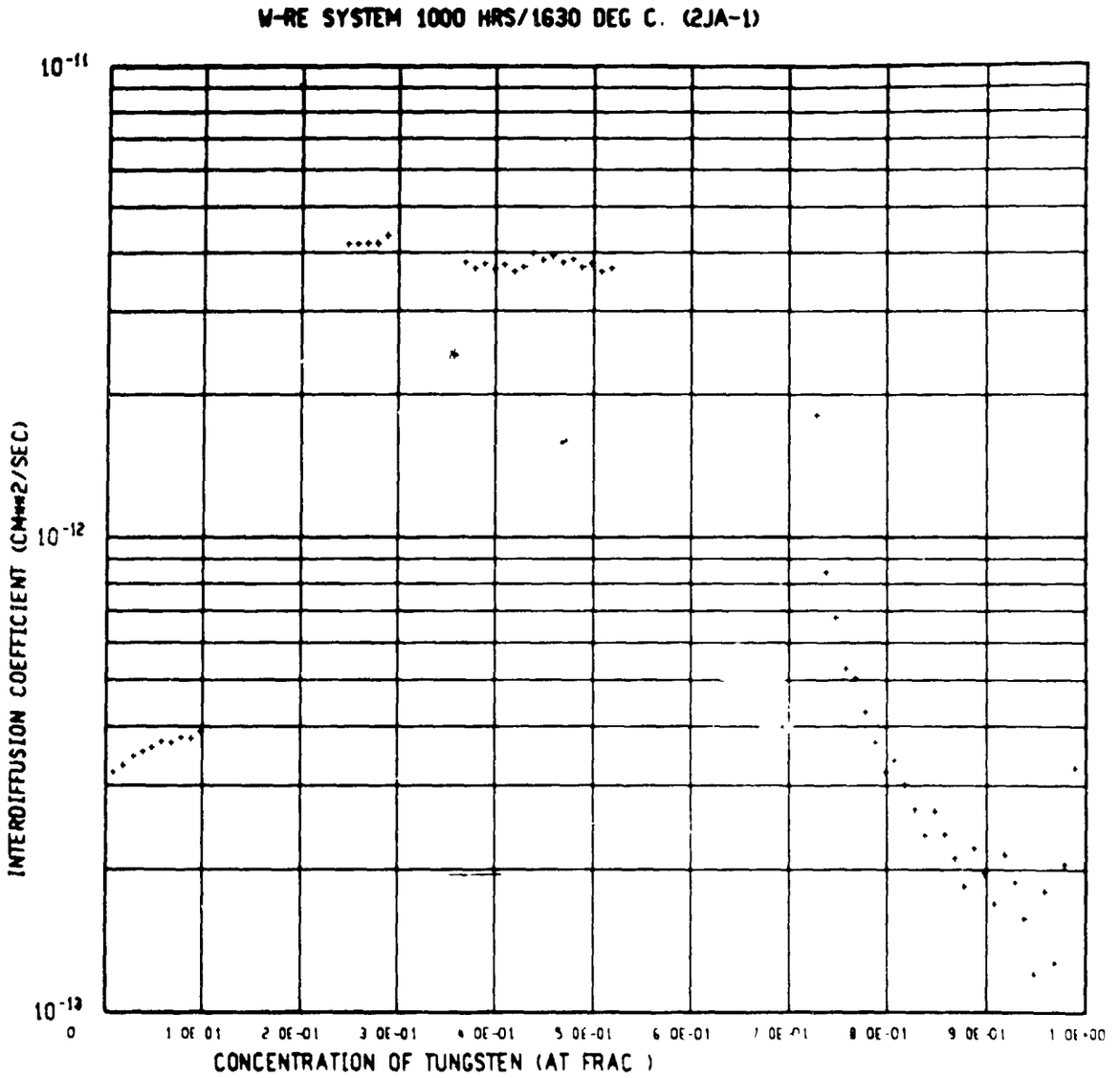

Figure 88. Tungsten-Rhenium Interdiffusion Coefficient at 1630°C (2JA-1)

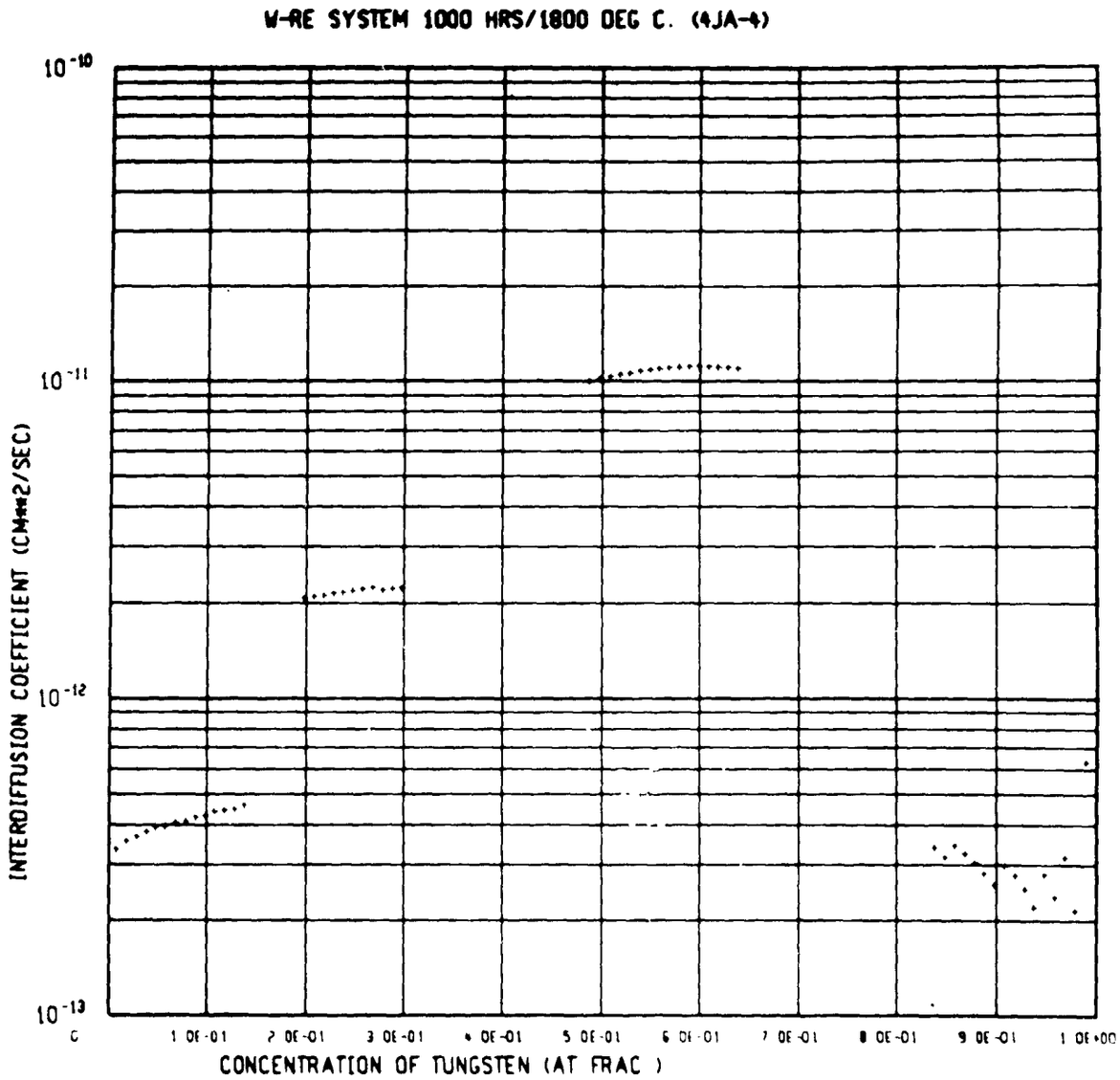

Figure 89. Tungsten-Rhenium Interdiffusion Coefficient at 1800°C (4JA-4).

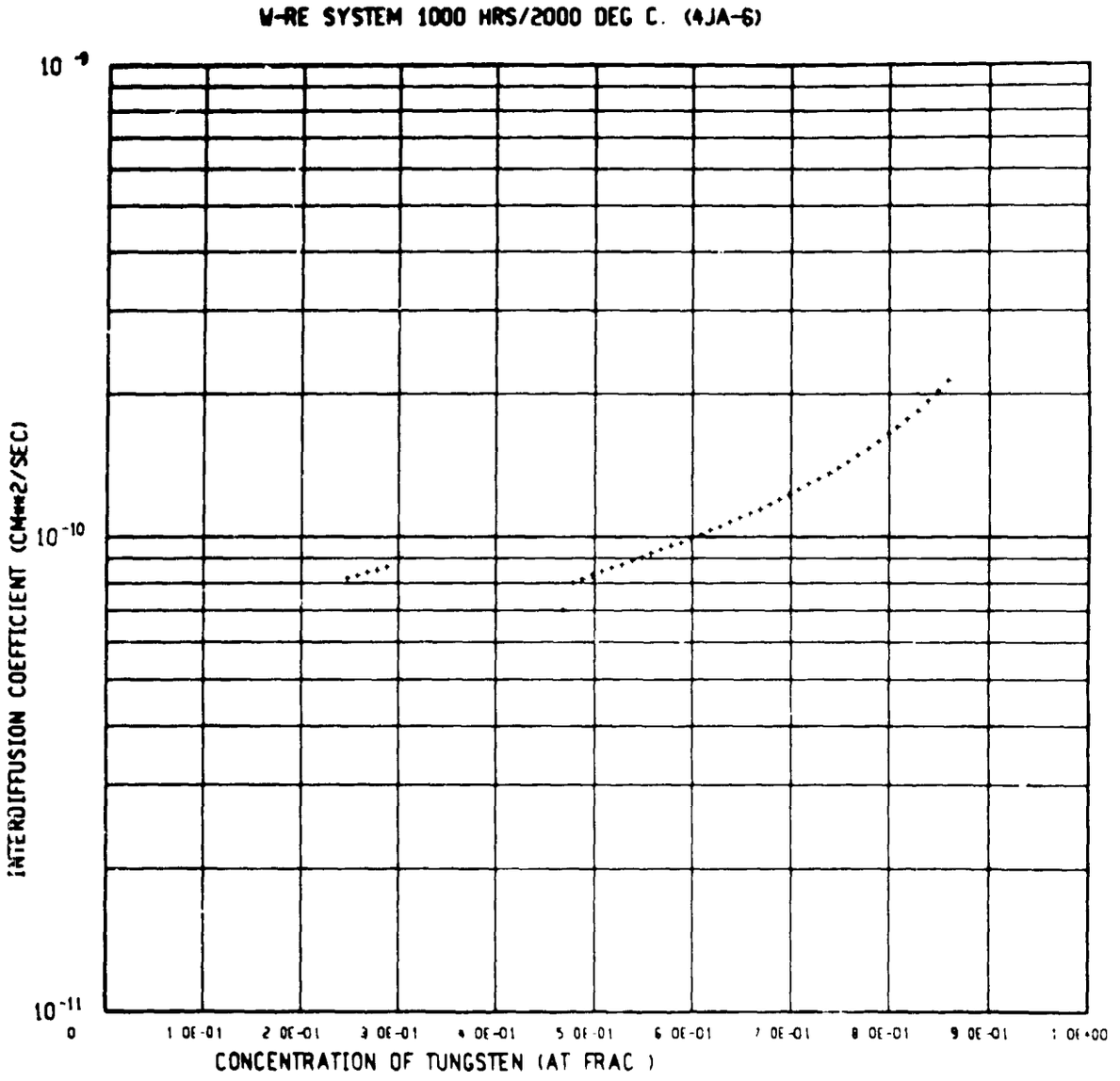

Figure 90. Tungsten-Rhenium Interdiffusion Coefficient at 2000°C (4JA-6)

are presented in Figure 91 because difficulties were experienced in least squares fitting the concentration curve in the β (high tungsten) and α (high rhenium) phase regions.

Figure 91 presents the Arrhenius interdiffusion relation for tungsten-rhenium interdiffusion as resolved in this study. The interdiffusion coefficients fall above that for tungsten self-diffusion and are plotted as mean $\tilde{D}$ values for each phase region. Self-diffusion data for rhenium was not found in the literature but should be larger than that for tungsten. Difficulty was encountered in resolving $\tilde{D}$ for the α and β phases due to the problem (previously described) of curve fitting to the data at 2000°C. The interdiffusion coefficient can be expressed for the σ and χ phases as:

$$\tilde{D}_{\sigma} \left(\frac{cm^2}{sec}\right) = 8.81 \times 10^{-4} \exp\left[-\frac{73,500}{RT}\right] \tag{28}$$

$$\tilde{D}_{\chi} \left(\frac{cm^2}{sec}\right) = 1.33 \times 10^{-3} \exp\left[-\frac{74,000}{RT}\right] \tag{29}$$

For the concentration (phase) regions of the phase diagram where they apply, and where T is in °K and R is the gas constant (1.987 cal/mole-°K).

2. Tungsten-25Rhenium to Tungsten Systems

The arc cast tungsten-25rhenium alloy to tungsten (arc cast, CVD) system diffusion couples formed solid solution interdiffusion zones. Couples for this system were the most difficult to autoclave HIP-weld and were all formed by hot press joining. Electron microprobe trace measured as-welded zero condition zone widths were 0.94×10^{-3} cm. Analysis of the arc cast tungsten-25rhenium alloy to tungsten interdiffusion zone widths are summarized in Table 30.

Figure 92 shows that some scatter for this system existed at 1500 and 1800°C, but there was no detectable difference between the systems. A grain boundary diffusion effect for preferentially

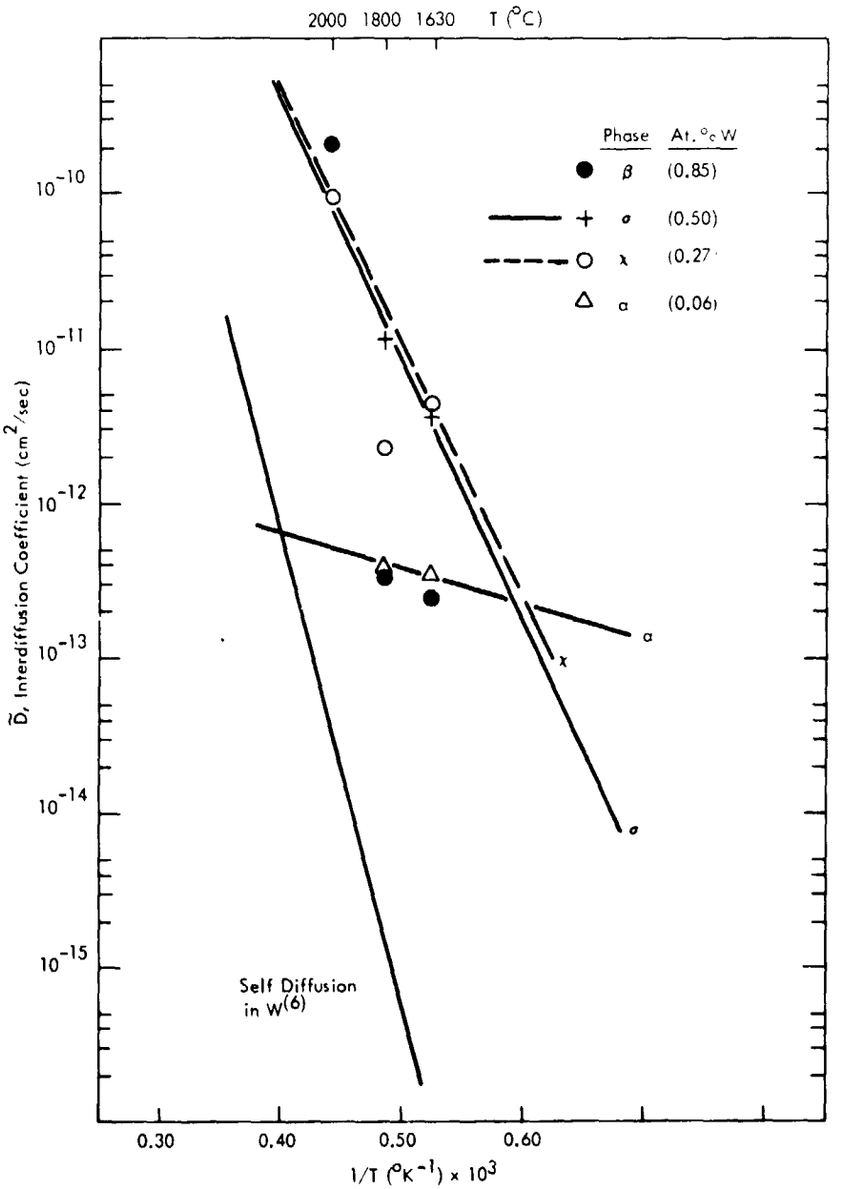

Figure 91. Arrhenius Interdiffusion Coefficient-Temperature Relation for the Tungsten-Rhenium System

Table 30. W-25Re/Tungsten-Rhenium Couple Systems
Corrected Interdiffusion Zone Widths

W-25Re Alloy Couple	Age Temp. (°C)	Age Time (t) (hrs.)	Age Time (t) (sec. x 10^{-6})	ΔX Interdiffusion Zone Width (cm x 10^3)* W Trace	ΔX Interdiffusion Zone Width (cm x 10^3)* Re	$\Delta X^2/t$ (cm^2/sec)
W-25Re/W_{arc} **	2000	1000	3.60	○ 19.21	--	1.03×10^{-10}
		100	0.36	6.10	--	1.03×10^{-10}
	1800	1000	3.60	7.92	--	1.74×10^{-11}
		100	0.36	2.37	--	1.56×10^{-11}
	1630	1000	3.60	2.43	--	1.65×10^{-12}
	1500	2000	7.20	3.06	--	1.30×10^{-12}
W-25Re/W_{CVD} ***	2000	1000	3.60	● 19.68	--	1.08×10^{-10}
		100	0.36	6.88	--	1.32×10^{-10}
	1800	1000	3.60	11.15	--	3.46×10^{-11}
		100	0.36	1.60	--	7.11×10^{-12}
	1630	1000	3.60	2.38	--	1.58×10^{-12}
	1500	2000	7.20	0.85	--	1.01×10^{-13}
W-25Re/$Re_{pdwr.}$ +	2000	1000	3.60	□ --	61.60	1.06×10^{-9}
		100	0.36	--	17.65	8.65×10^{-10}
	1800	1000	3.60	--	13.90	5.37×10^{-11}
		100	0.36	--	2.78	2.14×10^{-11}
	1630	1000	3.60	--	6.07	1.02×10^{-11}
	1500	2000	7.20	--	2.86	1.14×10^{-12}
W-25Re/Re_{CVD} *+	2000	1000	3.60	■ --	46.30	5.95×10^{-10}
		100	0.36	--	11.60	3.74×10^{-10}
	1800	1000	3.60	--	--	--
		100	0.36	--	2.54	1.79×10^{-11}
	1630	1000	3.60	--	7.72	1.65×10^{-11}
	1500	2000	7.20	--	1.34	2.49×10^{-13}

* Zone width = cm x 10^3, i.e., 1.72 = 1.72 x 10^{-3} cm
Zone width also corrected for as-welded condition.

** W_{arc} = arc cast tungsten product

*** W_{CVD} = chemical vapor deposited tungsten product

\+ Re_{powder} = powder metallurgy rhenium product

+* Re_{CVD} = chemical vapor deposited rhenium product

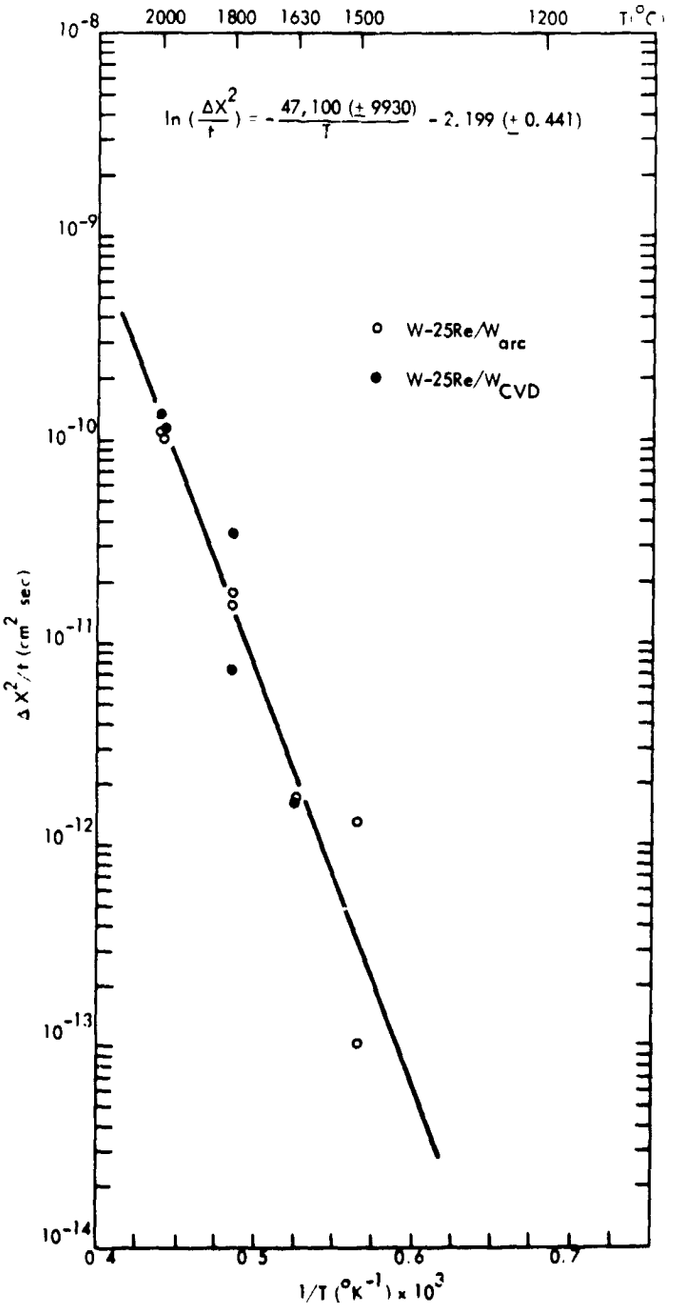

Figure 92. Arrhenius Model for Interdiffusion Zone Width in the Tungsten-25Rhenium to Tungsten Couple System

oriented CVD tungsten grains was not observed. Least squares computer analysis established the tungsten-25rhenium to tungsten interdiffusion model as:

$$\ln\left(\frac{\Delta X^2}{t}\right) = -\frac{47,100\ (\pm\ 9930)}{T} - 2.199\ (\pm\ 0.441) \qquad (30)$$

where ΔX is the net interdiffusion zone width (affected zone) in centimeters, t is age time in seconds, and T is age temperature in $^{\circ}K$. Ninety-five percent confidence limits are shown. The interdiffusion zone width extends from 98 to 75 atomic percent tungsten. Since this partial tungsten-rhenium couple is a binary system, only the tungsten concentration trace was followed. Literature reviews did not reveal other sources of zone width information for this couple system.

Figure 93 presents the interdiffusion zone width information as a function of age time, and extrapolations to long age times are provided with equation (30) from Figure 92. A least squares correlation coefficient of 0.966 was found for equation (30).

Metallographic study of the interdiffusion zone revealed that neither Kirkendall voids nor intermediate phases were present. Cracking did not occur in the interdiffusion zone. As described for the tungsten-rhenium diffusion couple system, grain boundary porosity developed in the CVD tungsten structure only after 2000°C ageing for 1000 hours. This porosity did not appear to affect the interdiffusion characteristics of the couple system.

Boltzmann-Matano analysis was not performed for this system since it is a partial couple to the tungsten-rhenium couple system, and results would have duplicated this system.

3. Tungsten-25Rhenium to Rhenium Systems

The arc cast tungsten-25rhenium alloy to rhenium (CVD, powder metallurgy product) system diffusion couples formed intermediate phase (σ , χ) concentration discontinuous profile

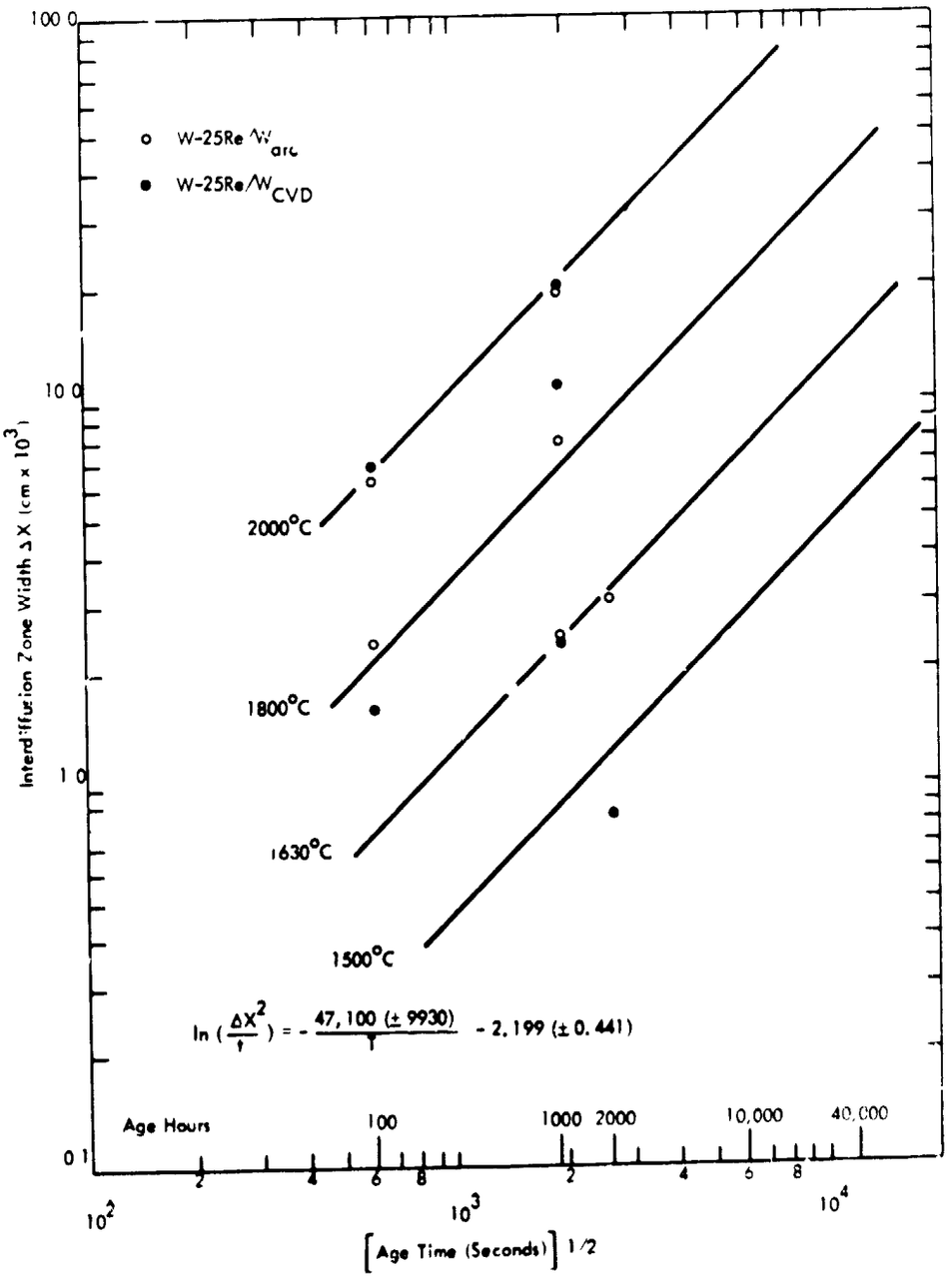

Figure 93. Illustrating Extrapolation of Zone Widths to Long Age Times for Tungsten-25Rhenium to Tungsten Interdiffusion

interdiffusion zones. Couples for this system were among the most difficult to autoclave HIP-weld and were all formed by hot press joining. Electron microprobe trace measured as-welded zero condition zone widths were 1.96×10^{-3} cm. Analysis of the arc cast tungsten-25rhenium alloy to rhenium interdiffusion zone widths are summarized in Table 30.

Figure 94 shows that this system possessed above average scatter and that there is a small trend for interdiffusion zone widths with powder metallurgy rhenium to be slightly larger than those with CVD rhenium. Since grain diameters were equal to or larger than the interdiffusion zone widths (Figure 95), this effect could not be assigned to a grain structural dependency. The CVD rhenium was layered due to deposition practices, and one layer junction plane paralleled the couple weld plane and occurred within the interdiffusion zone. The small pores and deposition disruption associated with this CVD layer zone could have contributed to the interdiffusion zone widths being smaller for the CVD rhenium couples.

Least squares computer analysis established the tungsten-25rhenium to rhenium interdiffusion model as:

$$\ln \left(\frac{\Delta X^2}{t}\right) = - \frac{53,990 \ (\pm 11,900}{T} + 2.415 \ (\pm 0.551) \qquad (31)$$

where ΔX is the net interdiffusion zone width (affected area) in centimeters, t is age time in seconds, and T is age temperature in °K. Ninety-five percent confidence limits are shown. The interdiffusion zone width extends from 98 to 25 atomic percent rhenium. Since this partial tungsten-rhenium couple is a binary system, only the rhenium concentration trace was followed. Literature reviews did not reveal other sources of zone width information for this couple system.

Figure 96 presents the interdiffusion zone width information as a function of age time, and extrapolations to long age times are provided with equation (31) from Figure 94. A least squares correlation coefficient of 0.761 was found for equation (31).

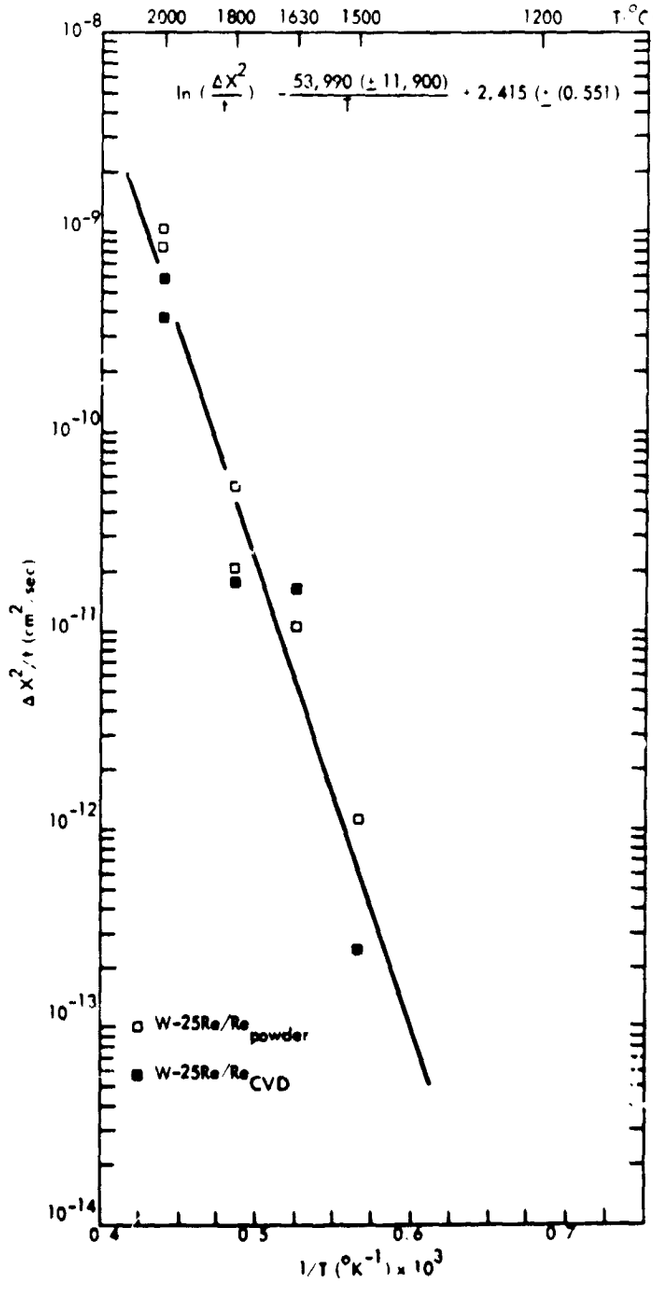

Figure 94. Arrhenius Model for Interdiffusion Zone Width in the Tungsten-25Rhenium to Rhenium Couple System

Figure 95. Tungsten-25Rhenium to Rhenium Interdiffusion Zone Width after 1000 hours at 1800°C (3GA-4) at 200X. Note that average grain size equals or exceeds interdiffusion zone width

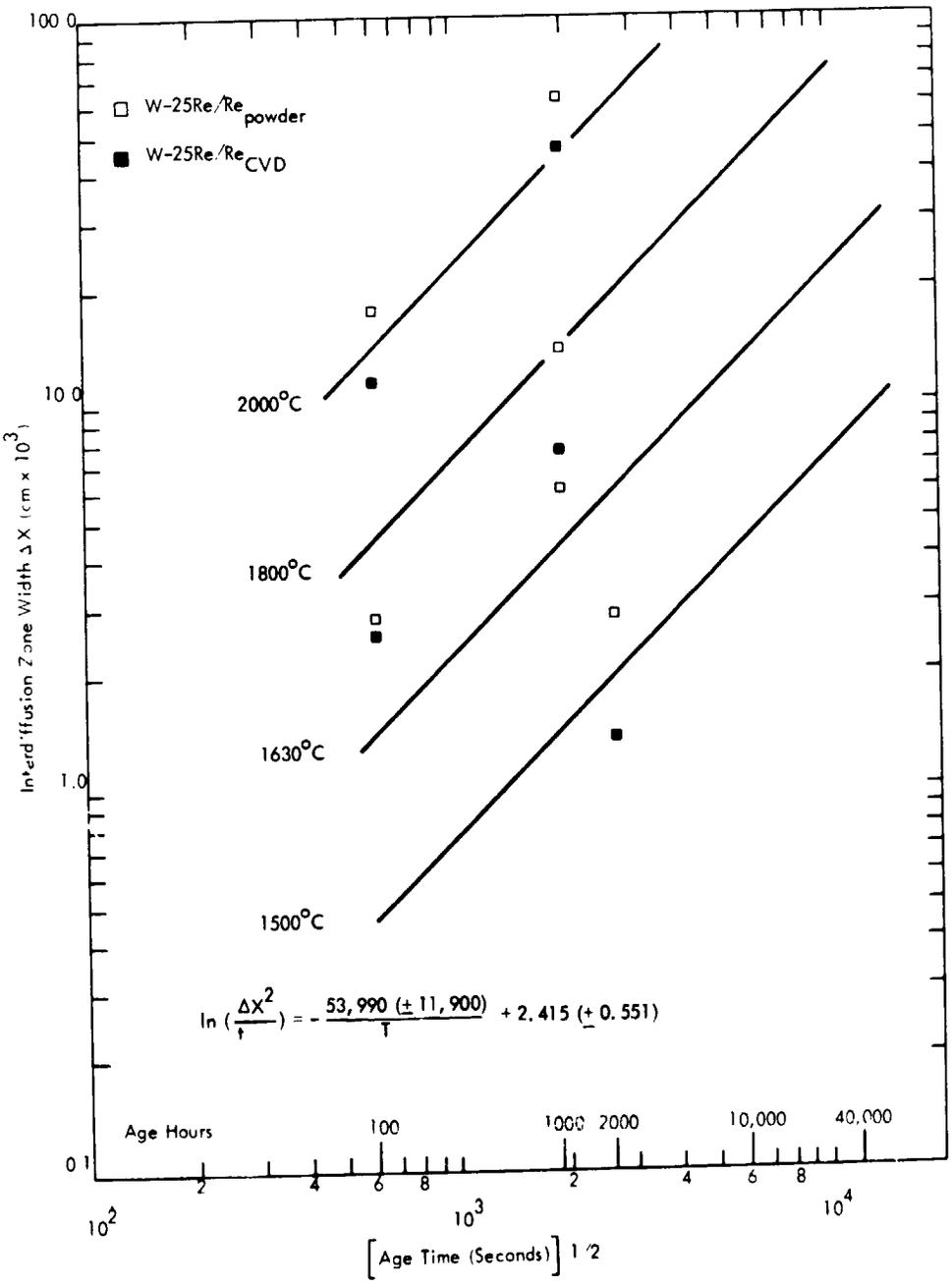

Figure 96. Illustrating Extrapolation of Zone Widths to Long Age Times for Tungsten-25Rhenium to Rhenium Interdiffusion

Metallographic study of the interdiffusion zone revealed that neither Kirkendall voids nor cracking were present. The χ phase: σ phase zone width ratio was constant at 1:5 for the age times and temperatures studied. The χ phase was not observed metallographically in those samples aged at 2000°C for 100 and 1000 hours. Microprobe concentration traces of the 2000°C age couples also failed to reveal a definite χ phase region. Since published phase diagrams establish a χ phase to 2200°C, its absence at 2000°C would only be assigned to its small concentration span at this temperature (i. e., 73 to 74 atomic percent), and thus low visibility on a concentration gradient trace. Also, since the diffusion coefficient of the χ phase is slightly larger than that of the σ phase (see Tungsten to Rhenium Systems), the σ phase diffusion should be rate controlling, and σ phase should grow at the expense of χ phase.

Boltzmann-Matano analysis was not performed for this system since it is a partial couple to the tungsten-rhenium couple system, and results would have duplicated this system.

VIII. DISCUSSION OF RESULTS

The selection of refractory metals and alloys for diffusion couple analysis was based on several considerations. Refractory metal structural alloys typical of thermionic support materials were joined to pure refractory metals, typical emitter structures, to simulate thermionic system application. Also, diffusion couple systems that were not reported in the literature were selected. Sufficient alloy family and partial couples* were selected to ascertain the effect of varying boundary conditions upon couple interdiffusion characteristics. Progressive alloys (Ta, Ta-10W, T-111, ASTAR-811C) were also selected for diffusion couples with tungsten or rhenium for similar purposes.

The diffusion couple systems selected were first joined by hot isostatic pressure welding. Lower strength materials such as Cb, Cb-1Zr, Ta, etc. were easily welded. Higher strength materials required secondary processing at more elevated temperatures (hot press joining) in order to achieve 100 percent welded interdiffusion interfaces. In both cases the as-welded interdiffusion zone width was minimal with respect to subsequent diffusion age thicknesses.

Ageing temperatures were selected to span typical thermionic application conditions. Ages at 1200°C were not expected to yield substantial interdiffusion zone widths, and age times of 1000 and 2000 hours were found in most cases to be marginal for accurate microprobe analysis. Ages at 2000°C were 100 and 1000 hours and resulted in substantial interdiffusion zone widths whose analysis showed substantially no differences between 100 hour and 1000 hour interdiffusion constants. The inadvertant shorting of the control thermocouple during the 1500°C age cycle was properly rectified by optical pyrometry to 1630°C and was later supported by the coincidence of the 1630°C data with diffusion characteristics at 1200, 1500, 1800, and 2000°C (i.e., ln $(\Delta X^2/t)$ vs. $1/T$ correlations).

---

* Where W/Ta is a full couple, W/Ta-10W is a partial couple, etc.

All interdiffusion zone width parameters followed the relation

$$\ln\left(\frac{\Delta X^2}{t}\right) = A + \frac{B}{T} \tag{32}$$

where ΔX is zone width in centimeters, t is age time in seconds, and T is age temperature in degrees Kelvin. Graphical presentation of experimental interdiffusion data as

$$\ln\left(\frac{\Delta X^2}{t}\right) \text{ vs } \frac{1}{T} \tag{33}$$

and

$$\ln(\Delta X) \text{ vs } \ln(t)^{1/2} \tag{34}$$

showed good correlation to equation (32). Table 31 presents the parameters A and B (in equation 32) for the interdiffusion couple systems of this study. Correlation coefficients were good considering the small number of data points available. Most of the correlation coefficients were 0.8 or better.

Classic interdiffusion coefficients were only calculated for a few of the systems. For instance, W/Cb, W/Ta, etc. were analyzed for $\tilde{D}$, but not W/Ta-10W or similar partial couples, since these partial couples would have yielded the same results. Also, ternary or higher alloy interdiffusion couples were not analyzed for $\tilde{D}_{ij}$ due to the lack of sufficient ternary interdiffusion at one temperature (i.e., crossing path technique*). Where classic interdiffusion coefficients were calculated, correlation with published data by other researchers was established.

Classic intrinsic diffusivities (i.e., Darken's analysis with marker motion correlations) were not calculated for this study since primary concern was predicting interdiffusion zone widths. Also, distortions around the fairly large marker wires (W-2% ThO_2 at 0.001 inch diameter) caused them to form unusual geometries as well as potential disruption to normal diffusion

*See Part II, Appendix B, References 26, 27, 28, etc.

Table 31. Interdiffusion Zone Width Analytical Model*

$$\ln\left(\frac{\Delta X^2}{t}\right) = B\left(\frac{1}{T}\right) + A$$

$$\Delta X = \sqrt{t}\ \ e^{A/2}\ \ e^{B/2T}$$

System	Correlation Coefficient	A	B
1. $W_{(Pow,\ CVD)}/Cb, Cb\text{-}1Zr$	0.934	-3.8689	-37,390
2. $Re_{(pow, CVD)}/Cb, Cb\text{-}1Zr$	0.866	-0.4899	-43,880
3. $W_{(arc, CVD)}/Ta, Ta\text{-}10W$	0.897	-7.3385	-35,290
4. $W_{(arc, CVD)}/T\text{-}111, ASTAR\text{-}811C$	0.815	-3.3589	-44,720
5. $Re_{(pow, CVD)}/Ta, Ta\text{-}10W$	0.971	-7.1124	-35,020
6. $Re_{(pow, CVD)}/T\text{-}111, ASTAR\text{-}811C$	0.939	-6.4489	-36,560
7. $W_{(arc, CVD)}/Mo\text{-}50Re$	0.894	+0.1554	-45,140
8. $Re_{(pow, CVD)}/Mo\text{-}50Re$	0.929	-8.4797	-30,140
9. $W_{(arc, CVD)}/W\text{-}30.9Re\text{-}20.1Mo$	0.771	-7.2084	-34,750
10. $Re_{(pow, CVD)}/W\text{-}30.9Re\text{-}20.1Mo$	0.791	-9.3027	-28,580
11. $W_{(arc, CVD)}/Re_{(pow, CVD)}$	0.584	-4.4641	-41,300
12. $W_{(arc, CVD)}/W\text{-}25Re$	0.966	-2.1992	-47,100
13. $Re_{(pow, CVD)}/W\text{-}25Re$	0.761	+2.4148	-53,990

* Least squares fit to $\left(\frac{\Delta X^2}{t}\right) = A' e^{B/T}$

paths. Microprobe trace and spot count analyses were therefore made in areas removed from the marker locations.

The use of microhardness traverses to determine interdiffusion zone widths has been historically inaccurate and qualitative but was attempted early in this study to establish correlations with microprobe analysis. Interdiffusion analysis by microhardness traverse of the interdiffusion zone was not continued in the study since: (1) Kirkendall voids disrupted these measurements, (2) interdiffusion zone widths of small dimension were beneath the resolution of the technique, and (3) microhardness changes across the interdiffusion zone were in some cases within statistical scatter.

The effect of varying grain size on interdiffusion characteristic within each alloy family was, if present, undetectable. For instance, interdiffusion characteristics for arc cast W to a couple material were the same as CVD W to the same material. In general, post-test grain sizes were all larger than the interdiffusion zone width for both sides of the diffusion couple by factors of 10 or more. As a result of this effect, grain boundary diffusion was not an influencing factor in the analysis of the couples. This is further illustrated by the fact that the graphical presentations of $\ln (\Delta X^2/t)$ vs $(1/T)$ were linear in all cases. If grain boundary effects had been present, the interdiffusion zone widths would have been larger than expected at low temperatures, and deviations above the linear relationship described above would have been observed. This was not the case.

Several system comparisons can be made for the diffusion couples of this study. For instance, Figure 97 demonstrates the interdiffusion characteristics for the Cb/W and Cb/Re systems. There is surprisingly little variation between the two systems even though one is a solid solution couple system and the other is one with an interphase interdiffusion zone. Differences between CVD W and arc cast W, and CVD Re and powder metallurgy Re were not noticed in the

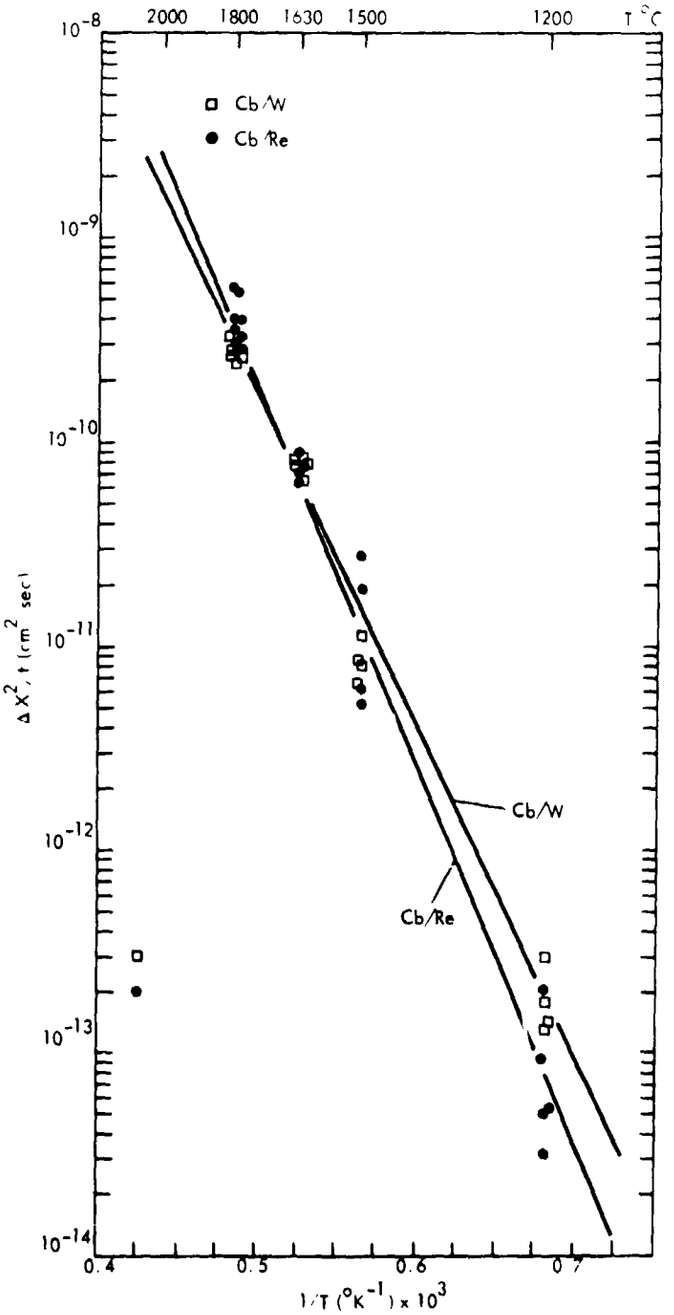

Figure 97. Interdiffusion Columbium/Tungsten and Columbium/Rhenium Systems

earlier presentation of these systems. Note also, the absence of a grain boundary effect. The statistical scatter at low temperatures is due to the resolution of analytical techniques and the small interdiffusion zone widths achieved in this temperature range. These analytical problems are not present at elevated temperatures.

Comparison of the W/Ta alloy systems is presented in Figure 98 as well as that of Re/Ta systems. The relationships of the interdiffusion characteristics are almost predictable. For instance, the interdiffusion zone width of Ta/W and W/Ta-10W couples is greater than those of T-111 and ASTAR-811C to W at low temperatures but almost equal at elevated temperatures. That the zone width of the Ta-10W/W partial couple is the same as that for the W/Ta couple was not entirely expected. As a comparison, the Re/Ta alloy systems possessed slightly higher zone widths than those of W/Ta, even though they formed multiple phase interdiffusion zones. This would be expected from a relative melting point consideration (Part II, Appendix C).

An interdiffusion predictive model was developed early in this study as an aid in predicting adequate age times and temperatures to employ (experimentally) in order to generate zone widths of analyzable dimensions. Part II, Appendix C describes the development of this model in detail. Basic interdiffusion Arrhenius equations were employed to relate the interdiffusion zone width to the entropy of the combined system. Since entropy and relative temperatures were shown to be related, the interdiffusion zone widths of various interdiffusion systems could all be related to one "family" line. The lowest melting point temperature of each binary (interdiffusion) system was selected as the point of highest entropy, and thus the point of diffusion characterization. Figure 99 presents the predicted interdiffusion/temperature relationship for the material combinations of this study, as well as the experimental line. Correlation was better than expected due to the "universality" assigned to the relationship. However, the interdiffusion characteristics of W and Re to group V and VI refractory metals and alloys can be predicted by Figure 99 with acceptable

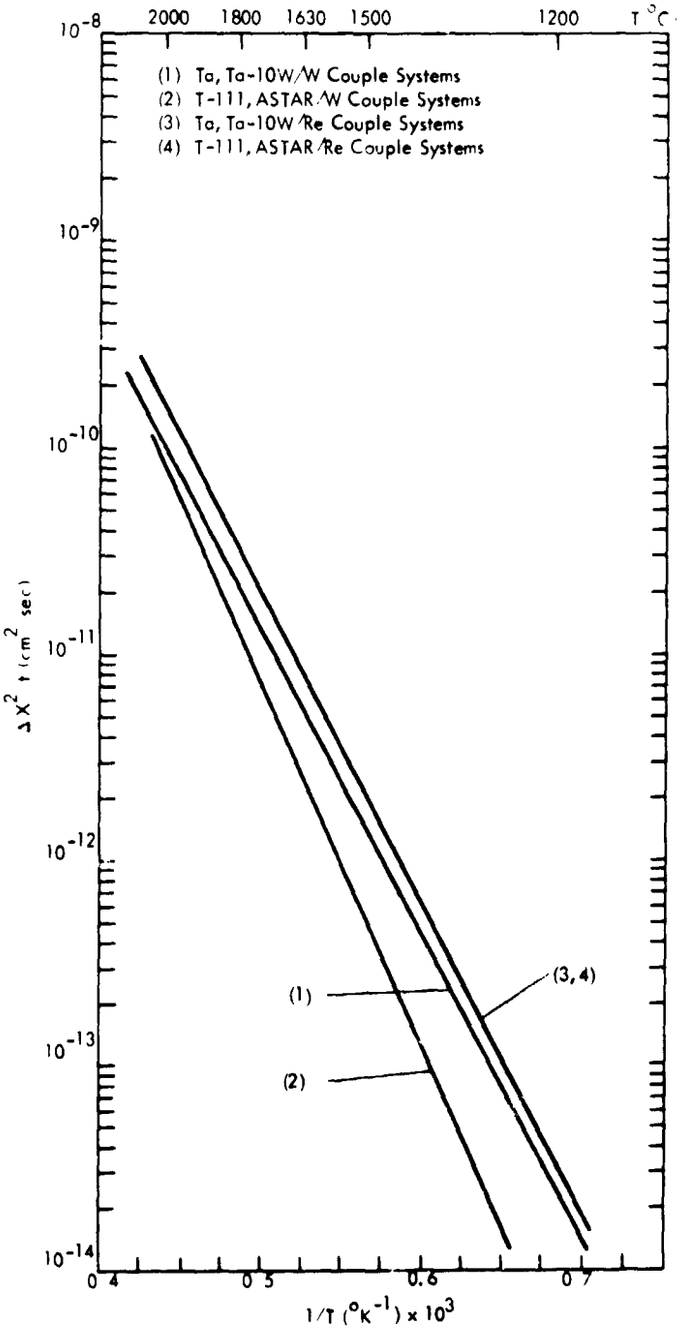

Figure 98. Interdiffusion of Tantalum Alloy Systems to Tungsten and Rhenium

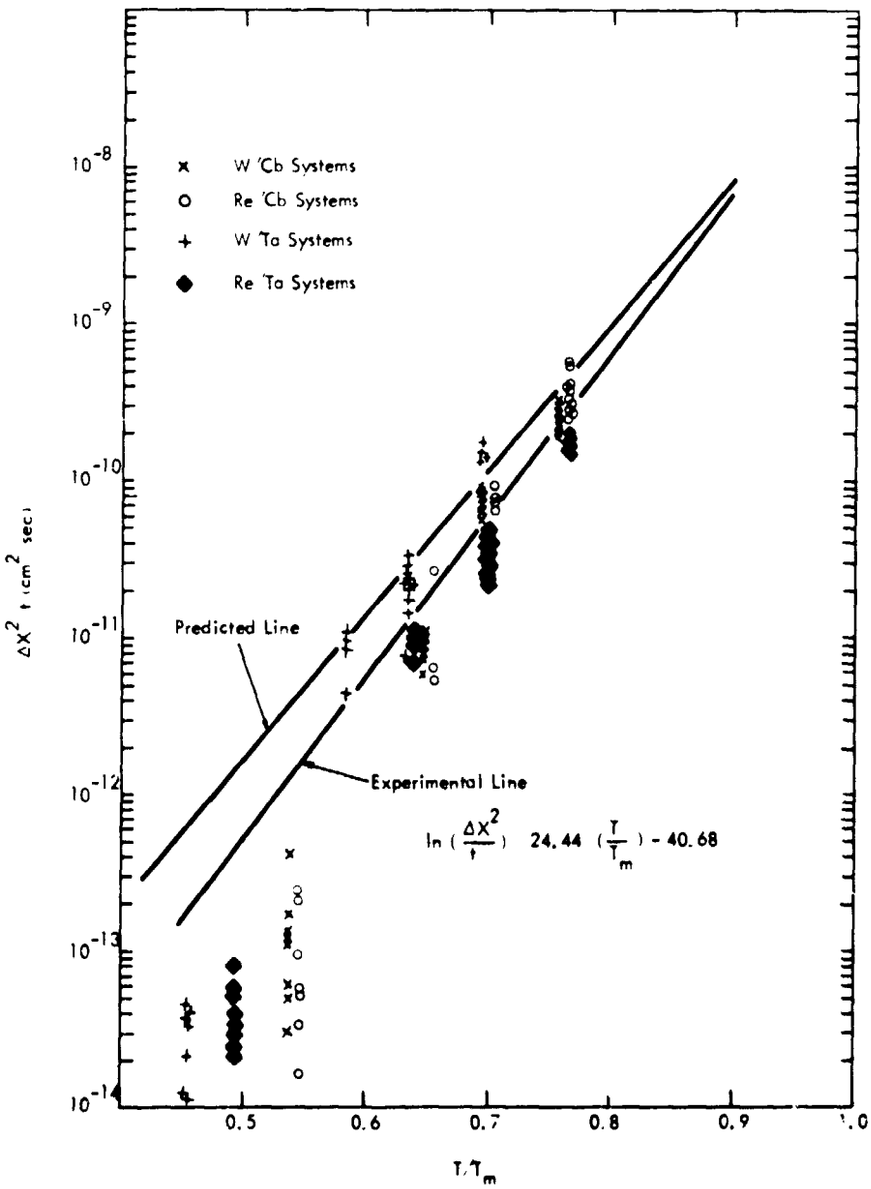

Figure 99. Comparing Predicted and Experimental Interdiffusion Predictive Models

accuracy when experimental data are not available.

Although all of the selected diffusion junctions survived their one age thermal cycle without fracture, several observations could be noted. Hot isostatic pressure welded interfaces with Re cannot be recommended for long term elevated temperature service due to brittle intermetallic phases and cracks which formed in their diffusion interfaces during short term thermal ageing. Nonplanar joints such as tubular (concentric cylinder) face joints with Re to Ta all cracked and fractured in the interdiffusion zone.* W joints to refractory metal alloys were not subject to joint cracking but were susceptible to considerable Kirkendall void formation. The most acceptable joints for long term high temperature service should be hose of W to alloys such as T-111 or ASTAR-811C after being pretreated for Kirkendall void inhibition (see Section IX, "Kirkendall Void Problems").

Since the experimental interdiffusion test pieces were all planar in geometry and small in dimension, the above recommendation of acceptable junction materials for long term high temperature service should be tempered with the fact that more tortuous tubular geometries may be more conducive to junction failure.

A means of inhibiting the formation and thus the deleterious effects of Kirkendall voids in dissimilar metal junctions is described in Section IX. Although the technique has been verified in this study with minimal experimental evidence, the implications are important enough to thermionic systems as well as other dissimilar metal junction applications to merit more thorough characterization.

---

*See Section IX, Kirkendall Void Problems.

IX. KIRKENDALL VOID PROBLEMS

A. PROBLEMS INTRODUCED BY KIRKENDALL VOIDS

When dissimilar metallic materials are joined (pressure welding, EB welding, etc.) and employed at elevated temperatures, they will interdiffuse. The interdiffusion is uneven in that the atoms of the lower melting point metal possess a higher mobility and diffuse across the junction more rapidly than those atoms of the higher melting point material moving in the opposite direction. This net flux of (low melting point material) atoms moving across the junction is compensated by a flux of vacancies moving in the opposite direction. These vacancies coalesce adjacent to the junction in the lower melting point material (Figure 100 This phenomenon is well documented in diffusion literature and is commonly referred to as the "Kirkendall Effect"[14]. Long diffusion thermal ageing inherent in the application of the dissimilar metal junction (i.e., thermionic emitter/structure joints such as CVD-tungsten or rhenium to ASTAR-811C, etc.) could result in the coalescence of these voids into an interconnecting (porous) structure[15] and,

- through interconnection, form paths that lead to junction through-leakage. Thus, in thermionic systems, vacuum or cesium plasma envelopes become compromised.
- The plane of Kirkendall voids is known to be easily fractured, due to its porous structure.
- Since the gross formation of Kirkendall voids forms in a plane, the cross sectional area for thermionic current is reduced, leading to I^2R losses and localized heating.

Employing dissimilar metal junctions of materials whose selection is dictated by other characteristics (i.e., thermionic emission) requires the prevention or inhibition of the gross growth of Kirkendall voids.

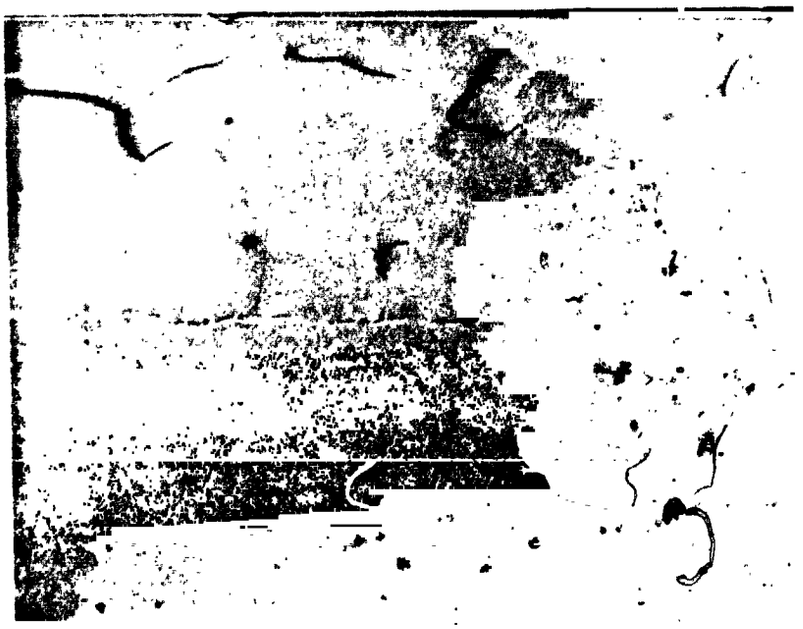

(a) W(crc cast)/Cb as HIP Welded Junction (400X)

(b) W(arc cast)/Cb Junction Aged at 1800°C/1000 hours (200X) (1AA-5)

Figure 100. Illustrating the Gross Kirkendall Void Structure Possible Through Thermal Ageing of Dissimilar Metal Junctions

Prior research has been directed toward inhibiting or retarding the interdiffusion of dissimilar metals by placing a layer of a third material, a "barrier", between them[16]. Here, the generally accepted concept is that the higher the melting point of the selected barrier material, the lower the extent of interdiffusion.

Selection of a "barrier" to interdiffusion, however, does not solve the void problem. For instance, if tungsten is coupled to columbium, no barrier of a higher melting point exists. Also, direct coupling of tungsten to columbium will still result in considerable Kirkendall void formation after brief (100-500 hours) ageing at elevated temperatures[17]. Also, if two dissimilar melting point metals are joined by a barrier with a much higher melting point, Kirkendall voids could form in each of the dissimilar metals adjacent to their interface with the barrier. Similarly, if the barrier were an intermediate melting point metal (melting point between that of the two joined metals), the Kirkendall voids could form in the lower melting point metal and in the barrier.

Often in thermionic power systems, the two metals to be joined are selected for thermionic emission and high temperature strength characteristics, and no consideration is given with respect to inhibiting the Kirkendall effect. For instance, an emitter material of CVD-tungsten or rhenium may be joined to a structural material such as ASTAR-811C, Cb-1Zr, or T-111. A means of retarding Kirkendall void formation and coalescence is required to maintain system integrity, vacuum or cesium plasma envelopes, etc. This requirement becomes more important when system lifetimes are expected to exceed 3 and 4 years without material compromise.

B. KIRKENDALL VOID INHIBITION (KVI) CONCEPTS

The objective of this cursory study is not to totally prevent Kirkendall void formation during the interdiffusion of two dissimilar metals at elevated temperatures, but to evaluate

C-3

the potential of a proposed method of reducing the coalescence and growth of such voids over that which would normally occur over the same age time/temperature conditions in junctions not treated to inhibit interdiffusion. Thus, the intent is to evaluate a method of preventing intervoid porosity and through leakage from occurring in junctions particularly susceptible to such degradation.

In order to minimize the formation of Kirkendall voids without utilizing a (dissimilar metal) barrier between two metallurgically joined dissimilar metals, the rates of interdiffusion must be investigated. The width or extent of the interdiffusion zone (ΔX) between the metals is related to their time (t) at the elevated temperature by the relationship

$$\Delta X = At^n \tag{35}$$

where n is usually found (experimentally) to be 1/2. Figure 101 illustrates the usual mode of graphically representing the interdiffusion zone width at one temperature. The information in Figure 101 can also be plotted as illustrated in Figure 102 where the rate of extent of interdiffusion is observed to decrease with time. This can also be shown by taking the time derivative of equation (IX-1):

i.e.,
$$\Delta X = At^{1/2} \tag{35}'$$

$$\frac{d\Delta X}{dt} = \frac{A}{2t^{1/2}} \tag{36}$$

Thus, from equation (35), the rate of growth of the interdiffusion zone width decreases with time. In Figure 102, the growth of the interdiffusion zone for time increment $(t_1 - 0)$ is ΔX_1, whereas for the same time increment $(t_2 - t_1)$ at a later time, the growth of the interdiffusion zone is ΔX_2 ($<< \Delta X_1$).

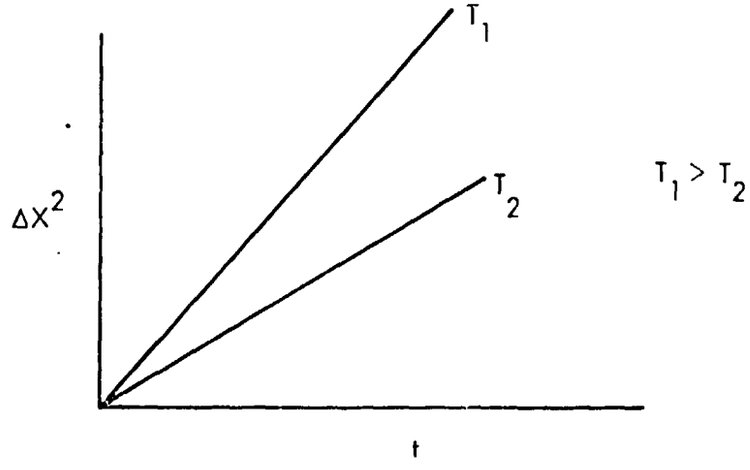

Figure 101. Extent of Interdiffusion Zone Width as a Function of Time at Temperature Ti.

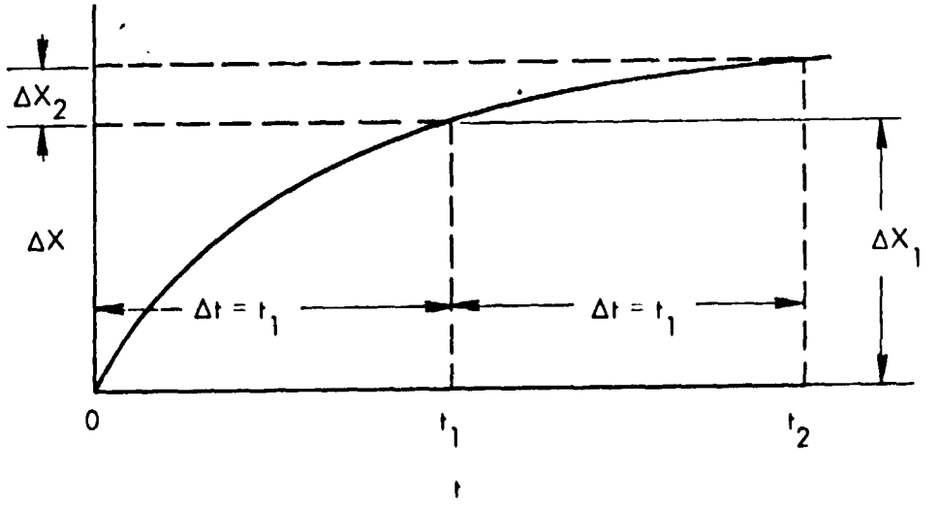

Figure 102. Illustrating Decrease in Rate of Extent of Interdiffusion with Time

Figure 103 illustrates that as the diffusion age time increases at one age temperature, the diffusion concentration profile between dissimilar metals A and B becomes lower in slope (gradient). Since the diffusion flux, J, is proportional to the concentration (activity) gradient, by the first Fick equation

$$J = -\tilde{D} \frac{\partial C}{\partial X} \tag{36}$$

where $\tilde{D}$ is the diffusion coefficient, the reason for the effect of Figure 102 is obvious. Several texts offer good reviews of concentration dependent interdiffusion ($\tilde{D}$) coefficients, the Boltzmann-Matano analysis for $\tilde{D}$, and the Kirkendall effect[18,19].

1. Alloy Layers

If a layer, ΔX_1, of material homogeneously composed of 50% A and 50% B is inserted between A and B of Figure 103, then the interdiffusion zone width at time zero is ΔX_1 (see Figure 102). Thus, the artificial interdiffusion zone width ΔX_1 forms a shallow concentration gradient to subsequent interdiffusion (Figure 104). In the following time interval t_1, the extent of further interdiffusion will be ΔX_2. More importantly, the interdiffusion at time zero now begins with the "artificial" interdiffusion zone ΔX_1, without the presence of Kirkendall voids; and the initiation and development of Kirkendall voids will now form at a reduced rate since the rate of interdiffusion has now been reduced by the void free Kirkendall Void Inhibition (KVI) layer.

The KVI layer can be expanded from the 100A/50A-50B/100B geometry to several KVI layers to further smooth the concentration (activity) gradients between A and B, i.e.,

100A/75A-25B/50A-50B/25A-75B/100B

where each layer is from a special melt.

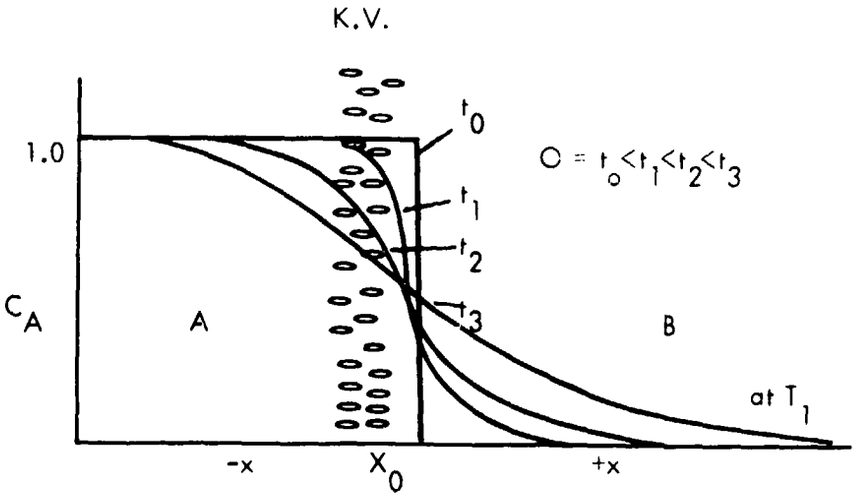

Figure 103. As the Diffusion Age Time t at Temperature T_1 is Increased, the Concentration Gradients Decrease. The Kirkendall voids Form in the Higher Mobility Metal.

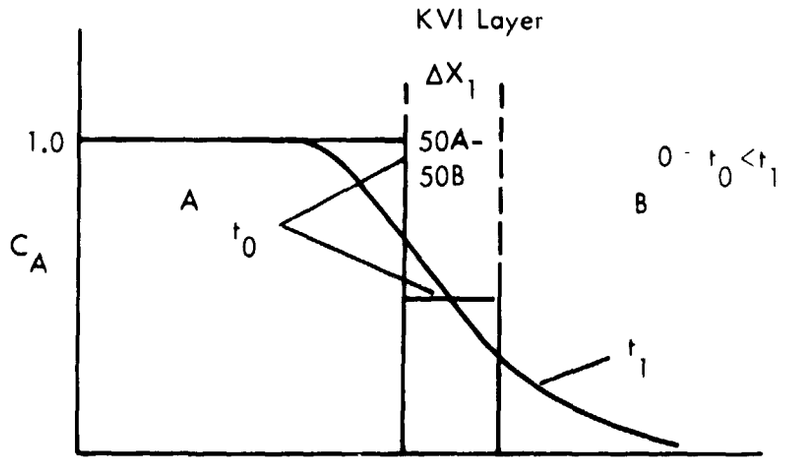

Figure 104. The Kirkendall Void Inhibition Layer Retards the Rate of Formation of Kirkendall Voids During Interdiffusion of A and B.

Or, the KVI layer may already exist as an industrial (commercially available) alloy of the two components of the junction, i,e.,

W/W-25Re/Re

The KVI layer may be formed separately and applied to the junction during metallurgical joining (hot isostatic pressure welding), or may be formed during joining (wide puddle during EB welding), or may be formed through short, elevated temperature anneals (discussed later).

It should be noted that the KVI layer is not a "barrier" but does utilize diffusion kinetics to extend the useful life of dissimilar metal joints at elevated temperatures by retarding the formation of Kirkendall voids.

Considerations such as brittle phases, KVI layer fabricability (from rolled sheet or HIP-weld junction as a powder, etc.), KVI layer thickness, etc., must also be accounted for in the selection of suitable systems.

2. Annealed Layers

If an interdiffusion couple is subjected to age time-temperature conditions which are insufficient to obtain Kirkendall voids, a mathematical approach can be employed to ascertain the position where the Kirkendall voids would appear with adequate ageing[20]. Consider Figure 105 where (a) illustrates the initial conditions of the as HIP-welded couple at time zero. In (b) the couple has been aged at temperature T for time t and presents a concentration gradient of constituent A. Boltzmann-Matano analysis results in the interdiffusion coefficient $\tilde{D}$. Knowledge of $\tilde{D}$ plus the marker (thoriated tungsten wire) motion (V) allows Darken's[21] calculation of the intrinsic diffusivities D_A and D_B. The constituency flux of A and B can then be determined from D_A and D_B and their respective concentration gradients as in Figure 105 (d). In this case, constituent B is the faster moving element, and the net flux if vacancies is into B. The rate of creation or destruction (coalescence)

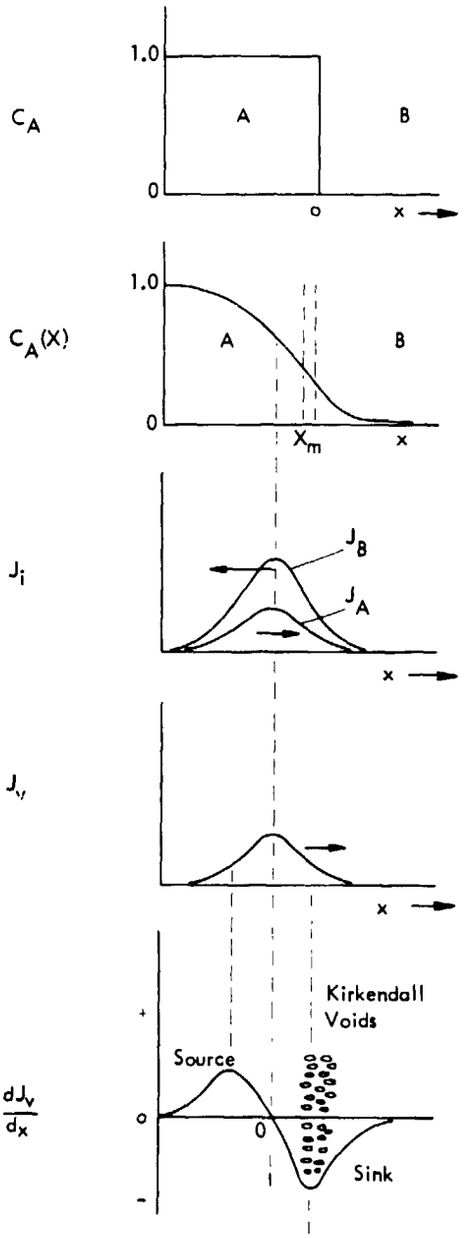

(a) Concentration plot of as HIP-welded couple at $t_o = 0$.

(b) Couple at T, $t > t_o$

Boltzmann-Matano solution yields $\tilde{D}$

Apply Darken's analysis

$$\tilde{D} = N_A D_B + N_B D_A$$

$$V_{marker} = (D_A - D_B) \frac{\partial N_A}{\partial X}$$

(c) Simultaneous solution to Darken's equations yield intrinsic D_A, D_B.

Then $J_A = -D_A \frac{\partial C_A}{\partial X}$

$$J_B = -D_B \frac{\partial C_A}{\partial X}$$

(d) The vacancy flux is

$$J_v = J_B - J_A$$

(e) The rate of creation or destruction (coalescence) of vacancies is the variance of the vacancy flux with position (i.e. $\frac{dJ_v}{dx}$).

Kirkendall voids form at the sink.

Figure 105. Predicting the Location of Kirkendall Voids

of vacancies is the variance of the vacancy flux with position, i.e., dJ_v/dX. Figure 105 (e) demonstrates the location of vacancy source and sink areas in this demonstration couple. Kirkendal' voids would be expected to form at the sink location in Figure 105 (e) if their rate of arrival exceeds the normal crystallographic mechanisms of their removal (i.e., dislocation motion, normal vacancy motion, grain boundaries, etc.).

Figure 106 demonstrates that this analysis must be further refined. Notice that as the concentration penetration profile (Figure 105 (b) becomes flattened and extended for longer age times, the vacancy source and sink peaks in Figure 106 will become shorter (i.e., fewer vacancies are being created or removed). Also, the location of the two peaks will be observed to move away from the original interface. Experimental evidence usually indicates a void free zone between the initial interface and the Kirkendall voids. This is probably an incubation zone which occurs prior to adequate vacancy density levels forming to initiate coalescence. There is probably a critical sink peak height below which the normal crystallographic removal rate of vacancies would equal or exceed their arrival rate. Thus, the optimum selection of the KVI layer composition as well as the thickness could result in no Kirkendall voids being formed. This critical sink (source) peak height is represented by the dashed lines (a, b) in Figure 106. This dashed line can be thought of as the normal vacancy equilibrium concentration supply rate found in the material of interest at the temperature being studied. Once the concentration penetration profile (Figure 105 (b)) becomes sufficiently extended so that the source and sink peaks (Figure 106) fall below the equilibrium lines, then the Kirkendall voids will cease to grow (coalesce). The KVI layer establishes this extended concentration-penetration profile immediately.

We should also note that as the diffusion age temperature is raised, the equilibrium vacancy concentration level (Figure 106, dotted line (a) will also rise while the peak heights would remain constant (i.e., derivative of $C(x,t)$ with respect to X). Thus, one would expect the absence of or a reduced Kirkendall effect at high temperatures when compared to low

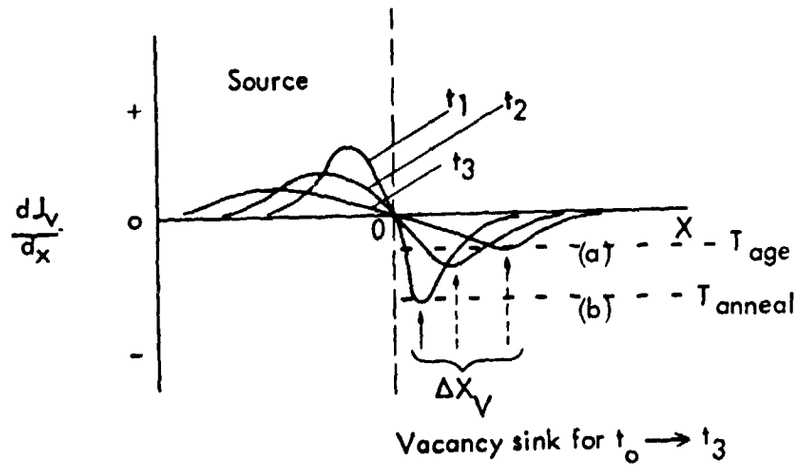

Figure 106. The Vacancy Coalescence Rate (sink) Decreases with Age Time, and the Zone of Vacancy Coalescence Moves With the Interdiffusion Profile With Age Time

temperatures. This has been shown to be true experimentally[13]. This also demonstrates that one may form the KVI layer by a short high temperature diffusion age to establish a Kirkendall void free extended concentration-penetration profile in the hardware junctions. Hudson[13] shows that the Kirkendall effect in W-Ta couples aged at 2200°C for 100 hours prior to their 400 hour ageing at 1650°C was substantially reduced over that in couples aged directly at 1650°C. This lends considerable credence to the KVI layer concept proposed in that Hudson's preage at 2200°C probably produced a KVI layer of graded concentration.

Also, since the Kirkendall voids are observed experimentally to form in one small zone in the diffusion couple, it can be proposed that the sink peak of Figure 106 exceeds the removal rate of vacancies for a brief period. Then, as the decreasing peak moves away from the interface, the normal vacancy removal rates exceed their arrival rate, and vacancy coalescence ceases to be a problem.

Thus, KVI layer junctions can also be grown through short, elevated temperature anneals where vacancy equilibrium levels and removal rates are high, and the opportunities for coalescence are minimized. Then, additional long term ageing at reduced temperatures would occur on the low growth rate part of the curve of Figure 102 and with the low sink peaks of Figure 106 resulting in little, if any, vacancy coalescence or void growth.

C. AGE SCHEDULE

Two groups of junctions were selected for cursory study: (1) a group fabricated with commercial alloy layers placed between the pure metal couples; and (2) a group with graded concentration layers grown through short, elevated temperature anneals to minimize Kirkendall void formation.

1. Alloy Layers

Tri-layer combinations to ascertain the validity of the KVI alloy layer concept were selected as:

KVI Layer (Tri-layer)	Control Couple (No KVI Layer)
W/W-25Re/Re	W/Re
Ta/Ta-10W/Ta	Ta/W

Table 32 presents the age time-temperature matrix for the KVI alloy layer study as well as the selected KVI layer initial thicknesses (ΔX). These thicknesses were determined from the predictive interdiffusion model (Part II, Appendix C) as values which bounded the maximum interdiffusion zone thicknesses expected for the control couple (no KVI layer) for the age time-temperature selected. Some thicknesses were selected to exceed expected control couple interdiffusion zones, and some were not. The commercially available alloy layers employed are not optimum KVI layers (i.e., 50-50 or graded combinations may have been preferred) but were adequate to verify or disprove the concept.

2. Annealed Layers

Diffusion couple material combinations selected to ascertain the validity of the KVI annealed (graded) layer concept were selected. It was decided to grow KVI layers through high temperature anneals for the following systems:

Re/Ta

W/Ta

CVD Re/Ta (tube)

Table 32. Alloy KVI Tri-layer Age Schedule

Code: X = Scheduled KVI layer couple
o = Control couple
( ) = KVI layer thickness (cm x 10^3)

T (°C)	t (Hours)	KVI Ta/Ta-10W/W	Control W/Ta	KVI W/W-25Re/Re	Control W/Re
2000	2000	X (25.4)	o	X (38.1)	o
	1000	X (25.4)	o	X (38.1)	o
	100				o
	10				
1800	2000	X (12.7)	o		
	1000	X (12.7)	o	X (25.4)	o
	100		o		o
	10				
1500	2000	X (12.7)	o	X (12.7)	o
	1000		o		o
	100				
	10				
1200	2000		o		
	1000		o		
	100				
	10				

The diffusion ages for annealed layers are presented in Table 33. The KVI annealed layer is a compositionally graded layer grown through a high temperature anneal, while the KVI alloy layer is a stepped layer produced through the hot isostatic pressure (HIP) welding or hot press welding of stratified alloy sheets.

The interdiffusion predictive model (Part II, Appendix C) was used to predict the KVI layer anneal conditions (time, temperature) required to produce the desired layer thicknesses (at $T/T_m = 0.94$) illustrated in Table 34. The KVI annealed layer thicknesses, as can be seen in Table 34 were not selected to eliminate all Kirkendall voids but to encompass the predicted interdiffusion zone growths expected for low temperature ageing. This method (controlled experiment) of reducing Kirkendall voids was expected to yield more information than their total reduction through the employment of a wide KVI annealed layer. Wide KVI layers were not desired since they could also create problems in embrittlement, subsequent handling, thermal cycling, and a resultant lack of measurable data.

Ramp time corrections to the preage anneal (i.e., heatup and quench contributions to KVI zone width growth) are treated in Part II, Appendix D.

3. Preparation and Age

The alloy interlayer KVI couples were prepared as described earlier by vacuum encapsulation in molybdenum containers and HIP welding. The annealed KVI layers were prepared by short time anneals at 0.95 T/T_m in a 10^{-5} torr tungsten mesh resistance furnace. Temperatures were monitored by optical pyrometry and power-temperature curve extrapolations from lower temperatures. The anneal time-temperature conditions selected for KVI growth are described in Table 34, footnote 2. These conditions were selected to give grown interdiffusion layers of thicknesses which fell on either side of the thickness which would occur in non-preannealed, aged couples (i.e., control couples).

Table 33. KVI (Annealed) Layer Age Schedule

Age Condition	KVI Combination						
	Ta/Re ΔX_1*	Ta/Re ΔX_2	Ta/W ΔX_3	Ta/W ΔX_4	Ta/CVD Re		
					ΔX_5=O Tube	ΔX_1 Tube	ΔX_2 Tube
1800°C							
1000 hrs	X	X	X	X	X	X	X
100 hrs	X	X	X	X	X	X	X
1500°C							
2000 hrs	X	X	X	X	X	X	X
1000 hrs	X	X	X	X	X	X	X
Control (No age)	X	X	X	X	X	X	X

* ΔX_1 and ΔX_2 denote KVI annealed layer thickness

See Table IX-3. $\Delta X_1 = 25.4 \times 10^{-3}$ cm

$\Delta X_2 = 7.6 \times 10^{-3}$ cm

$\Delta X_3 = 15.2 \times 10^{-3}$ cm

$\Delta X_4 = 5.1 \times 10^{-3}$ cm

ΔX_5 = As deposited, no KVI layer (ΔX = 0 cm)

Table 34. KVI (Annealed) Layer Predicted Thicknesses (cm x 10^3) to be Aged

Diffusion Age Conditions		W/Ta				Re/Ta			
		Predicted	Programmed KVI ΔX**			Predicted	Programmed KVI ΔX**		
(°C)	(hrs.)	ΔX*	ΔX_3	ΔX_4	ΔX_0	ΔX*	ΔX_1	ΔX_2	ΔX_0
1800	1000	5.48	15.2	5.1	0***	9.38	25.4	7.6	0***
	100	1.73	15.2	5.1	0***	2.97	25.4	7.6	0***
1500	2000	4.24	15.2	5.1	0***	6.00	25.4	7.6	0***
	1000	3.00	15.2	5.1	0***	4.24	25.4	7.6	0***

* Predicted interdiffusion zone thickness for a non-KVI layer couple from interdiffusion predictive model of Appendix C.

** KVI growth conditions at 0.95 T/Tm

W/Ta 15.2×10^{-3}cm = ΔX_3; 2800°C for 3.6 hours

W/Ta 5.1×10^{-3}cm = ΔX_4; 2800°C for 0.4 hours

Re/Ta 25.4×10^{-3}cm = ΔX_1; 2500°C for 10 hours

Re/Ta 7.6×10^{-3}cm = ΔX_2; 2500°C for 0.9 hours

*** Non-KVI layered control couples.

All KVI couples were indexed (see Appendix F, Diffusion Couple Age/Identification Chart), and were aged with the interdiffusion couples as described earlier in this report. As reported earlier, age temperatures did not vary by $\pm 20^{\circ}C$, and vacuum conditions were $1.2 \times 10^{-6} N/m^2$ (10^{-8} torr) or better for the duration of the age cycle (except for a brief, 1 hour, period at $10^{-3} N/m^2$ (10^{-5} torr) during age startup).

D. RESULTS AND DISCUSSION

The effectiveness of the KVI preage treatment upon subsequent Kirkendall void formation was evaluated qualitatively. Comparison of Kirkendall void structure between KVI treated couples and control couples showed the KVI treatments to be effective in reducing or eliminating Kirkendall voids.

Figure 107 presents the as-welded and aged control couple, $W_{arc\ cast}/Ta$ - 1800°C/ 1000 hours, while Figure 108 presents a similar couple for the W_{CVD}/Ta system. Note in both systems that the Kirkendall void structure is the same, i.e., elongated, interconnected voids on the Ta side of the weld interface. Figure 109 presents the W/Ta interface of the annealed (2650°C - 0.4 hour) KVI couple prior to and after ageing at 1800°C for 1000 hours. Figure 110 also illustrates other zones of the interdiffusion interface of the W/Ta KVI couple and demonstrates that the Kirkendall voids of Figures IX-8 and 108 are almost entirely eliminated.

If the W/Ta KVI couple is initially annealed at 2650°C for 3.6 hours (rather than 0.4 hours), the post-age results are as illustrated in Figure 111. The reduced number of Kirkendall voids, which do form (over those appearing in non-KVI treated couples), are located further away from the weld (juncture) interface than those in Figure 110, aged at 2650°C for 0.4 hour. This is compatible with the extended concentration/penetration profiles grown at the longer anneal times at 2650°C. Contrary to expectation, the density of

(a) W(arc cast)/Ta As Welded Diffusion Couple (200X)

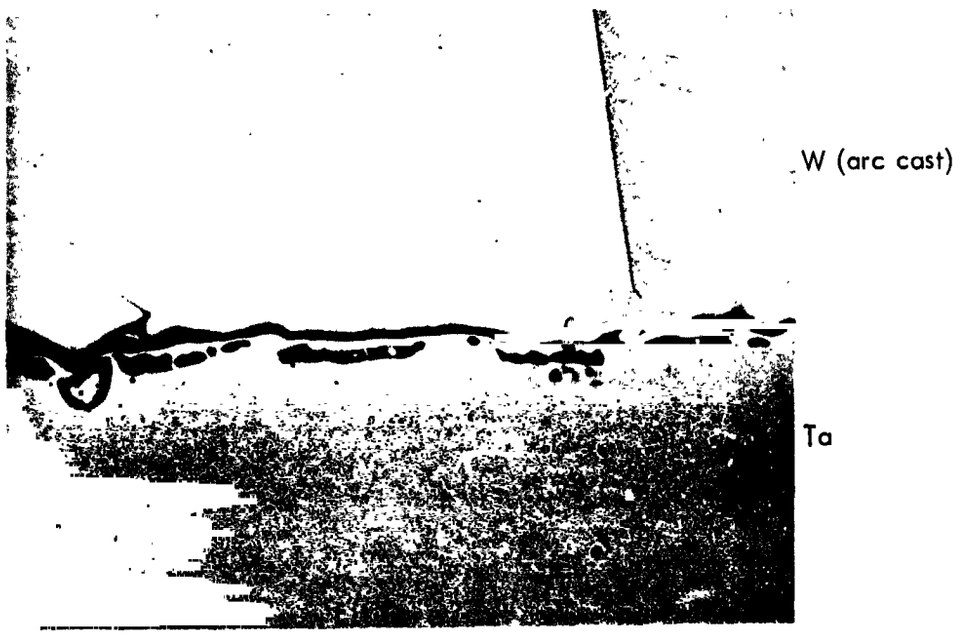

(b) W(arc cast)/Ta After Ageing at 1800°C/1000 hours (200X)

Figure 107. The W/arc cast)/Ta Control Couple. Note the Coalesced Void Structure in the Ta Side of the Interface

(a) W(CVD)/Ta as HIP Welded Diffusion Couple (400X)

(b) W(CVD)/Ta After Ageing at 1800°C/1000 hours (200X)

Figure 108. W(CVD)/Ta Control Couple Note the Coalesced Void Structure in the Ta Side of the Interface

(a) W/Ta Interface After Preanneal at 2650°C for 0.4 hours (200X)

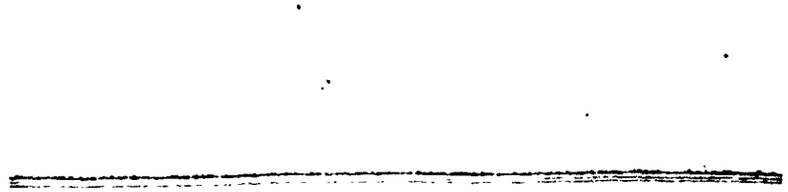

(b) W/Ta Preannealed Couple After Ageing at 1800°C for 1000 Hours (200X)

Figure 109. The Preannealed W/Ta KVI Diffusion Couple, Preannealed at 2650°C for 0.4 hours Prior to Ageing at 1800°C for 1000 hours.
(Continued on next page)

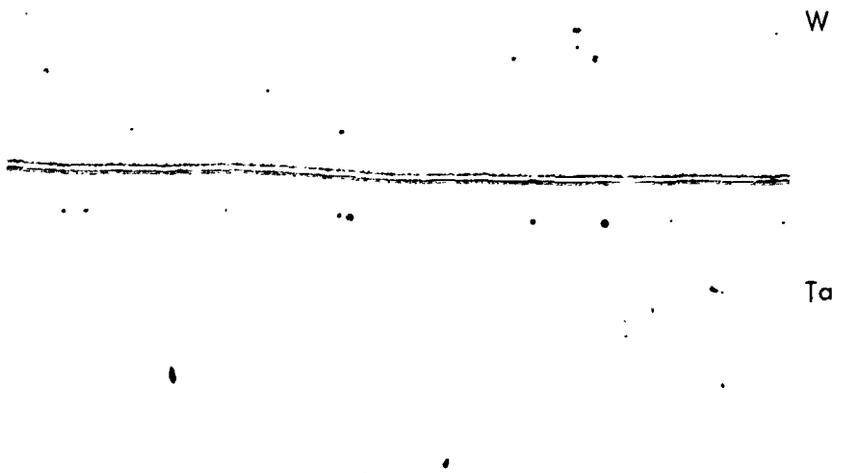

(c) W/Ta Preanneal Couple (2650°C/0.4 hours) After Ageing at 1800°C/1000 hours (200X)

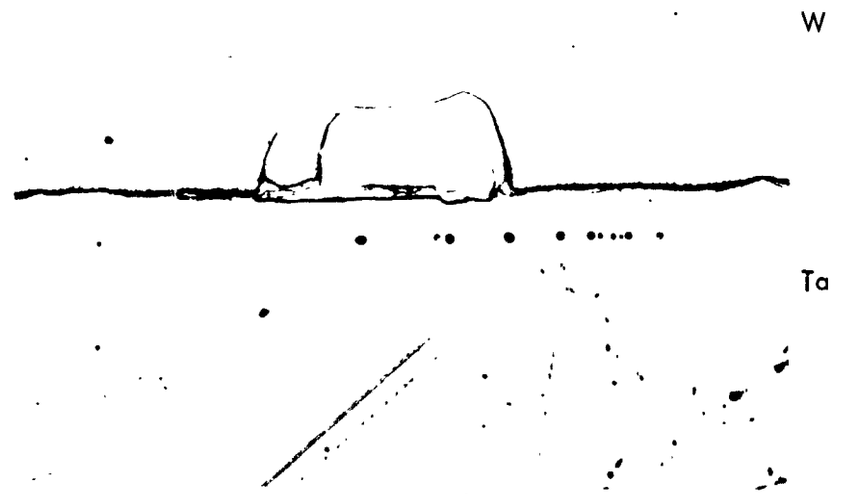

(d) W/Ta Preannealed Couple (2650°C/0.4 hours) After Ageing at 1800°C/1000 hours (200X)

Figure 110. (Continued from previous page)

(a) W/Ta Interface After Preanneal at 2650°C for 3.6 hours (200X)

(b) W/Ta Preannealed Couple After Ageing at 1800°C for 1000 Hours (200X)

Figure 111. The Preannealed W/Ta KVI Diffusion Couple, Preannealed at 2650°C for 3.6 hours Prior to Ageing at 1800°C for 1000 Hours

Kirkendall voids appears to be slightly larger than that resulting from anneals at 2650°C for 0.4 hour prior to 1800°C/1000 hour ageing. This may be a statistical variation in sample structure or could be real. Further study will be necessary to resolve this issue.

Inhibiting Kirkendall void structures from forming in the Ta/W system was also attempted with alloy KVI layers. Figure 112 (a) presents, again, the $W_{arc\ cast}$/Ta control couple aged 1000 hours at 1800°C. Figure 112 (b) demonstrates that the insertion of a Ta-10W alloy interlayer of 5 mils (0.013 cm) thickness considerably reduces the density of Kirkendall voids over that occurring in the control couple.

The void density, which does appear, is not, however, as limited as that which resulted from high temperature preageing. The voids appear in the Ta-10W alloy layer next to the W/alloy junction and are in a plane. The plane is further from the couple interface than that occurring in the pure Ta/W control couple.

Figures 113, 114, 115, and 116 present the results of the KVI concept feasibility study. Results were more positive for the W/Ta systems than for the Re/Ta systems since the latter: (1) possessed closer melting points and were therefore less susceptible to Kirkendall void formation, and (2) formed brittle intermetallic phases in the interdiffusion zone which cracked and could have affected interdiffusion. Also, high temperature pre-annealing of the interdiffusion couples appeared more promising in eliminating Kirkendall voids than alloy tri-layer insertion.

Consider Figure 116. If a dissimilar metal junction is aged at an elevated temperature, 0.90 Tm or higher, then the Kirkendall void structure which results will be considerably reduced over that which occurs at a lower temperature, since vacancy removal rates through bulk diffusion, dislocations, and grain boundaries are higher (i.e., T_{anneal} line (b)

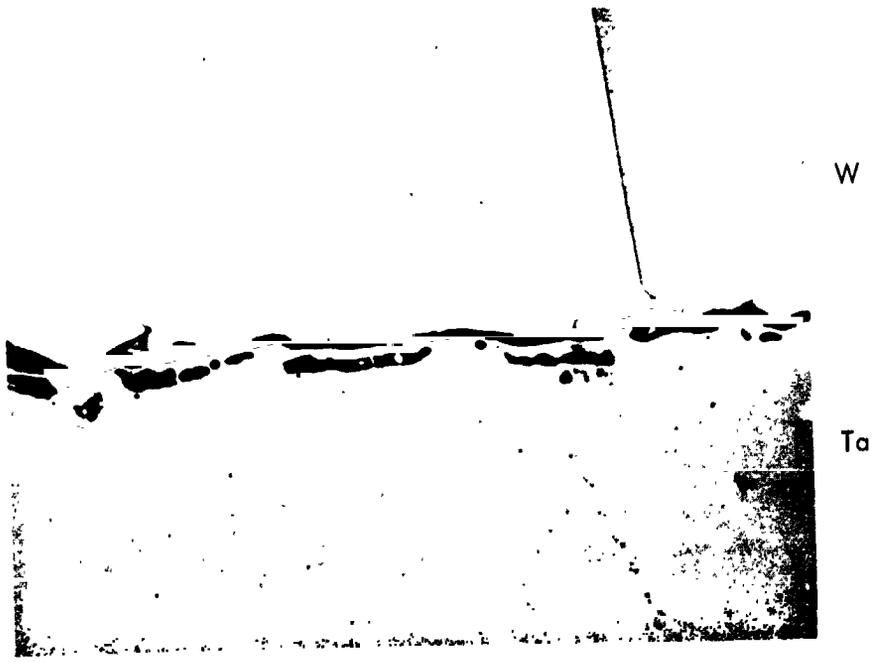

(a) W(arc cast)/Ta Junction After 1800°C/1000 hours Ageing (Control) (200X)

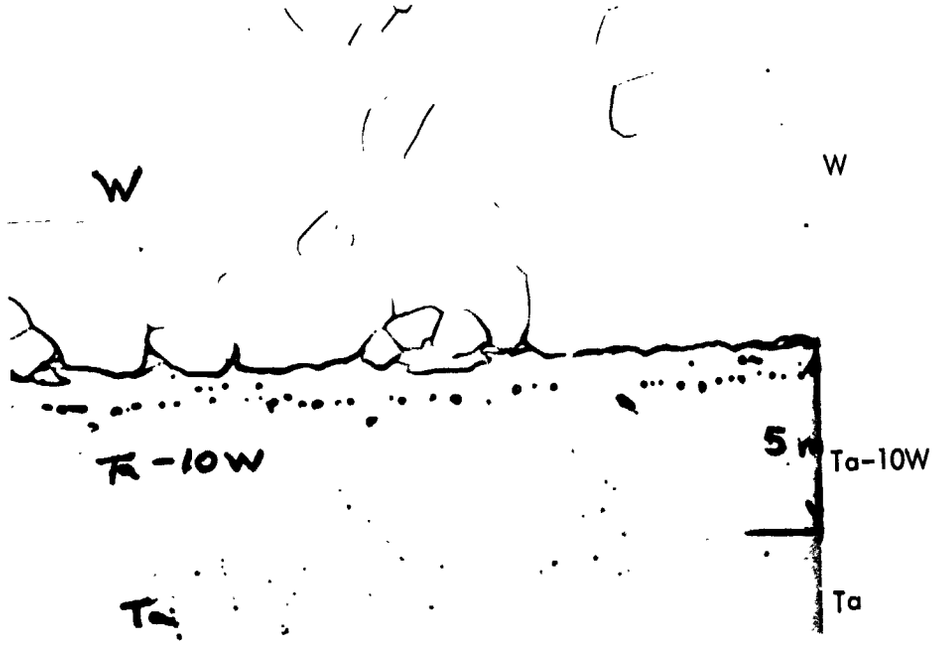

(b) A W/Ta-10W/Ta Alloy KVI Layer (.005-inches) After Ageing at 1800°C/1000 Hours (200X)

Figure 112. The Effect of a KVI Alloy Layer Between Junction Materials

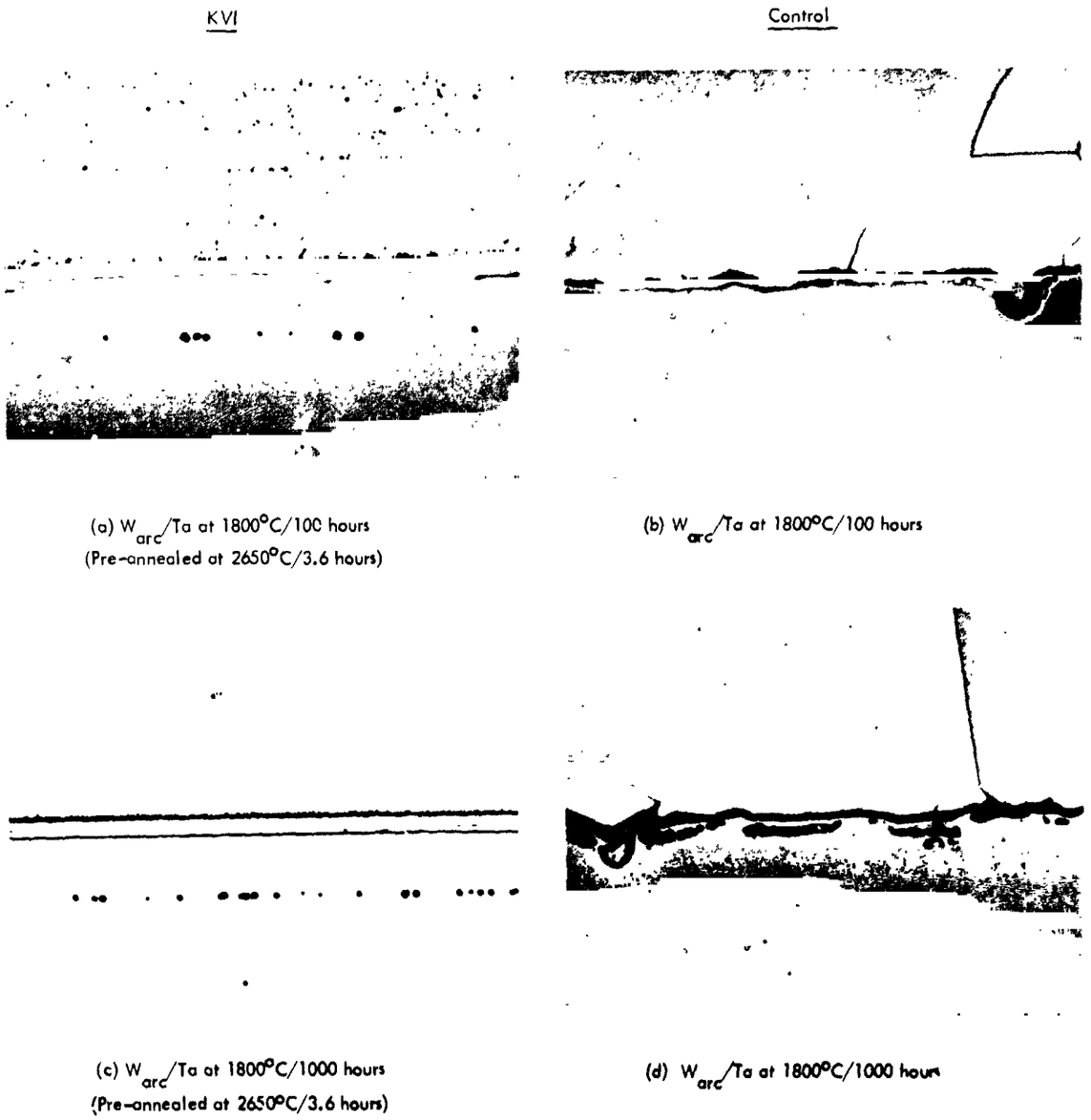

(a) W_{arc}/Ta at 1800°C/100 hours
(Pre-annealed at 2650°C/3.6 hours)

(b) W_{arc}/Ta at 1800°C/100 hours

(c) W_{arc}/Ta at 1800°C/1000 hours
(Pre-annealed at 2650°C/3.6 hours)

(d) W_{arc}/Ta at 1800°C/1000 hours

Figure 113. Post-Age KVI Observations: W/Ta Pre-Annealed Aged Couples
(All photomicrographs at 200X)

KVI

Control

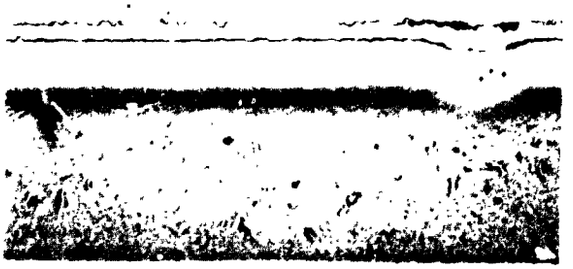

(a) $Re_{(p)}/Ta$ at 1800°C/100 hours
(Pre-annealed at 2500°C/0.9 hours)

(b) $Re_{(p)}/Ta$ at 1800°C/100 hours

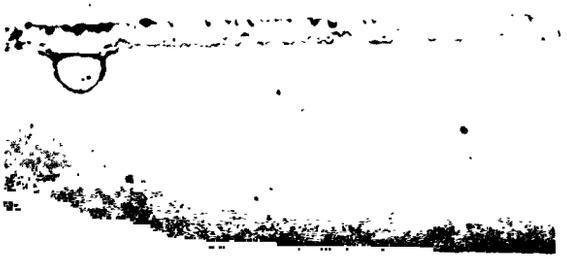

(c) $Re_{(p)}/Ta$ at 1800°C/1000 hours
(Pre-annealed at 2500°C/0.9 hours)

(d) $Re_{(p)}/Ta$ at 1800°C/1000 hours

Figure 114. Post-Age KVI Observations: Re/Ta Pre-Annealed Aged Couples
(All photomicrographs at 200X)

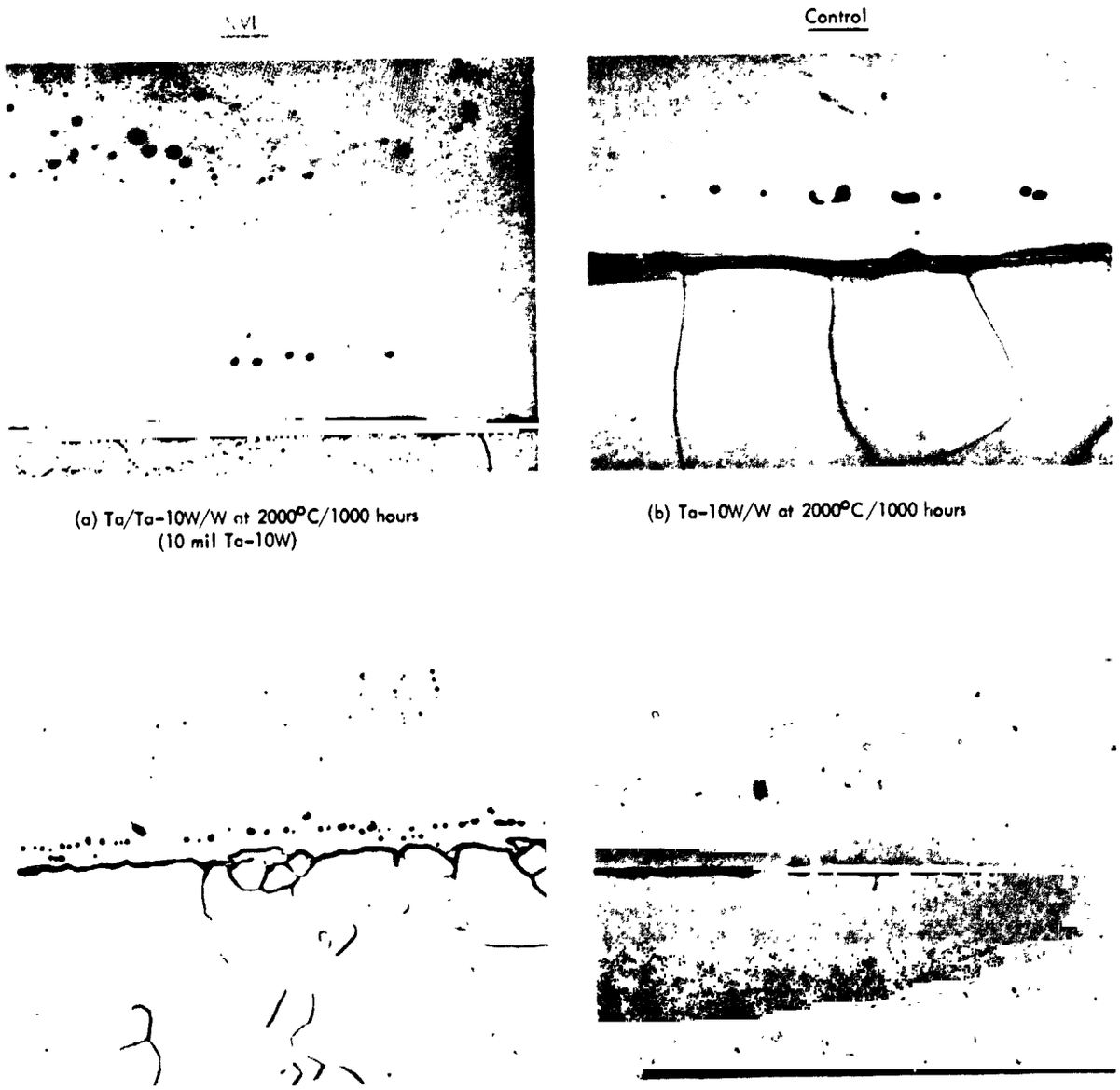

(a) Ta/Ta-10W/W at 2000°C/1000 hours
(10 mil Ta-10W)

(b) Ta-10W/W at 2000°C/1000 hours

(c) Ta/Ta-10W/W at 1800°C/1000 hours
(10 mil Ta-10W)

(d) Ta-10W/W at 1800°C/1000 hours

Figure 115. Post-Age KVI Observations: Ta/Ta-10W/W Alloy Tri-Layer Couples (All photomicrographs at 200X)

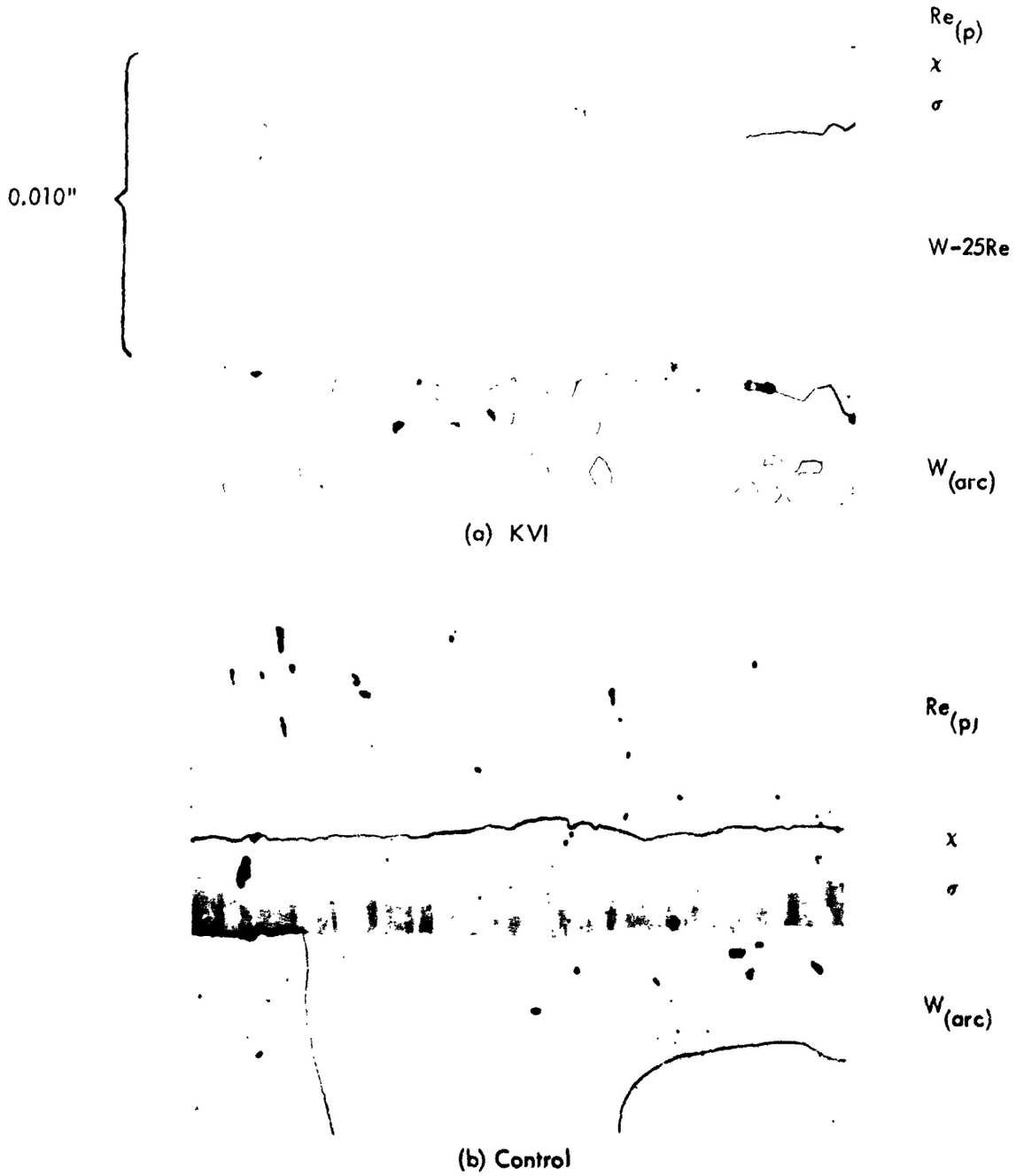

Figure 116. Post-Age KVI Observations: W/W-25Re/Re Alloy Tri-Layer Couples Age at 1800°C/1000 hours (All photomicrographs at 200X)

of Figure 106 as opposed to T_{age} line (a)). Also, vacancy equilibrium concentration levels are higher. It may also be hypothesized that long age treatment of dissimilar metal junctions at low temperatures would result in reduced Kirkendall effects. At low temperatures the vacancy flux would be very small, and again normal crystallographic short circuiting paths such as dislocctions, grain boundaries, etc. would remove excess vacancies before they could accumulate or coalesce as voids. Figure 117 thus demonstrates that Kirkendall voids are more likely to form at intermediate temperatures and are more gross in density and appearance in this select temperature range.

Similarly, short time ages will result in little if any void structure since an incubation period is required before sufficient vacancies can coalesce to form an optically visible void. Once formed, voids will grow rapidly until the vacancy arrival .ate diminishes. This occurs when the interdiffusion concentration penetration profile becomes sufficiently distended that the vacancy flux then equals or becomes lower than the active vacancy removal rate (see Figure 105). This observation is illustrated in Figure 118, where the maximum vacancy growth rate occurs during a short period of the total age time. Observation of voids of couples aged for 1000 hours and 2000 hours found voids of nearly the same dimension. It would appear, then, that maximum void growth occurred early in the age cycle when diffusional fluxes were high.

The location of the void plane in the lower melting point material with respect to the weld interface will also be observed to vary with temperature. For instance, in preannealed Ta/W KVI couples, the void plane in couples preannealed at 2650°C for 3.6 hours is farther from the weld plane than the void plane of the Ta/W couple preannealed at 2650°C for 0.4 hour (both aged at 1900°C for 1000 hours). This appearance of Kirkendall voids at the same concentration level (i.e., point in the concentration-penetration profile) was also observed by Hehemann[4]. Further study will be necessary to resolve, if this plane is

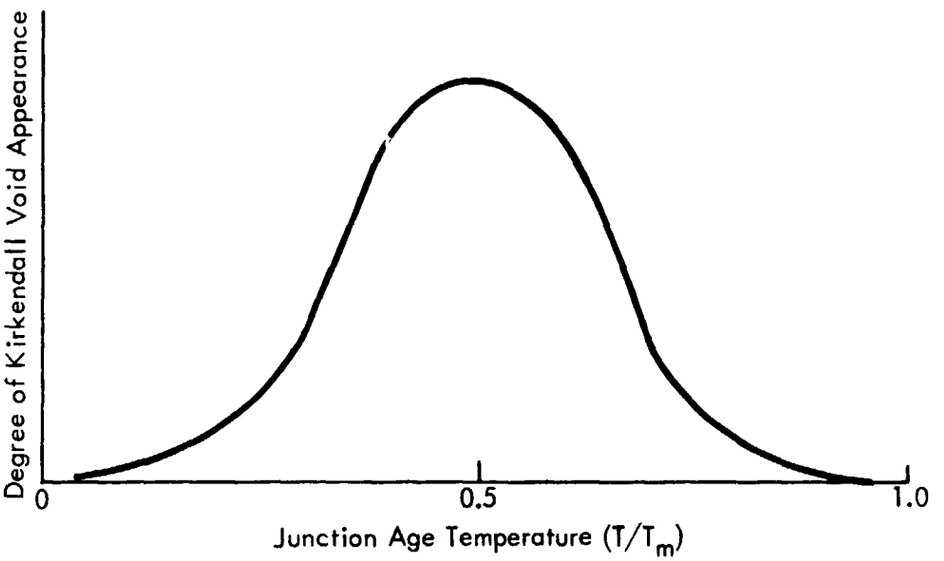

Figure 117. Kirkendall Voids Are More Likely to Form at Intermediate Temperatures Than at Low or Elevated Temperatures

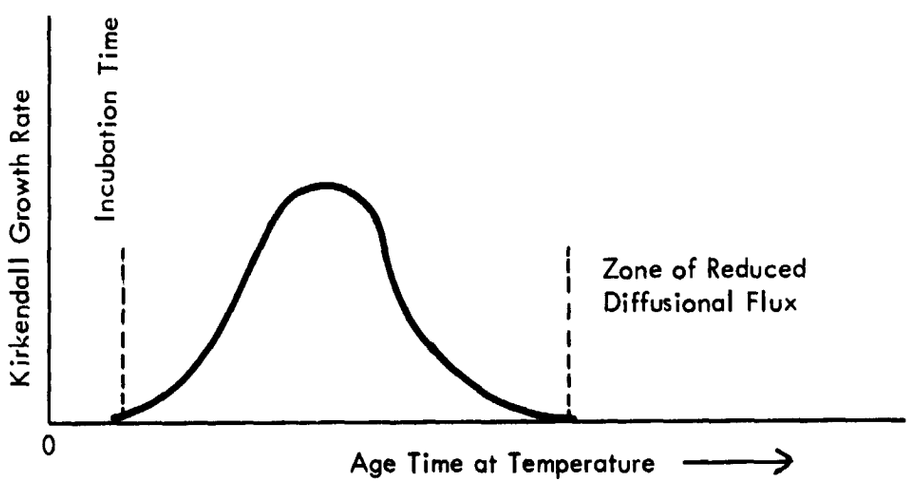

Figure 118. The Kirkendall Void Structure Will Grow Only Until the Vacancy Arrival Flux Equals the Vacancy Removal Rate

consistently the inflection point of the vacancy flux profile (Figure 105 (d, e)). A parabolic plot of the void plane distance from the weld plane with respect to age time and microprobe concentration correlations at void locations should resolve this issue.

Further quantitative study beyond this cursory investigation should be performed. Initial evidence indicates that the Kirkendall void structure can be reduced if not entirely eliminated through the proper formation (alloy layer) or thermal pretreatment (anneal layer) of dissimilar metal junctions destined for long term thermal environments.

X. ELECTRON BEAM WELD STUDIES

A. MATERIAL SELECTION

As discussed in Section I of this report, the typical thermionic system of interest would employ a high temperature emitter material joined to the necessary structural elements. The tubular type configurations involved lend themselves to welding as the simplest assembly approach, if welds with satisfactory properties could be produced. Thus an evaluation of electron beam welding applied to dissimilar metals applicable to thermionic designs was performed.

A review of the desired materials for the emitter and structural portion of the thermionic system led to the selection by NASA program management of Re to Cb-1Zr and W-25Re to Cb-1Zr for this study. It was recognized that rhenium forms brittle intermetallics, Sigma and Xi, in combination with columbium. However, success in welding had been achieved in other systems, for example stainless steel to Ta by adjusting heat balance to achieve a braze type joint. While joints of this type may not be recommended for high strength applications, they could be resistant to thermal cycle stresses and serve as effective seals for a closed system. Thus it was felt that the ability of the electron beam process to control intermixing during welding, through parameter selection and joint design variation, should be explored on the material combinations noted.

Flat sheet material .05 x 8.9 cm (.020 thick x 3-1/2" long) was employed in these tests. Powder metallurgy Re and arc cast W-25Re were utilized. The characteristics and prior history of these materials and the Cb-1Zr sheet are discussed elsewhere in this report.

Simple holddown clamps provided the required fixturing for these butt welds produced in a 150 KV, Hamilton Standard Electron Beam Welder.

B. BUTT WELDING

A series of sheet butt joints .05 cm thick (.020") were produced with variations in speed, preheat, and beam position relative to the weld seam. In all cases weld current was adjusted

to that required for full penetration. Table 35 details the results of these weld tests on both material combinations. It can be seen that defect free welds, as revealed by visual and dye penetrant examination, were produced between W-25Re and Cb-1Zr alloy with parameter combinations that minimized material intermixing. These conditions required low weld speed and electron beam placement preferentially on the Cb-1Zr side of the weld seam. In this manner the lower melting temperature Cb-1Zr was fused and flowed against the W-25Re alloy. Figures 119, 120, and 121 show typical weld cross sections produced in this manner. Obviously control of this technique is difficult and duplication of results was not consistent.

Satisfactory weld configurations could not be achieved when placing the beam on the W-25Re. Power levels adequate to completely melt the higher melting point material caused excessive melt back of the Cb-1Zr alloy. Even when bonding was achieved, with apparent limited intermixing, cracking would occur in the melt zone immediately adjacent to the W-25Re. This can be observed in Figures 122 and 123.

Regardless of the butt weld technique employed, no success was obtained in joining the Re to the Cb-1Zr. Similar weld zone configurations could be produced but cracking always occurred. Typical conditions are shown in the cross section of Figure 124. The weld parameters in this case duplicated those that had produced some success in the other material combination.

C. LAP WELDING

Experience at WANL with lap type weld configurations in other systems had indicated better control of material intermixing could be achieved with this joint design. The lower melting material would be heated preferentially and melted against the higher melting point material. This approach was pursued and a number of short length (approximately 3.8 cm (1.5")) welds were successfully produced between Cb-1Zr and Re. These joints were free of cracks as revealed by dye penetrant examination. The conditions were successfully reproduced on

Table 35. Sheet Butt Welding Parameter Evaluation, Electron Beam Process
(120 KV, 3 to 5.5 milliamps selected for correct penetration)

A. Cb-1Zr to W-25Re

	15 ipm (38 cpm) Weld Speed			60 ipm (151 cpm) Weld Speed	
Beam Center Position	Room Temperature	426°C Preheat	704°C Preheat	Room Temp.	426°C Preheat
.010" (.025 cm) on Cb-1Zr	No. 1. Good Weld No. 2. Trans. Cracking	Good Weld		Trans. Cracking	
Seam	Trans. Cracking			Lack of Fusion (Edge Rollback)	
.010" (.025 cm) on W-25Re	Longitudinal Edge Cracking			Lack of Fusion Trans. Cracking	
B. Cb-1Zr to Re					
.010" (.025 cm) on Cb-1Zr	Trans. Cracking	Trans. Cracking	Trans. Cracking	Lack of Fusion (Edge Rollback)	
Seam				Complete Long. Cracking	
.010" (.025 cm) on Re	Complete Long. Cracking			Complete Long. Cracking + Lack of Fusion	

Figure 119. W-25Re to Cb-1Zr (Weld No. 1), Electron Beam Positioned .010" (.025 cm) on Cb-1Zr (50X)

Figure 120. Melt Zone - W-25Re interface of Weld Shown in Figure 1A(400X)

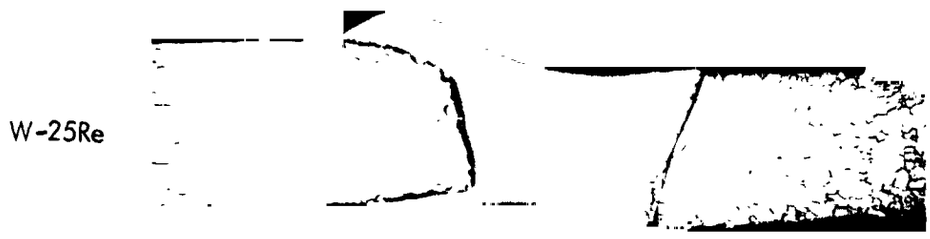

(50X)

Figure 121. W-25Re to Cb-1Zr, Electron Beam Positioned .010" on Cb-1Zr

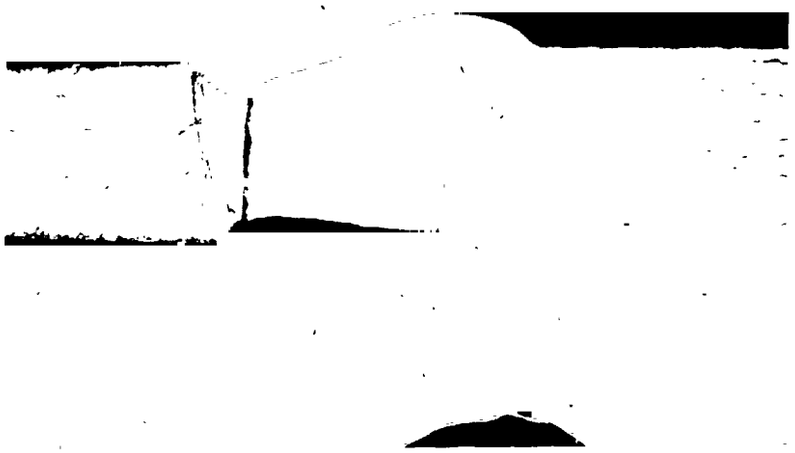

(50X)

Figure 122. Cb-1Zr to W-25Re, Electron Beam Positioned .010" (.025 cm) on W-25Re

(400X)

Figure 123. Longitudinal Cracking at Interface of Melt Zone and W-25Re on Weld Shown in Figure X-3A.

(50X)

Figure 124. Cb-1Zr to Re, Electron Beam Positioned .010" (.025 cm) on Cb-1Zr, Cracking Occurs Near the Cb-1Zr - Melt Zone Interface.

8.9 cm (3-1/2") length specimens (standard for this program). As in the production of butt welds, lap welding of the Cb-1Zr to W-25 Re material was achieved with lesser difficulty.

Tables 36 and 37 list the parameters employed for each of the lap weld tests. It can be seen that lower speeds, 12.7 cm/min (5 ipm),were most successful. Figures 125, 126, 127, and 128 are cross sections of typical crack free joints. In this case the Cb-1Zr had been heated preferentially and melted against the rhenium.

The weld schedule which produced successful and reproducible lap joints in both material combinations was as follows:

Standard Lap Joint Weld Procedures

Weld Parameter	
Overlap	1/32 inch (.079 cm) (Cb-1Zr on top)
Beam center location from seam	.015 inch (.038 cm) in Cb-1Zr
Weld speed	5 ipm (12.7 cm/min)
Voltage	110 KV
Current	3.5 MA
Deflection	None
Work distance	6.5 inches (16.5 cm)
Pre-heat	None
Beam focus	Defocus to .025" (.064 cm) diameter

It was apparent from these tests that whenever intermixing of fusion zones in the dissimilar metals occurred, severe cracking could not be avoided.

Attempts to heat the higher melting point material (Re) and through conductive heating cause localized melting and bonding to the Cb-1Zr were unsuccessful in all but one case (see Figures 129 and 130). This short 3.8 cm (1.5") joint could not be duplicated with similar weld parameters. It does illustrate however that where minimal intermixing occurs (a braze type joint) a sound joint may be achieved.

Table 36. Lap Welding of Rhenium to Columbium-1Zirconium Alloy .020" Sheet

Lap Weld No.	Overlap (in.)	Overlap (cm)	Beam Center Location from Seam	Weld Speed (ipm)	Weld Speed (cpm)	Voltage (KV)	Current (MA)	Focus	Deflection	Remarks
1	Re, 1/32	(.08 cm)	.020" (.051 cm) on Re	10	(25.4 cpm)	120	6	Sharp	None	Melting and burn thru
2	Re, 1/32	"	.020" (.051 cm) on Re	10	(25.4 cpm)	120	4	Sharp	None	Re edge melted, some surface fusion, no cracks
3	Re, 1/32	"	.020" (.051 cm) on Re	10	"	120	4	Defocused	None	Both materials melted, cracking
4	Re, 1/32	"	.020" (.051 cm) on Re	10	"	110	3	Sharp	None	Re edge melted and flowed to Cb-1Zr, cracking
5	Re, 1/32	"	.020" (.051 cm on Re)	10 (multipass)	"	110	2	Sharp	.031" (.079 cm)	No fusion
6	Re, 1/32	"	.020" (.051 cm on Re)	10 (multipass)	"	110	2	Sharp	.031" (.079 cm)	Re edge melted, no fusion to Cb-1Zr
7	Re, 1/32	"	050" (.127 cm) on Re	5	(12.7 cpm)	110	2	Defocused	095" (.241 cm) (all on Re)	No fusion
8	Re, 1/32	"	.025" (.063 cm) on Re	5	(12.7 cpm)	110	2	Sharp	.095" (.241 cm) (25% on Cb-1Zr)	Surface melting of Re, no fusion to Cb-1Zr
9	Re, 1/32	"	.025" (.063 cm) on Re	5	(12.7 cpm)	115	3	Sharp	.095" (.241 cm) (25% on Cb-1Zr)	Re melted to Cb-1Zr, cracking
10	Cb-1Zr, 1/32	"	.045" (.114 cm) on Cb-1Zr	10	(25.4 cpm)	110	3	Slight Defocused	.090" (.228 cm)	Insufficient melt down, Some fusion with no cracks
11	Cb-1Zr, 1/32	"	.045" (.114 cm) on Cb-1Zr	10	(25.4 cpm)	110	4	Defocused	.090" (.228 cm)	No fusion
12	Cb-1Zr, 1/32	"	.045" (.114 cm) on Cb-1Zr	5	(12.7 cpm)	110	4	Defocused	090" (.228 cm)	Visual & dye penetrant good, no cracks
13	Cb-1Zr, 1/32	"	.090" (.228 cm) on Cb-1Zr	5	(12.7 cpm)	110	3	Sharp	180" (.456 cm)	Visual & dye penetrant good, no cracks (3-1/2" lgth) (8.9 cm)
14	Cb-1Zr, 3/32	(.24 cm)	.090" (.228 cm) on Cb-1Zr	5	(12.7 cpm)	110	4	Sharp	.180" (.456 cm)	Visual & dye penetrant good, no cracks (3-1/2" lgth) (8.9 cm)

Table 37. Lap Welding of Tungsten-25 Rhenium Alloy to Columbium-1Zirconium Alloy

Lap Weld No.	Overlap (in.)	(cm)	Beam Center Location from Seam	Weld Speed (ipm)	(cpm)	Voltage (KV)	Current (MA)	Focus	Deflection	Remarks
1A	Cb-1Zr 3/32	(.24 cm)	.090" on Cb-1Zr (.228 cm)	5	(12.7 cpm)	110	4	Sharp	.180" (.456 cm)	Visual & dye penetrant good, no cracks
2A	Cb-1Zr, 3/32	"	.090" on Cb-1Zr "	"	"	110	4	Sharp	.180" (.456 cm)	Visual & dye penetrant good, no cracks
3A	Cb-1Zr, 3/32	"	.045" on Cb-1Zr (.114 cm)	"	"	110	4	Sharp	.090" (.228 cm)	Thru penetration, weld cracks
4A	Cb-1Zr, 1/32	(.08 cm)	.045" on Cb-1Zr "	"	"	110	6	Wide Defocus	None	Complete penetration, weld cracks
5A	Cb-1Zr, 1/32	"	.045" on Cb-1Zr "	"	"	110	3.5	Defocused	None	Visual & dye penetrant good, no cracks
6A	Cb-1Zr, 1/32	"	.045" on Cb-1Zr	"	"	110	4	Defocused	.090" (.228 cm)	Excess melting of Cb-1Zr, no cracks
7A	Cb-1Zr, 1/32	"	.045" on Cb-1Zr "	"	"	110	3	Defocused	None	Insufficient melting of Cb-1Zr
8A	Cb-1Zr, 1/32	"	.045" on Cb-1Zr "	"	"	110	3.5	Defocused	None	Visual & dye penetrant good, no cracks (3-1/2") (8.9 cm) length

Figure 125. Lap Weld No. 12. Melt Down of Cb-1Zr Against Unfused Rhenium

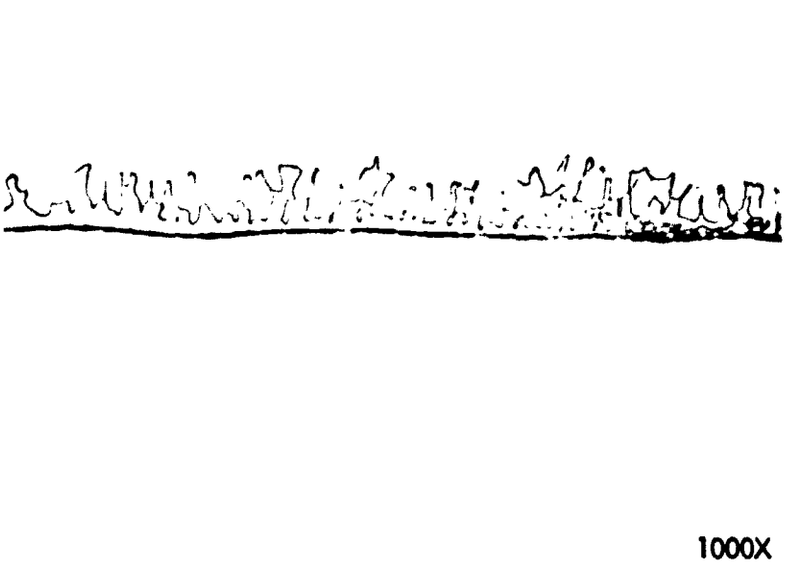

Figure 126. Lap Weld No. 12. Interface Between Fused Cb-1Zr and Rhenium Showing Limited Intermixing of Material.

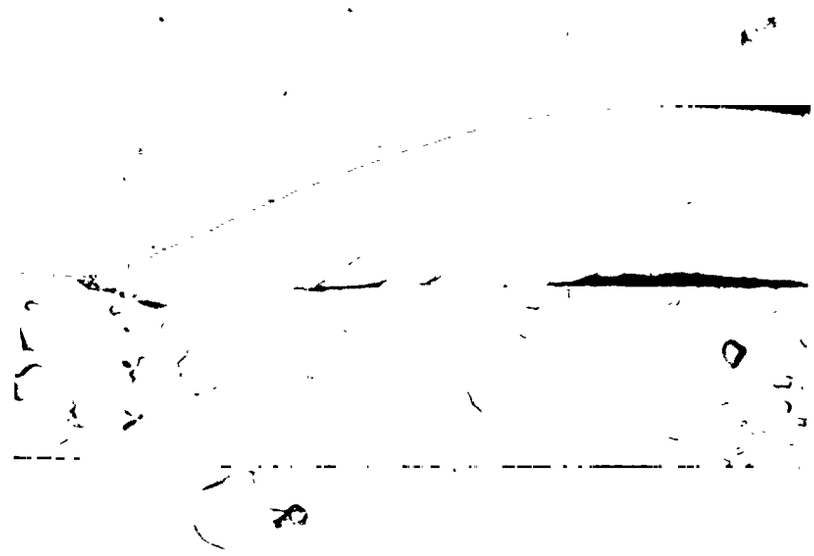

50X

Figure 127. Lap Weld No. 13. Melt Down of Cb-1Zr Against Unfused Rhenium

1000X

Figure 128. Lap Weld No. 13. Interface Between Fused Cb-1Zr and Rhenium Showing Limited Intermixing of Material.

(50X)

Figure 129. Lap Weld No. 2. Melting of Cb-1Zr Against Unfused Rhenium

(1000X)

Figure 130. Lap Weld No. 2. Braze Type Interface Showing Limited Intermixing of Material

Regardless of the ability to produce joints with apparent as welded integrity, the extreme brittleness of the intermetallic interface could be expected to create severe handling and use problems. For example, the cutting of samples for metallographic inspection or bend specimen preparation was difficult due to the extreme brittleness of the joints in both material combinations. The Cb-1Zr to W-25Re joints were successfully sectioned, however, by clamping the sheet between 1.27 cm (1/2") thick layers of sponge rubber and slowly cutting using a soft abrasive cut-off wheel. Electrical discharge machining was also successful with this material combination. Similar procedures did not resolve the problem with the Cb-1Zr to Re welds. Approximately 50% of specimens in this combination developed cracks even when the shock and vibration free electrical discharge machining was employed. Figure 131 illustrates the brittle nature of the interface area which fractured during metallographic preparation.

Elevated temperature bend testing was performed on lap joints. While this test would obviously be nonstandard and not comparable to other ductile-brittle transition temperature data, it was felt that some feel for joint ductility at temperature might be obtained. As the data shown in Table 38 illustrates, extreme brittle behavior occurred even at the maximum bend test temperature of 704°C (1300°F).

D. RECOMMENDATIONS

While limited in nature this welding study demonstrated that joining of the W-25Re and Re to Cb-1Zr alloy was feasible. The basic principle of melting the lower melting point alloy against the more refractory material did result in joints with no apparent defects in the as welded condition. This type of process is difficult to control on flat sheet specimens. However the round, tubular joints typical of thermionic systems would undoubtedly be more amenable to the process.

The extreme brittle nature of the joints produced must be considered in any application. It is suggested that before actual use, production configurations be carefully evaluated for performance through thermal cycling and other design requirements.

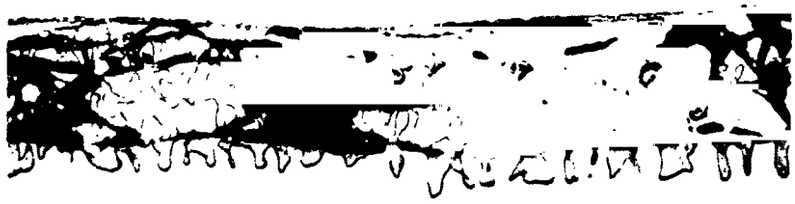

1000X

Figure 131. Lap Weld No. 14. Interface Between Fused Cb-1Zr and Rhenium. Cracking and Fragmentation Occurred During Metallographic Preparation.

Table 38. Longitudinal Bend Test Data on Lap Welds

Lap Weld Type	Test Temp. °C	Test Atmosphere	Final Bend Angle After Springback*	Results
Cb-1Zr to W-25Re	538	Argon	74°	Single large weld zone cracks
	543	Vacuum	68°	Many small weld zone cracks
	649	Vacuum	79°	Many small weld zone cracks
	704	Vacuum	55°	Many small weld zone cracks
Cb-1Zr to Re	704	Vacuum	83°	Crack-weld fusion zone shattered
	704	Vacuum	83°	Crack-weld fusion zone shattered

*Bent to 90° in test

XI. CONCLUSIONS

- The interdiffusion zone width of W or Re coupled to group V or VI refractory metals or alloys can be characterized with 95% accuracy by the following

$$\ln\left(\frac{\Delta X^2}{t}\right) = B\left(\frac{1}{T}\right) + A \qquad (37)$$

where ΔX is zone width in centimeters, t is age time in seconds, T is age temperature in ^{o}K, and A and B are as expressed in Table 39.

- Although the interdiffusion relationship expressed above was derived from 1000 and 2000 hour age experiments, data trends indicate valid extrapolation to 10,000 hours.

- A general interdiffusion zone width predictive model for any refractory metal junctions of W or Re to group V and VI elements of the periodic table can be expressed as

$$\ln\left(\frac{\Delta X^2}{t}\right) = -40.7 + 24.4\ \frac{T}{T_m} \qquad (38)$$

where ΔX is interdiffusion zone width in centimeters, t is age time in seconds, T is age temperature in ^{o}K, and T_m is lowest binary system melting point (i.e., eutectic, etc.) in ^{o}K. This predictive model is applicable only at T/T_m greater than 0.6.

- A general interdiffusion zone width predictive model for any refractory metal junctions of W or Re to group V and VI elements of the periodic table can be expressed as

$$\ln\left(\frac{\Delta X^2}{t}\right) = 24.44\left(\frac{T}{T_m}\right) - 40.68 \qquad (39)$$

Table 39. Parameters to Predict Net Interdiffusion Zone Width As a Function of Age Time (t-seconds) and Temperature (T - °K)

$$\ln\left(\frac{\Delta X^2}{t}\right) = B\left(\frac{1}{T}\right) + A$$

(with 95% confidence limits)

System	A	B
W/Cb, Cb-1Zr	-3.8689 ± 0.2266	-37,390 ± 2810
Re/Cb, Cb-1Zr	-0.4899 ± 0.2266	-43,880 ± 3060
W/Ta, Ta-10W	-7.3385 ± 0.1891	-35,290 ± 2210
W/T-111, ASTAR	-3.3585 ± 0.1530	-44,720 ± 3760
Re/Ta, Ta-10W	-7,1024 ± 0.0980	-35,020 ± 1100
Re/T-111, ASTAR	-6.4489 ± 0.1374	-36,560 ± 1730
W/Mo-50Re	+0.1554 ± 0.1921	-45,140 ± 4500
Re/Mo-50Re	-8,4797 ± 0.1466	-30,140 ± 2940
W/W-30.9Re-20.1Mo	-7.2084 ± 0.1719	-34,750 ± 3890
Re/W-30.9Re-20.1Mo	-9.3027 ± 0.1440	-28,580 ± 3290
W/Re	-4.4641 ± 0.3317	-41,300 ± 7470
W/W-25Re	-2.1992 ± 0.4407	-47,100 ± 9930
Re/W-25Re	+2.4148 ± 0.5513	-53,990 ± 11,900

where ΔX is interdiffusion zone width in centimeters, t is age time in seconds, T is age temperature in ^{o}K, and T_m is lowest binary system melting point,(i.e., eutectic etc.) in ^{o}K. This predictive model is applicable only at T/T_m greater than 0.6.

- The appearance of Kirkendall voids upon ageing of metallurgically coupled dissimilar metals can be inhibited if not prevented by the introduction of Kirkendail Void Inhibition (KVI) layers either by thermal pre-age treatments, or the introduction of interdictory alloy layers (of the same coupled materials) upon couple formation.

- W to T-111 or ASTAR-811C appear to be the best junctions for long time thermionic applications since their Kirkendall void structures are minimal (of the 39 junctions studied here). Re couples should be avoided since brittle intermetallics and subsequent junction cracking occur.

- Limited application lap welds between Cb-1Zr and Re or W-25Re can be formed by melting the Cb-1Zr onto the second material (braze type welds). Only sheet geometries were studied. Welds between these materials cannot be recommended without further development since they are brittle.

- Hot isostatic pressure (HIP) welding at 1400°C for 1/2 to 1 hour at 190 Mn/m^2 (28,000 psi) is an excellent method for joining W or Re to group V and VI elements and alloys of the periodic table with minimal joint thicknesses.

XII. RECOMMENDATIONS FOR FUTURE WORK

- This study has demonstrated the feasibility of eliminating Kirkendall voids from dissimilar metal junctions by proper pre-age heat treatments or insertion of alloy interdictory layers. Analytical and experimental characterization of these pre-age treatments must be developed on a formal basis with respect to vacancy flux, pre-age anneal temperature, time, vacancy coalescense, etc.

- The possibilities of joining complex thermionic power structures in the hot isostatic pressure (HIP) weld autoclave should be investigated. Complex geometries may be premachined as simple components and joined by HIP welding.

- Further definition and parameter analysis will be required to resolve the feasibility and utility of Cb-1Zr to Re or W-25Re welds.

XIII. REFERENCES

1. Taylor, A., X-Ray Metallography, Wiley, New York pp 242-245, 1961.
2. Stoner, D. R. and Lessmann, G. G., "Operation of 10^{-10} Torr Vacuum Heat Treating Furnaces in Routine Processing", WANL-SP-010, June 1965.
3. Hudson, R. G. et al., "Some Investigations of Refractory Metal Systems of Thermionic Interest", NASA-CR-111593, November 1969.
4. Hehemann, R. F. and Leber, S., "Chemical Diffusion in the Columbium-Tungsten System", AIME Trans., Vol. 236, p. 1040, July 1966.
5. Vergasova, L. L., Prokoshkin, D. A., and Vasileva, E. V., "Concentrational and Temperature Correlation of Interdiffusion Coefficients in Binary Nb Alloys", Izv. Akad. Naak, SSSR, Metal., No. 4, 1970, pp 198-204. As cited in Diffusion Data, No. 1, 1971, p. 53, Diffusion Information Center, Cleveland, Ohio.
6. Pawel, R. E. and Lundy, T. S., "Tracer Diffusion in Tungsten", Acta Met., Vol. 17, No. 8, p. 979, August 1969.
7. Lundy, T. S., Winslow, F. R., Pawel, R. E., and McHargue, C. J., "Tracer Diffusion in Columbium", ORNL-3617, June 1964. (Also in AIME Trans. 1965)
8. Ivanov, A. N., Krasil'nikova, G. B., and Mitiu, B. S., "Determining the Diffusion Parameters in Mo-Ta and W-Ta Systems", The Physics of Metals and Metallography, Vol. 29, No. 1, p. 215, May 1971.
9. Tregubov, I. A., Kuzina, L. N., and Ivanov, O. S., "Mutual Diffusion of Ta and W", (in Russian) Dokl. Akad. Nauk. SSSR., Vol. 180, No. 2, p. 423, 1968.
10. Pawel, R. E., and Lundy, T. S., J. Phys. Chem. Solids, 1965 as cited in Askil. J., "A Bibliography on Tracer Diffusion in Metals, Part I", ORNL-3795, May 1965.
11. DMIC Report No. 152, "Binary and Ternary Phase Diagrams of Columbium, Molybdenum, Tantalum, and Tungsten", p. 167, April 28, 1961.
12. Danneberg, W. and Krautz, E., Z. Naturforsch., 16a(a), p. 854, 1961 as cited in Askil, J., "A Bibliography on Tracer Diffusion in Metals, Part I", ORNL-3795, May 1965.
13. Hudson, R. G and Yang, L., "Diffusion and Electron Emission Properties of Duplex Refractory Metal Thermionic Emitters", Refractory Metals and Alloys, IV, Research and Development, Vol. II, AIME French Lick, Indiana Conference, Oct. 3-5, 1965, p. 1253, Gordon-Breach Publishers, 1967.

REFERENCES (Cont'd.)

14. Kirkendall, E. O. and Smigelskas, A. D., Metals Tech. 13, Tech. Publ. 2071, 1946.

15. Phillips, W. M., "Welding and Ageing of Bimetallic Refractory Metal Joints", IEEE Conference on Thermionic Conversion, Oct. 26-29, 1970 (70 C 53-ED).

16. Passmore, E. M., et al., "Investigation of Diffusion Barriers for Refractory Metals", ASD-TDR-62-432, WPAFB, July 1962.

17. Hehemann, R. F. and Leber, S., "Chemical Diffusion in the Columbium-Tungsten System", Trans. of the AIME, Vol. 236, p. 1040, July 1966.

18. Jost, W., Diffusion in Solids, Liquids, and Gases, Academic Press, 1960.

19. Shewmon, P. G., Diffusion in Solids, McGraw Hill, 1963.

20. Adda, Y., et al., "Application de la Thermodynamique des Processes Irreversilles a la Diffusion a L'etate Solide", Thermodynamics, Vol. II, p. 255, IAEA, Vienna, 1966.

21. Darken, L., AIME IMD, Metals Technol. 15, Tech. Publs. 2311 and 2433, 1948.